USGS
science for a changing world

Prepared in cooperation with the State of Hawai‘i Department of Hawaiian Home Lands, State of Hawai‘i Office of Hawaiian Affairs, and County of Maui Department of Water Supply

Numerical Simulation of Groundwater Availability in Central Moloka‘i, Hawai‘i

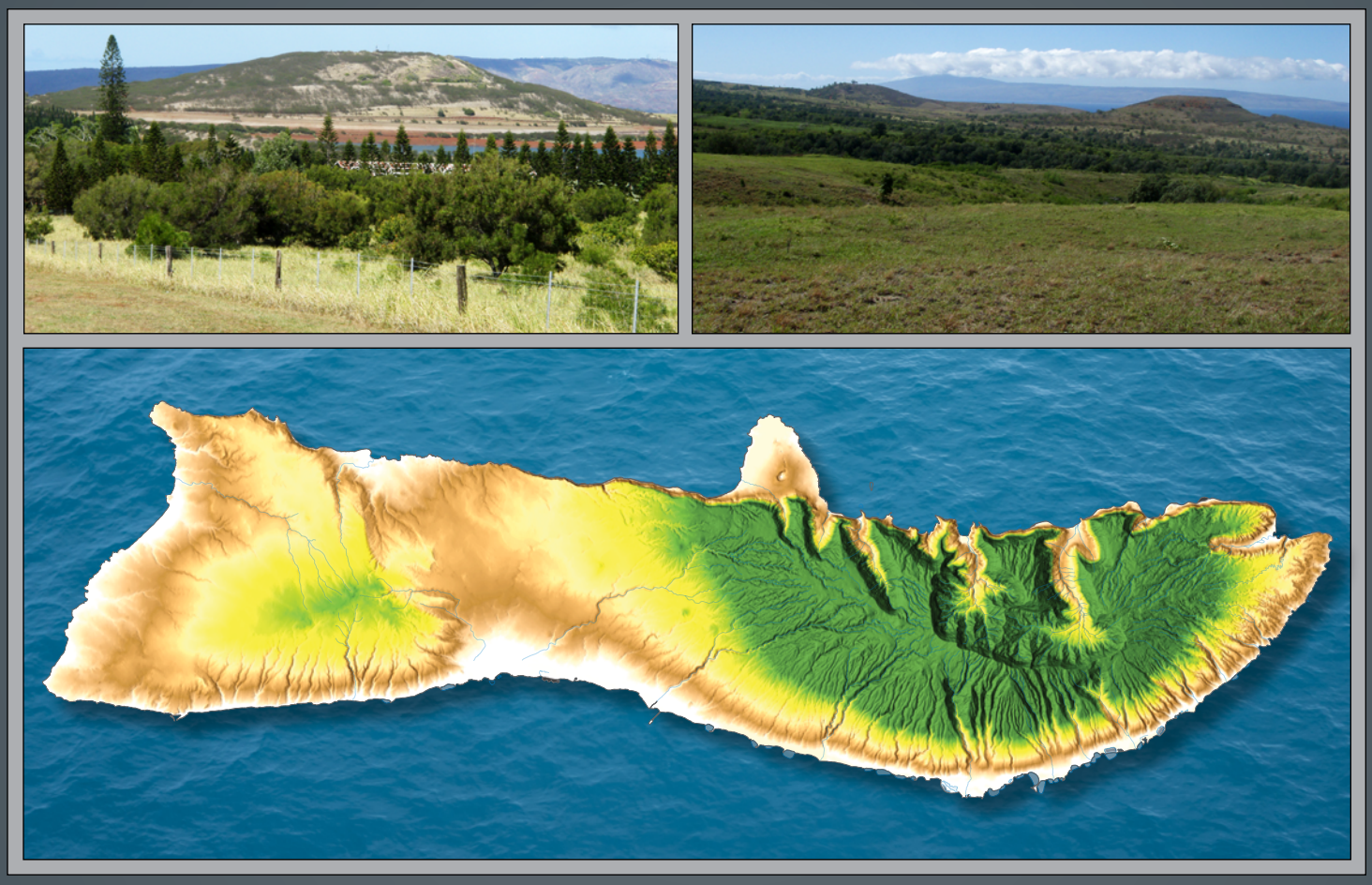

Scientific Investigations Report 2019–5150

U.S. Department of the Interior
U.S. Geological Survey

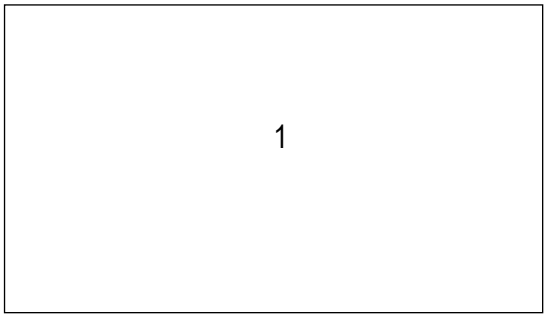

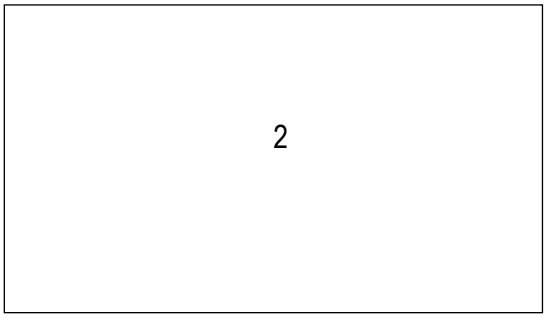

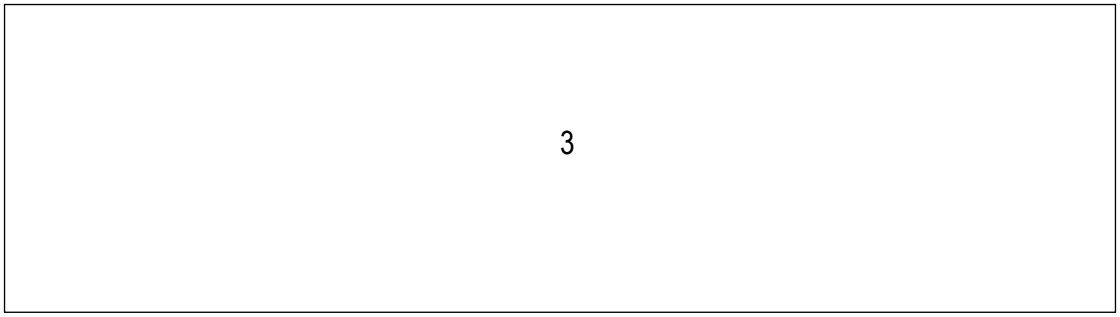

Cover images:

(1) Photograph of the volcanic vent Kualapuʻu in the Kualapuʻu area, Molokaʻi, Hawaiʻi, with the eroded remnants of West Molokaʻi volcano in the background.

(2) Photograph of the volcanic vents Kākalahale and Puʻu Luahine in the Kualapuʻu area, Molokaʻi, Hawaiʻi, with the island of Lānaʻi in the background.

(3) Generalized map of island of Molokaʻi, Hawaiʻi.

Numerical Simulation of Groundwater Availability in Central Molokaʻi, Hawaiʻi

By Delwyn S. Oki, John A. Engott, and Kolja Rotzoll

Prepared in cooperation with the State of Hawaiʻi Department of Hawaiian Home Lands, State of Hawaiʻi Office of Hawaiian Affairs, and County of Maui Department of Water Supply

Scientific Investigations Report 2019–5150

U.S. Department of the Interior
U.S. Geological Survey

U.S. Department of the Interior
DAVID BERNHARDT, Secretary

U.S. Geological Survey
James F. Reilly II, Director

U.S. Geological Survey, Reston, Virginia: 2020

Suggested citation:
Oki, D.S., Engott, J.A., and Rotzoll, K., 2020, Numerical simulation of groundwater availability in central Moloka'i, Hawai'i: U.S. Geological Survey Scientific Investigations Report 2019–5150, 95 p., https://doi.org/10.3133/sir20195150.

ISSN 2328-0328 (online)

Acknowledgments

The State of Hawai'i Department of Hawaiian Home Lands, State of Hawai'i Division of Forestry and Wildlife, Kamehameha Schools, Kawela Plantation, Maui Electric Company, Limited, and Pauline and Skip Castanera provided access to wells that were monitored for this study. Monthly pumpage data were provided by the State of Hawai'i Commission on Water Resource Management. Additional detailed pumpage data for the period August to September 2009 were supplied by the State of Hawai'i Department of Hawaiian Home Lands, County of Maui Department of Water Supply, and Moloka'i Properties Limited (Moloka'i Ranch). Ed Carlson, National Geodetic Survey, led a surveying effort, using global positioning system methods, to determine altitudes of reference marks near monitor wells. Jeff A. Perreault, Adam G. Johnson, Todd K. Presley, Sarah N. Rosa, Craig A. Senter, and Maoya Bassiouni from the U.S. Geological Survey assisted with activities related to this study.

Contents

Figures

Appendix Figures

Tables

Appendix Tables

Conversion Factors

U.S. customary units to International System of Units

Multiply	By	To obtain
	Length	
inch (in.)	25.4	millimeter (mm)
foot (ft)	0.3048	meter (m)
mile (mi)	1.609	kilometer (km)
	Area	
acre	4,047	square meter (m^2)
square foot (ft^2)	0.09290	square meter (m^2)
square mile (mi^2)	2.590	square kilometer (km^2)
	Volume	
gallon (gal)	3.785	liter (L)
gallon (gal)	0.003785	cubic meter (m^3)
million gallons (Mgal)	3,785	cubic meter (m^3)
cubic foot (ft^3)	0.02832	cubic meter (m^3)
	Flow rate	
foot per second (ft/s)	0.3048	meter per second (m/s)
foot per day (ft/d)	0.3048	meter per day (m/d)
cubic foot per second (ft^3/s)	0.02832	cubic meter per second (m^3/s)
gallon per day (gal/d)	0.003785	cubic meter per day (m^3/d)
million gallons per day (Mgal/d)	0.04381	cubic meter per second (m^3/s)
inch per year (in/yr)	25.4	millimeter per year (mm/yr)
	Mass	
pound, avoirdupois (lb)	0.4536	kilogram (kg)
	Pressure	
atmosphere, standard (atm)	101.3	kilopascal (kPa)
bar	100	kilopascal (kPa)
pound per square foot (lb/ft^2)	0.04788	kilopascal (kPa)
pound per square inch (lb/in^2)	6.895	kilopascal (kPa)
	Density	
pound per cubic foot (lb/ft^3)	16.02	kilogram per cubic meter (kg/m^3)
	Hydraulic conductivity	
foot per day (ft/d)	0.3048	meter per day (m/d)
	Hydraulic gradient	
foot per mile (ft/mi)	0.1894	meter per kilometer (m/km)

Temperature in degrees Celsius (°C) may be converted to degrees Fahrenheit (°F) as °F = (1.8 × °C) + 32.
Temperature in degrees Fahrenheit (°F) may be converted to degrees Celsius (°C) as °C = (°F – 32) / 1.8.

Datum

Vertical coordinate information is referenced to local mean sea level.

Horizontal coordinate information is referenced to the North American Datum of 1983 (NAD 83)].

Altitude, as used in this report, refers to distance above the vertical datum.

Supplemental Information

Specific conductance is given in microsiemens per centimeter at 25 degrees Celsius (µS/cm at 25 °C).

Concentrations of chemical constituents in water are given in either milligrams per liter (mg/L) or micrograms per liter (µg/L).

Abbreviations

CWRM	State of Hawai‘i Commission on Water Resource Management
DHHL	Department of Hawaiian Home Lands
EPA	U.S. Environmental Protection Agency
MDWS	County of Maui Department of Water Supply
MIS	Moloka‘i Irrigation System
OHA	Office of Hawaiian Affairs
SUTRA	saturated-unsaturated transport groundwater model computer code
USGS	U.S. Geological Survey
WRPP	Water Resource Protection Plan (the 1990 version is referred to as the Water Resources Protection Plan)

Numerical Simulation of Groundwater Availability in Central Molokaʻi, Hawaiʻi

By Delwyn S. Oki, John A. Engott, Kolja Rotzoll

Abstract

Since the 1990s, increased chloride concentrations of water pumped from wells (much of which is used for drinking water) and the effects of withdrawals on groundwater-dependent ecosystems have led to concerns over groundwater availability on the island of Molokaʻi, Hawaiʻi. An improved understanding of the hydrologic effects of proposed groundwater withdrawals is needed to ensure effective management of the groundwater resources of Molokaʻi, plan for possible growth, and accommodate cultural, social, and economic concerns.

To address the information needs of managers and community stakeholders on Molokaʻi, the U.S. Geological Survey developed a numerical groundwater model capable of simulating salinity change and reduction in groundwater discharge in coastal areas of central and southern Molokaʻi. Estimates of groundwater recharge needed as input to the numerical groundwater model were made using a daily water budget for each decade during 1940−2012 (the period 2000−12 spanned 13 years) and the most current available data, including the distributions of monthly rainfall and potential evapotranspiration. Total island recharge during the decadal periods ranged from a low of about 189 Mgal/d during the 1970s to a high of 278 Mgal/d during the 1960s. These recharge estimates were used to develop an island-wide numerical groundwater model with simplifying assumptions (sharp interface between freshwater and saltwater; two-dimensional flow). The island-wide model provided estimates of groundwater inflows to the main area of interest simulated with a three-dimensional numerical groundwater model.

Simulated withdrawal scenarios were selected in consultation with water managers and stakeholders and consisted of: (1) a baseline scenario using average recharge (1978−2007 rainfall and 2010 land cover) and average 2016−17 withdrawals; (2) a scenario using average recharge and withdrawals from existing wells at pending (as of January 2019) water-use permit rates; (3) six scenarios using average recharge and selected withdrawals from existing and proposed wells; and (4) a scenario using reduced recharge and selected withdrawals from existing and proposed wells. Results of the simulated withdrawal scenarios indicate that wells may be capable of producing groundwater with chloride concentrations below 250 mg/L at withdrawal rates exceeding average 2016−17 rates. However, the quality of water withdrawn from production wells is dependent on the rate and distribution of the withdrawals. For all nonbaseline scenarios, simulated groundwater discharge to the nearshore environment is reduced relative to the baseline scenario. Areas of discharge reduction may correspond to areas used for cultural or subsistence purposes.

The three-dimensional numerical groundwater model developed for this study utilizes the latest available hydrologic and geologic information and is a useful tool for understanding the hydrologic effects of additional groundwater withdrawals in central Molokaʻi. The model has several limitations, including its nonuniqueness and inability to account for local-scale heterogeneities.

Introduction

Groundwater demand on the island of Molokaʻi, Hawaiʻi (fig. 1), has increased since the 1970s. Known island-wide groundwater withdrawals averaged about 0.4 million gallons per day (Mgal/d) during 1970, peaked at greater than 5.7 Mgal/d during 2002 and 2003, and averaged between about 3 and 5 Mgal/d from 2004 to 2017. Federal, State, and County agencies and private entities on Molokaʻi withdraw groundwater, which is primarily used as drinking water. The increase in groundwater demand is partly related to the 40 percent increase in resident population on Molokaʻi from 1970 (resident population 5,261) to 2010 (resident population 7,345) (State of Hawaiʻi, 2011). In 1992, the State of Hawaiʻi Commission on Water Resource Management (CWRM) designated the entire island of Molokaʻi as a Water Management Area for groundwater. With this designation, any increase in groundwater withdrawal on Molokaʻi requires a water-use permit issued by CWRM. CWRM may deny an application for a water-use permit if the applicant does not establish that the proposed use of water (1) can be accommodated with the available water source; (2) is a reasonable-beneficial use; (3) will not interfere with any existing legal use of water; (4) is consistent with the public interest; (5) is consistent with state and county general plans and land-use designations; (6) is consistent with county land-use plans and policies; and (7) will not interfere with the rights of the Department of Hawaiian Home Lands as provided in the Hawaiian Homes Commission Act (Hawaiʻi Revised Statutes, Chapter 174C, State Water Code, Section 174C-49).

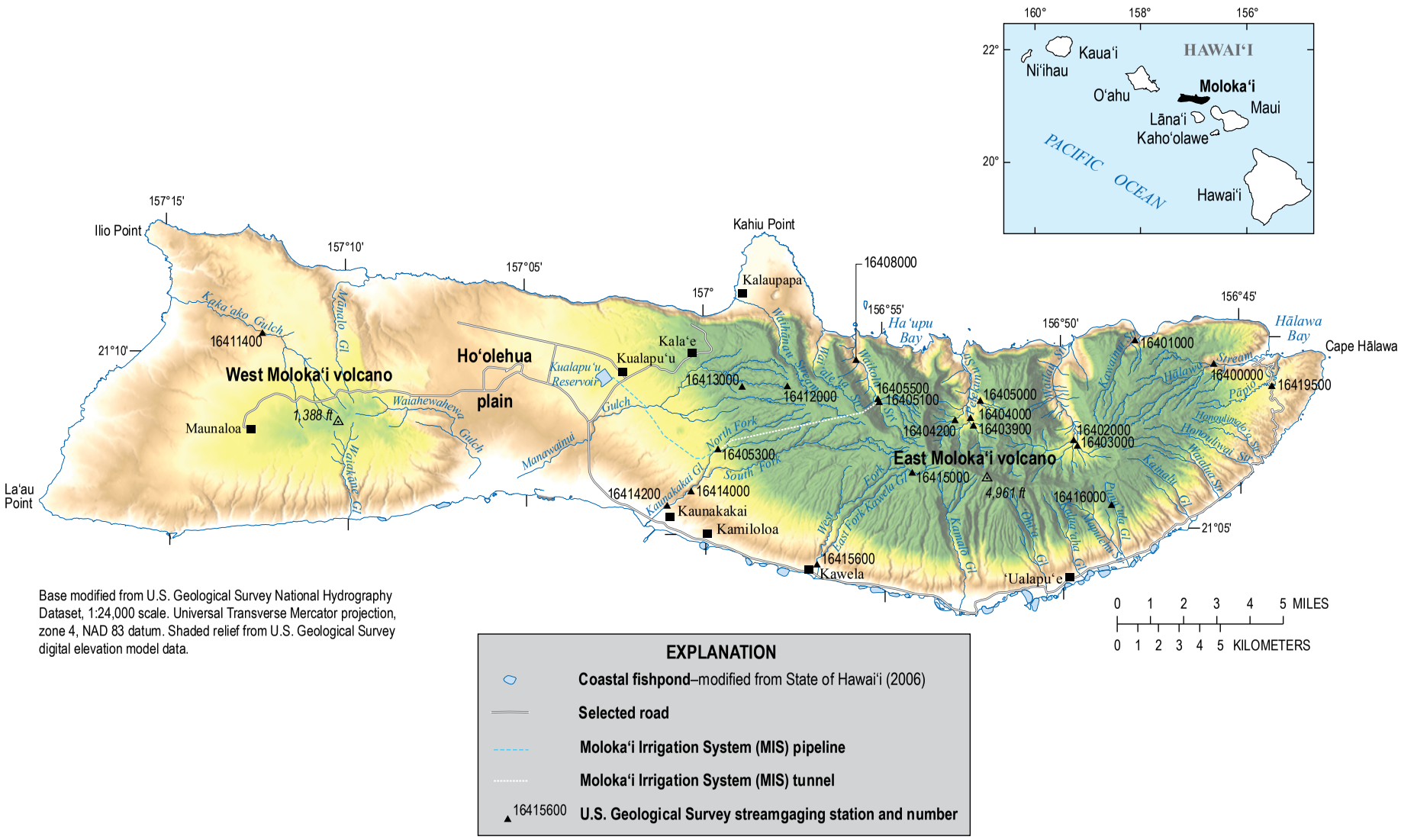

Base modified from U.S. Geological Survey National Hydrography Dataset, 1:24,000 scale. Universal Transverse Mercator projection, zone 4, NAD 83 datum. Shaded relief from U.S. Geological Survey digital elevation model data.

Figure 1. Map of Moloka'i, Hawai'i showing selected geographic features and Moloka'i Irrigation System (MIS) Tunnel.

For management purposes, CWRM has divided the island of Molokaʻi into 16 management areas called aquifer systems (fig. 2). The aquifer-system boundaries do not necessarily coincide with known hydrogeologic barriers to groundwater flow. Nearly all of the CWRM aquifer-system boundaries on Molokaʻi are along topographic divides, which may not be related to subsurface hydrogeologic conditions (Mink and Lau, 1992). Thus, groundwater may cross aquifer-system boundaries, and withdrawals from one aquifer system may affect conditions in nearby aquifer systems. The Kualapuʻu aquifer system in central Molokaʻi is one of the most important aquifer systems on the island and reported withdrawals from this aquifer system averaged about 1.5 Mgal/d during 2016–17. In addition, the State of Hawaiʻi Department of Hawaiian Home Lands (DHHL) has an existing (as of 2019) groundwater reservation of 2.905 Mgal/d from the Kualapuʻu aquifer system. The CWRM-estimated sustainable yield of the Kualapuʻu aquifer system is 5 Mgal/d (State of Hawaiʻi, 2008). Decisions related to future infrastructure development and alternate sources of freshwater will depend on the long-term sustainability of the groundwater resources in the Kualapuʻu aquifer system, as well as other aquifer systems on Molokaʻi. The current estimates of sustainable yield used by CWRM are based on an analytical equation that does not account for aquifer heterogeneities and the spatial distribution of withdrawals (Oki and Meyer, 2001). These limitations can be addressed with numerical groundwater models.

In a freshwater-lens system, increased groundwater withdrawals will, in the long term, result in a decline in water levels, a rise in the transition zone between freshwater and saltwater, and a reduction of natural groundwater discharge to streams or the ocean. The extents to which water levels decline, the transition zone rises, and natural discharge reduces are dependent on factors including the distribution and rates of withdrawals and the hydraulic characteristics of the aquifer system. In some cases, withdrawal from a well may induce brackish water to enter the well if the withdrawal rate is too high or the well is too deep.

Since the 1990s, the chloride concentrations of water pumped from some wells on Molokaʻi have increased (Oki, 2006), leading to concern over the long-term sustainability of withdrawals from wells on Molokaʻi. To ensure effective management of the groundwater resources of Molokaʻi and to plan for possible growth on the island, an improved understanding of the hydrologic effects of proposed groundwater withdrawals is needed. An accurate understanding of how much fresh groundwater in the Kualapuʻu aquifer system can be developed for future needs is critically important from economic, cultural, and resource standpoints.

A growing concern related to groundwater development in Hawaiʻi is the effect of withdrawals on groundwater-dependent ecosystems. This concern was raised during a contested-case hearing related to proposed withdrawal from the Kamiloloa aquifer system of south-central Molokaʻi (State of Hawaiʻi, 1998) and, more recently, this concern has been raised in relation to potential future groundwater development in the western part of the island of Hawaiʻi (National Park Service, 2013). Along the southern coast of Molokaʻi, numerous ancient Hawaiian coastal fishponds (fig. 1) (Farber, 1997) were once used for aquaculture, and some of these cultural sites have been restored in recent years. References to fishpond construction on Molokaʻi date back to the 16th century, and the most recently constructed fishpond on the island was built about 1829 (Farber, 1997). Discharge of fresh or brackish groundwater to these fishponds may be a factor controlling productivity by providing nutrients for algae on which the fish feed (Farber, 1997). Stearns and Macdonald (1947, p. 56) suggested that fishponds along the southern shore of Molokaʻi indicate the presence of coastal springs, some of which discharge more than 0.5 Mgal/d. In addition to the fishponds, numerous nearshore subsistence sites were identified by the Governor's Molokaʻi Subsistence Task Force as important for ocean gathering, fishing, or future protection (Matsuoka and others, 1994). For example, residents of Molokaʻi gather edible limu (marine algae) in productive nearshore areas. Because limu productivity may be dependent on groundwater discharge (State of Hawaiʻi, 1998), increased groundwater withdrawals have the potential to affect subsistence gathering activities.

An existing USGS numerical groundwater-flow model of Molokaʻi (Oki, 1997, 2006, 2007) was used to develop updated numerical models to address information needs related to: (1) quantifying the effects of pumping existing or proposed wells on salinity of groundwater and discharge of groundwater near the coast, (2) identifying areas for new groundwater development in central Molokaʻi, (3) distributing pumping to increase the overall amount of fresh groundwater developed in the Kualapuʻu area, and (4) estimating the long-term effects of potential reductions in groundwater recharge on groundwater availability.

Purpose and Scope

The purpose of this report is to describe an evaluation of groundwater availability in central Molokaʻi, Hawaiʻi, for selected withdrawal scenarios. Groundwater levels and salinity in central Molokaʻi were estimated with a three-dimensional numerical groundwater model capable of simulating density-dependent flow and salinity transport. Estimates of groundwater recharge from the soil zone, needed as input to the numerical groundwater model, were made using a daily water budget of each decade during 1940−2012 (the period 2000−12 spanned 13 years) and the most current available data, including the distributions of monthly rainfall and potential evapotranspiration (Frazier and others, 2016; Giambelluca and others, 2013; 2014). A two-dimensional, sharp-interface groundwater-flow model covering the entire island was used to estimate subsurface inflows at the boundaries of the central Molokaʻi groundwater model. Aquifer hydraulic properties for the numerical groundwater model were estimated using available water-level and salinity information. Simulated withdrawal scenarios were selected in consultation with water managers and stakeholders and consisted of: (1) a baseline scenario using average recharge (1978−2007 rainfall and 2010 land cover) and average 2016−17 withdrawals; (2) a scenario using average recharge and withdrawals from existing wells at pending (as of

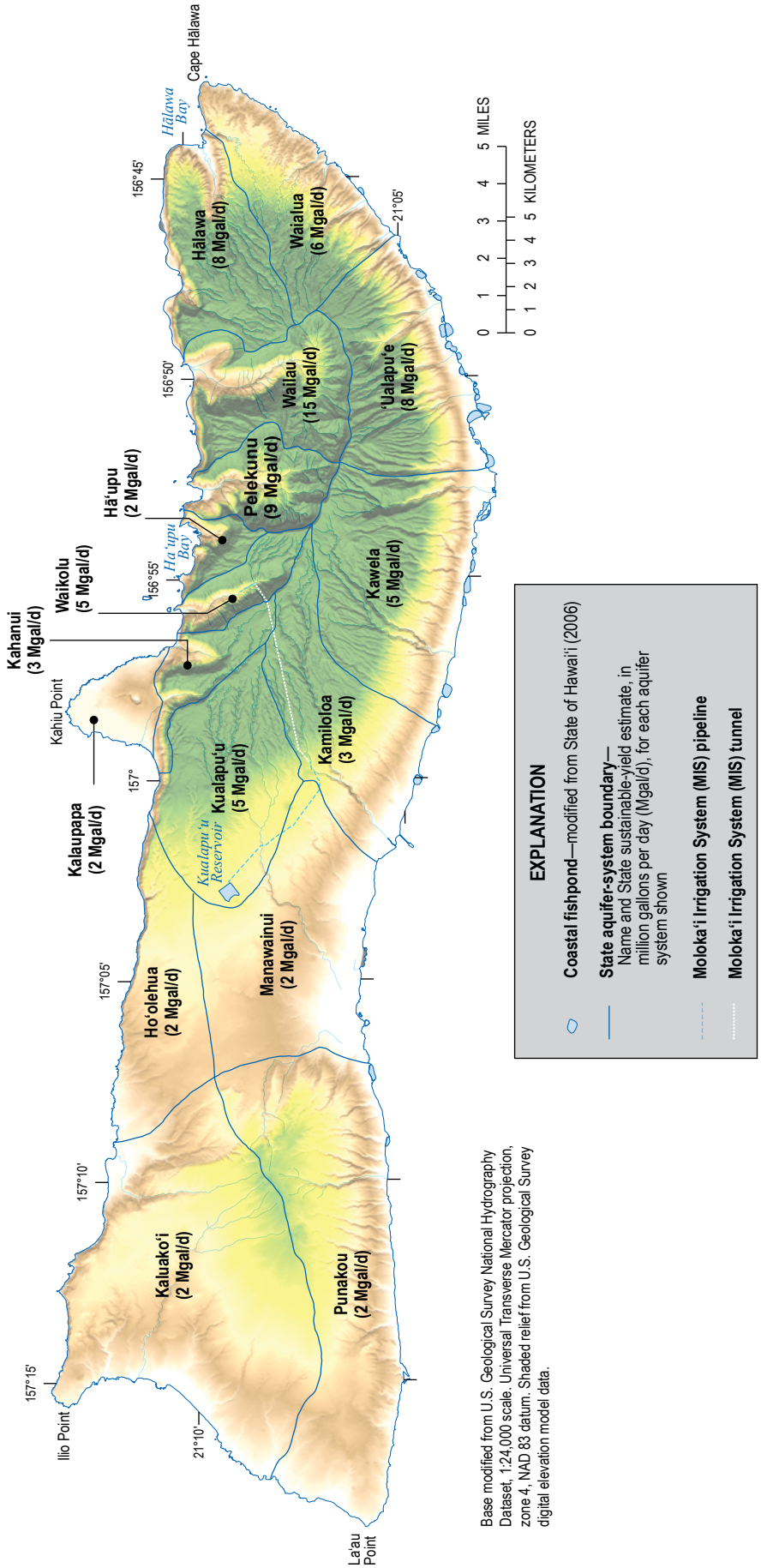

Figure 2. Map of Moloka'i, Hawai'i aquifer systems delineated by the Hawai'i Commission on Water Resource Management.

January 2019) water-use permit rates; (3) six scenarios using average recharge and selected withdrawals from existing and proposed new wells; and (4) a scenario using reduced recharge and selected withdrawals from existing and proposed new wells.

Description of Study Area

The island of Molokaʻi, the fifth largest of the Hawaiian Islands, occupies an area of 260 square miles (mi^2; Juvik and Juvik, 1998) between lat 21°00'–21°15' N. and long 157°20'–156°40' W. (fig. 1). The island primarily consists of two shield volcanoes (Stearns and Macdonald, 1947): the older West Molokaʻi volcano, which rises to an altitude of 1,388 ft, and the younger East Molokaʻi volcano, which rises to an altitude of 4,961 ft. The town of Kualapuʻu lies on the eastern margin of the Hoʻolehua plain, a relatively flat area of land in the central saddle area of the island. The main study area is the Kualapuʻu aquifer system in central Molokaʻi, although groundwater models developed for this study include other areas.

Climate

The climate on Molokaʻi is characterized by mild temperatures, cool and persistent trade winds, a rainy winter season from October through April, and a dry summer season from May through September (Blumenstock and Price, 1967; Sanderson, 1993). The climate is controlled primarily by topography and the position of the North Pacific anticyclone, a large-scale clockwise circulation of winds around an area of high atmospheric pressure north of the Hawaiian Islands, and other migratory weather systems relative to the island. During the dry season, the stability of the North Pacific anticyclone produces persistent northeasterly winds known locally as trade winds. Summer trade winds blow 80 to 95 percent of the time. During the rainy season, frequent passage of migratory high-pressure systems by the Hawaiian Islands results in less persistent trade winds. Winter trade winds blow 50 to 80 percent of the time. Southerly winds associated with low-pressure systems can bring heavy rains to the island. The dry coastal areas receive much of their rainfall as a result of these low-pressure systems.

Rainfall

The windward (northeastern) part of Molokaʻi is the wettest part of the island, a trait controlled by the orographic lifting of moisture-laden northeasterly trade winds along the windward slope of East Molokaʻi volcano. The moisture-laden air mass cools as it rises up the slopes of the volcano, resulting in condensation, cloud formation, and high rainfall near the crest of the mountains. West Molokaʻi volcano is considerably drier because it does not extend upward into the cloud-forming zone at higher altitudes.

Annual rainfall averaged over the entire island of Molokaʻi during 1920–2012 ranged from 24 to 77 in. and averaged about 48 in. (Frazier and others, 2016). Rainfall on Molokaʻi is characterized by maxima at high altitudes and steep spatial gradients (fig. 3). Mean annual rainfall during 1978–2007 was greatest over the eastern part of East Molokaʻi volcano, where it exceeded 160 in. (Giambelluca and others, 2013). Over most of West Molokaʻi volcano, mean annual rainfall during 1978–2007 was less than about 25 in., and along the coastal areas of the southern and western parts of the island, mean annual rainfall was less than 15 in.

Geology

The overall geology of Molokaʻi has been described by numerous investigators (for example, Lindgren, 1903; Stearns and Macdonald, 1947; Beeson, 1976; Macdonald and others, 1983; Stearns, 1985; Sherrod and others, 2007). The reader is referred to these sources for a more detailed description than the brief description provided here.

Molokaʻi was built mainly during the shield stage of volcanic activity, when more than 95 percent of West and East Molokaʻi volcanoes were formed by lava flows that originated from rift zones as well as the central caldera area of East Molokaʻi volcano. Intrusive dikes formed by rising magma that penetrated the rift zones and caldera area. The postshield stage is recognized by a change in lava chemistry and characteristics. Postshield-stage volcanic rocks on Molokaʻi consist of alkalic basalt, hawaiite, mugearite, and trachyte. On East Molokaʻi volcano, lava from the post-shield stage seems to have erupted from both within and outside the main rift zones and forms a veneer atop the shield-stage basalt. Following a period of volcanic quiescence, lava issued from a vent during the rejuvenated stage of volcanic activity and formed Kalaupapa Peninsula, the peninsular landmass containing the town of Kalaupapa. Langenheim and Clague (1987) described the stratigraphic framework of volcanic rocks on Molokaʻi. Collectively, the volcanic rocks of West Molokaʻi volcano are known as the West Molokaʻi Volcanics, and the exposed rocks of East Molokaʻi volcano are named the East Molokaʻi Volcanics and the Kalaupapa Volcanics (Langenheim and Clague, 1987; Sherrod and others, 2007) (fig. 4). Erosion has modified the topography of the volcanoes, particularly in the wetter parts of East Molokaʻi volcano where erosion has exposed dikes in valleys.

Volcanic Rocks

The volcanic rocks of Molokaʻi can be divided into two main types on the basis of their mode of emplacement: (1) extrusive lava flows, and (2) intrusive dikes, sills, stocks, and plugs. In general, lava flows that erupt from rift zones are less than 10 feet (ft) thick and composed either of pāhoehoe, which is characterized by smooth or ropy surfaces, or ʻaʻā, which contains a massive central core sandwiched between rubbly

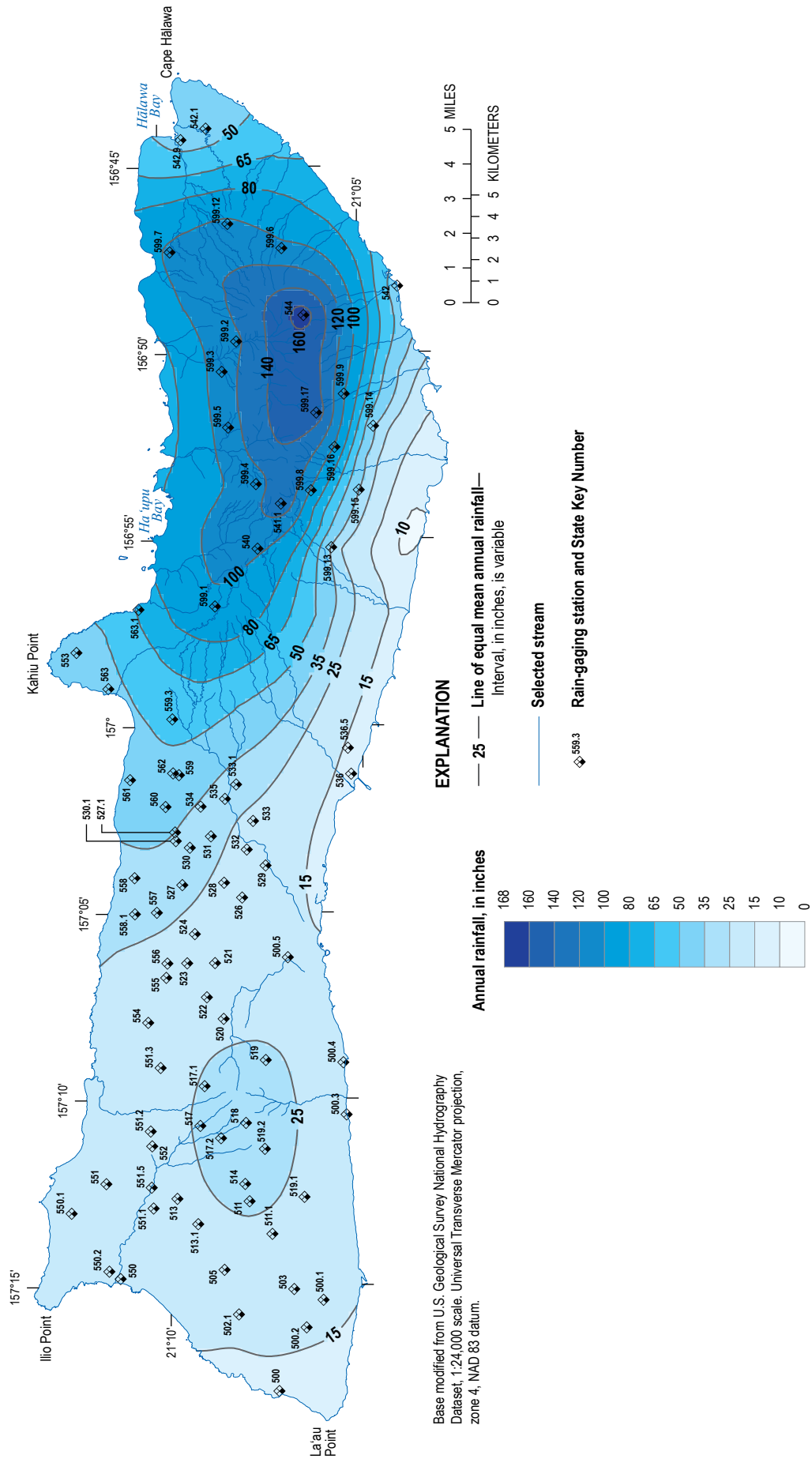

Figure 3. Map of Moloka'i, Hawai'i showing mean annual rainfall distribution during 1978–2007 (modified from Giambelluca and others, 2013).

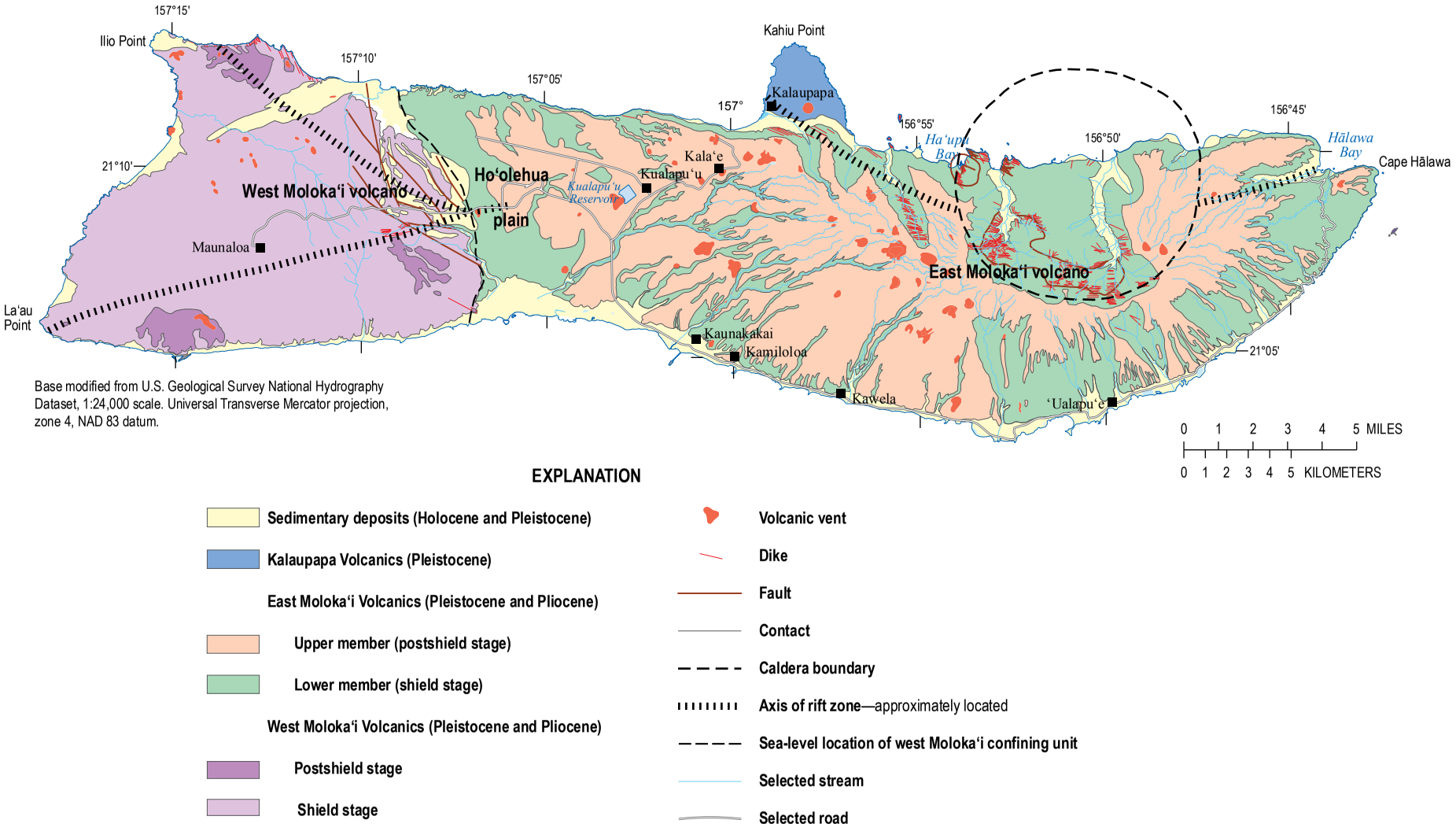

Figure 4. Map of Moloka'i, Hawai'i showing generalized surface geology and geologic features (modified from Sherrod and others, 2007 and Langenheim and Clague, 1987).

clinker layers (Wentworth and Macdonald, 1953). ʻAʻā flows are typically more abundant at greater distances from eruptive sources (Lockwood and Lipman, 1987).

Dikes are thin, near-vertical sheets of dense intrusive volcanic rock that formed when rising magma cut through existing rock and cooled beneath the land surface. Dikes are an important hydrologic control on groundwater because they have low permeability and tend to impede flow of groundwater, causing groundwater levels to build up behind them. Dikes are commonly exposed by erosion within the central and marginal parts of rift zones of older volcanoes (see Takasaki and Mink, 1985), including West and East Molokaʻi volcanoes. In the central part of a rift zone, dikes can number as many as 1,000 per mile of horizontal distance and compose 10 percent or more of the total rock volume (Takasaki and Mink, 1985). The central part of the rift zone, where dikes compose 10 percent or more of the total rock volume, commonly is referred to as a dike complex. The number of dikes decreases toward the outer edges of a rift zone within the marginal dike zone, where dikes generally compose less than 5 percent of the total rock volume (Takasaki and Mink, 1985). Wentworth and Macdonald (1953) estimated that 200 dikes are needed to vertically build 1,000 ft of a shield volcano.

West Molokaʻi Volcano

The primary rift zones of West Molokaʻi volcano trend approximately northwest and southwest (fig. 4) in the same direction as broad ridges that extend from near the summit of the volcano. A positive gravity anomaly that extends from near the summit region of West Molokaʻi volcano through Lāʻau Point at the southwest tip of the island (Moore and Krivoy, 1965; Flinders and others, 2013) indicates the presence of dense intrusive dikes associated with the southwestern rift zone. A few southeast-trending dikes exposed near the southern coast may be evidence of a third rift zone associated with West Molokaʻi volcano. No surface evidence of a summit caldera has been observed on West Molokaʻi volcano (Beeson, 1976; Langenheim and Clague, 1987). Numerous fault scarps, 100 to 500 ft high, are exposed on the northeastern part of the volcano (Stearns and Macdonald, 1947). The exposed rocks of West Molokaʻi volcano are shield-stage tholeiitic basalt and postshield-stage hawaiite and alkalic basalt.

East Molokaʻi Volcano

The primary rift zones of East Molokaʻi volcano trend northwest and east from a central caldera complex (fig. 4). Macdonald (1956) suggested a possible southern rift zone emanating from the caldera. Furthermore, Malahoff and Woollard (1966) interpreted results from a magnetic survey as indicating a possible southwestern rift zone emanating from the caldera complex. The northwestern and eastern rift zones are marked by numerous nearly vertical to vertical intrusive dikes (Stearns and Macdonald, 1947). The caldera complex of East Molokaʻi volcano is exposed in Pelekunu and Wailau Stream valleys (figs. 1 and 4), and is composed of stocks, plugs, crater fills, ponded lavas, and talus and fault breccias cut by dike swarms (Langenheim and Clague, 1987; Stearns and Macdonald, 1947).

Stearns and Macdonald (1947) mapped numerous vent features, including cinder and spatter cones, along the western and southern flanks of East Molokaʻi volcano (fig. 4). Many of these features do not seem to lie along the trends of the two primary rift zones of the volcano, possibly indicating the presence of (1) a marginal dike zone or (2) more than two primary rift zones. Presence of dikes in these areas is consistent with positive gravity anomalies mapped by Flinders and others (2013).

The East Molokaʻi Volcanics is divided into two informal members: a lower member consisting of shield-stage tholeiitic, olivine-tholeiitic, and picritic-tholeiitic basalts and postshield-stage alkalic basalt; and an upper member consisting of postshield-stage mugearite and lesser amounts of hawaiite and trachyte (Langenheim and Clague, 1987). The upper member forms a relatively thin (approximately 50–500 ft thick) veneer over the lower member (Stearns and Macdonald, 1947); the upper member may obscure vent features associated with the lower member. The Kalaupapa Volcanics consists of the rejuvenated-stage alkalic basalt and basanite that form Kalaupapa Peninsula (Clague and others, 1982; Langenheim and Clague, 1987).

Estimated ages of the rocks of West and East Molokaʻi volcanoes (McDougall, 1964; Naughton and others, 1980; Langenheim and Clague, 1987) indicate that the volcanoes may have formed almost contemporaneously. Stearns and Macdonald (1947) noted, however, that an erosional unconformity, which dips about 10° E., is exposed at an altitude of 250 ft in the eastern bank of Waiahewahewa Gulch (fig. 1). The West Molokaʻi Volcanics form the base of the observed outcrop and is overlain by 3 ft of soil and 6 ft of spheroidally weathered basalt, which separate the West Molokaʻi Volcanics from the East Molokaʻi Volcanics at this site. This sequence indicates that the West Molokaʻi Volcanics is older than the East Molokaʻi Volcanics at the site of the exposed unconformity.

Coastal Deposits

Off the northern coast of Molokaʻi, a thin veneer of recent sediment derived from wave erosion covers the insular shelf (Mathewson, 1970). A coral reef extends from the southern coast of the island to about 1 mile (mi) offshore, and limestone also has been described in geologic logs from wells near the southern coast (Lindgren, 1903; Lum, 2003). In addition, along the southern shore of East Molokaʻi volcano and the Hoʻolehua plain, an apron of alluvium has formed by deposition of eroded soil. Geophysical and geological information is limited on the thickness of the sedimentary deposits overlying the volcanic rocks in nearshore and offshore areas. The thickness can be determined if the depth of the base of the sedimentary deposits is known or estimated. Off the southern coast of Molokaʻi, the base of the sedimentary deposits can be estimated by extrapolating the assumed uneroded slope of shield-building lavas offshore (fig. 5). The thickness of the sedimentary deposits can then be determined from the difference in altitudes of the ocean

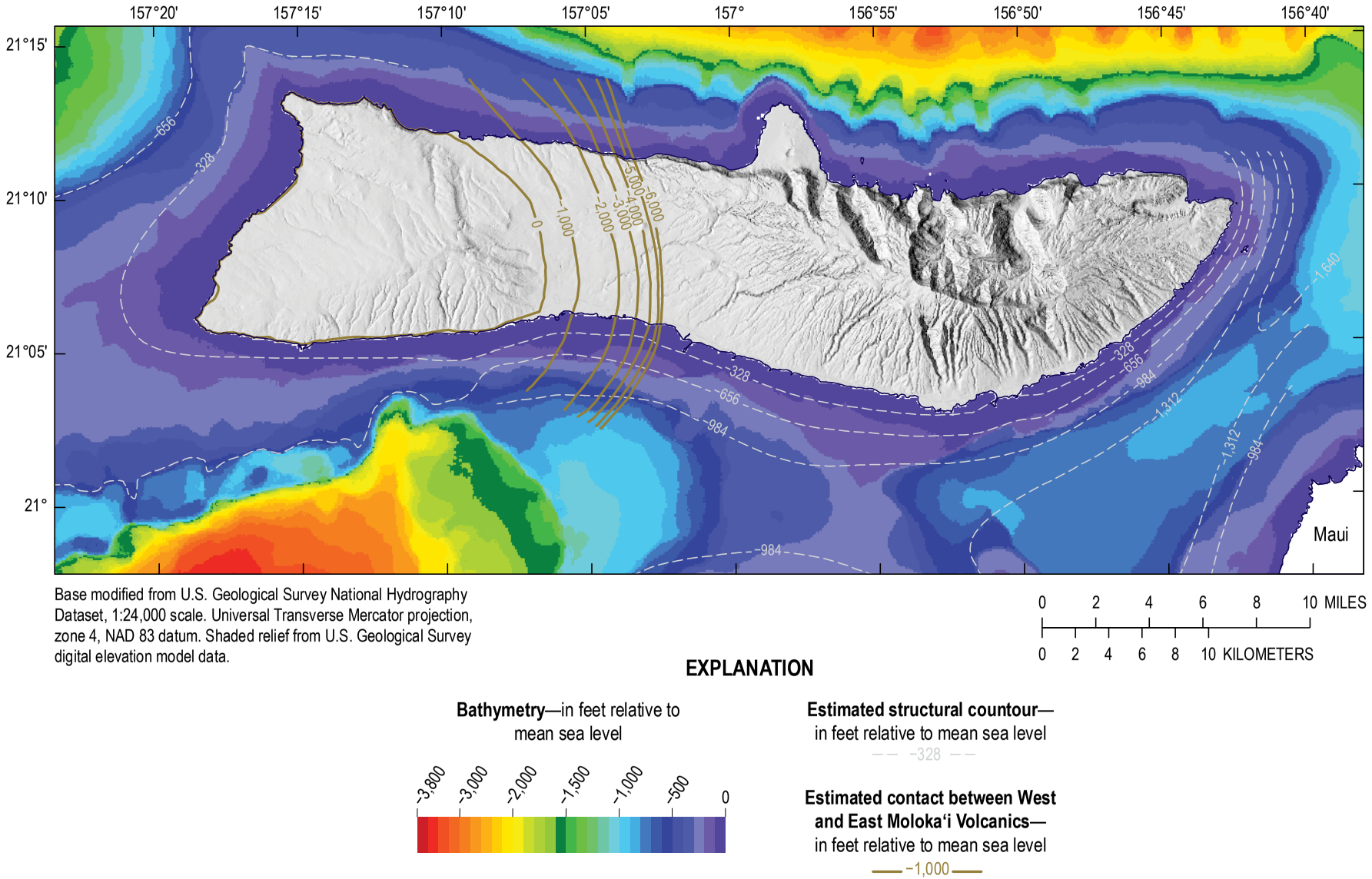

Figure 5. Map of Moloka'i, Hawai'i showing generalized bathymetry and estimated structural contours representing the base of offshore sedimentary deposits.

bottom and estimated base of sedimentary deposits. Off the northeastern coast, large submarine landslides have modified the original shape of the East Molokaʻi volcano, which makes estimation of the sediment thickness off the northeastern coast highly uncertain using the above method.

Hydraulic Conductivity of the Rocks

Hydraulic conductivity and permeability are quantitative measures of the capacity of a rock to transmit water. The term "permeability" is also commonly used to indicate the ease of fluid movement through a porous rock in a qualitative sense (see Domenico and Schwartz, 1990). The permeability of volcanic rocks varies with a number of factors, including the presence of clinker zones, voids, fractures, and lava tubes, extent of weathering, and the mode of emplacement.

Lava Flows

In a layered sequence of subaerial, shield-stage lava flows of a Hawaiian volcano, in which dike intrusions are absent, the overall permeability generally is high (Stearns and Macdonald, 1947). The main features of lava flows contributing to the high permeability are (1) clinker zones associated with ʻaʻā flows, (2) voids along the contacts between flows, (3) cooling joints normal to flow surfaces, and (4) lava tubes associated with pāhoehoe flows. On the basis of a numerical-model analysis, Oki (1997) estimated the horizontal hydraulic conductivity of the dike-free, shield-stage lava flows of Molokaʻi at 1,000 feet per day (ft/d).

Dikes

Although most dikes are less than 10 ft thick, they are hydrologically important because of their low permeability and can extend vertically and laterally for thousands of feet. Within a dike complex, dikes intersect at various angles and compartmentalize the more permeable intruded rock, resulting in impoundment of groundwater to high altitudes. Because dikes lower overall rock porosity and permeability, the average hydraulic conductivity of a dike complex decreases as the number of dike intrusions increases. Although the geometry and local-scale hydrologic effects of the unexposed dikes that fed the scattered vents of East Molokaʻi volcano near Kualapuʻu are unknown, these dikes intrude the aquifer and probably lower the overall permeability of the aquifer.

On the basis of a numerical-model analysis, Oki (1997) estimated the overall hydraulic conductivity of the dike complexes of West and East Molokaʻi volcanoes at 2 and 0.02 ft/d, respectively, and the bulk horizontal hydraulic conductivity of the marginal dike zone near Kualapuʻu at 100 ft/d. The marginal dike zone of East Molokaʻi volcano is assumed to occur in the area of vent features in the central part of the island (see Oki, 1997).

Weathering

Weathering generally reduces the permeability of volcanic rocks. The zone of weathered West Molokaʻi Volcanics and soil beneath the East Molokaʻi Volcanics likely impedes groundwater flow between East and West Molokaʻi volcanoes. In this report, this weathered zone separating the West Molokaʻi Volcanics from the overlying East Molokaʻi Volcanics is referred to as the West Molokaʻi confining unit. No data are available to determine whether this unit is truly an effective barrier to groundwater flow; however, Oki (1997) estimated the hydraulic conductivity of the West Molokaʻi confining unit (1 ft/d) on the basis of information from weathered volcanic rocks and a similar geohydrologic barrier on Oʻahu (Oki, 1998).

Coastal Deposits

Coastal deposits and underlying weathered volcanic rocks impede the seaward discharge of freshwater near the southern part of the island. The permeability of the interbedded coastal deposits may vary widely, from low-permeability compacted alluvium to cavernous limestone deposits. Oki (1997) estimated the overall vertical hydraulic conductivity of the coastal deposits in the southern part of the island at 0.5 to 5 ft/d.

Regional Groundwater-Flow System

Precipitation (rainfall and fog interception) is the source of all freshwater on Molokaʻi. The precipitation either (1) runs off, (2) evaporates or is transpired by vegetation, (3) recharges the groundwater system, or (4) is stored in the soil and underlying unsaturated rocks. Groundwater levels are highest in the mountainous interior of the island, particularly in the northeast, and lowest near the coast. Thus, groundwater flows from the mountainous interior areas to coastal discharge areas. Groundwater originating from the eastern part of the island also flows toward the central Hoʻolehua plain, where it then flows to either the northern or southern coast.

Groundwater that is not withdrawn from wells and tunnels discharges naturally from the aquifer to onshore springs and seeps in deeply incised valleys and to subaerial and submarine coastal springs and seeps. In the northeastern part of the island, springs form where erosion has cut through dike compartments and lowered the land surface such that the water table intersects the land surface. Groundwater discharge at these springs contributes to the base flow of streams.

Recharge

Groundwater is recharged by direct infiltration of rainfall over much of the island. Over West Molokaʻi volcano and the Hoʻolehua plain; however, groundwater-recharge rates are low because of low rainfall and high evaporation rates. The area of

greatest recharge is near the topographic peak of East Moloka‘i volcano, where rainfall is greatest. Recharge from rainfall may be supplemented locally by other sources of water, including cloud-water interception by vegetation in high-altitude areas, irrigation water, leakage from surface reservoirs and water-transmission pipes, or discharge of wastewater.

Groundwater recharge of Moloka‘i was estimated for this study using a daily water budget (appendix 1), which generally is expected to provide more accurate recharge estimates relative to annual and monthly water budgets. Details of the water-budget computation and maps showing land cover and the distribution of recharge over the island are provided in appendix 1. For 1978–2007 rainfall and 2010 land-cover conditions, island-wide recharge estimated for this study was about 227 Mgal/d. During the seven decadal periods from 1940–2012 (the last decadal period 2000–12 covered 13 years), recharge estimated for this study ranged from about 189 to 278 Mgal/d.

Discharge to Streams

Streams on Moloka‘i have steeper gradients in the mountainous, high-rainfall areas and flatter gradients near the coast. Streams in the windward, northeastern valleys are perennial through most of their lengths because they receive groundwater discharge from the dike-impounded groundwater body. In contrast, no perennial streams exist in the western part of the island or the central Ho‘olehua plain. Most of the streams that drain to the southern coast of East Moloka‘i volcano are perennial only in their upper reaches where rainfall is persistent or where water drains from marshes or springs. These streams generally are perennial only where they flow over lavas of the upper member of the East Moloka‘i Volcanics. Where streams flow over more permeable lavas of the lower member, surface water may be lost to infiltration (Stearns and Macdonald, 1947, p. 47).

Groundwater Levels

Measured water levels are available primarily in wells along the southern coast and in the central Ho‘olehua plain. In the vicinity of Kualapu‘u, Hawai‘i, water levels are about 8 to 10 ft above sea level; near the southern shore, water levels are 1 to 3 ft above sea level between Pālā‘au and Kawela, Hawai‘i and 2 to 5 ft above sea level between about Kamalō and Pūko‘o, Hawai‘i (fig. 6). Within the dike-intruded areas of east Moloka‘i, water levels may be tens to hundreds of feet above sea level. At the northern margin of the dike complex, near Kalaupapa Peninsula, the water level in well 1058–01 (fig. 7) was reported to be 9 ft above sea level, which represents an approximate upper limit of the water-table altitude in the Kalaupapa Volcanics. Results from an electrical-resistivity survey indicated that the freshwater lens in the Kalaupapa Volcanics is thin, probably less than a few tens of feet thick (Kauahikaua, 1983; Takasaki, 1986).

In the West Moloka‘i Volcanics, Stearns and Macdonald (1947, p. 61) reported the water level in well 1011–01 to be 5.6 ft above sea level in 1946. MacCarthy (1941) used electrical-resistivity measurements to determine the depth to saltwater, then applied the Ghyben-Herzberg relation to estimate the altitude of the water table in the western part of the island (fig. 6). For hydrostatic conditions and specific-gravity values of 1.000 and 1.025 for freshwater and saltwater, respectively, the Ghyben-Herzberg relation can be used to estimate the thickness of freshwater floating on saltwater and predicts that every foot of freshwater above sea level must be balanced by 40 ft of freshwater below sea level. MacCarthy estimated that the water-table altitude in the western part of the island ranges from about 1 to 14 ft above sea level. The water-level estimates made from resistivity measurements are only approximate because use of the Ghyben-Herzberg relation to predict water levels from estimated depths to saltwater (1) ignores the freshwater-saltwater transition zone and (2) does not account for dynamic conditions in the aquifer where vertical flow is present. Furthermore, unquantified errors are probably associated with the resistivity measurements and the geophysical models used to represent actual subsurface conditions.

Groundwater Occurrence

Groundwater on Moloka‘i is unconfined in inland areas. Along the southern coast, groundwater may be confined by sedimentary deposits that impede the seaward discharge of fresh groundwater. Similar coastal sedimentary deposits form confining units on other Hawaiian islands (see for example, Izuka and others, 2018). Fresh groundwater on Moloka‘i occurs in two main forms: (1) as a lens-shaped body of freshwater, called a freshwater lens, floating on denser, underlying saltwater within permeable dike-free volcanic rocks; and (2) as dike-impounded water that is underlain by saltwater (underlying saltwater is primarily observed in areas where water levels are low). The depth at which freshwater and saltwater exist in the dike-impounded groundwater system where water levels are hundreds of feet above sea level is not known. A measured seismic-velocity discontinuity near an altitude of about −6,000 ft in southwestern O‘ahu, Hawai‘i may coincide with a reduction in porosity and permeability of the volcanic rocks (Furumoto and others, 1970). Kauahikaua (1993) also indicated that a reduction in porosity on the island of Hawai‘i may occur near an altitude of −6,000 ft. Although the base of the aquifer on Moloka‘i is uncertain, it may extend to an altitude near −6,000 ft. Stearns and Macdonald (1947) also suggested that perched water (groundwater at higher levels than the main groundwater body and separated from the main groundwater body by an unsaturated zone) exists on Moloka‘i, although this form of groundwater is much less voluminous than groundwater in freshwater-lens and dike-impounded systems.

Freshwater-Lens System

Within the dike-free volcanic rocks of Moloka‘i, measured groundwater levels generally are less than 7 ft above mean sea level. The freshwater-lens systems within dike-free volcanic

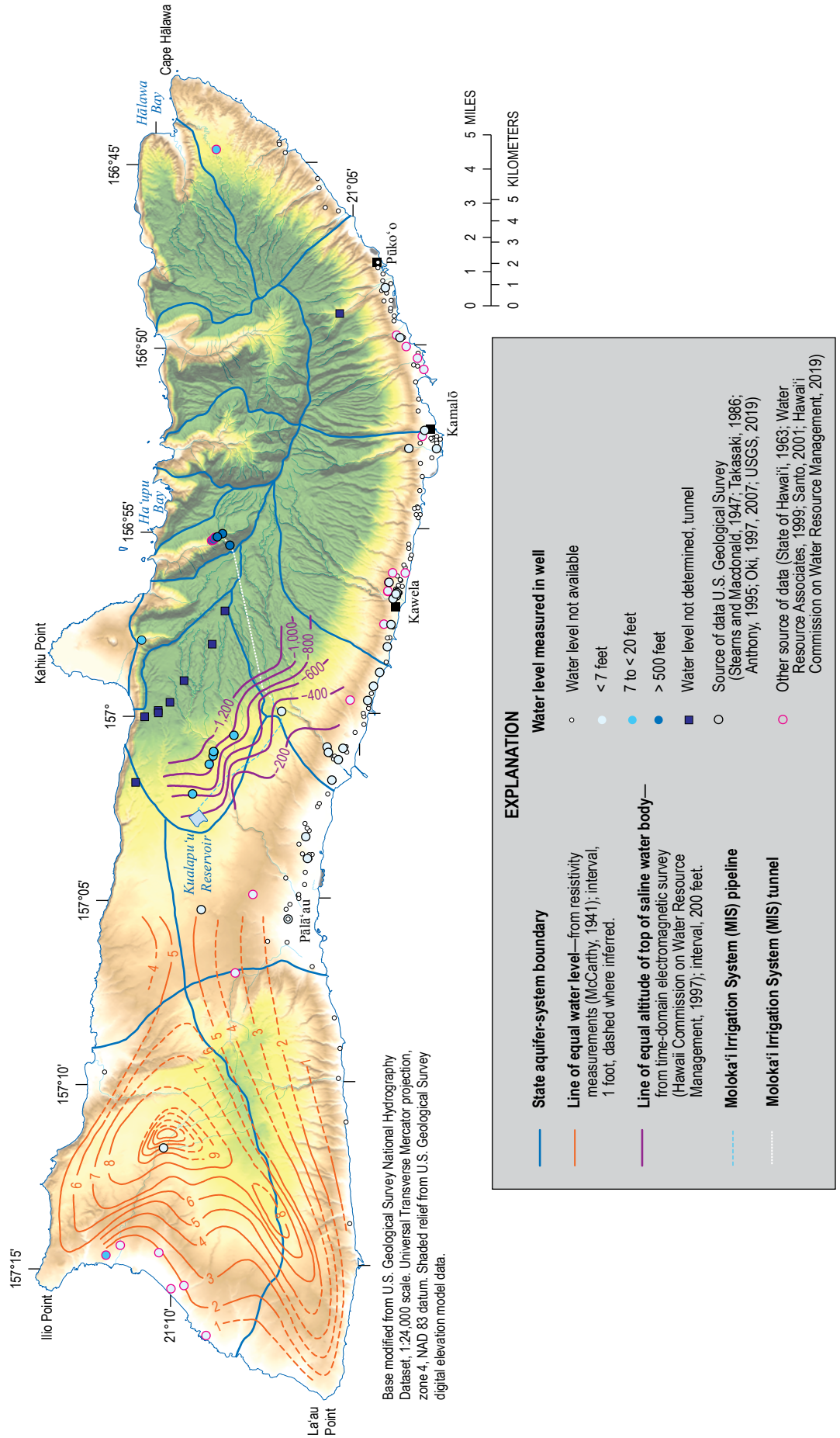

Figure 6. Map of Moloka'i, Hawai'i showing groundwater levels from wells and resistivity measurements.

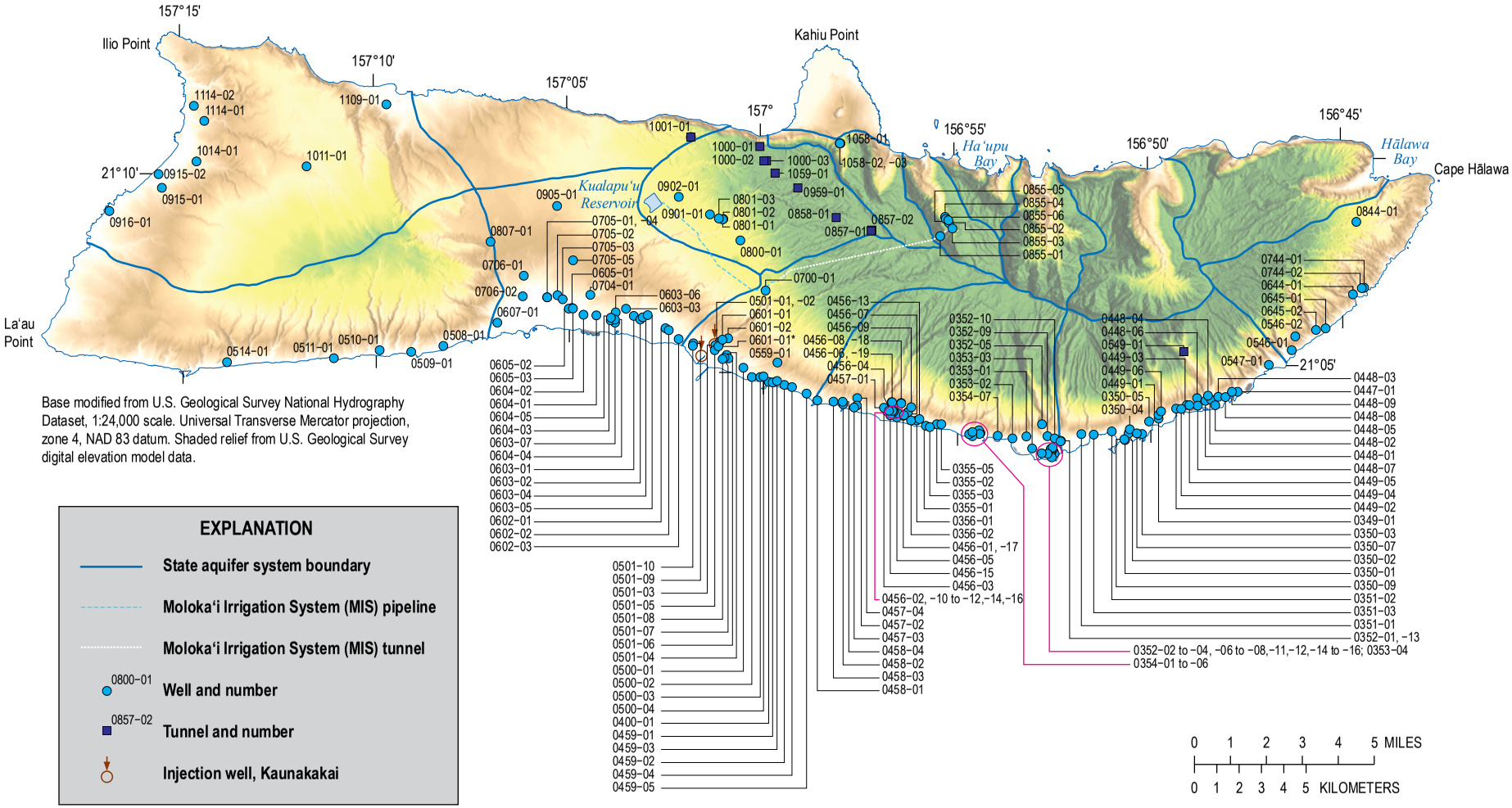

Figure 7. Map of Moloka'i, Hawai'i showing locations of wells and tunnels. Well 0601–01* is a production well recognized by the Hawai'i Commission on Water Resource Management as well "0601–001." Well 0601–01 is a monitoring well from which the U.S. Geological Survey has been collecting water-level data since the 1950s.

rocks consist of a lens-shaped body of freshwater overlying a zone of brackish water (transition zone), which in turn overlies saltwater originating from the ocean. Fresh groundwater is derived mainly from recharge of rainfall and also from recharge associated with irrigation water, leakage from surface reservoirs and water-transmission pipes, or discharge of wastewater. The zone of brackish water is formed by the mixing of seaward flowing freshwater with underlying saltwater. A saltwater-circulation system exists beneath the freshwater lens. Saltwater enters the aquifer from the ocean and flows landward. The saltwater then rises and becomes entrained with the seaward flowing freshwater, forming the brackish-water transition zone.

Dike-Impounded Groundwater System

Within the dike complex of East Molokaʻi volcano, fresh groundwater is impounded to high levels in the volcanic rocks between low-permeability dikes. In the valleys of the northeastern part of the island, the presence of springs indicates that groundwater in the dike complex is probably impounded to altitudes higher than 2,000 ft above sea level (Stearns and Macdonald, 1947, p. 75). Because of low recharge rates in the western part of the island, water levels in the dike complex of West Molokaʻi volcano are probably less than about 15 ft above sea level (fig. 6; MacCarthy, 1941). The abundance of dikes in a rift zone increases with depth, reducing the overall permeability of the dike complex with depth. No data exist that indicate the depth to which rocks are saturated with freshwater in the dike complex where water levels are high. In the marginal dike zone, where dike intrusions are few and water levels are lower than those in the dike complex, freshwater floats on saltwater.

Freshwater Thickness

Salinity profiles from deep open boreholes (deep monitor wells) commonly are used in Hawaiʻi to estimate the thicknesses of the freshwater lens and freshwater-saltwater transition zone. The USGS drilled deep monitor well 0800–01 from a ground-surface altitude of about 982 ft to an altitude of about −603 ft in the Kualapuʻu area (fig. 7) (Oki and Bauer, 2001), and have collected salinity profiles from this well since 2001. Although the Kualapuʻu deep monitor well is likely located in an area where unexposed dikes exist, salinity profiles collected from this well indicate the presence of a zone of freshwater underlain by a brackish-water transition zone and deeper saltwater. Measured salinity profiles indicate a freshwater zone, about 260 to 280 ft thick, defined by a fluid specific conductance less than 1,000 microsiemens per centimeter (µS/cm). The thickness of this freshwater zone may vary over time because of changes in recharge or withdrawal rates. The upper part of the freshwater-saltwater transition zone, as indicated by fluid specific conductance between 1,000 and 23,000 µS/cm, generally is about 150 ft thick (fig. 8). The highest fluid specific conductance measured in the well is about 46,000 µS/cm, which is assumed to represent the specific conductance of saltwater in the area.

Since 2001, measured water levels in well 0800–01 have ranged from about 8 to 10 ft above mean sea level. Using the Ghyben-Herzberg relation, the bottom of the freshwater is expected to be near an altitude of −320 to −400 ft. The depth in the transition zone where salinity is about half that of saltwater is commonly consistent with the base of freshwater predicted by the Ghyben-Herzberg relation in deep monitor wells in Hawaiʻi. However, for well 0800–01, the measured depth in the transition zone where salinity is about half that of saltwater is deeper than the base of the freshwater predicted by the Ghyben-Herzberg relation.

Salinity profiles from deep open boreholes, such as well 0800–01 (fig. 8), may be affected by flow in the borehole (Paillet and others, 2002; Rotzoll, 2012) caused by both natural and withdrawal-induced vertical-head differences in the aquifer. In areas where the head (the height above a specified datum at which the water rises in a piezometer that is open at a particular depth) decreases with depth, downward borehole flow may occur, leading to an overestimate of the aquifer freshwater thickness based on the recorded salinity profile.

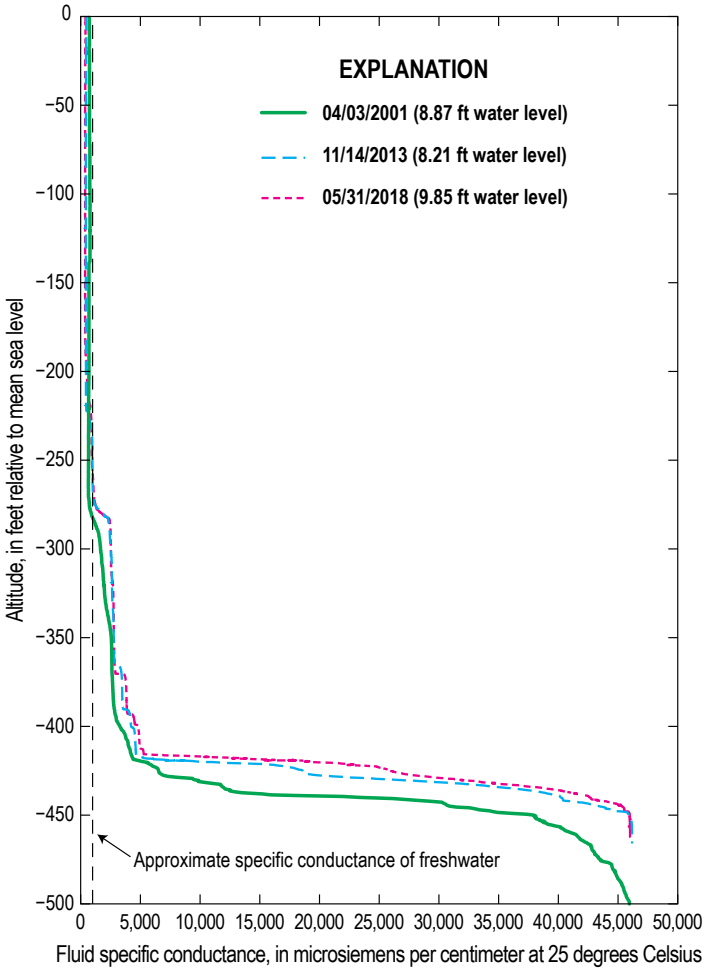

Figure 8. Line graph showing selected fluid specific-conductance profiles from the Kualapuʻu deep monitor well 0800-01, Molokaʻi, Hawaiʻi.

The head may increase with depth in the aquifer near partially penetrating pumped wells or coastal discharge areas, and an increase in head in the aquifer with depth may lead to upward flow within an open borehole. Upward borehole flow may cause saltwater to flow upward in the borehole, leading to an underestimate of the aquifer freshwater thickness based on the recorded salinity profile.

Chloride Concentration of Pumped Water

Chloride concentration is commonly used as an indicator of salinity, which may increase as a result of saltwater intrusion into a fresh groundwater body. The U.S. Environmental Protection Agency (EPA) secondary standard for chloride concentration in drinking water is 250 milligrams per liter (mg/L). Water with a chloride concentration above 250 mg/L may have a salty taste. The chloride concentration of water pumped from wells in the Kualapu‘u area generally has been less than 200 mg/L except in well 0902–01 (also known as Well 15) (fig. 9). During 1950–63, the chloride concentration of water pumped from well 0902–01 ranged from 252 to 430 mg/L (Oki, 1997). For comparison, the chloride concentration of rainfall is typically less than 10 to 20 mg/L (Swain, 1973), and that of ocean water is about 19,500 mg/L (Wentworth, 1939). Since 1980, chloride concentrations of water pumped from well 0901–01 (well 17) generally have been less than 100 mg/L, and chloride concentrations of water pumped from wells 0801–01 (Kauluwai 1), 0801–02 (Kauluwai 2), and 0801–03 (Kualapu‘u Mauka) generally have ranged from 50 to 200 mg/L (fig. 9).

Before the early 1980s, chloride concentrations of water pumped from the Kawela shaft (well 0457–01, fig. 7) were less than 100 mg/L (fig. 9). During 1980–2001, chloride concentrations of water pumped from Kawela shaft remained less than 200 mg/L, but during 2002–05, chloride concentrations commonly exceeded 200 mg/L and at times exceeded 300 mg/L. With reduced withdrawals from Kawela Shaft during 2008–2015, chloride concentrations of pumped water generally have been less than 100 mg/L.

Before 2002, chloride concentrations of water pumped from the ‘Ualapu‘e shaft (well 0449–01, fig. 7) generally were less than 70 mg/L (fig. 9); during 2003–06, however, chloride concentrations generally were more than 70 mg/L, reaching a maximum of 100 mg/L during 2004. During 2007–15, chloride concentrations of water pumped from the ‘Ualapu‘e shaft have remained less than 100 mg/L.

Groundwater Withdrawals

Most of the groundwater withdrawn on Moloka‘i is from the Kualapu‘u area, the southeastern coastal area, and the dike complex in the northeastern part of the island. Annual withdrawal from wells (excluding discharge from tunnels) on Moloka‘i has increased since the 1940s and peaked in 2002 and 2003 when withdrawal exceeded 5.7 Mgal/d. From 2004 to 2017, annual withdrawal was between about 3 and 5 Mgal/d (fig. 10).

Five production wells (0801–01, 0801–02, 0801–03, 0901–01, and 0902–01, fig. 7) have been drilled in the Kualapu‘u aquifer system for either irrigation or domestic use. Wells 0901–01 and 0902–01, drilled in 1950 and 1946, respectively, originally were used to irrigate pineapple fields in the Ho‘olehua plain area. Well 0902–01 was abandoned in 1964 when surface water from the Moloka‘i Irrigation System (MIS) tunnel (fig. 1) became available. Since 1976, water from well 0901–01 has been used for domestic and irrigation purposes, mainly in the western part of the island. Kualapu‘u wells 0801–01 (Kauluwai 1) and 0801–02 (Kauluwai 2) (fig. 7) were completed in 1949 and 1979, respectively, and well 0801–03 (Kualapu‘u Mauka) was drilled in 1987. Annual withdrawal from the five production wells in the Kualapu‘u aquifer system increased from the 1940s to the 1990s, reaching a peak of about 2.7 Mgal/d during 1994 (fig. 10). From 1995 to 2008, annual withdrawal from the five production wells in the Kualapu‘u aquifer system ranged from 1.8 to 2.6 Mgal/d, and from 2009 to 2017, annual withdrawal was less than about 1.9 Mgal/d.

Near the southern coast, groundwater withdrawals for domestic or public-supply uses are primarily from the Kawela and ‘Ualapu‘e aquifer systems. In the Kawela aquifer system, annual withdrawals prior to 1992 and after 2002 were less than 0.5 Mgal/d. During 1992–2002, annual withdrawals from the Kawela aquifer system exceeded 0.5 Mgal/d, peaking in 1998 at about 0.75 Mgal/d. In the ‘Ualapu‘e aquifer system, annual withdrawals have remained below 0.5 Mgal/d, although withdrawals generally have increased over time (fig. 10). Total unreported withdrawals from drilled wells and numerous shallow dug wells along the southern coast are probably small.

Six production wells, three drilled in 1961 (0855–01, 0855–02, 0855–03) and three drilled in 1988 (0855–04, 0855–05, 0855–06) (fig. 7), withdraw water from the dike complex in the northeastern part of the island. Information on withdrawal from the six wells generally is incomplete from 1961 to 1987. During 1988–2015, reported total withdrawal from these wells averaged about 1 Mgal/d. Water from these wells enters the MIS, which includes the MIS tunnel that captures (gains) additional groundwater (Hirashima, 1963). The direct capture of groundwater from the MIS tunnel plus the discharge from well 0855–01, which was drilled in the MIS tunnel, can be estimated from the difference between discharge measured at USGS gaging station 16405300 (downstream) and discharge at gaging station 16405100 (upstream). Water flowing past the downstream gaging station 16405300 includes some or all of the direct capture of groundwater from the MIS tunnel, the discharge from well 0855–01, and the water flowing past the upstream gaging station 16405100. During 1966–2002, the combined gain in groundwater (from the tunnel and well 0855–01) between the upstream and downstream gaging stations averaged about 1.7 Mgal/d. The combined discharge of the MIS tunnel and well 0855–01 was determined from existing records or estimated as an average during a selected period when data were unavailable.

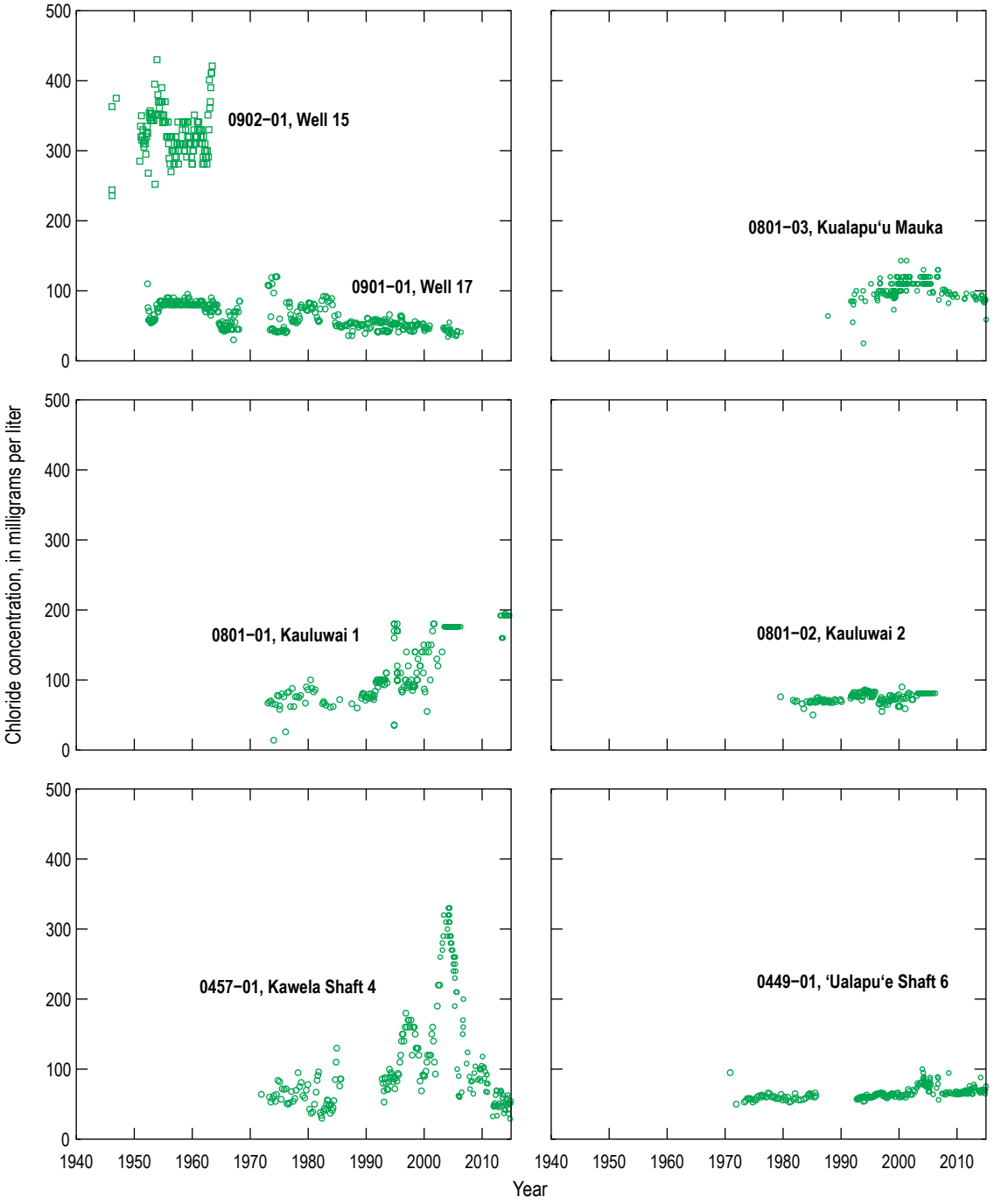

Figure 9. Multiple time-series graphs showing chloride concentration of pumped water from selected wells, Molokaʻi, Hawaiʻi. Data are from U.S. Geological Survey National Water Information System database, Anthony (1995), and unpublished data from Maui Department of Water Supply and Hawaiʻi Commission on Water Resource Management.

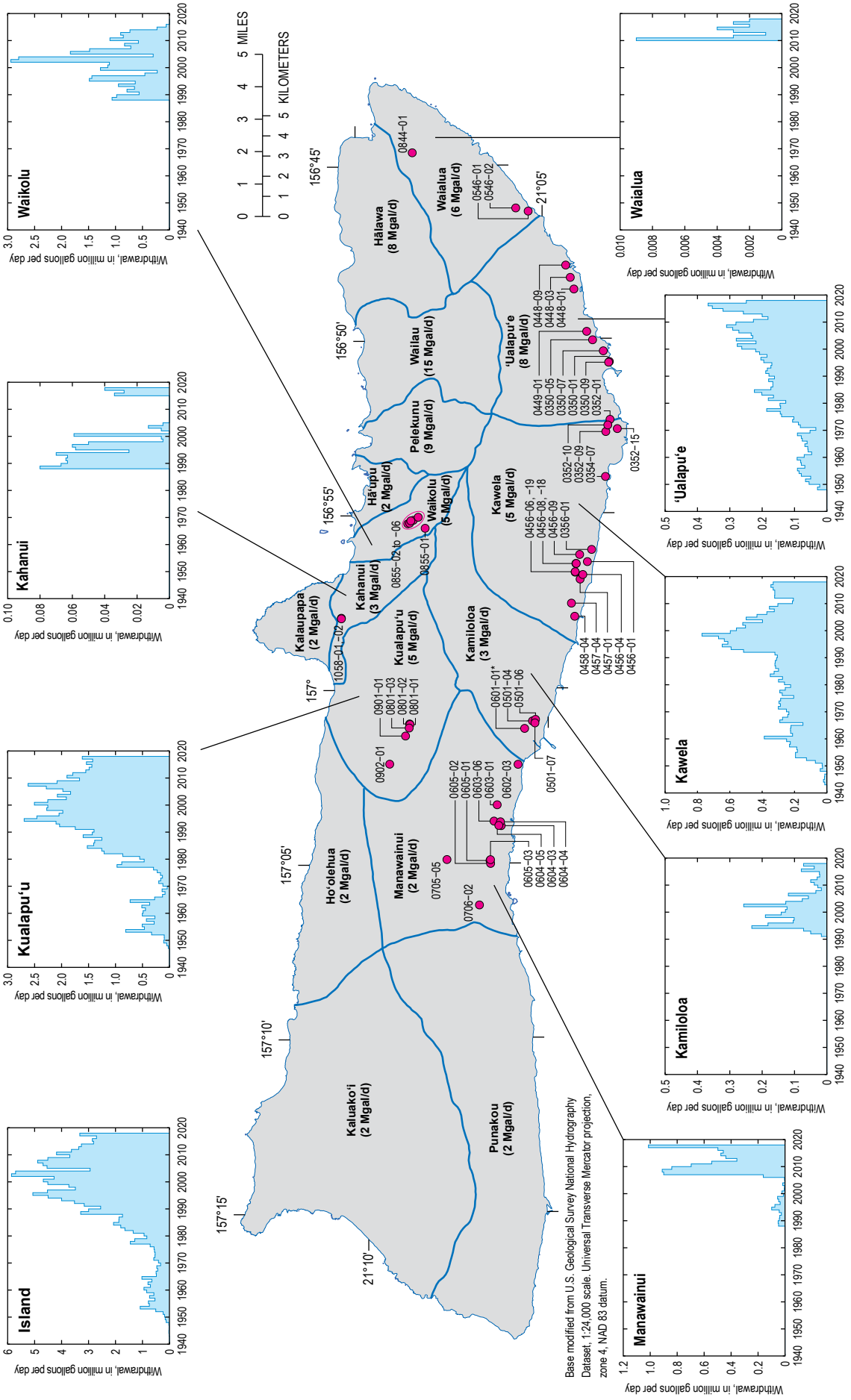

Figure 10. Map of Moloka'i, Hawai'i showing annual reported pumpage by aquifer system.

Island-Wide Two-Dimensional Numerical Groundwater-Flow Model

An island-wide, two-dimensional, sharp-interface numerical groundwater-flow model was developed to estimate groundwater inflows to the main area of interest in central Molokaʻi. These inflow estimates are needed for the three-dimensional flow and salinity-transport model of central Molokaʻi. The island-wide model was developed using the computer code SHARP that simulates groundwater flow in both the freshwater and saltwater zones (Essaid, 1990). However, SHARP does not represent the mixing of freshwater and saltwater and the formation of a brackish-water transition zone. Rather, SHARP assumes that freshwater and saltwater are separated by a sharp interface with no mixing of the two fluids. This assumption generalizes the groundwater-flow system but maintains an accurate accounting of total freshwater flow.

The island-wide groundwater-flow model was developed using temporally varying recharge and withdrawal conditions during 1940–2012. The model accounts for spatially varying hydraulic properties of the geologic materials, recharge, and discharge. The hydraulic properties of the rocks were estimated from available data and were modified by varying them in the model to obtain reasonable agreement between model-calculated and observed water levels and stream base flows. Model development also was guided by available geophysical surveys that estimated the depth to the transition zone between freshwater and saltwater (see for example, MacCarthy, 1941; State of Hawaiʻi, 1997).

Model Grid

The finite-difference model grid used in this study consists of 166 rows and 446 columns of square cells, each 492 ft on a side. The grid is oriented with its short side in a north-south direction. The geographic origin of the grid is on the southwest corner at long 157°20’07” W., lat 21°01’36” N. based on the North American Datum of 1983 (fig. 11). The grid covers the entire island of Molokaʻi and extends offshore at least a mile to include the entire zone where fresh groundwater is expected to discharge to the ocean.

Representation of the System

For modeling purposes, the island of Molokaʻi was divided into 23 horizontal-hydraulic-conductivity zones, some of which were assigned the same hydraulic properties in the model (fig. 11). Because the CWRM aquifer-system boundaries do not necessarily represent subsurface hydrogeologic features, the zones generally were not aligned with the aquifer-system boundaries. One zone each was used to represent the dike-free West Molokaʻi Volcanics, the dike-intruded West Molokaʻi Volcanics, the West Molokaʻi confining unit, the Kalaupapa Volcanics, a presumed west-trending minor rift zone of East Molokaʻi volcano, and a presumed south-trending minor rift zone of East Molokaʻi volcano; five zones were used to represent the dike complex and main rift zones of East Molokaʻi volcano in the northeastern part of the island, including a small zone near Waikolu, Hawaiʻi that primarily served to allow simulation of appropriate water levels near the MIS tunnel; eight zones were used to represent the marginal dike zone of East Molokaʻi volcano in the central part of the island, including four zones representing groundwater barriers (dikes) and four zones representing marginal dike-zone compartments between groundwater barriers; and four zones—one of which represents a narrow zone between adjacent, larger hydraulic-conductivity zones, and was assigned the average hydraulic-conductivity value of the adjacent zones—were used to represent the mostly dike-free East Molokaʻi Volcanics. The West Molokaʻi confining-unit zone represents the zone, formed by weathered volcanic rocks and soil, separating West and East Molokaʻi Volcanics. The West Molokaʻi confining unit is represented in the two-dimensional model as a barrier to horizontal flow with a zone of reduced hydraulic conductivity. The dike complex of East Molokaʻi volcano in the northeastern part of the island was divided into five zones to enable representation of water levels needed to simulate groundwater discharge to streams and the MIS tunnel. The marginal dike zone of East Molokaʻi volcano in the central part of the island was divided into eight zones to enable representation of water levels and to create a compartmentalized groundwater system consistent with the presence of dikes. The mostly dike-free East Molokaʻi Volcanics was divided into four zones to enable representation of the spatial distribution of water levels.

Boundary Conditions

SHARP supports three types of boundary conditions: (1) specified head, (2) specified flow, including no flow, and (3) head-dependent discharge. Specified-head boundary conditions were not used for this study. The perimeter rows and columns of the grid are no-flow boundaries. The base of the model was a no-flow boundary and assigned an altitude of −5,906 ft (−1,800 m), relative to mean sea level, to coincide with an assumed aquifer bottom near an altitude of −6,000 ft (Furumoto and others, 1970; Kauahikaua, 1993).

Freshwater discharge near coastal areas and to streams in northeastern Molokaʻi valleys was modeled using a head-dependent discharge boundary condition, where the aquifer is presumed to be overlain by sedimentary deposits that form a confining unit that impedes discharge from the aquifer. The head-dependent discharge boundary condition requires specification of (1) the head overlying the confining unit and (2) the confining-unit leakance. The confining-unit leakance is a lumped parameter defined as the quotient of the confining-unit vertical hydraulic conductivity and the confining-unit thickness.

For coastal-discharge boundaries, the head above the confining unit at offshore boundaries was set equal to the freshwater equivalent head of the saltwater column overlying the

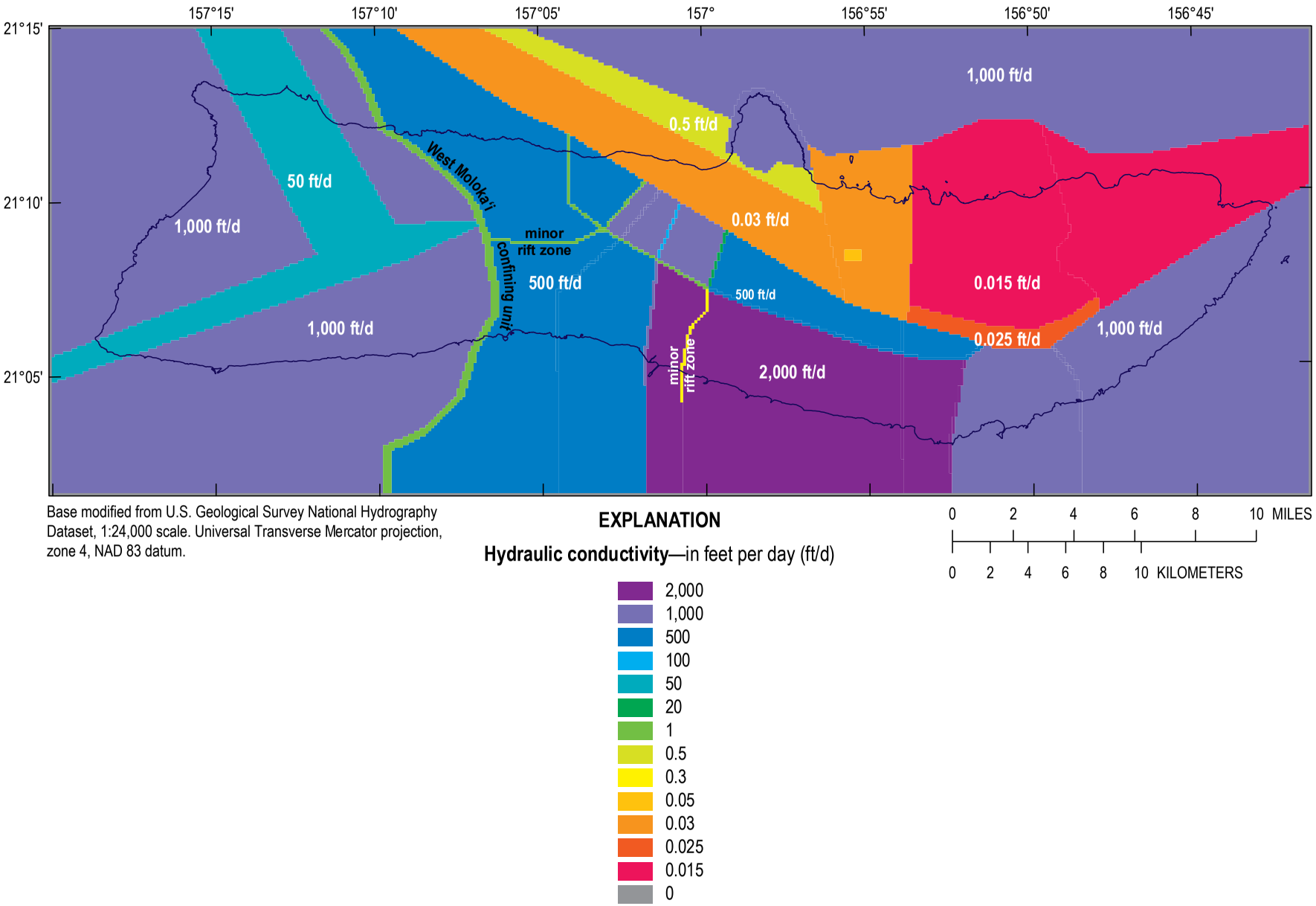

Figure 11. Map of Moloka'i, Hawai'i showing horizontal-hydraulic-conductivity zones used in the island-wide, sharp-interface groundwater model.

ocean floor. In some coastal areas of southern Molokaʻi, onshore sediments may form a confining unit and for these areas, the head above the confining unit was assigned a value of 0 ft. For streams in northeastern Molokaʻi, the head above the confining unit was set equal to the stream-bed altitude.

For coastal discharge cells of southern Molokaʻi, the confining-unit thickness was assigned values equal to the estimated thickness of sediments overlying the aquifer. The thickness of sediments was estimated in southern Molokaʻi by projecting the slope of the shield-stage volcanic rocks offshore and determining the altitude difference between the existing bathymetry (National Oceanic and Atmospheric Administration, 2010) and projected surface of the shield-building volcanic rocks (fig. 5). Estimated thickness of sediments ranged from several feet to over 1,000 ft near the eastern coast of the island. No attempt was made to estimate separate values for the confining-unit vertical hydraulic conductivity and thickness of northern Molokaʻi coastal discharge cells, because of a lack of information to define these values separately; instead, the lumped parameter leakance was estimated by trial and error. For stream cells in northeastern Molokaʻi, a unit thickness (1 ft) was assumed for the estimation of leakance values.

Recharge

For this study, a daily water budget was used to estimate average groundwater recharge during the six decadal periods from 1940 to 1999 (1940–49, 1950–59, 1960–69, 1970–79, 1980–89, 1990–99), and the 13-year period 2000–12 (appendix 1). Recharge is greatest near the mountainous parts of eastern Molokaʻi, exceeding 100 inches per year (in/yr), and least in western Molokaʻi and coastal areas of central and southern Molokaʻi. For areas receiving irrigation or where pineapple (a xerophytic plant) was cultivated, recharge may be slightly higher than in adjacent nonagricultural areas.

Recharge for each model cell was based on the area-weighted average recharge from the irregularly shaped water-budget-model subareas (appendix 1) within each model cell. Recharge used in the groundwater model may differ slightly from that estimated by the water budget because of discretization near the coast that causes some onshore areas to be assigned to offshore cells.

Withdrawals

Information on groundwater withdrawals was obtained from CWRM, the County of Maui Department of Water Supply (MDWS), and previously published studies (Oki, 1997, 2006). Island-wide groundwater withdrawals have generally been less than a few percent of island-wide recharge. Locally (within some aquifer systems), however, groundwater withdrawals are a larger percentage of recharge. In the Kualapuʻu aquifer system, for example, groundwater withdrawals during 2016–17 were about 12 percent of average recharge (based on 1978–2007 rainfall and 2010 land-cover conditions). For model cells containing multiple wells, the withdrawals from wells within the cell were summed.

Injection Wells

Recharge to the aquifer from two wastewater injection-well facilities near Kaunakakai, Hawaiʻi (fig. 7) averaged about 0.2 Mgal/d during 2004–12 using data provided by the County of Maui. However, this recharge was excluded from the island-wide model because the inclusion of the coastal injection-well recharge would not substantively affect the estimated groundwater inflows to the main area of interest in central Molokaʻi, which ultimately is the main output needed from the island-wide model. The injection wells were included in the three-dimensional model of central Molokaʻi (described below) capable of simulating variable salinity.

Groundwater Discharge to Streams (Base Flow)

Groundwater discharges to and sustains perennial base flows of streams in the valleys of northeastern Molokaʻi. As part of the water-budget computation, measured discharge at streamgaging stations was separated into runoff and base-flow components (appendix 1). Estimated base flows in northeastern Molokaʻi streams ranged from about 0.5 to more than 10 Mgal/d and were used to estimate aquifer hydraulic properties for the model.

Water Properties

In the model, the specific gravities of freshwater and saltwater were assigned values of 1.0 and 1.025, respectively. Hydraulic conductivity is dependent on fluid viscosity, which is a function of temperature and, to a lesser extent, pressure and salinity. Freshwater and saltwater dynamic viscosities at 20 °C are 2.09×10^{-5} pound force second per square foot ($lb \cdot s/ft^2$) (Freeze and Cherry, 1979) and 2.24×10^{-5} $lb \cdot s/ft^2$ (Weast and others, 1989), respectively. The specific-gravity and viscosity values were assumed to remain constant for all simulations with SHARP.

Estimation of Hydraulic Properties

Hydraulic conductivity and effective porosity values were estimated by trial and error. A steady-state simulation using average recharge during the 1940s and zero withdrawals was

used to generate initial conditions for the 1940–2012 transient simulation. A 1-day time step was used for the final steady-state and transient simulations. Freshwater and saltwater specific-storage values assigned in the model were 7.6×10^{-6} per foot (1/ft) and 7.8×10^{-6} (1/ft), respectively, and the effective porosity was assigned a value of 0.05.

The estimated hydraulic-conductivity values generally are consistent with previous estimates and with the conceptual model of higher values for the dike-free volcanic rocks and lower values for the dike-intruded areas. For the mostly dike-free volcanic rocks, estimated hydraulic-conductivity values were 500, 1,000 or 2,000 ft/d; for the marginal dike-zone compartments between groundwater barriers (zones with dikes), hydraulic-conductivity values were 500 or 1,000 ft/d; for the dike complex, hydraulic conductivity values were less than 1 ft/d for East Molokaʻi volcano and 50 ft/d for West Molokaʻi volcano; and for the zones representing groundwater barriers to flow (dikes or erosional surfaces), estimated hydraulic-conductivity values were between 0.3 and 100 ft/d (fig. 11). The hydraulic-conductivity values assigned for the mainly dike-free volcanic rocks on Molokaʻi are within the range of values previously estimated for Oʻahu and Maui (see for example, Izuka and others, 2018)

Discharge from head-dependent discharge cells is controlled by the thickness of the confining unit and the hydraulic conductivity of the confining unit. The ratio of confining-unit hydraulic conductivity to confining-unit thickness forms the lumped parameter leakance. Leakance values were estimated from (1) the individual values of confining-unit hydraulic conductivity and confining-unit thickness in southern Molokaʻi and (2) as a lumped parameter by assuming a unit thickness (1 ft) in northern Molokaʻi. Confining-unit vertical hydraulic conductivity values assigned in the model ranged from 0.01 ft/d for stream cells in northeastern Molokaʻi to 20 ft/d for the confining unit in the southeastern part of the island (fig. 12).

Simulation Results

The spatial distribution of simulated water levels is in general agreement with the conceptual model of high water levels in the dike complex of northeastern Molokaʻi and lower water levels in western and southern Molokaʻi (fig. 13). In areas with steep topography, the simulated water level may exceed the altitude of the top of the cell, which is attributed to (1) using an average land-surface altitude to define the top of the cell (in some areas of the model, a cell may cover a range of land-surface altitudes of several hundred feet), and (2) possibly not representing springs that may exist in areas of steep topography. Simulated transient water levels also are in reasonable agreement with observed water levels (fig. 14). In general, simulated transient water levels are within about a foot of available observed water levels.

The simulated average base flows of streams in northeastern Molokaʻi are in general agreement with the estimated concurrent base flows from streamgaging stations (fig. 15). On an annual basis, the model may not accurately represent the base flows, which is mainly attributed to the decadal representation of recharge in the model. That is, year-to-year variability in rainfall and recharge were not represented in the groundwater model because the timing of rainfall relative to recharge at the water table is poorly known. Instead, recharge variability was represented at the decadal scale, which represents a smoothing of the year-to-year variability in recharge.

The estimated boundary flows from the dike-complex area of northeastern Molokaʻi to central and southern Molokaʻi were determined for selected boundary zones of a three-dimensional numerical groundwater model (see next section) (fig. 16; table 1). The magnitude of the boundary flows reflects the distribution of groundwater flow but also is affected by the length of the boundary. Relative boundary inflows are greatest in the central zones (zones 5–7), where inflows range from about 2.5 to 3.3 Mgal/d per mile, and least in western zones (zones 1–3), where inflows range from about 0.03 to 0.2 Mgal/d per mile.

Table 1. Recharge input to the top and boundary-inflow zones of the three-dimensional model mesh, Molokaʻi, Hawaiʻi.

Period	Recharge for top of model, in million gallons per day	Recharge for indicated boundary inflow zone (see fig. 16), in million gallons per day									Total, in million gallons per day
		1	2	3	4	5	6	7	8	1–8	
1940–49	47.4	0.05	0.03	0.1	0.9	17.4	7.9	5.8	14.1	46.3	93.8
1950–59	55.4	0.05	0.05	0.1	1.0	17.2	8.0	6.0	14.2	46.6	102.0
1960–69	69.3	0.07	0.07	0.1	1.1	17.6	8.6	6.6	15.0	49.1	118.4
1970–79	43.7	0.08	0.06	0.1	1.1	17.0	8.5	6.4	14.5	47.8	91.5
1980–89	57.8	0.08	0.06	0.1	1.1	17.1	8.4	6.3	14.7	47.8	105.6
1990–99	50.6	0.07	0.06	0.1	1.1	17.4	8.6	6.6	15.0	49.0	99.5
2000–12	48.0	0.06	0.05	0.1	1.0	16.7	8.7	6.6	14.8	48.1	96.1
1978–2007	55.2	0.06	0.05	0.1	1.1	17.2	8.1	6.5	14.9	48.1	103.4

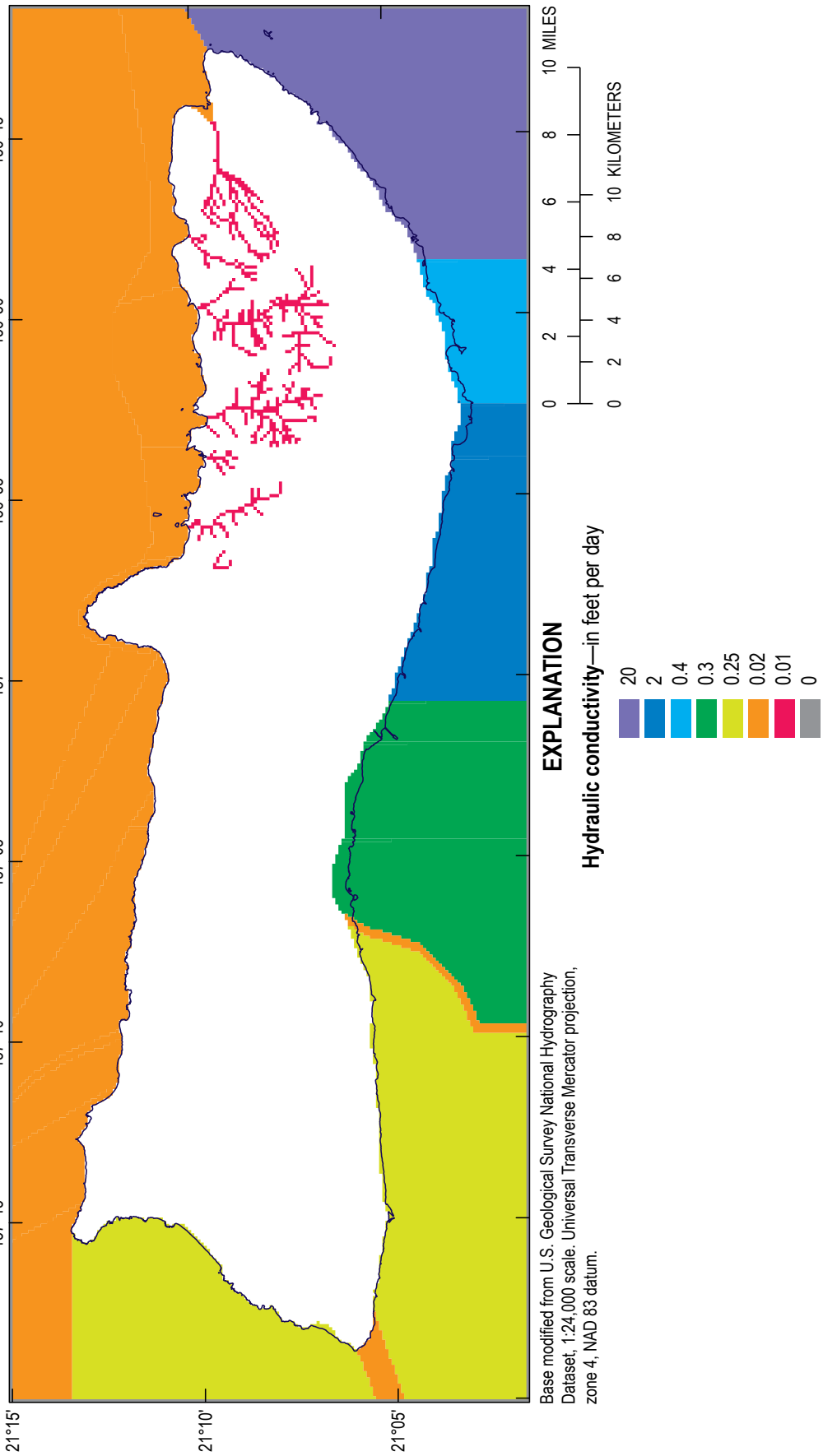

Figure 12. Map of Moloka‘i, Hawai‘i showing vertical-hydraulic-conductivity zones used in the island-wide, sharp-interface groundwater model.

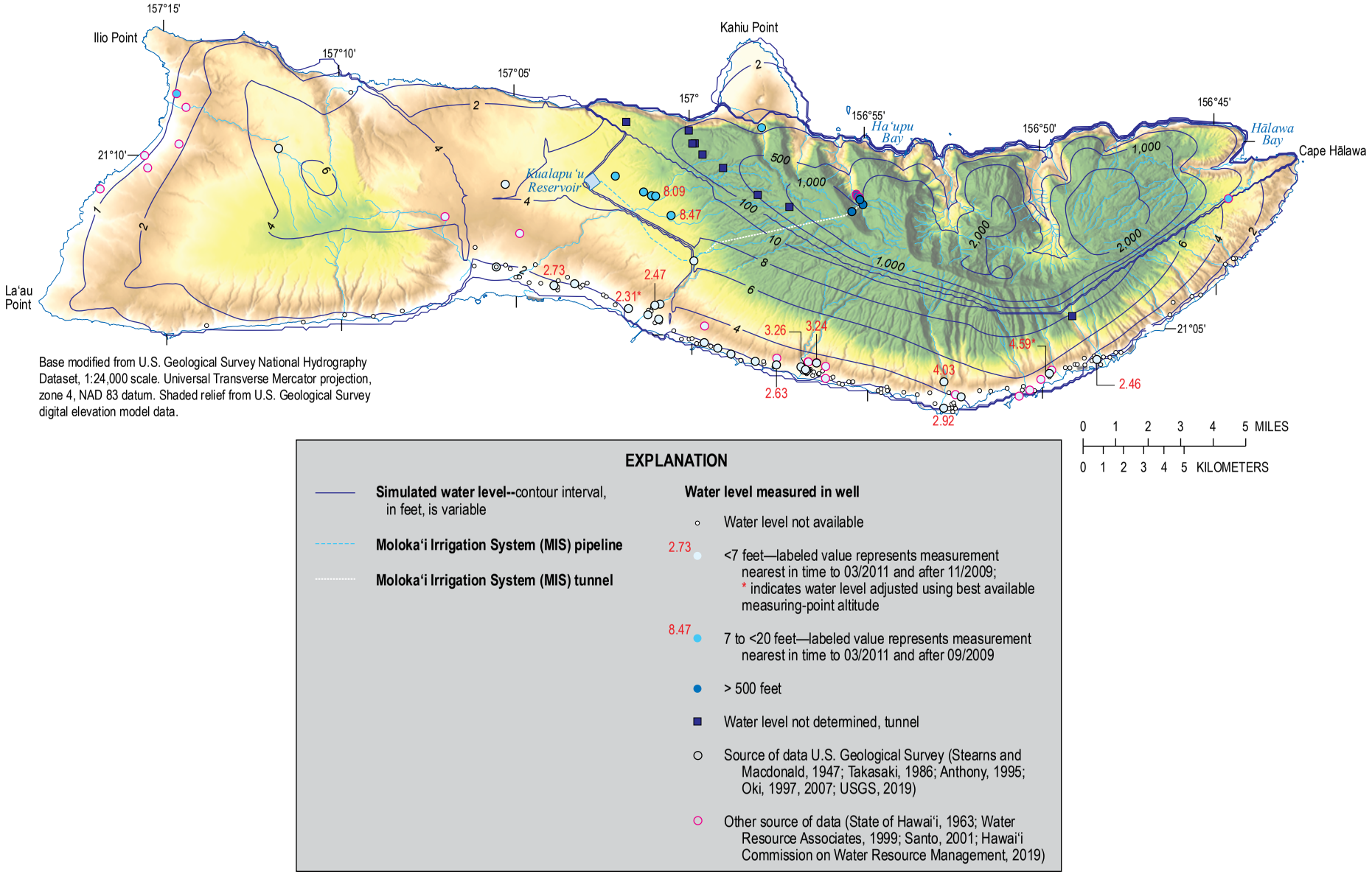

Figure 13. Map of Moloka'i, Hawai'i showing groundwater levels under 2011 conditions simulated with the two-dimensional, island-wide numerical groundwater model.

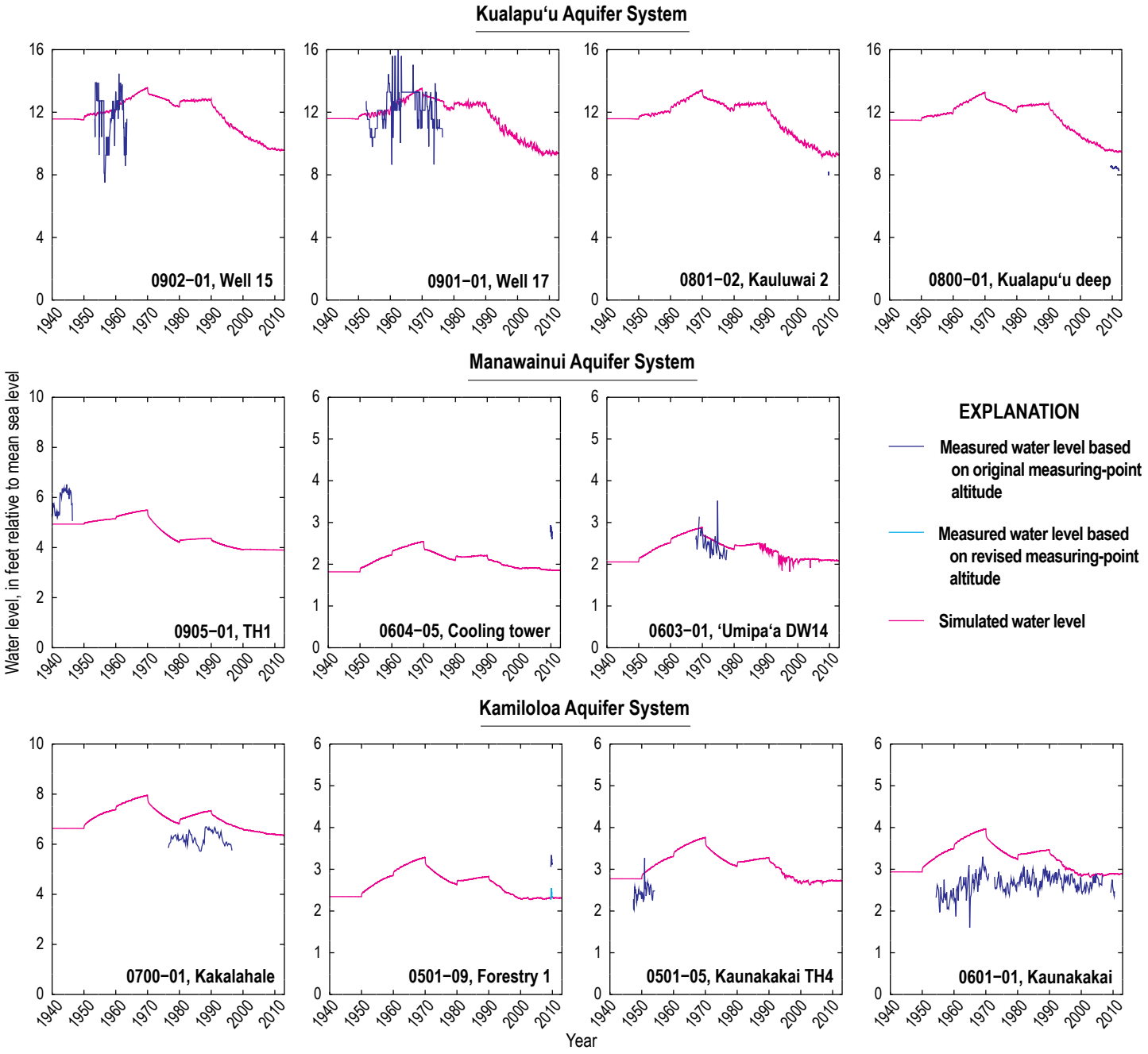

Figure 14. Multiple line graphs showing measured and simulated water levels at selected wells during 1940–2012, Moloka‘i, Hawai‘i. Explanation of water level based on revised measuring-point altitude is discussed on p. 33.

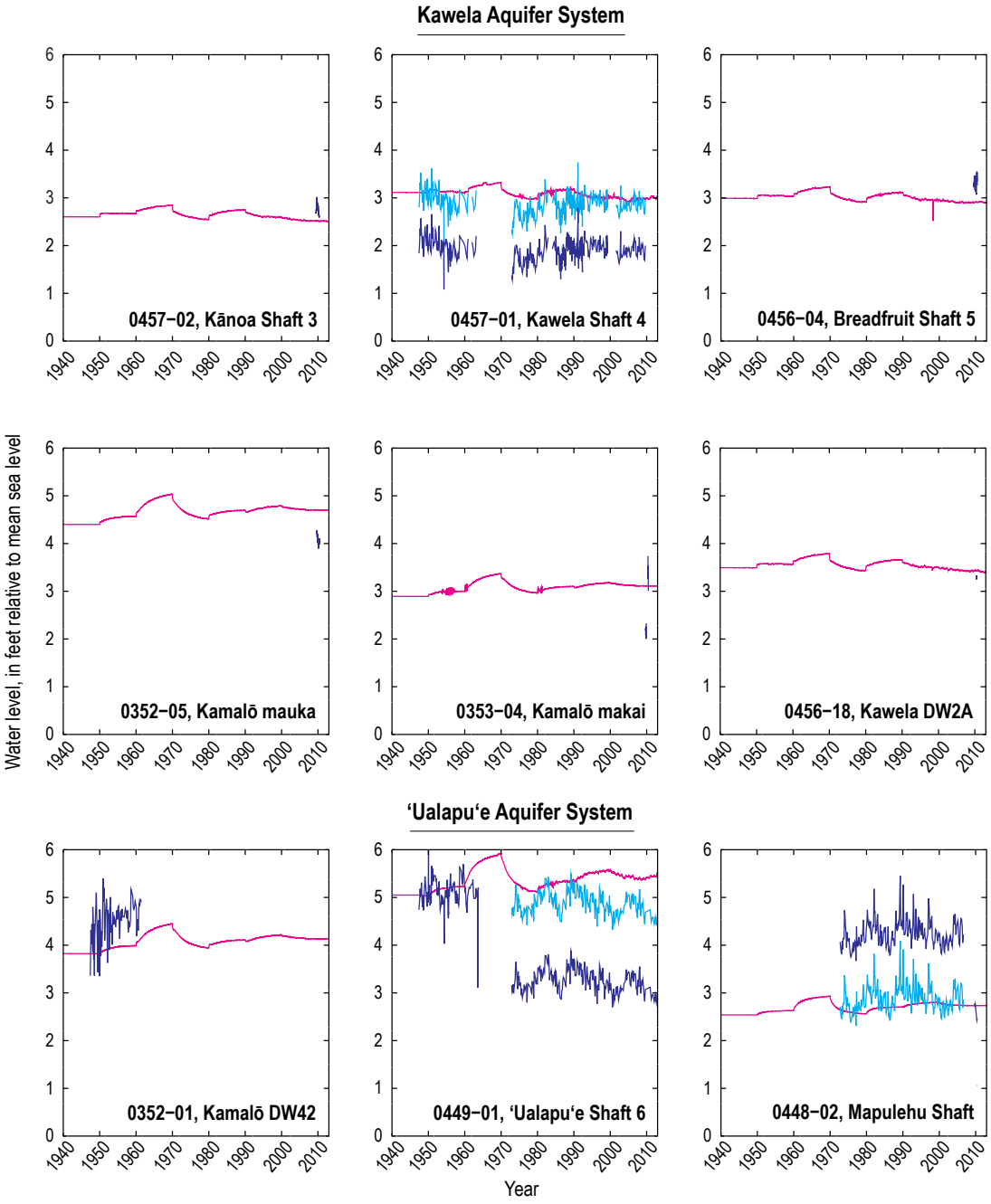

Figure 14.—Continued

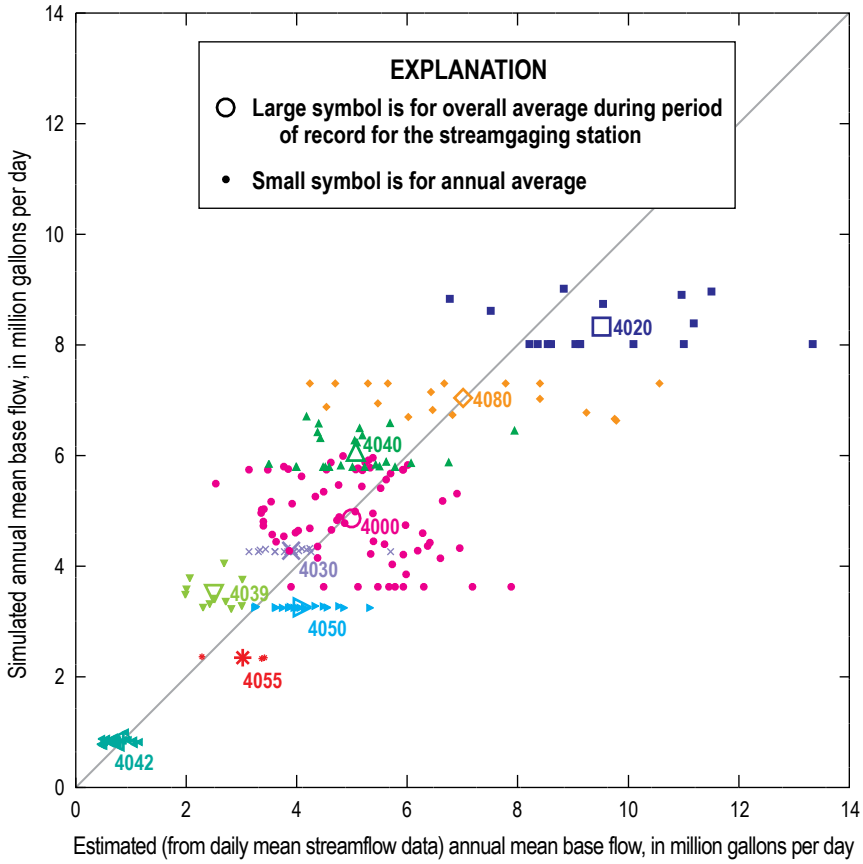

Figure 15. Scatterplot of estimated (from daily mean streamflow data) and simulated base flow during 1940–2012, Moloka‘i, Hawai‘i. Numbers represent the U.S. Geological Survey streamgaging station abbreviated number (full number is preceeded by “16” and ends in “00”). For each streamgaging station, the same color is used for the label and symbols.

Three-Dimensional Numerical Groundwater-Flow and Salinity Model

A three-dimensional numerical groundwater-flow and salinity-transport model was developed for part of the East Moloka‘i volcano in central and southern Moloka‘i using information from the two-dimensional island-wide groundwater-flow model. The three-dimensional model was developed using the saturated-unsaturated transport computer code (SUTRA; Voss and Provost, 2010), which simulates density-dependent groundwater-flow and salinity transport. For this study, SUTRA was used to represent the mixing of freshwater and saltwater and the formation of a brackish-water transition zone.

The three-dimensional groundwater-flow and salinity-transport model of central Moloka‘i was developed using temporally varying recharge and withdrawal conditions during 1940–2012. The model accounts for spatially varying hydraulic properties of the rocks, recharge, and discharge. The hydraulic properties of the rocks were estimated from available data and were modified by varying them in the model to obtain reasonable agreement between model-calculated and observed water levels and salinities of pumped water. Model development also was guided generally by available geophysical surveys that estimated the depth to the middle of the transition zone between freshwater and saltwater (see for example, MacCarthy, 1941; State of Hawai‘i, 1997).

Model Mesh

The finite-element model mesh used in this study consists of 520,821 nodes and 495,388 variably sized elements (fig. 16). In the vertical direction, the mesh has 64 elements (layers) where the top of the model is not truncated by the ocean or the bottom of the model is not truncated by West Moloka‘i Volcanics. The mesh has as few as 17 elements in the vertical direction near the eastern, offshore boundary where the ocean truncates the top of the model. The mesh covers the dike-free and marginal dike zone of East Moloka‘i volcano and excludes the dike-complex area. The southern extent of the dike-complex area of East Moloka‘i volcano forms the northern boundary of the model domain. Groundwater inflow from the dike complex is included and estimated from the island-wide model. The western boundary of the model is the confining unit at the presumed contact between West and East Moloka‘i volcanoes. The mesh extends offshore to include the entire zone where fresh groundwater is expected to discharge to the ocean.

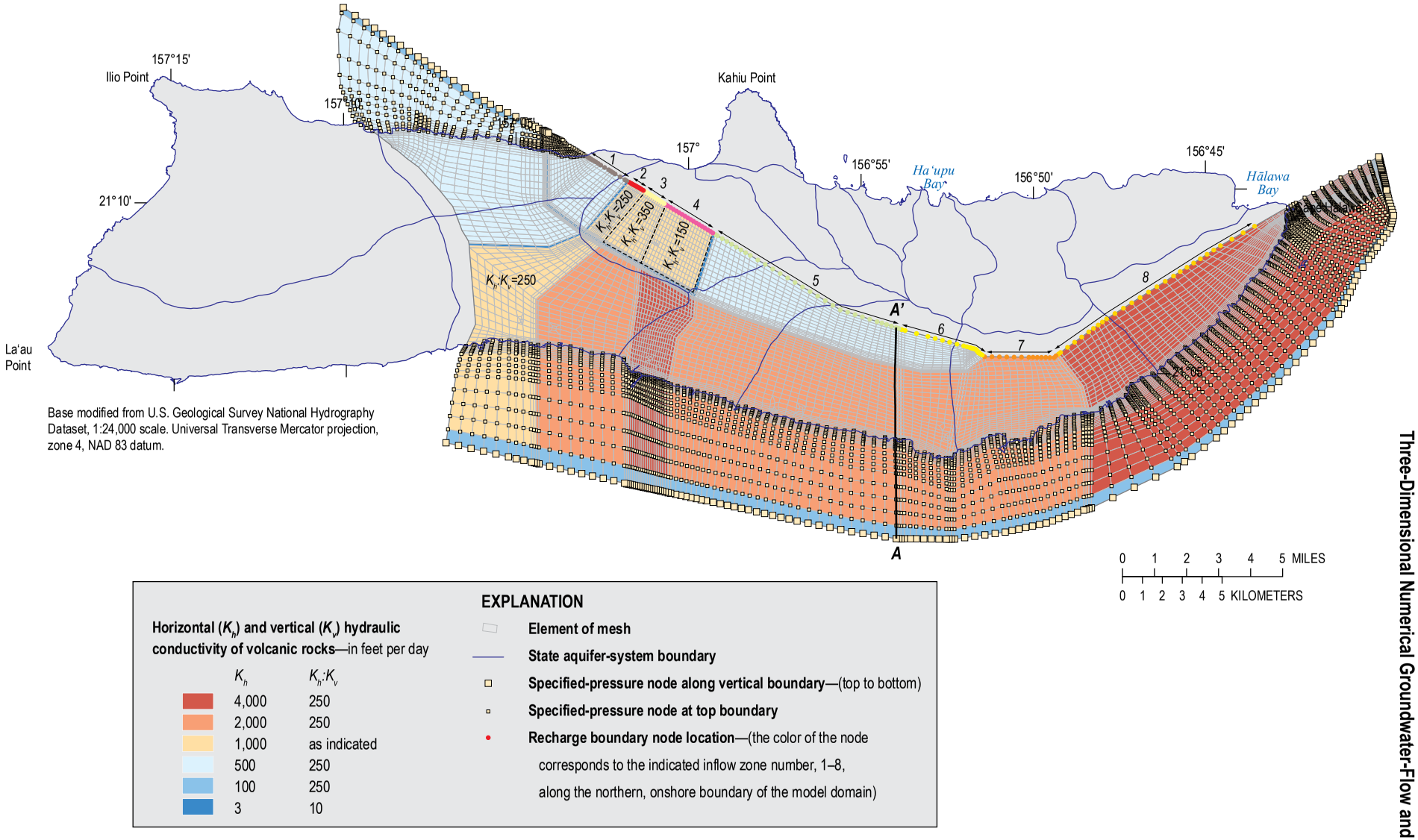

Figure 16. Hydraulic-conductivity zones for the volcanic rocks and boundary-condition nodes in the three-dimensional numerical groundwater model, Moloka'i, Hawai'i.

The top of the model domain in onshore areas ranged between altitudes of 6.56 ft near the coast to 19.7 ft in inland areas and was truncated to include the water table without also including the entire unsaturated zone to the land surface. That is, the top of the model domain in onshore areas was set high enough to simulate unconfined, water-table conditions, but did not extend to the ground surface in most areas to avoid the need to simulate the entire unsaturated zone. Offshore, the top of the model was defined by the ocean floor. The bottom of the model domain was assumed to be a no-flow boundary defined by either the estimated contact between West and East Moloka‘i volcanoes (fig. 5) near the western part of the model domain or an assumed aquifer bottom (Souza and Voss, 1987) and seismic-velocity discontinuity (Furumoto and others, 1970; Kauahikaua, 1993) at 5,906 ft below mean sea level. The bottom boundary near the model's western margin was assumed to deepen from west to east, defined by the estimated dip of the contact between West and East Moloka‘i volcanoes (fig. 5). To avoid simulating an aquifer of near zero thickness, the bottom boundary was assigned an altitude of −500 ft where the estimated contact between West and East Moloka‘i volcanoes was above that altitude. The depth of the bottom boundary increased in an eastward direction to an altitude of −5,906 ft (fig. 5).

Node spacing is variable in both the vertical and horizontal directions, and spacing is finest in the upper part of the aquifer and near areas of groundwater discharge or potential barriers to groundwater flow. The vertical spacing between nodes ranged from 1.64 ft in onshore areas above sea level to 924 ft near the bottom of the mesh where only saltwater is simulated (fig. 17).

Representation of the System

For modeling purposes, the model domain was divided into hydraulic-conductivity zones representing the volcanic rocks (fig. 16) and hydraulic-conductivity zones representing the coastal sediments overlying the volcanic rocks (fig. 18). Hydraulic conductivity is related to permeability, which is the parameter used by SUTRA, according to the following equation:

$$K = k\rho g/\mu \quad (1)$$

where

- K is hydraulic conductivity in units of length per unit time [LT^{-1}],
- k is permeability in units of area [L^2],
- ρ is fluid density in units of mass per unit length cubed [ML^{-3}],
- g is gravitational acceleration in units of length per unit time squared [LT^{-2}], and
- μ is fluid dynamic viscosity in units of mass per unit length per unit time [$ML^{-1}T^{-1}$], or force-time per unit area.

Because the CWRM aquifer-system boundaries do not necessarily represent subsurface hydrogeologic features, the zones generally were not aligned with the aquifer-system boundaries. The marginal dike zone of East Moloka‘i volcano in the central part of the island was divided into six zones to enable representation of water levels and to create a compartmentalized groundwater system consistent with the presence of dikes. The mostly dike-free East Moloka‘i Volcanics was divided into six zones to enable representation of the spatial distribution of water levels. A west-trending minor rift zone of East Moloka‘i volcano extends toward the western boundary of the model. Zones were created along the northern and southern offshore boundaries to simulate resistance to inflow and outflow of ocean water into the modeled domain.

Boundary Conditions

The lateral extent of the model domain is defined by boundaries that are either no-flow, recharge, or specified-pressure boundaries. The western boundary is formed by the eroded contact between West and East Moloka‘i volcanoes and is treated as a no-flow boundary in the model. The northern boundary is formed by the southern extent of the East Moloka‘i volcano dike complex and is a no-flow boundary offshore and a recharge or no-flow boundary onshore. Recharge from the East Moloka‘i volcano dike complex is allowed to enter the onshore northern boundary between altitudes of −3.3 to −82 ft in the northwestern and southeastern parts (inflow zones 1 and 8 in fig. 16); between altitudes of −3.3 to −262 ft within the marginal dike zone area (inflow zones 2–6); and between altitudes of −3.3 to −164 ft for inflow zone 7 (fig. 16). Recharge rates along the onshore northern boundary were determined from the island-wide model and the depths were selected to allow recharge to occur mainly within the freshwater part of the groundwater body. The onshore northern boundary, below where recharge is allowed to occur, is treated as a no-flow boundary. The no-flow assumption is reasonable given that changing conditions within the modeled area are not expected to substantively affect hydrologic conditions within the low-permeability dike complex (see for example, Oki, 2006). The offshore, vertical boundaries of the model domain in both northern and southern Moloka‘i are represented with a specified-pressure (hydrostatic ocean-water) boundary condition, except where the boundary is defined by the East Moloka‘i volcano dike complex and assumed to be a no-flow boundary. At the offshore, vertical specified-pressure boundaries of the model, pressure at each node is equal to the pressure of a column of ocean water extending from the node to sea level. Water may either enter or exit the flow system across the vertical specified-pressure boundaries of the model. Water entering at the vertical specified-pressure boundaries has salinity equal to that of ocean water, and water exiting at the boundary has salinity equal to that in the adjacent aquifer.

The top of the offshore model domain is defined by the ocean-bottom bathymetry (fig. 5) (National Oceanic and Atmospheric Administration, 2010) and is a specified-pressure (hydrostatic ocean-water) boundary condition. Ocean water may enter the model domain at the top boundary in offshore areas or water from the aquifer may exit at the top boundary in offshore areas. The top of the onshore model domain is assumed to be at an altitude of 6.56 to 19.7 ft to account for

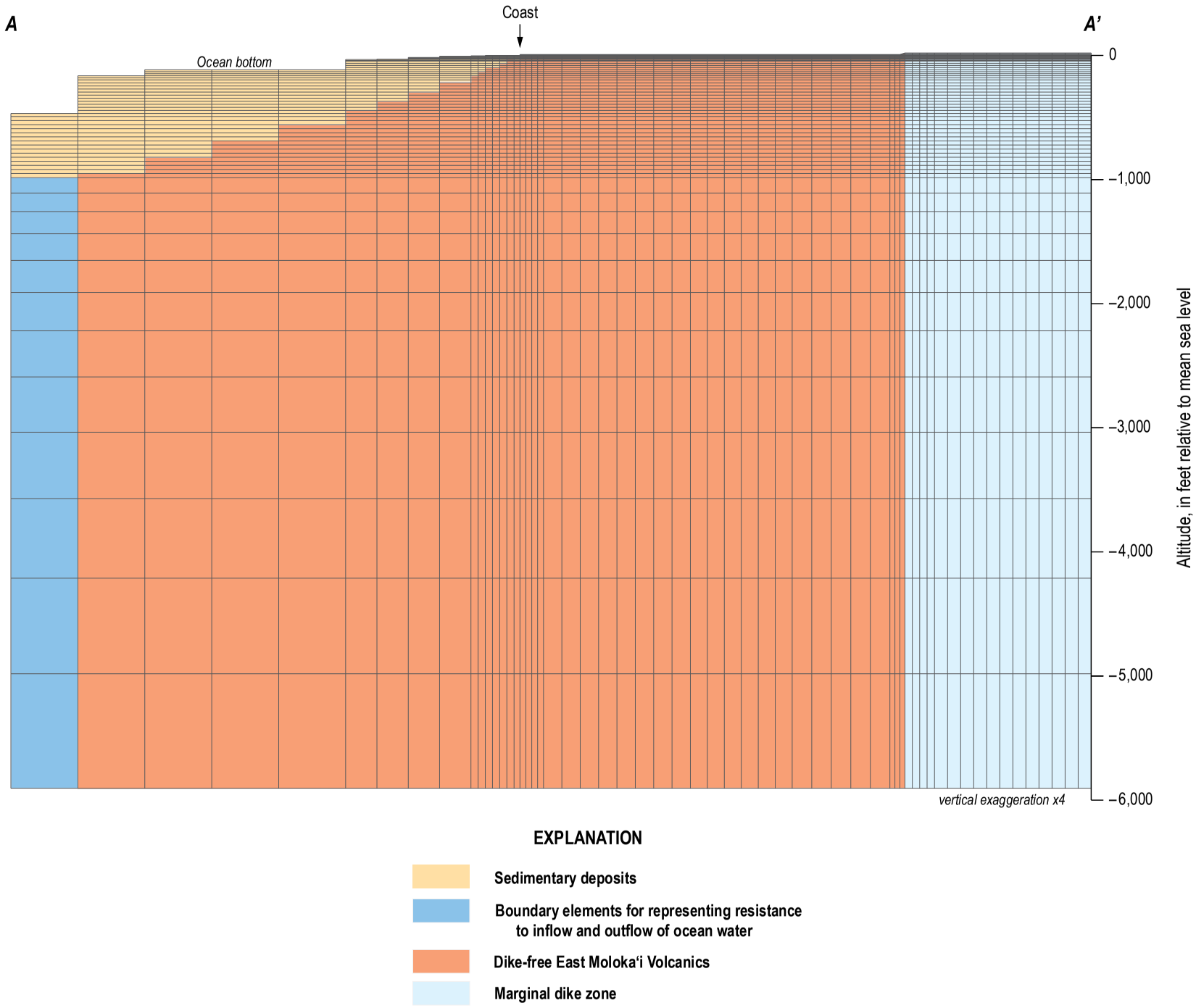

Figure 17. Vertical cross section of Moloka'i, Hawai'i model mesh through section A–A'. See figure 16 for location of section.

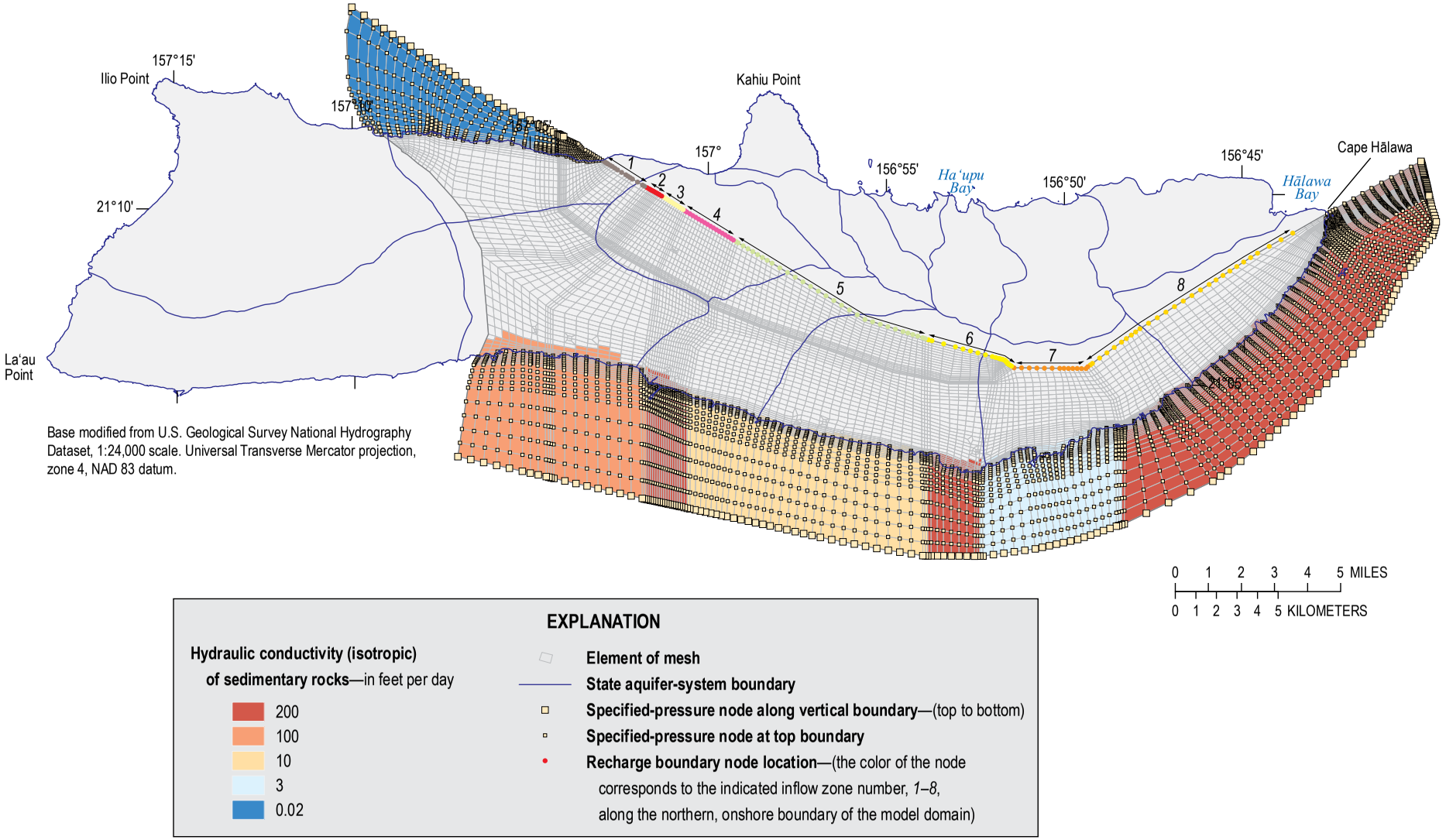

Figure 18. Map of Moloka'i, Hawai'i hydraulic-conductivity zones for the sedimentary rocks and boundary-condition nodes in the three-dimensional numerical groundwater model.

the water table. A simplified representation of the hydraulic characteristics of the unsaturated rocks was used in SUTRA to simulate the location of the water-table boundary.

Recharge

For this study, recharge to the onshore, top boundary of the model was estimated from a daily water budget of the six decadal periods from 1940 to 1999 (1940–49, 1950–59, 1960–69, 1970–79, 1980–89, 1990–99), and the 13-year period 2000–12 (appendix 1). Recharge assigned to each onshore node at the top of the model domain was based on the area-weighted average recharge from the irregularly shaped water-budget-model subareas within a Thiessen polygon surrounding the node. Recharge at the top of the model domain for the seven decadal periods ranged from about 44 to 69 Mgal/d (table 1). Recharge used in the groundwater model may differ slightly from that estimated by the water budget because of discretization near the coast that causes some onshore areas to be assigned to offshore cells. The recharge water at the top of the model domain was assumed to have a salinity 0.1 percent that of ocean water, except near the western part of the modeled area (west of Kaunakakai) where the recharge was assumed to have a salinity 0.2 percent that of ocean water to account for increased evapotranspiration. A salinity value 0.1 percent that of ocean water corresponds to a chloride concentration of about 20 mg/L (assuming ocean water has a chloride concentration of about 19,500 mg/L), which generally is consistent with lowest chloride concentrations in groundwater from wells on Moloka‘i (U.S. Geological Survey, 2019).

Recharge from the inflow of groundwater from the East Moloka‘i volcano dike complex was estimated from the island-wide model described above. For the six decadal periods from 1940 to 1999 (1940–49, 1950–59, 1960–69, 1970–79, 1980–89, 1990–99), and the 13-year period 2000–12 average total groundwater inflow from the East Moloka‘i volcano dike complex ranged from about 46.3 to 49.1 Mgal/d (table 1). The inflow from the inland boundary was assumed to have a salinity 0.05 percent that of ocean water. This salinity value corresponds to a chloride concentration of about 10 mg/L that is consistent with values for rainfall in Hawai‘i (Swain, 1973).

Withdrawals

Information on groundwater withdrawals was obtained from CWRM, the County of Maui Department of Water Supply (MDWS), and previously published studies (Oki, 1997, 2006). The open or screened interval of each pumped well was represented in the model using one or more nodes within a vertical column of nodes in the mesh (table 2). Except for two wells in the Kualapu‘u area, withdrawals were uniformly distributed with depth. For the two exceptions (wells 0801–01 and 0801–02), withdrawals were assumed to be distributed nonuniformly based on information from well 0801–01 indicating improved production when the well was deepened from an altitude of about −51 ft to −91 ft. In the model, 90 percent of the withdrawals from wells 0801–01 and 0801–02 were distributed to the bottom node of the vertical column of nodes representing each well, and the remaining 10 percent of the withdrawals were assigned to the other nodes representing each well. This nonuniform distribution was estimated during model calibration to match the salinity of pumped water from these wells. Simulated chloride concentrations from withdrawal wells represented by multiple nodes in the model were determined by weighting the salinity by the withdrawal at each node, which produces the overall withdrawal-weighted average.

Injection Wells

Total recharge to the aquifer from two wastewater injection-well facilities near Kaunakakai (fig. 7) was included in the model and averaged about 0.2 Mgal/d during 2004–12 based on data provided by the County of Maui (at the time of publication, the data had not been published by the County of Maui). During 2015, combined recharge from the two facilities averaged 0.29 Mgal/d. The injected wastewater was assumed to have a salinity of 1 percent that of ocean water, generally corresponding to the higher salinity values of pumped groundwater (fig. 9).

Water and Gravity Properties

For all model simulations, water was assigned a single fluid-compressibility value of 2.14×10^{-8} square feet per pound (ft^2/lb; 4.47×10^{-10} Pa^{-1}) and a dynamic-viscosity value of 2.1×10^{-5} slug/(ft·s) [0.001 kg/(m·s)]. Viscosity is a property of a fluid that measures its resistance to deformation (flow). Dynamic viscosity is the ratio of shear stress (shear force per unit area) to velocity gradient.

Solute concentrations in the model are expressed as a mass fraction: mass of total dissolved solids (TDS) per unit mass of fluid. Pure freshwater was assigned a TDS concentration of zero and 100 percent saltwater was assigned a TDS concentration of 0.0357 kilograms per kilograms (kg/kg). For this study, the simulated chloride concentration of water was estimated from the TDS concentration using the following equation:

$$Cl = TDS \times 19{,}500 / 0.0357 \quad (2)$$

where

Cl is chloride concentration, in mg/L, and
TDS is simulated total dissolved solids concentration, in kg/kg.

The density of water was assumed to increase linearly with salinity from 62.32 pounds per cubic foot (lb/ft^3; 998.23 kilograms per cubic meter [kg/m^3]) for freshwater to 63.96 lb/ft^3 (1,024.51 kg/m^3) for saltwater. The saltwater specific gravity used for this study is consistent with the value of 1.026 from Wentworth (1939).

Table 2. Values of top and bottom altitudes of open well interval used in the three-dimensional numerical groundwater model, Molokaʻi, Hawaiʻi.

[--, no reliable data available]

Well no.	Top altitude, in meters[1]	Bottom altitude, in meters[2]	Altitude, in feet[3]	Bottom of solid casing depth , in feet	Bottom of open hole depth , in feet
0350–01	−31.1	−66.1	3.01	105	220
0350–05	0.0	−2.0	56	56	62.5
0350–07	−0.5	−3.5	22.5	24	34
0350–09	−66.1	−102.7	8	225	345
0352–01	0.0	−1.0	43.23	--	40
0352–09	−3.7	−6.1	83	95	103
0352–10	0.0	−9.8	42	42	74
0352–15	0.0	−1.0	--	--	15
0354–07	0.0	−2.1	24	24	31
0356–01	0.0	−1.0	20	--	19
0448–01	0.0	−1.0	--	--	12
0448–03	0.0	−1.0	30	--	32
0448–09	0.0	−1.0	--	--	--
0449–01	0.0	−1.0	42	41.5	41.5
0456–01	0.0	−1.0	14	--	15
0456–04	0.0	−2.7	25	--	34
0456–06	0.0	−3.0	223	223	233
0456–08	0.0	−3.0	225.24	225	235
0456–09	0.0	−2.9	234.56	234	244
0456–18	0.0	−2.3	225.59	223	233
0456–19	0.0	−2.6	224.33	220	233
0457–01	0.0	−1.0	38	--	39
0457–04	0.0	−2.7	235	234	244
0458–04	0.0	−2.3	39.56	37	47
0501–04	0.0	−1.0	28	--	28
0501–06	0.0	−1.8	15	13	21
0501–07	0.0	−8.8	31	--	60
0501–98	−29.0	−59.4	10	105	205
0501–99	0.0	−1.0	28	--	27.3
0546–01	0.0	−1.0	20	--	20
0546–02	−0.6	−14.6	386	388	434
0601–01*	0.0	−2.1	52	32	59
0602–03	0.0	−2.1	3	--	10
0603–01	0.0	−1.0	15	16	17
0603–06	0.0	−1.0	84	78	--
0604–03	0.0	−1.0	16	--	19
0604–04	0.0	−2.7	36	28	45
0604–05	0.0	−1.2	34	--	38
0605–01	0.0	−31.6	16	--	120
0605–02	0.0	−56.0	16	--	200
0605–03	0.0	−1.0	--	--	--
0705–05	0.0	−8.2	254	251	281
0706–02	0.0	−1.0	23	--	25
0801–01	−0.9	−27.1	1006	1009	1095
0801–02	−8.2	−26.5	1013	1040	1100
0801–03	0.0	−29.3	1040	1027	1136
0901–01	0.0	−25.2	981.3	870	1064
0902–01	0.0	−23.9	884.5	883	963

[1]Underlined values indicate estimate or reassignment to zero if top altitude is above sea level.

[2]Underlined values indicate estimate or reassignment to −1.0 m if bottom altitude is above an altitude of −1.0 m.

[3]Underlined values indicate estimate based on topographic map or reported depth to water and assumed water level.

In the model, molecular diffusion of a solute is driven by concentration gradients in the fluid and may take place in the absence of groundwater flow. Molecular diffusion of a solute in a fluid is characterized by the molecular diffusivity. In the model, molecular diffusivity was assigned a value of 1.1×10^{-8} square feet per second (ft^2/s; 1.0×10^{-9} square meters per second [m^2/s]). In the model, acceleration due to gravity was assigned a value of 32.1 ft/s^2 (9.79 m/s^2).

Unsaturated Zone

For this study, the unsaturated zone characteristics were represented using simple linear relations between water saturation and pressure and between water saturation and relative permeability. Voss (1999) indicates that the details of the unsaturated zone are not important for tracking the water table and can be simplified using linear relations to reduce computational effort needed for the variable-density simulation. The simplified saturation-pressure relation is of the form:

$$S = 1 + (P - P_{entry}) \times (1 - S_{res}) / (P_{entry} - P_{min}) \quad (3)$$

where

S is saturation constrained to the range from S_{res} to 1 (volume fraction, unitless),

P is pressure in units of force per unit area [$ML^{-1}T^{-2}$],

P_{entry} is entry pressure above which $S = 1$, assigned a value of zero [$ML^{-1}T^{-2}$],

P_{min} is minimum pressure below which $S = S_{res}$, assigned a value of −1,021 lb/ft^2 (−48,863 Pa) [$ML^{-1}T^{-2}$], and

S_{res} is residual saturation, assigned a value of 0.01.

The simplified saturation-permeability relation is of the form:

$$k_{rel} = (S - 0.01) / 0.99 \quad (4)$$

where

k_{rel} is relative permeability (a multiplier for permeability), constrained to the range from 0 to 1 (unitless).

Initial Conditions and Time Step

A steady-state simulation using recharge values from the 1940s and zero withdrawals was used to generate initial conditions for the 1940–2012 transient simulation. A 0.5-day time step was used for the transient simulation.

Estimation of Hydraulic Properties

Hydraulic conductivity and effective porosity values were estimated by trial and error. Rock-matrix compressibility was assigned a value of 1.2×10^{-7} ft^2/lb (2.5×10^{-9} Pa^{-1}), and the effective porosity was assigned a value of 0.05.

The estimated hydraulic-conductivity values generally are consistent with previous estimates and are consistent with the conceptual model of higher values for the dike-free volcanic rocks and lower values for the dike-intruded areas. Estimated horizontal hydraulic-conductivity values were 500, 1,000 or 2,000 ft/d for the mainly dike-free volcanic rocks; 500 or 1,000 ft/d for the marginal dike-zone compartments between groundwater barriers; 3 ft/d for the zones representing groundwater barriers to flow (dikes or other features); and between 0.02 and 200 ft/d for coastal sedimentary deposits overlying volcanic rocks (figs. 16, 18). Horizontal anisotropy was not represented in the model. Vertical anisotropy (ratio of horizontal-to-vertical hydraulic conductivity) was 250:1 for the mainly dike-free volcanic rocks; 150:1, 250:1, or 350:1 for marginal dike-zone compartments between groundwater barriers; 10:1 for the zones representing groundwater barriers to flow (dikes or other features); and 1:1 for sedimentary deposits.

For regional solute-transport simulation, SUTRA requires specification of three longitudinal dispersivity values and three transverse dispersivity values. Above an altitude of −1,312 ft, longitudinal dispersivity values used in the model were 250 ft, 250 ft, and 5 ft in directions of maximum (horizontal longitudinal) hydraulic conductivity, middle (horizontal transverse) hydraulic conductivity, and minimum (vertical) hydraulic conductivity, respectively. Above an altitude of −1,312 ft, transverse dispersivity values used in the model were 0.16 ft in all three directions (maximum hydraulic conductivity, middle hydraulic conductivity, and minimum hydraulic conductivity). Below an altitude of −1,312 ft, which is entirely within the saltwater zone represented in the model, longitudinal dispersivity values were multiplied by a factor of 2 and transverse dispersivity values were multiplied by a factor of 20 to enhance numerical stability without otherwise affecting the results.

Simulation Results

Simulated transient water levels are in reasonable agreement with observed water levels (fig. 19). At a few sites, available water levels (U.S. Geological Survey, 2019) are uncertain because of uncertainty in the reference, measuring-point altitude used at the site. For example, water levels measured at well 0449–01 appear to shift downward by about 2 ft starting in the 1970s until mid-2014. However, updated (2014) surveying indicates that this downward shift may have been related to an inaccurate starting, reference-mark altitude used for a 1973 survey. Additional surveying in 2015 indicates that water levels at well 0501–09 may be high by about 0.8 ft and water levels at well 0457–01 may be low by about 1 ft. Although these survey results reflect the best available information, determining the accuracy of the earlier surveys may not be possible given potential site changes over time and unretrievable starting reference marks used for the early surveys.

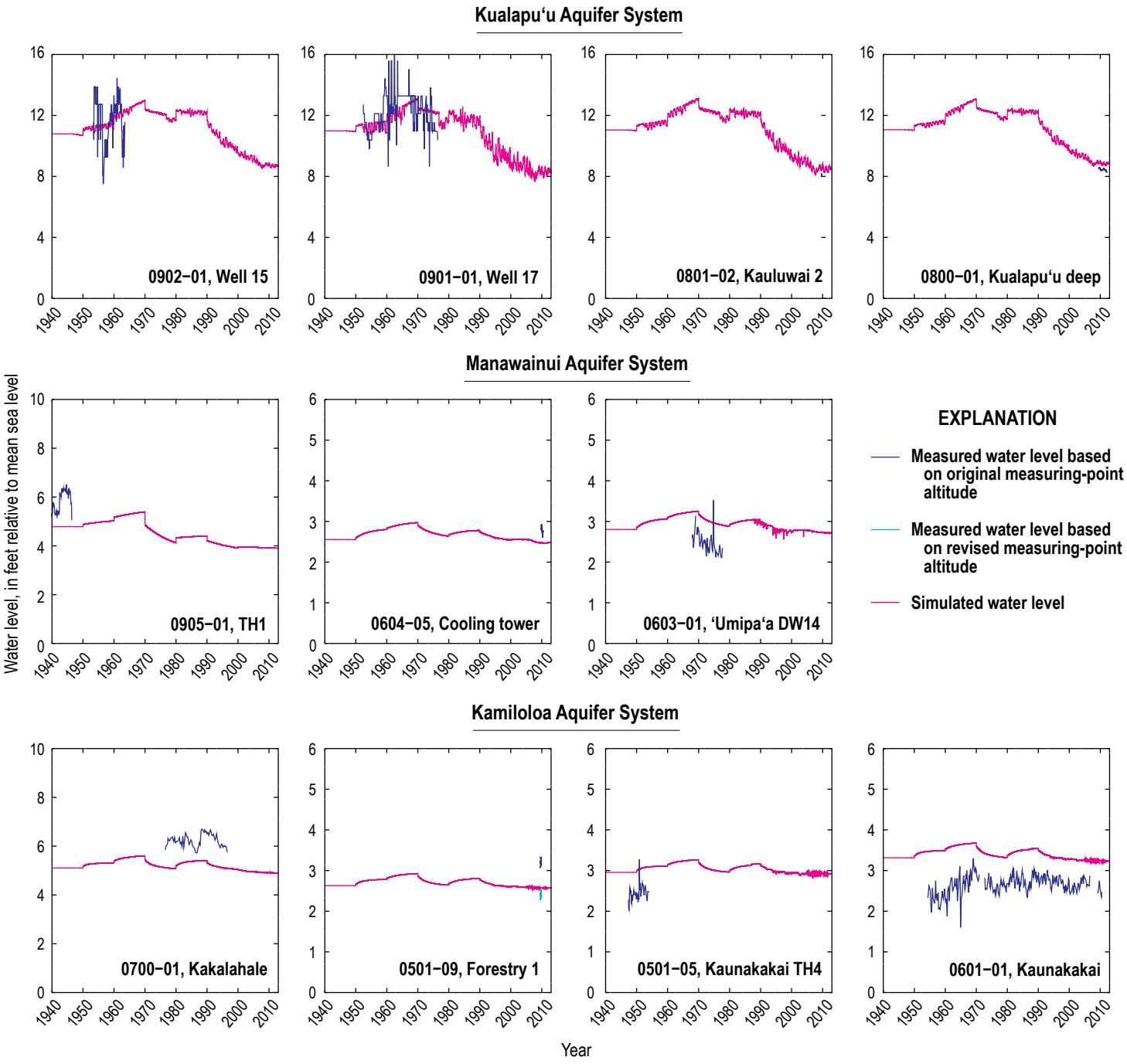

Figure 19. Multiple line graphs showing measured and simulated (from three-dimensional numerical groundwater model) water levels at selected wells during 1940–2012, Moloka‘i, Hawai‘i.

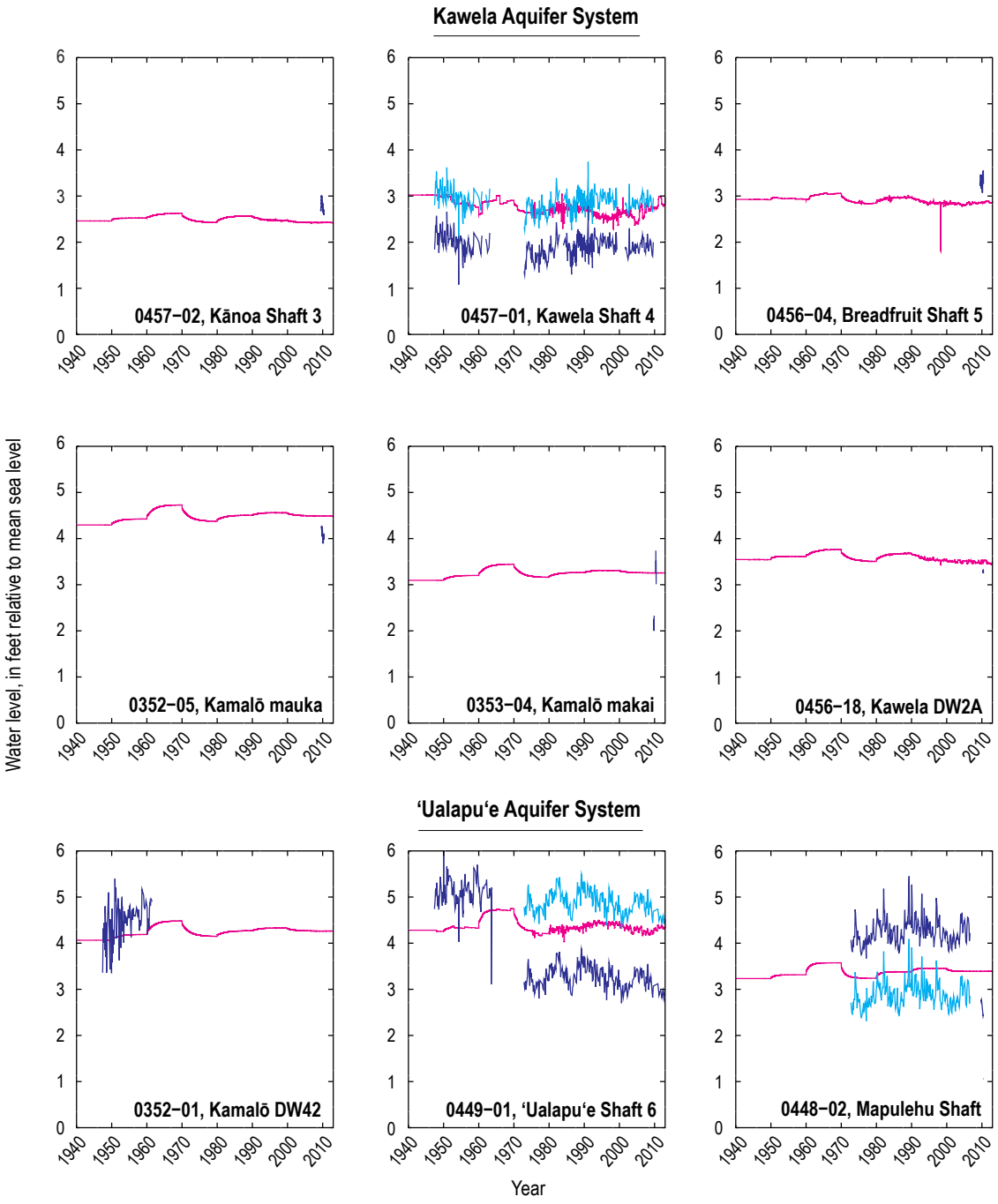

Figure 19.—Continued

Simulated chloride concentrations of water withdrawn by wells are in general agreement with observed chloride concentrations, with the exception of chloride concentrations from well 0902–01, which has unexpectedly high observed concentrations (fig. 20). Because of large uncertainties in local-scale aquifer heterogeneity that can affect the quality of water withdrawn by a well, the model cannot be expected to produce an exact match between simulated and observed chloride concentrations. However, the model does appear to generally capture the overall quality of water withdrawn by wells in the Kualapuʻu area.

Deep monitoring well 0800–01 in the Kualapuʻu area is open to the aquifer from the water table to the bottom of the well (Oki and Bauer, 2001). Vertical salinity profiles are collected from this well by trolling a logging tool down the well. The logging tool records fluid specific conductance with depth during its descent. For this study, chloride concentrations were estimated from the fluid specific-conductance values using the following equation:

$$Cl = SC \times 19{,}500 / 46{,}000 \quad (5)$$

where

Cl is chloride concentration, in milligrams per liter (mg/L), and

SC is measured fluid specific conductance, in microsiemens per centimeter (µS/cm).

The simulated and measured salinity profiles, in terms of estimated chloride-concentration (fig. 21), indicate that the model underestimates the thickness of freshwater near well 0800–01. This underestimation of freshwater thickness may reflect model inaccuracy or possibly intraborehore flow that can occur in wells of this type with long open or screened intervals (see for example, Rotzoll, 2012). The simulated

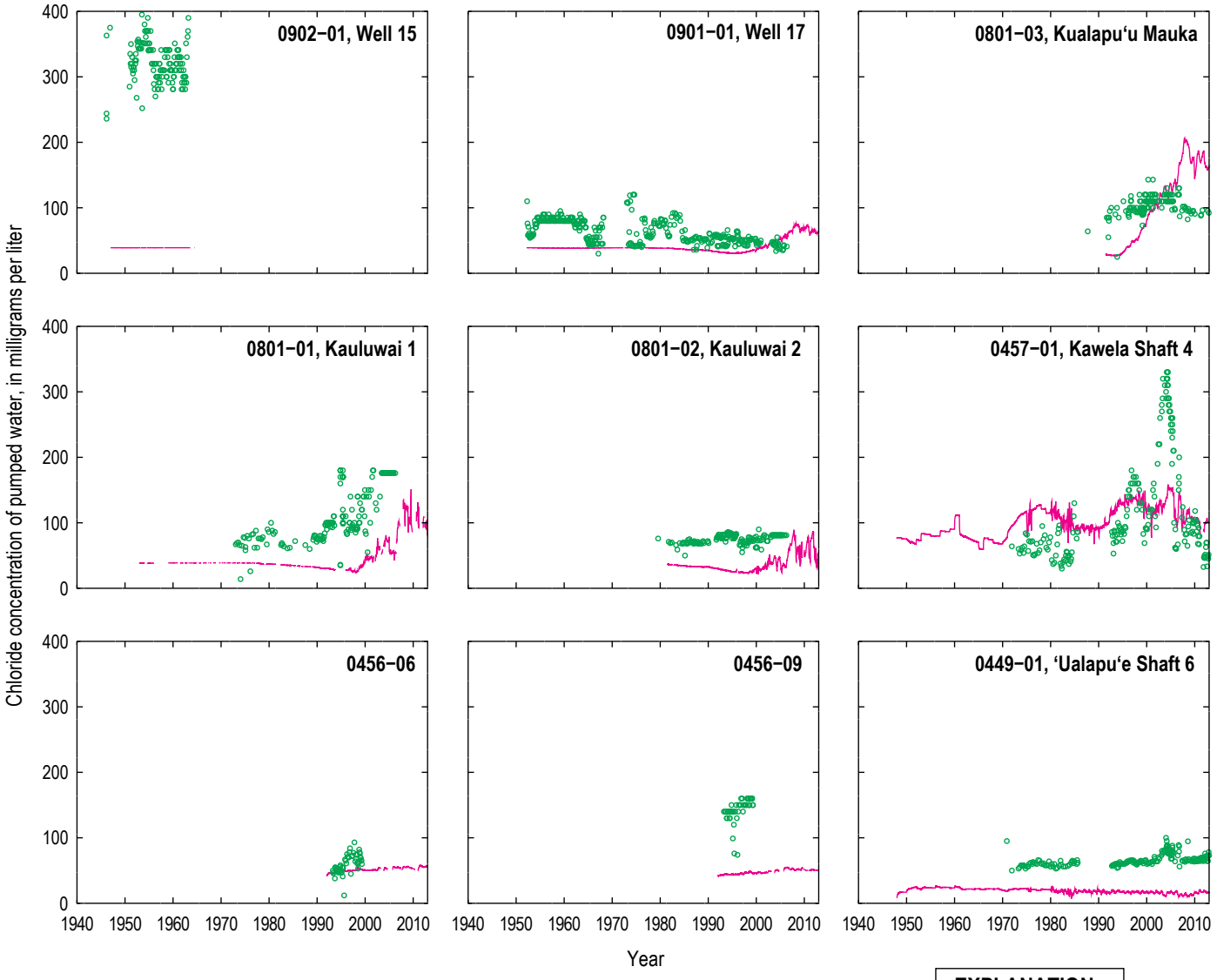

Figure 20. Multiple time-series graphs showing measured and simulated chloride concentration of pumped water from selected wells during 1940–2012, Molokaʻi, Hawaiʻi.

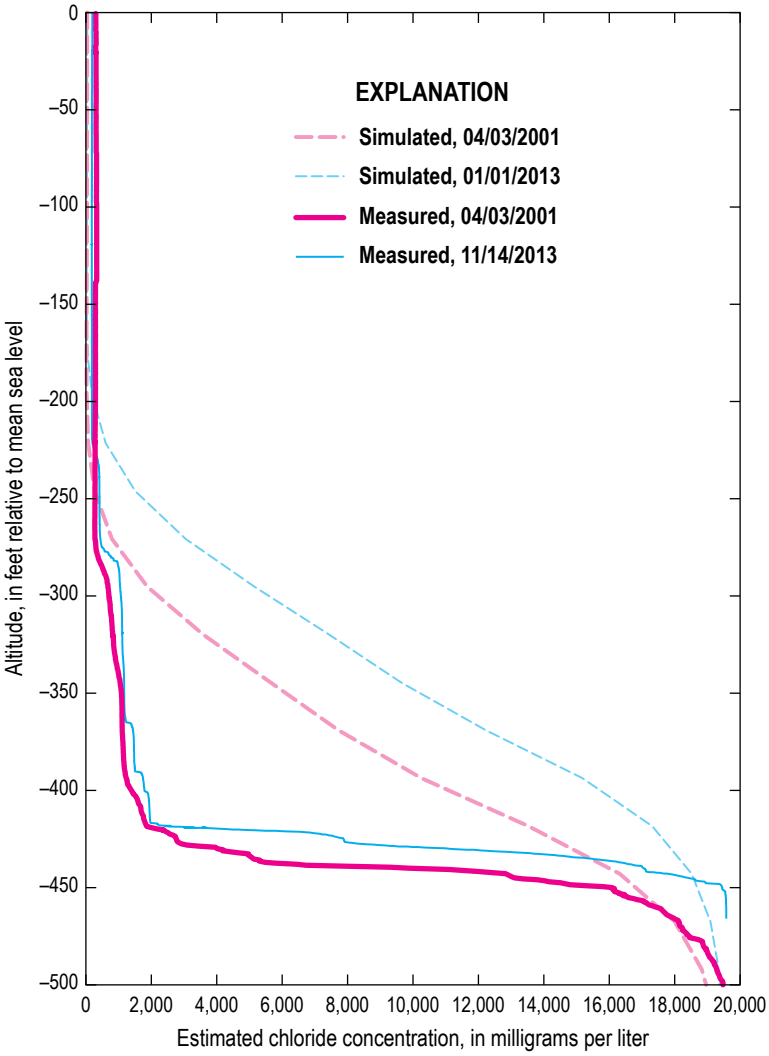

Figure 21. Simulated and measured salinity profiles from selected times in terms of estimated chloride concentration, Kualapu‘u deep monitor well 0800–01, Moloka‘i, Hawai‘i.

freshwater thickness near well 0800–01 potentially can be increased by reducing the hydraulic conductivity in the model below an altitude of about −150 ft near well 0800–01. In both simulated dates, the model tends to be conservative from the standpoint of freshwater thickness near well 0800–01.

Simulation of Selected Withdrawal Scenarios

The hydrologic effects of withdrawals on the quality of water withdrawn by wells and coastal discharge of groundwater were simulated with the three-dimensional numerical groundwater-flow and salinity-transport model. The following simulated withdrawal scenarios were selected in consultation with water managers and stakeholders: (1) a baseline scenario using average recharge (1978−2007 rainfall and 2010 land cover) and average 2016−17 withdrawals; (2) a scenario using average recharge and withdrawals from existing wells at pending (as of January 2019) water-use permit rates; (3) six scenarios using average recharge and selected withdrawals from existing and proposed new wells; and (4) a scenario using reduced recharge and selected withdrawals from existing and proposed new wells. Selected withdrawal scenarios of interest (table 3) were developed in collaboration with representatives from MDWS, DHHL, Office of Hawaiian Affairs, and CWRM. All simulations were run for a sufficient time to reach steady-state conditions.

For each scenario, the estimated chloride concentration (derived from the simulated total dissolved solids concentration; see equation 2 above) of groundwater withdrawn by each well in the Kualapu‘u aquifer system was generalized into one of three categories: (1) less than 100 mg/L; (2) greater than or equal to 100 mg/L and less than or equal to 200 mg/L; and (3) greater than 200 mg/L (or possibly greater than 250 mg/L in some cases). Although the EPA secondary standard for chloride concentration in drinking water is 250 mg/L, maintaining the chloride concentration of produced water less than 200 mg/L helps provide a buffer to avoid concentrations greater than 250 mg/L.

Coastal groundwater discharge from model nodes was summed into 1,640 by 1,640 ft (500 by 500 m) cells to provide a generalized representation of discharge conditions. For this study, the freshwater component of coastal groundwater discharge was used to evaluate changes in discharge associated with each scenario relative to a baseline scenario. The freshwater discharge was computed from a salinity mass balance, assuming freshwater has zero salinity. For example, if the salinity of the groundwater discharge is 25 percent that of ocean water, then the discharge represents a mixture of 25 percent ocean water and 75 percent freshwater. Thus, if the discharge from a cell is 1 Mgal/d and the salinity of the discharge is 25 percent that of ocean water, then the saltwater component of the discharge is estimated to be 0.25 Mgal/d and the freshwater component of the discharge was estimated to be 0.75 Mgal/d. Although the groundwater model can be used to quantify the reduction in fresh groundwater discharge associated with increased withdrawals, the model cannot ascertain whether the reductions are ecologically, culturally, societally, or economically acceptable or not. Whether or not a reduction in fresh groundwater discharge is acceptable may be dependent on factors including the sensitivity of nearshore ecosystems to salinity change and the importance of the area from cultural or subsistence perspectives.

Scenario 1—Baseline

A baseline scenario was developed to provide a basis for evaluating existing withdrawals in the Kualapu‘u aquifer system, in terms of salinity from production wells, and estimating change in coastal groundwater discharge associated with each withdrawal scenario. The baseline scenario used average recharge conditions,

Table 3. Withdrawal rates used in the modeled scenarios, Kualapuʻu, Molokaʻi.

[Green values indicate simulated chloride concentration of pumped water is less than 100 mg/L; orange, italicized values indicate simulated chloride concentration of pumped water is between 100 and 200 mg/L; bold purple, underlined values indicate simulated chloride concentration is greater than 200 mg/L; *, simulated chloride concentration of pumped water exceeds 250 mg/L; mg/L, milligrams per liter; Mgal/d, million gallons per day; --, no withdrawal simulated]

Scenario	Withdrawal rate, in Mgal/d									Recharge, in Mgal/d
	Kauluwai 1, 0801–01	Kauluwai 2, 0801–02	Kualapuʻu Mauka, 0801–03	Well 17, 0901–01	Proposed Well A	Proposed Well B	Proposed Well C	Proposed Well D	Total	
1. Baseline with 2016–17 average withdrawals	0.0897	0.3556	0.5634	0.5128	--	--		--	1.5215	103.4
2. Pending water-use permit rates in the Kualapuʻu aquifer system	--	0.6370	*0.9000*[1]	1.1440	--	--		--	2.6810	103.4
3. Increased rate for well 0801–03; domestic-need rate for well 0901–01; add Proposed Well B	--	0.5950	0.9500	0.1380	--	0.7926		--	2.4756	103.4
4. Increased rate for well 0801–03; pending water-use permit rate for well 0901–01; add Proposed Well B	--	**0.5950***	**0.9500***[1]	*1.1440*	--	0.7926		--	3.4816	103.4
5. Proposed Well A replaces well 0801–03; domestic-need rate for well 0901–01; add Proposed Well B	--	0.5950	--	0.1380	0.9500	0.7926		--	2.4756	103.4
6. Proposed Well A replaces well 0801–03; pending water-use permit rate for well 0901–01; add Proposed Well B	--	**0.5950**	--	**1.1440***	*0.9500*	0.7926		--	3.4816	103.4
7. Proposed Well B replaces well 0801–03; pending water-use permit rate for well 0901–01; add Proposed Well A	--	**0.5950**	--	**1.1440**	*0.7926*	0.9500		--	3.4816	103.4
8. Proposed Well B replaces well 0801–03; pending water-use permit rate for well 0901–01; add Proposed Wells C and D	--	**0.5950***	--	*1.1440*	--	*0.9500*	**0.7926**[1]	1.0000	4.4816	103.4
9. Same as scenario 6 but reduce recharge by 15 percent	--	**0.5950***	--	**1.1440***	**0.9500***	**0.7926***		--	3.4816	87.9

[1]Negative chloride concentration in the freshwater zone simulated at one to three of the 16 nodes representing the well was assigned a value of 195 mg/L.

estimated using 1978–2007 rainfall and 2014 land-cover conditions, and average withdrawals during 2016–17. Recharge values from the baseline scenario were about 48 Mgal/d from the inland boundary and 55 Mgal/d from the top, onshore boundary within the modeled area. Total simulated withdrawal represented in the model from wells in the Kualapu‘u aquifer system was 1.5215 Mgal/d (0.0897 Mgal/d from well 0801–01; 0.3556 Mgal/d from well 0801–02; 0.5634 Mgal/d from well 0801–03; and 0.5128 Mgal/d from well 0901–01). An average injection rate of 0.3 Mgal/d was assumed for the injection-well facilities near Kaunakakai for this baseline scenario and all other scenarios.

For the baseline scenario, the estimated chloride concentrations of groundwater withdrawn from wells in the Kualapu‘u aquifer system are less than 100 mg/L (fig. 22). Model results from the Kualapu‘u aquifer system indicate that withdrawals under the baseline condition will produce water with chloride concentrations below the EPA secondary standard for drinking water, although the model likely does not represent the exact salinity of withdrawn water from an individual well for several reasons (see Limitations section below).

Simulated freshwater coastal discharge varies spatially and ranges from less than 10,000 gallons per day to more than 2 Mgal/d within the 1,640 by 1,640 ft cells (fig. 22). Rates of freshwater coastal discharge generally are low in the drier western part of the modeled area, where groundwater recharge rates are low. Within the modeled area, most of the fresh groundwater discharges to the southern coast rather than the northern coast, which is related to the longer southern coastline and the relation between areas of recharge and discharge. Although the simulated distribution of fresh groundwater discharge may not accurately represent local conditions, simulated fresh groundwater discharge occurs in and near areas of coastal fishponds and subsistence sites (Matsuoka and others, 1994) (fig. 22).

Scenario 2—Pending (January 2019) Water-Use Permit Rates in Kualapu‘u Aquifer System

Scenario 2 includes the same recharge and withdrawals as the baseline scenario, except simulated withdrawals from wells in the Kualapu‘u aquifer system were changed to the CWRM pending water-use permit rates (as of January 2019), which correspond to a total withdrawal of 2.6810 Mgal/d in the Kualapu‘u aquifer system (0.6370 Mgal/d from well 0801–02; 0.9000 Mgal/d from well 0801–03; and 1.1440 Mgal/d from well 0901–01). In the model, permitted withdrawals from wells 0801–01 and 0801–02 were combined and simulated at well 0801–02, which is consistent with the typical operation of these wells (with well 0801–02 serving as the primary source).

For scenario 2, the estimated chloride concentrations of groundwater withdrawn from wells 0801–02 and 0901–01 are less than 100 mg/L, whereas the estimated chloride concentration of groundwater withdrawn from well 0801–03 is in the 100 to 200 mg/L category (fig. 23). The simulated chloride concentrations from production wells indicate that withdrawals from the Kualapu‘u aquifer system for scenario 2 remain below the EPA secondary standard.

Increased withdrawals in scenario 2 relative to the baseline scenario cause a reduction of freshwater discharge to the nearshore area (fig. 23). In general, the simulated reductions in freshwater discharge are greatest in areas nearest the Kualapu‘u aquifer system, although the effects are widespread. The discharge reductions are more widespread along the southern coast relative to the northern coast, partly because the simulated discharge to the northern coast is limited, which is the case in all scenarios. The greatest simulated reduction in fresh groundwater discharge from a 1,640 by 1,640 ft cell occurs northwest of the Kualapu‘u aquifer system and was 0.080 Mgal/d, representing 13 percent of the baseline discharge from that cell. The greatest simulated relative reduction in fresh groundwater discharge from any 1,640 by 1,640 ft cell was 25 percent, corresponding to a reduction of 0.012 Mgal/d (fig. 23).

Scenario 3—Increased Rate for Well 0801–03; Domestic-Need Rate for Well 0901–01; Additional Withdrawal from Proposed Well B

Scenario 3 includes the same recharge and withdrawals as the baseline scenario, except simulated withdrawals from wells in the Kualapu‘u aquifer system totaled 2.4756 Mgal/d (0.5950 Mgal/d from well 0801–02; 0.9500 Mgal/d from well 0801–03; 0.1380 Mgal/d from well 0901–01; and 0.7926 Mgal/d from proposed well B). For scenario 3, combined withdrawals from wells 0801–01 and 0801–02 were increased to 0.5950 Mgal/d relative to the 2016–17 rate (0.4453 Mgal/d) in the baseline scenario. As in scenario 2, the withdrawals from wells 0801–01 and 0801–02 were combined and simulated at well 0801–02, consistent with the typical operation of these wells. For scenario 3, withdrawal from well 0801–03 was increased to 0.9500 Mgal/d relative to the 2016–17 rate (0.5634 Mgal/d) in the baseline scenario to account for projected demand, and withdrawal from well 0901–01 was reduced to 0.1380 Mgal/d relative to the average 2016–17 rate (0.5128 Mgal/d) in the baseline scenario. The reduced rate is intended to represent the withdrawal from well 0901–01 used to meet mainly domestic needs only. Also included in scenario 3 is additional withdrawal of 0.7926 Mgal/d from proposed well B to account for projected demand.

For scenario 3, the estimated chloride concentrations of groundwater withdrawn from wells 0801–02, 0801–03, 0901–01, and proposed well B are less than 100 mg/L (fig. 24). The simulated chloride concentrations from production wells indicate that withdrawals from the Kualapu‘u aquifer system for scenario 3 remain below the EPA secondary standard.

Increased withdrawals in scenario 3 relative to the baseline scenario cause a reduction of freshwater discharge to the nearshore area (fig. 24). The pattern of freshwater discharge reduction for scenario 3 (and all other scenarios) is similar to that of scenario 2, with widespread reductions but greatest reductions in areas nearest the Kualapu‘u aquifer system. The greatest simulated reduction in fresh groundwater discharge from any 1,640 by 1,640 ft cell occurs northwest of the Kualapu‘u aquifer system and was 0.063 Mgal/d, representing 10 percent of the baseline discharge from that cell. The greatest

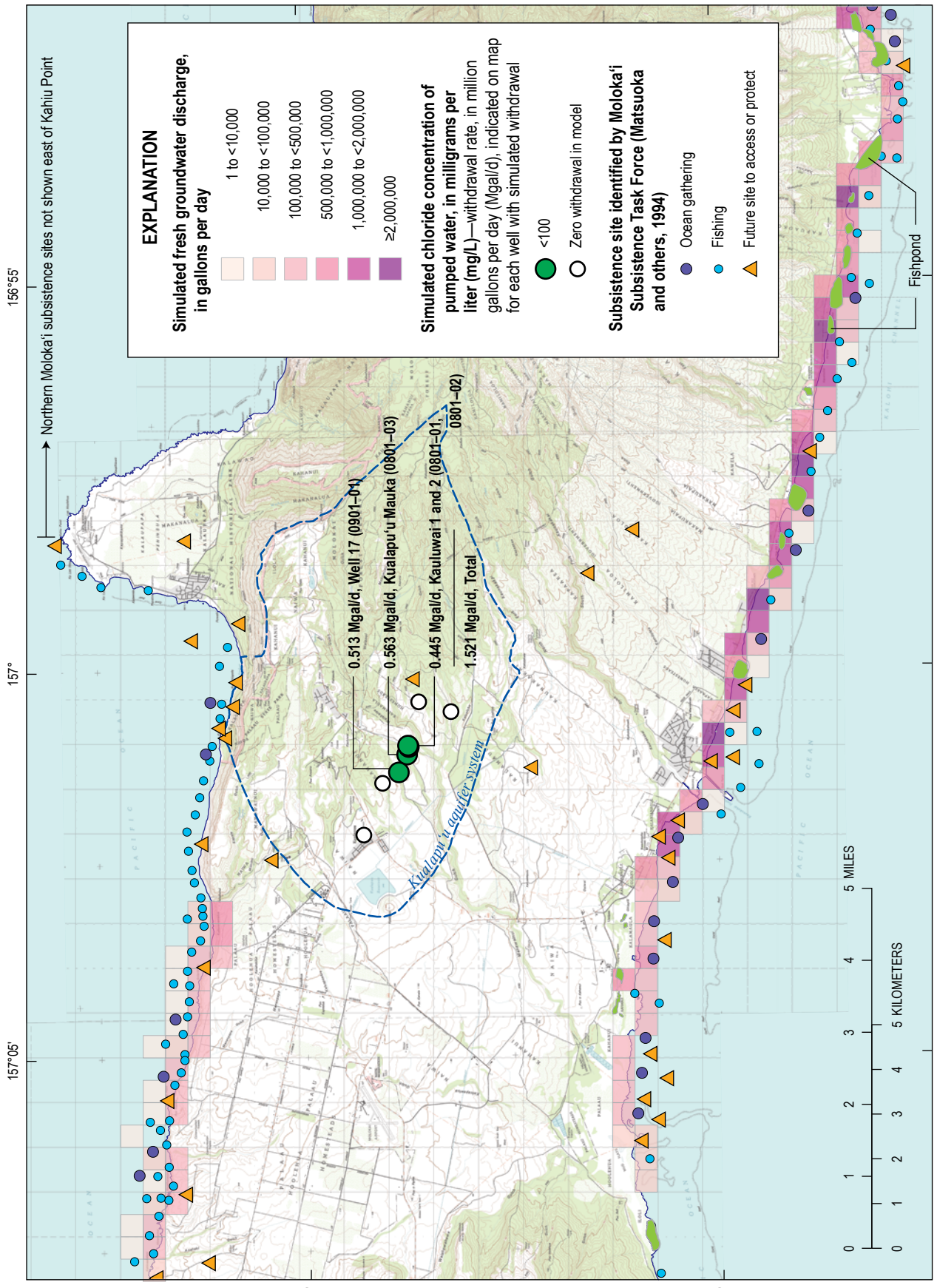

Base modified from U.S. Geological Survey Digital Raster Graphics topographic map, 1:24,000 scale.
Universal Transverse Mercator projection, zone 4, NAD 83 datum.

Figure 22. Map of the Kualapu'u aquifer system on Moloka'i, Hawai'i showing scenario 1 (baseline condition) withdrawal rates from wells and fresh groundwater discharge.

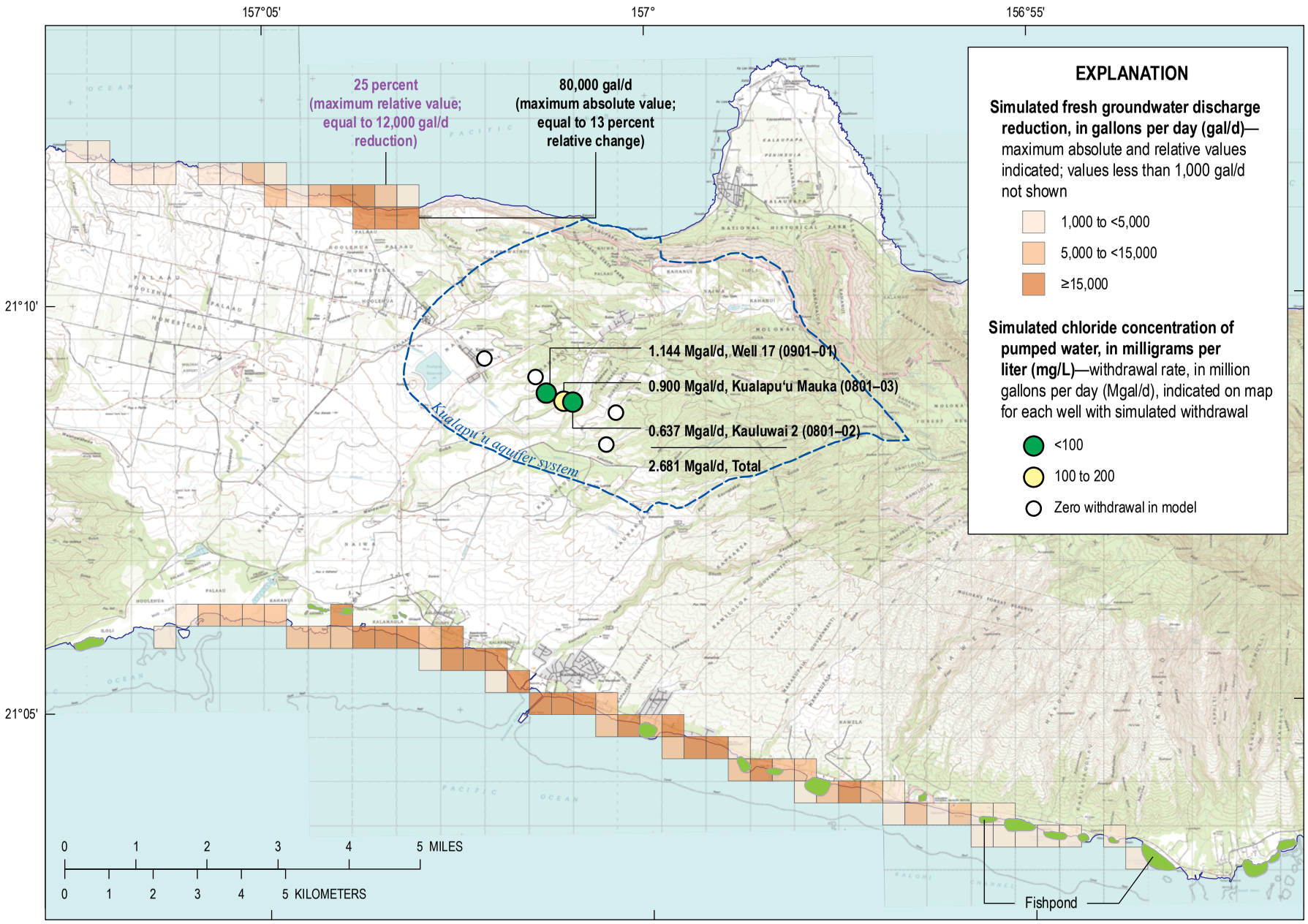

Base modified from U.S. Geological Survey Digital Raster Graphics topographic map, 1:24,000 scale.
Universal Transverse Mercator projection, zone 4, NAD 83 datum.

Figure 23. Map of the Kualapu'u aquifer system on Moloka'i, Hawai'i showing scenario 2 withdrawal rates from wells and fresh groundwater-discharge reduction (relative to scenario 1).

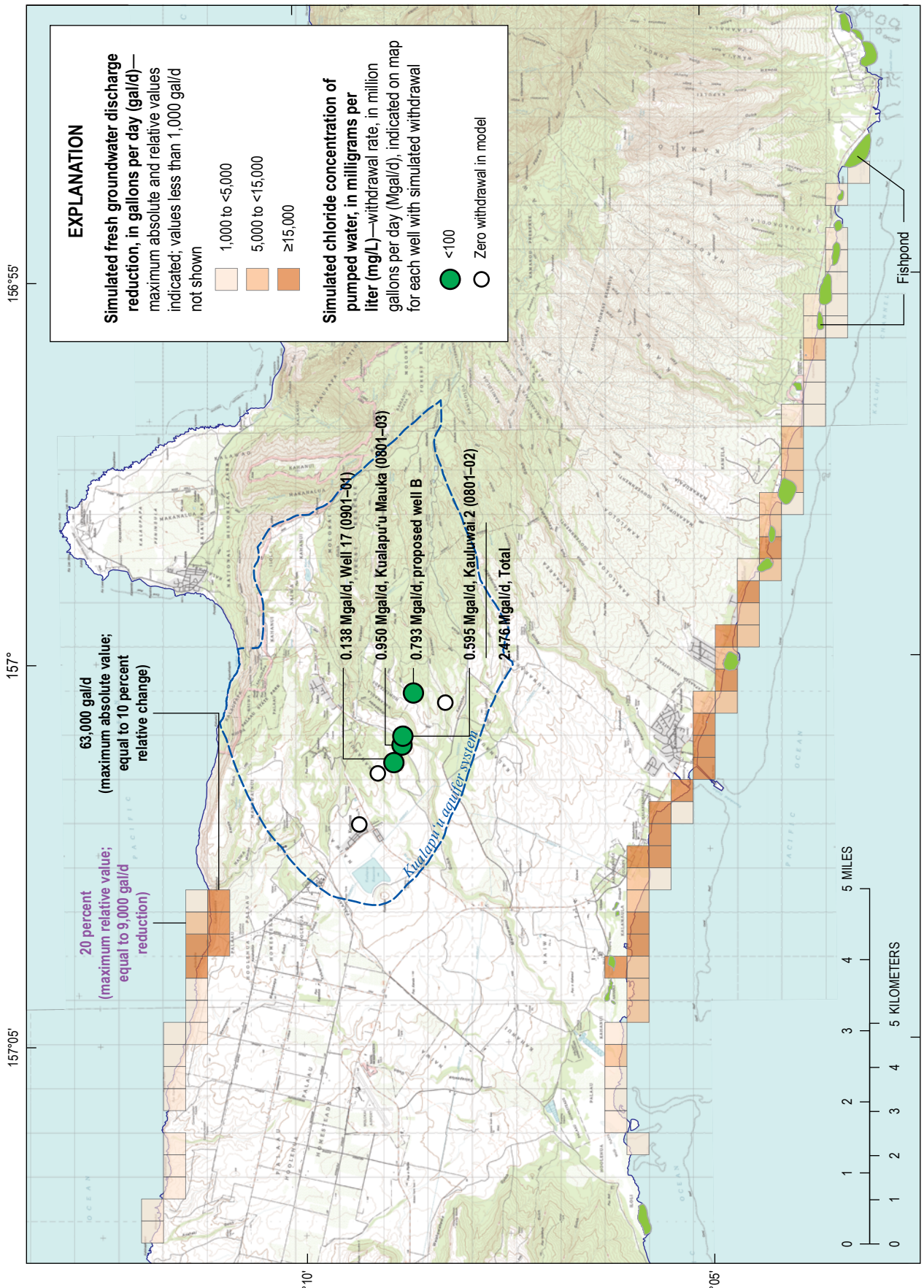

Base modified from U.S. Geological Survey Digital Raster Graphics topographic map, 1:24,000 scale.
Universal Transverse Mercator projection, zone 4, NAD 83 datum.

Figure 24. Map of the Kualapu'u aquifer system on Moloka'i, Hawai'i showing scenario 3 withdrawal rates from wells and fresh groundwater-discharge reduction (relative to scenario 1).

simulated relative reduction in fresh groundwater discharge from any 1,640 by 1,640 ft cell was 20 percent, corresponding to a reduction of 0.009 Mgal/d (fig. 24).

Scenario 4—Increased Rate for Well 0801–03; Pending Water-Use Permit Rate for Well 0901–01; Additional Withdrawal from Proposed Well B

Recharge and withdrawals in scenario 4 are identical to those in scenario 3, except the withdrawal from well 0901–01 was increased from 0.1380 to 1.1440 Mgal/d, consistent with the pending water-use permit rate. For scenario 4, total withdrawal from wells in the Kualapu‘u aquifer system is 3.4816 Mgal/d.

For scenario 4, the estimated chloride concentration of groundwater withdrawn from proposed well B is less than 100 mg/L, the estimated chloride concentration of groundwater withdrawn from well 0901–01 is between 100 and 200 mg/L, and the estimated chloride concentrations of groundwater withdrawn from wells 0801–02 and 0801–03 exceed the EPA secondary standard of 250 mg/L (fig. 25). Blending water from wells 0801–02 and 0801–03 with water produced from other wells could be considered as an option to supply water with chloride concentration less than 250 mg/L.

Increased withdrawals in scenario 4 relative to the baseline scenario cause a reduction of freshwater discharge to the nearshore area (fig. 25). The greatest simulated reduction in fresh groundwater discharge from any 1,640 by 1,640 ft cell occurs northwest of the Kualapu‘u aquifer system and was 0.133 Mgal/d, representing 21 percent of the baseline discharge from that cell. The greatest simulated relative reduction in fresh groundwater discharge from any 1,640 by 1,640 ft cell was 39 percent, corresponding to a reduction of 0.019 Mgal/d (fig. 25).

Scenario 5—Proposed Well A Replaces Well 0801–03; Domestic-Need Rate for Well 0901–01; Additional Withdrawal from Proposed Well B

Recharge and withdrawals in scenario 5 are identical to those in scenario 3, except the withdrawal of 0.9500 Mgal/d from well 0801–03 was transferred to proposed well A. This scenario is intended to reflect a possible new well site, with well 0801–03 being retained for standby purposes. For scenario 5, total withdrawal from wells in the Kualapu‘u aquifer system is 2.4756 Mgal/d, identical to the total withdrawal in scenario 3 and greater than the total withdrawal in the baseline scenario (1.5215 Mgal/d).

For scenario 5, the estimated chloride concentrations of groundwater withdrawn from wells 0801–02, 0901–01, and proposed wells A and B are less than 100 mg/L (fig. 26). Spreading out withdrawals from the Kualapu‘u aquifer system in scenario 5, relative to scenario 3, causes an overall improvement in the simulated quality of water withdrawn from production wells in the Kualapu‘u aquifer system.

Increased withdrawals in scenario 5 relative to the baseline scenario cause a reduction of freshwater discharge to the nearshore area (fig. 26). The greatest simulated reduction in fresh groundwater discharge from any 1,640 by 1,640 ft cell occurs northwest of the Kualapu‘u aquifer system and was 0.065 Mgal/d, representing 10 percent of the baseline discharge from that cell. The greatest simulated relative reduction in fresh groundwater discharge from any 1,640 by 1,640 ft cell was 20 percent, corresponding to a reduction of 0.010 Mgal/d (fig. 26).

Scenario 6—Proposed Well A Replaces Well 0801–03; Pending Water-Use Permit Rate for Well 0901–01; Additional Withdrawal from Proposed Well B

Recharge and withdrawals in scenario 6 are similar to those in scenario 4, except the withdrawal of 0.9500 Mgal/d from well 0801–03 was transferred to proposed well A. For scenario 6, the total withdrawal from wells in the Kualapu‘u aquifer system is 3.4816 Mgal/d, identical to the total withdrawal in scenario 4.

For scenario 6, the estimated chloride concentration of groundwater withdrawn from proposed well B is less than 100 mg/L, the estimated chloride concentration of groundwater withdrawn from proposed well A is between 100 and 200 mg/L, the estimated chloride concentration of groundwater withdrawn from well 0801–02 exceeds 200 mg/L, and the estimated chloride concentration of groundwater withdrawn from well 0901–01 exceeds 250 mg/L (but is less than 275 mg/L) (fig. 27). Thus, spreading out withdrawals from the Kualapu‘u aquifer system in scenario 6, relative to scenario 4, results in improved water quality from using proposed well A instead of well 0801–03, but also causes an increase in chloride concentration of groundwater withdrawn from well 0901–01.

Increased withdrawals in scenario 6 relative to the baseline scenario cause a reduction of freshwater discharge to the nearshore area (fig. 27). The greatest simulated reduction in fresh groundwater discharge from any 1,640 by 1,640 ft cell occurs northwest of the Kualapu‘u aquifer system and was 0.136 Mgal/d, representing 22 percent of the baseline discharge from that cell. The greatest simulated relative reduction in fresh groundwater discharge from any 1,640 by 1,640 ft cell was 40 percent, corresponding to a reduction of 0.019 Mgal/d (fig. 27).

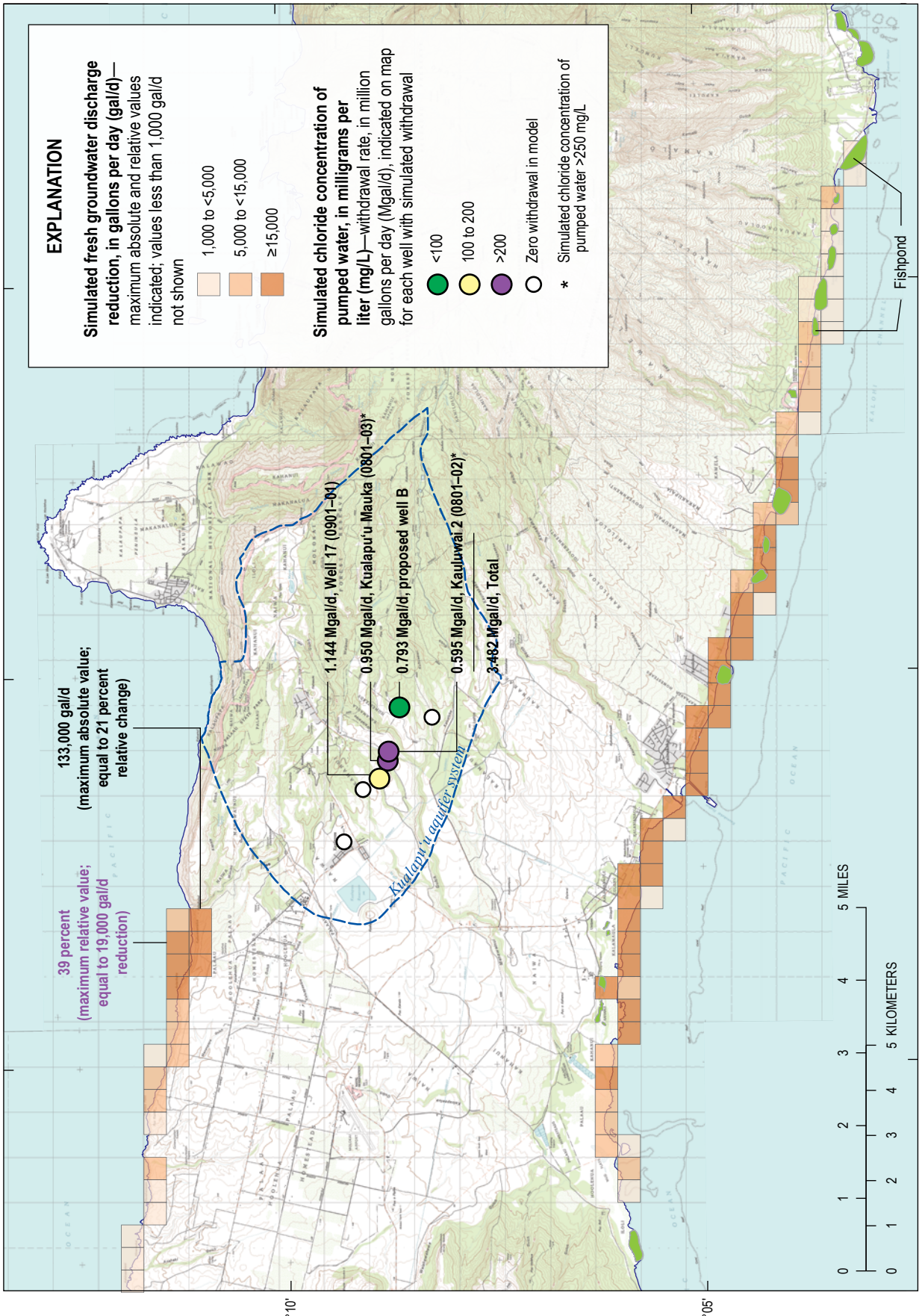

Base modified from U.S. Geological Survey Digital Raster Graphics topographic map, 1:24,000 scale.
Universal Transverse Mercator projection, zone 4, NAD 83 datum.

Figure 25. Map of the Kualapu'u aquifer system on Moloka'i, Hawai'i showing scenario 4 withdrawal rates from wells and fresh groundwater-discharge reduction (relative to scenario 1).

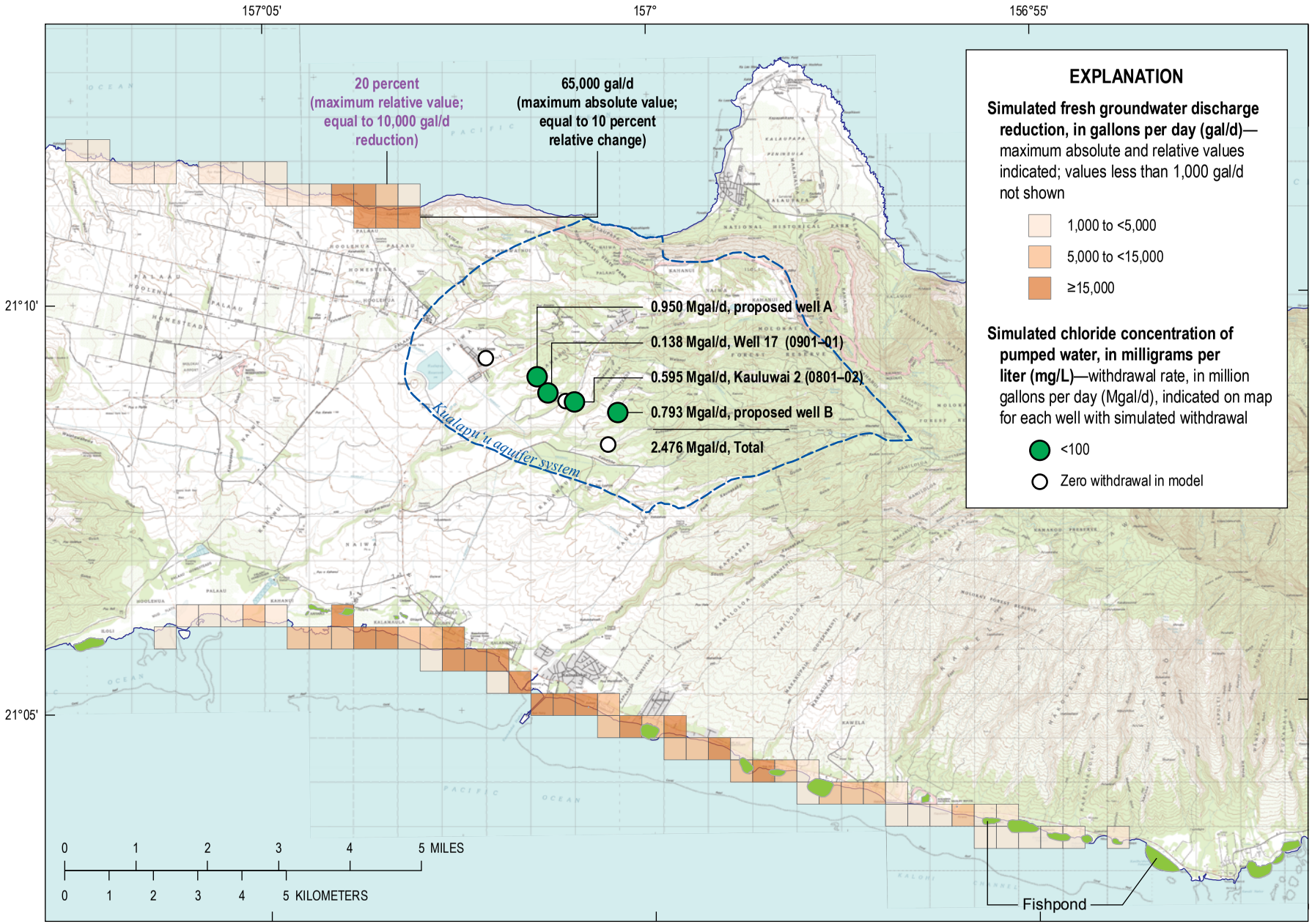

Base modified from U.S. Geological Survey Digital Raster Graphics topographic map, 1:24,000 scale.
Universal Transverse Mercator projection, zone 4, NAD 83 datum.

Figure 26. Map of the Kualapu'u aquifer system on Moloka'i, Hawai'i showing scenario 5 withdrawal rates from wells and fresh groundwater-discharge reduction (relative to scenario 1).

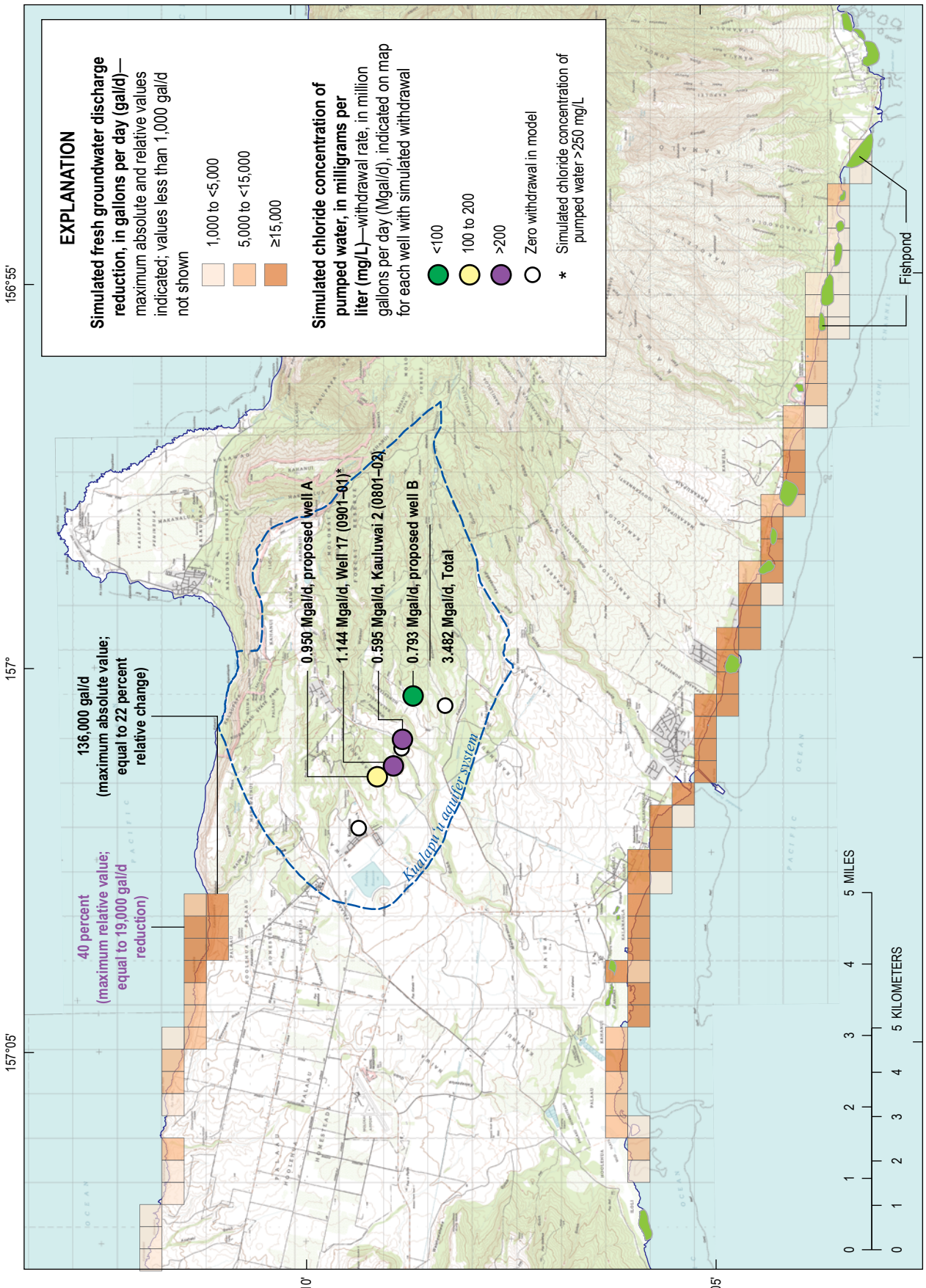

Base modified from U.S. Geological Survey Digital Raster Graphics topographic map, 1:24,000 scale.
Universal Transverse Mercator projection, zone 4, NAD 83 datum.

Figure 27. Map of the Kualapu'u aquifer system on Moloka'i, Hawai'i showing scenario 6 withdrawal rates from wells and fresh groundwater-discharge reduction (relative to scenario 1).

Scenario 7— Proposed Well B Replaces Well 0801–03; Pending Water-Use Permit Rate for Well 0901–01; Additional Withdrawal from Proposed Well A

Recharge and withdrawals in scenario 7 are similar to those in scenario 6, except the withdrawal rates from proposed wells A and B are switched. For scenarios 6 and 7, total withdrawal from wells in the Kualapu‘u aquifer system is 3.4816 Mgal/d.

For scenario 7, the estimated chloride concentration of groundwater withdrawn from proposed well B is less than 100 mg/L, the estimated chloride concentration of groundwater withdrawn from proposed well A is between 100 and 200 mg/L, and the estimated chloride concentrations of groundwater withdrawn from wells 0801–02 and 0901–01 exceed 200 mg/L (less than 250 mg/L) (fig. 28). Thus, reducing the withdrawal from proposed well A in scenario 7, relative to scenario 6, results in a slight improvement in the simulated quality of water withdrawn from nearby well 0901–01.

Increased withdrawals in scenario 7 relative to the baseline scenario cause a reduction of freshwater discharge to the nearshore area (fig. 28). The greatest simulated reduction in fresh groundwater discharge from any 1,640 by 1,640 ft cell occurs northwest of the Kualapu‘u aquifer system and was 0.135 Mgal/d, representing 22 percent of the baseline discharge from that cell. The greatest simulated relative reduction in fresh groundwater discharge from any 1,640 by 1,640 ft cell was 40 percent, corresponding to a reduction of 0.019 Mgal/d (fig. 28).

Scenario 8— Proposed Well B Replaces Well 0801–03; Pending Water-Use Permit Rate for Well 0901–01; Additional Withdrawal from Proposed Wells C and D

Recharge and withdrawals in scenario 8 are similar to those in scenario 7, except the withdrawal from proposed well A (0.7926 Mgal/d) was transferred farther east to proposed wells C and D and increased by 1 Mgal/d to 1.7926 Mgal/d. In scenario 8, total withdrawal from wells in the Kualapu‘u aquifer system is 4.4816 Mgal/d.

For scenario 8, the estimated chloride concentration of groundwater withdrawn from proposed well D is less than 100 mg/L, the estimated chloride concentrations of groundwater withdrawn from wells 0901–01 and proposed well B are between 100 and 200 mg/L, the estimated chloride concentration of groundwater withdrawn from proposed well C exceeds 200 mg/L, and the estimated chloride concentration of groundwater withdrawn from well 0801–02 exceeds 250 mg/L (less than 275 mg/L) (fig. 29). Simulation results from scenario 8 indicate that the chloride concentrations from production wells in the Kualapu‘u aquifer system mostly remain below the EPA secondary standard. However, hydrogeologic conditions in the eastern part of the Kualapu‘u aquifer system are uncertain because of a lack of drilled wells in the area.

Increased withdrawals in scenario 8 relative to the baseline scenario cause a reduction of freshwater discharge to the nearshore area (fig. 29). The greatest simulated reduction in fresh groundwater discharge from any 1,640 by 1,640 ft cell occurs directly south of the Kualapu‘u aquifer system and was 0.211 Mgal/d, representing 10 percent of the baseline discharge from that cell. The greatest simulated relative reduction in fresh groundwater discharge from any 1,640 by 1,640 ft cell was 40 percent, corresponding to a reduction of 0.019 Mgal/d (fig. 29).

Scenario 9—Reduced Recharge; Proposed Well A Replaces Well 0801–03; Pending Water-Use Permit Rate for Well 0901–01; Additional Withdrawal from Proposed Well B

In scenario 9, recharge was everywhere reduced by 15 percent relative to the recharge in the other scenarios, and simulated withdrawals in scenario 9 are identical to those in scenario 6. The reduced recharge is a simplified scenario that generally is consistent with end-of-century drying projected for Moloka‘i (Elison Timm and others, 2015).

For scenario 9, the estimated chloride concentrations of groundwater withdrawn from wells 0801–02, 0901–01, proposed well A, and proposed well B are greater than 250 mg/L. Thus, model results indicate that a reduction in recharge can have a substantial negative effect on the simulated quality of water withdrawn from production wells in the Kualapu‘u aquifer system. Relative to scenario 6, the reduction in fresh groundwater discharge in scenario 9 is equal to the 15 percent reduction in freshwater recharge simulated in scenario 9.

Implications of Scenarios

Results of the simulated withdrawal scenarios indicate that increased withdrawals, relative to 2016–17 rates, may produce groundwater with chloride concentrations below the EPA secondary standard of 250 mg/L. However, the quality of water withdrawn from production wells is dependent on the rate and distribution of the withdrawals. High rates of withdrawal from closely spaced wells tend to enhance the potential for increased salinity of the water withdrawn from production wells in the Kualapu‘u aquifer system. Spreading out withdrawals may help to produce water of acceptable quality. However, hydrogeologic conditions and groundwater quality in parts of the Kualapu‘u aquifer system (primarily in the eastern part) are uncertain because of the lack of drilled wells and, thus, model results also contain unquantified uncertainty. Model results also indicate that the rate of groundwater recharge may be a controlling factor for the quality of water withdrawn from production wells in the Kualapu‘u aquifer system. A reduction in groundwater recharge in the future (all other factors remaining equal) would tend to cause increased salinity of water withdrawn from production wells.

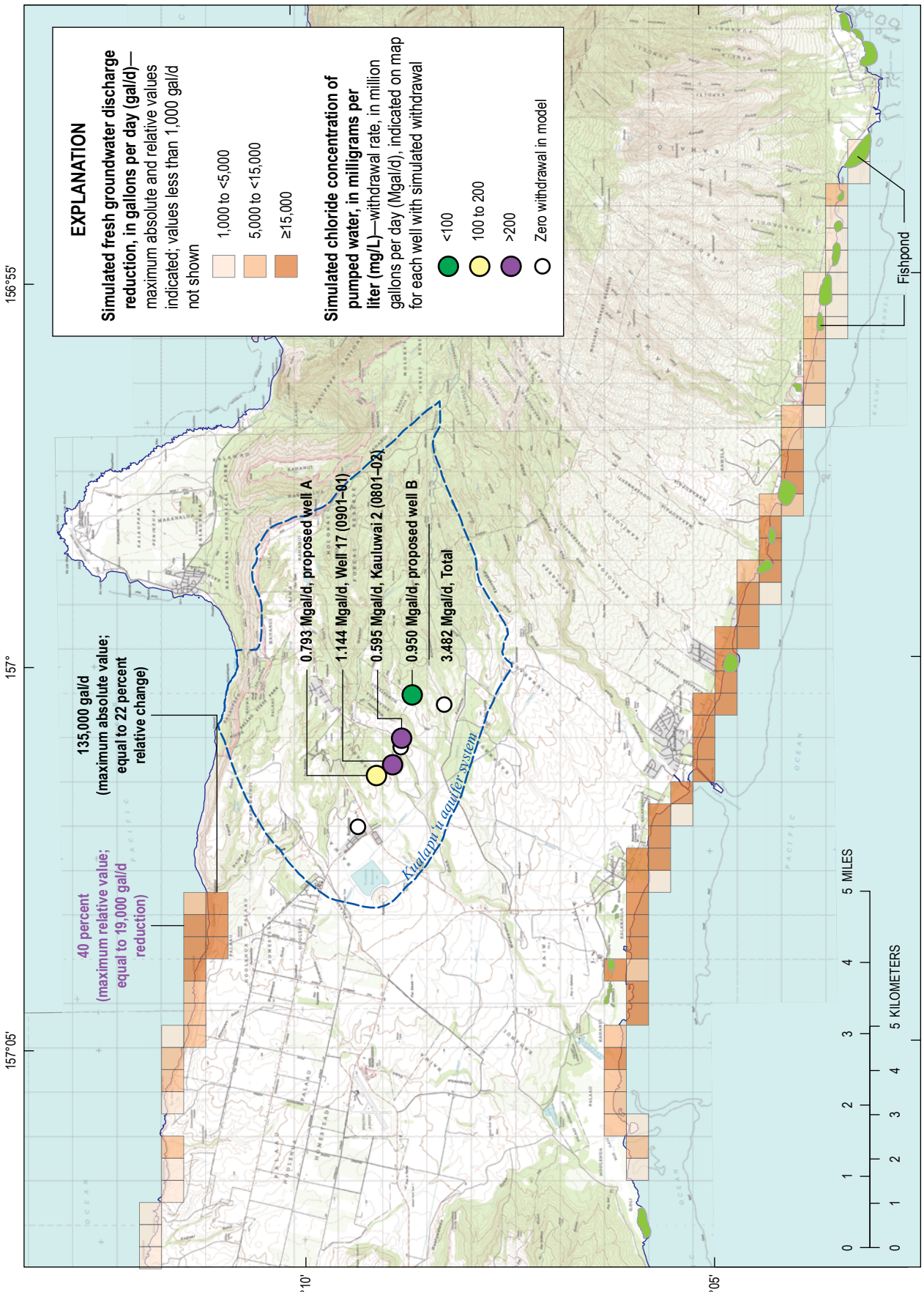

Base modified from U.S. Geological Survey Digital Raster Graphics topographic map, 1:24,000 scale.
Universal Transverse Mercator projection, zone 4, NAD 83 datum.

Figure 28. Map of the Kualapu‘u aquifer system on Moloka‘i, Hawai‘i showing scenario 7 withdrawal rates from wells and fresh groundwater-discharge reduction (relative to scenario 1).

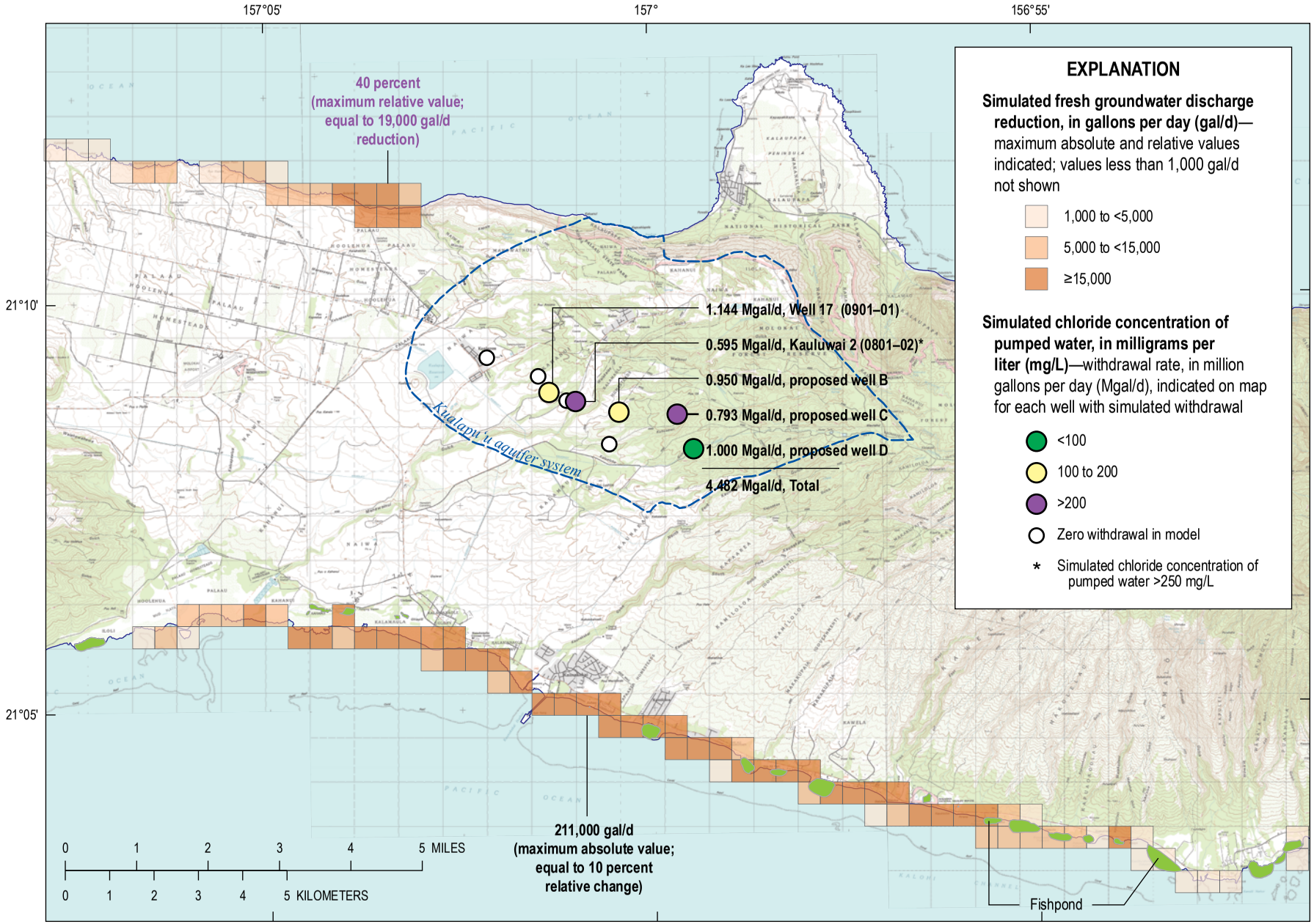

Base modified from U.S. Geological Survey Digital Raster Graphics topographic map, 1:24,000 scale.
Universal Transverse Mercator projection, zone 4, NAD 83 datum.

Figure 29. Map of the Kualapu'u aquifer system on Moloka'i, Hawai'i showing scenario 8 withdrawal rates from wells and fresh groundwater-discharge reduction (relative to scenario 1).

Limitations

The numerical groundwater models developed for this study have several limitations, including their nonuniqueness and inability to account for local-scale heterogeneities. Different distributions of hydraulic properties and recharge may result in comparable model results, although recharge estimates were based on the best available information. Data from a limited number of wells are available to constrain the model. For example, no wells are available in the eastern part of the Kualapuʻu aquifer system to understand hydrogeologic conditions and groundwater quality there. The numerical models developed for this study also simulate conditions on a regional scale and may not accurately predict either the water level at an individual well or the salinity of water withdrawn from that well. Salinity of water pumped from a well may be controlled by local heterogeneities in the aquifer that are not represented in the model. Also, the level of model discretization affects the numerical accuracy with which transport mechanisms are simulated. The model has several other limitations for predictive purposes because of the various assumptions used and possible uncertainties in input data. These limitations are discussed below.

Differences between measured and simulated water levels are greater in some areas than others, which may reflect uncertainties in recharge or withdrawal, boundary conditions, assigned parameter values in the model, or representations of the different hydrogeological features in the model. Recharge estimates in Hawaiʻi generally are based on water-budget computations that could be improved with a better understanding of the spatial distributions of rainfall, evapotranspiration, runoff, and land-cover characteristics. Additional climate stations and continuous-record streamgaging stations on Molokaʻi would lead to improved recharge estimates. Other studies that could enhance understanding of recharge include (1) quantifying rates of evapotranspiration of native and nonnative forest species, (2) directly measuring recharge using field lysimeters, (3) measuring changes in soil moisture below the plant root zone, (4) quantifying increases in the chloride concentration of infiltrating water caused by evapotranspiration, (5) measuring groundwater discharge with offshore seepage meters, and (6) developing an integrated surface-water/groundwater model. Improved recharge estimates in the study area will lead to improved estimates for parameter values in the numerical groundwater model and greater confidence in model results.

Withdrawals represented in the model were based on available information. Unreported withdrawals and uncertainties in reported withdrawals that cannot be quantified also affect the accuracy of model results.

For this study, no-flow boundaries were assigned in the west, which precludes movement of groundwater across this boundary. Although some flow likely takes place across this boundary, the amount simulated with the island-wide model was small (less than 0.0005 Mgal/d).

Heterogeneity in the groundwater system likely exists but is currently poorly understood. Values assigned to model hydraulic parameters generally were based on existing estimates and controlled by observed hydrogeologic conditions. However, some of these parameter values may be poorly known. Simulated water levels are typically controlled by the hydraulic-conductivity values assigned in the model. Simulated salinity can be controlled by various hydraulic parameters. A sensitivity analysis of selected hydraulic parameters is included in appendix 2. Results of the sensitivity analysis indicate that the simulated chloride concentration of pumped water in the Kualapuʻu area is sensitive to the effective porosity, dispersivity, and vertical anisotropy of the aquifer.

Additional wells or geophysical studies in areas with limited information would improve the understanding of hydrogeologic conditions, presence and geometry of barriers to flow, thickness of coastal sedimentary deposits, and distribution of hydraulic characteristics. Controlled aquifer tests that monitor withdrawal and water-level conditions throughout the aquifer can improve estimates of the distribution of hydraulic characteristics in the study area. Accurate water-level and withdrawal data can be used for calibration of numerical groundwater models, particularly during periods when recharge does not vary.

Confidence in model results can be improved by addressing the limitations described in this section. In particular, improved estimates of recharge and the distribution of model parameters will lead to an increase of model reliability.

Summary

Since the 1990s, the chloride concentrations of water pumped from some wells on Molokaʻi have increased, which has led to concern over groundwater availability. A growing concern related to groundwater development on Molokaʻi is the effect of withdrawals on groundwater-dependent ecosystems. To ensure effective management of the groundwater resources of Molokaʻi and to plan for possible growth on the island, an improved understanding of the hydrologic effects of proposed groundwater withdrawals is needed. An accurate understanding of how much fresh groundwater in the Kualapuʻu aquifer system can be developed for future needs is critically important, from economic, cultural, and resource standpoints.

To address the information needs of managers and community stakeholders on Molokaʻi, the U.S. Geological Survey developed a numerical groundwater model capable of simulating salinity change and reduction in groundwater discharge in coastal areas of central and southern Molokaʻi. Estimates of groundwater recharge from the soil root zone, needed as input to the numerical groundwater model, were made using a daily water budget for each decade during 1940−2012 (the period 2000−12 spanned 13 years) and the most current available data, including the distributions of monthly rainfall and potential evapotranspiration. Total island

recharge during the decadal periods ranged from a low of about 189 Mgal/d during the 1970s to a high of 278 Mgal/d during the 1960s. These recharge estimates were used to develop an island-wide numerical groundwater model with simplifying assumptions (sharp interface between freshwater and saltwater; two-dimensional flow). The island-wide model provided estimates of groundwater inflows that were used for the main area of interest simulated with a three-dimensional numerical groundwater model.

Aquifer hydraulic properties for the three-dimensional numerical groundwater model were estimated using available water-level and salinity information. Simulated withdrawal scenarios were selected in consultation with water managers and stakeholders and consisted of: (1) a baseline scenario using average recharge (1978−2007 rainfall and 2010 land cover) and average 2016−17 withdrawals; (2) a scenario using average recharge and withdrawals from existing wells at pending (as of January 2019) water-use permit rates; (3) six scenarios using average recharge and selected withdrawals from existing and proposed new wells; and (4) a scenario using reduced recharge and selected withdrawals from existing and proposed new wells.

Results of the simulated withdrawal scenarios indicate that increased withdrawals, relative to 2016–17 rates, may produce groundwater with chloride concentrations below 250 mg/L. However, the quality of water withdrawn from production wells is dependent on the rate and distribution of the withdrawals. For all nonbaseline scenarios, simulated groundwater discharge to the nearshore environment is reduced relative to the baseline scenario. Areas of discharge reduction may correspond to areas used for cultural or subsistence purposes. Although the numerical groundwater model is capable of quantifying the rate of groundwater-discharge reduction associated with each withdrawal scenario, the model cannot determine whether the reduction is acceptable or not. Such a determination is dependent on evaluating the cultural, social, and economic benefits and costs associated with increased groundwater withdrawals.

Model results indicate that the rate of groundwater recharge may be a controlling factor for the quality of water withdrawn from production wells in the Kualapuʻu aquifer system. A reduction in groundwater recharge in the future (all other factors remaining equal) would tend to cause increased salinity of water withdrawn from production wells.

The three-dimensional numerical groundwater model developed for this study has several limitations, including its nonuniqueness and inability to account for local-scale heterogeneities. Data from a limited number of wells are available to constrain the model. For example, no wells are available in the eastern part of the Kualapuʻu aquifer system to understand hydrogeologic conditions and groundwater quality there. The numerical model developed for this study may not accurately predict the salinity of water withdrawn from a production well because salinity of water pumped from a well may be controlled by local heterogeneities in the aquifer that are not represented in the model. The model has several other limitations for predictive purposes because of the various assumptions used and possible uncertainties in input data. Nevertheless, the three-dimensional numerical groundwater model developed for this study utilizes the latest available hydrologic and geologic information, and it is considered a useful tool for understanding the hydrologic effects of additional groundwater withdrawals.

References Cited

Anthony, S.S., 1995, Evaluation of ground-water resources from available data, 1992, East Molokai Volcano, Hawaii: U.S. Geological Survey Water-Resources Investigations Report 95–4180, 32 p., accessed June 10, 2019, at https://doi.org/10.3133/wri954180.

Beeson, M.H., 1976, Petrology, mineralogy, and geochemistry of the East Molokai Volcanic Series, Hawaii: U.S. Geological Survey Professional Paper 961, 53 p., accessed November 15, 2018, at https://doi.org/10.3133/pp961.

Blumenstock, D.I., and Price, S., 1967, Climate of Hawaii *in* Climates of the States, no. 60–51, Climatography of the United States: Washington, D.C., U.S. Department of Commerce, 27 p.

Domenico, P.A., and Schwartz, F.W., 1990, Physical and chemical hydrogeology: New York, John Wiley, 824 p.

Elison Timm, O., Giambelluca, T.W., and Diaz, H.F., 2015, Statistical downscaling of rainfall changes in Hawai‘i based on the CMIP5 global model projections: Journal of Geophysical Research: Atmospheres, v. 120, p. 92–112, accessed November 15, 2018, at https://doi.org/10.1002/2014JD022059.

Essaid, H.I., 1990, The computer model SHARP, a quasi-three-dimensional finite-difference model to simulate freshwater and saltwater flow in layered coastal aquifer systems: U.S. Geological Survey Water-Resources Investigations Report 90–4130, 181 p., accessed November 15, 2018, at https://doi.org/10.3133/wri904130.

Farber, J.M., 1997, Ancient Hawaiian fishponds, can restoration succeed on Molokaʻi: Encinitas, California, Neptune House, 99 p.

Flinders, A.F., Ito, G., Garcia, M.O., Sinton, J.M., Kauahikaua, J., and Taylor, B., 2013, Intrusive dike complexes, cumulate cores, and the extrusive growth of Hawaiian volcanoes: Geophysical Research Letters, v. 40, p. 3367–3373, https://doi.org/10.1002/grl.50633.

Frazier, A.G., Giambelluca, T.W., Diaz, H.F., and Needham, H.L., 2016, Comparison of geostatistical approaches to spatially interpolate month-year rainfall for the Hawaiian Islands: International Journal of Climatology, v. 36, no. 3, p. 1459–1470, https://doi.org/10.1002/joc.4437.

Freeze, R.A., and Cherry, J.A., 1979, Groundwater: Englewood Cliffs, N.J., Prentice-Hall, Inc., 604 p.

Furumoto, A.S., Campbell, J.F., and Hussong, D.M., 1970, Seismic studies of subsurface structure in the Ewa coastal plain, Oahu, Hawaii: Pacific Science, v. 24, no. 4, p. 529–542, accessed August 29, 2019, at https://hdl.handle.net/10125/6267.

Giambelluca, T.W., Chen, Q., Frazier, A.G., Price, J.P., Chen, Y.-L., Chu, P.-S., Eischeid, J.K., and Delparte, D.M., 2013, Online rainfall atlas of Hawaiʻi: Bulletin of the American Meteorological Society, v. 94, p. 313–316, https://doi.org/10.1175/BAMS-D-11-00228.1.

Hawaiʻi Groundwater and Geothermal Resources Center, 2019, Hawaiʻi State water wells: digital well files of the Hawaiʻi Commission on Water Resource Management, accessed June 10, 2019, at https://www.higp.hawaii.edu/hggrc/projects/hawaii-state-waterwells/.

Hirashima, G.T., 1963, Aspects of ground-water storage and depletion along the Molokai Irrigation Tunnel, Molokai, Hawaii: State of Hawaiʻi, Department of Land and Natural Resources, Circular C20, 21 p.

Izuka, S.K., Engott, J.A., Rotzoll, K., Bassiouni, M., Johnson, A.G., Miller, L.D., and Mair, A., 2018, Volcanic aquifers of Hawaiʻi —hydrogeology, water budgets, and conceptual models (ver. 2.0, March 21018): U.S. Geological Survey Scientific Investigations Report 2015–5164, 158 p., accessed November, 15, 2018, at https://doi.org/10.3133/sir20155164.

Juvik, S.O., and Juvik, J.O., 1998, Atlas of Hawaiʻi (3d ed.): Honolulu, University of Hawaii Press, 333 p.

Kauahikaua, J. 1983, Estimation of fresh water abundances by electrical resistivity sounding on the Kalapapa Penninsula, island of Molokaʻi, Hawaiʻi: U.S. Geological Survey Open-File Report 83–65, variously paged, accessed August 29, 2019, at https://doi.org/10.3133/ofr8365.

Kauahikaua, J., 1993, Geophysical characteristics of the hydrothermal systems of Kilauea Volcano, Hawaiʻi: Geothermics, v. 22, no. 4, p. 271–299, accessed August 29, 2019, at https://doi.org/10.1016/0375-6505(93)90004-7

Langenheim, V.A.M., and Clague, D.A., 1987, The Hawaiian-Emperor volcanic chain, part II, stratigraphic framework of volcanic rocks of the Hawaiian Islands, chap. 1 *of* Decker, R.W., Wright, T.L., and Stauffer, P.H., eds., Volcanism in Hawaii: U.S. Geological Survey Professional Paper 1350, v. 1, p. 55–84, accessed November 15, 2018, at https://doi.org/10.3133/pp1350.

Lindgren, W., 1903, The water resources of Molokai, Hawaiian Islands: U.S. Geological Survey Water-Supply and Irrigation Paper 77, 62 p., accessed November 15, 2018, at https://doi.org/10.3133/wsp77.

Lockwood, J.P., and Lipman, P.W., 1987, Holocene eruptive history of Mauna Loa Volcano, chap. 18 *of* Decker, R.W., Wright, T.L., and Stauffer, P.H., eds., Volcanism in Hawaii: U.S. Geological Survey Professional Paper 1350, v. 1, p. 509–535, accessed November 15, 2018, at https://doi.org/10.3133/pp1350.

Lum, D.A., 2003, Geologic log of drill cuttings, Oceanic Institute salt water well, Keawanui/Kaamoloa, Molokai: Hawaiʻi Commission on Water Resource Management file for well 4-0350-009, accessed November 15, 2018, at https://www.higp.hawaii.edu/csav/WaterWells/Molokai/4-0350-009/4-0350-009.pdf.

MacCarthy, G.R., 1941, Geophysical studies on the island of Molokai, Territory of Hawaii: U.S. Department of the Interior Press Release 160579, October 3, 1941, 2 p.

Macdonald, G.A., 1956, The structure of Hawaiian volcanoes: Verhandelingen Van Het Koninklijk Nederlandsh Geologisch Mijnbouwkundig Genootschap, v. 16, p. 1–22.

Macdonald, G.A., Abbott, A.T., and Peterson, F.L., 1983, Volcanoes in the sea; the geology of Hawaii (2d ed.): Honolulu, University of Hawaiʻi Press, 517 p.

Malahoff, A., and Woollard, G.P., 1966, Magnetic surveys over the Hawaiian Islands and their geologic implications: Pacific Science, v. 20, no. 3, p. 265–311.

Mathewson, C.C., 1970, Submarine canyons and the shelf along the north coast of Molokai Island, Hawaiian Ridge: Pacific Science, v. 24, no. 2, p. 235–244.

Matsuoka, J., McGregor, D, Minerbi, L., and Akutagawa, M., eds., 1994, Governor's Molokaʻi Subsistence Task Force: Final Report, Honolulu, Hawaiʻi, June 1994, 225 p.

McDougall, I., 1964, Potassium-argon ages from lavas of the Hawaiian Islands: Geological Society of America Bulletin, v. 75, no. 2, p. 107–128.

Mink, J.F., and Lau, L.S., 1992, Aquifer identification and classification for Molokaʻi—Groundwater protection strategy for Hawaiʻi: University of Hawaiʻi Water Resources Research Center Technical Report no. 187, 31 p., accessed November 15, 2018, at http://hdl.handle.net/10125/1968.

Moore, J.G., and Krivoy, H.L., 1965, A reconnaissance gravity survey of the Island of Molokai, Hawaii: Pacific Science, v. 19, no. 3, p. 343–345.

National Oceanic and Atmospheric Administration, 2010, National Geophysical Data Center GEODAS on-line design-a-grid system, digital data, accessed May 26, 2010, at http://www.ngdc.noaa.gov/mgg/gdas/gd_designagrid.html.

National Park Service, 2013, Petition to designate the Keauhou aquifer system a Water Management Area: Petition for Water Management Area action submitted to the Hawai‘i Commission on Water Resource Management, 63 p., accessed June 11, 2019, at https://dlnr.hawaii.gov/cwrm/groundwater/activities/keauhou/.

Naughton, J.J., Macdonald, G.A., and Greenberg, V.A., 1980, Some additional potassium-argon ages of Hawaiian rocks; the Maui Volcanic Complex of Molokai, Maui, Lanai and Kahoolawe: Journal of Volcanology and Geothermal Research, v. 7, no. 3–4, p. 339–355.

Oki, D.S., 1997, Geohydrology and numerical simulation of the ground-water flow system of Molokai, Hawaii: U.S. Geological Survey Water-Resources Investigations Report 97–4176, 62 p., accessed November 15, 2018, at https://doi.org/10.3133/wri974176.

Oki, D.S., 2006, Numerical simulation of the hydrologic effects of redistributed and additional ground-water withdrawal, Island of Molokai, Hawaii: U.S. Geological Survey Scientific Investigations Report 2006–5177, 49 p., accessed November 15, 2018, at https://doi.org/10.3133/sir20065177.

Oki, D.S., 2007, Effects of ground-water withdrawal on Kaunakakai Stream environmental restoration plan, Moloka‘i, Hawai‘i: U.S. Geological Survey Scientific Investigations Report 2007–5128, 25 p., accessed November 15, 2018, at https://pubs.usgs.gov/sir/2007/5128/.

Oki, D.S., and Bauer, G.R., 2001, Drilling, construction, water-level, and water-quality information for the Kualapuu deep monitor well 4–0800–01, Molokai, Hawaii: U.S. Geological Survey Open-File Report 01–350, 19 p., accessed November 15, 2018, at https://doi.org/10.3133/ofr2001350.

Oki, D.S., and Meyer, W., 2001, Analytical versus numerical estimates of water-level declines caused by pumping, and a case study of the Iao aquifer, Maui, Hawaii: U.S. Geological Survey Water-Resources Investigations Report 00–4244, 31 p., accessed November 15, 2018, https://doi.org/10.3133/wri20004244.

Paillet, F.L., Williams, J.H., Oki, D.S., and Knutson, K.D., 2002, Comparison of formation and fluid-column logs in a heterogeneous basalt aquifer: Ground Water, v. 40, no. 6, p. 577–585.

Rotzoll, K., 2012, Numerical simulation of flow in deep open boreholes in a coastal freshwater lens, Pearl Harbor Aquifer, O‘ahu, Hawai‘i: U.S. Geological Survey Scientific Investigations Report 2012–5009, 39 p., accessed November 15, 2018, at https://doi.org/10.3133/sir20125009.

Sanderson, M., ed., 1993, Prevailing trade winds; weather and climate in Hawai‘i: Honolulu, University of Hawai‘i Press, 126 p.

Santo, L.T., 2001, Assessment and improvement recommendations for the Molokai Irrigation System: Hawaii Agriculture Research Center, Aiea, Hawaii, 49 p. plus appendixes, accessed June 10, 2019, at https://hdoa.hawaii.gov/wp-content/uploads/2013/07/ADCannual2001.pdf.

Sherrod, D.R., Sinton, J.M., Watkins, S.E., and Brunt, K.M., 2007, Geologic map of the State of Hawaii: U.S. Geological Survey Open-File Report 2007–1089, 83 p., 8 plates, scales 1:100,000 and 1:250,000, with GIS database, accessed November 15, 2018, at https://doi.org/10.3133/ofr20071089.

Souza, W.R., and Voss. C.I., 1987, Analysis of an anisotropic coastal aquifer system using variable-density flow and solute transport simulation: Journal of Hydrology, v. 92, p. 17–41, accessed August 29, 2019, at https://doi.org/10.1016/0022-1694(87)90087-4.

State of Hawai‘i, 1963, Summary of drilling log and pumping test for Kamiloloa Well 19, Kamiloloa, Molokai: Department of Land and Natural Resources, Division of Water and Land Development Circular C22, 9 p. plus plate.

State of Hawai‘i, 1997, Commission on Water Resource Management contested case hearing on water use, well construction and pump installation permit applications filed by Wai‘ola O Molokai, Inc. and Molokai Ranch, Limited, case CCH–MO96–1: Wai‘ola O Molokai, Inc. and Molokai Ranch Ltd.’s brief in support of water use permit application CCH–MO96–1, exhibit A–18, 1 p.

State of Hawai‘i, 1998, Commission on Water Resource Management contested case hearing on water use, well construction, and pump installation permit applications filed by Waiola O Molokai and Molokai Ranch, Limited, case CCH–MO96–1: Findings of Fact, Conclusions of Law, and Decision and Order, 73 p.

State of Hawai‘i, 2006, Hawaii statewide GIS program: State of Hawaii Office of Planning, accessed April 5, 2006 at http://www.hawaii.gov/dbedt/gis/fishponds.htm.

State of Hawai‘i, 2008, Water resource protection plan, June 2008: State of Hawai‘i, Commission on Water Resource Management, variously paginated, accessed November 15, 2018, at http://dlnr.hawaii.gov/cwrm/planning/hiwaterplan/wrpp/wrpp2008/.

State of Hawai‘i, 2011, Island population and housing units, State of Hawaii: 2010: State of Hawai‘i, Department of Business, Economic Development, and Tourism, Hawai‘i State Data Center Report 2010–3, 24 p., accessed December 16, 2019, at https://files.hawaii.gov/dbedt/census/Census_2010/PL94-171/Island_Report_Final.pdf.

Stearns, H.T., 1985, Geology of the State of Hawaii (2d ed.): Palo Alto, Pacific Books Publishers, 335 p.

Stearns, H.T., and Macdonald, G.A., 1947, Geology and ground-water resources of the island of Molokai, Hawaii: Hawaii Division of Hydrography Bulletin 11, 113 p., accessed November 15, 2018, at https://pubs.er.usgs.gov/publication/70161790.

Swain, L.A., 1973, Chemical quality of ground water in Hawaii: State of Hawaiʻi, Department of Land and Natural Resources, Report R48, 54 p.

Takasaki, K.J., 1986, Results of exploratory drilling for water in Waihanau Valley, Molokai, Hawaii: U.S. Geological Survey Water-Resources Investigations Report 85–4332, 26 p., accessed November 15, 2018, at https://doi.org/10.3133/wri854332.

Takasaki, K.J., and Mink, J.F., 1985, Evaluation of major dike-impounded ground-water reservoirs, island of Oahu: U.S. Geological Survey Water-Supply Paper 2217, 77 p., accessed November 15, 2018, at https://doi.org/10.3133/wsp2217.

U.S. Geological Survey, 2019, National Water Information System data available on the World Wide Web (USGS Water Data for the Nation), accessed June 10, 2019, at https://nwis.waterdata.usgs.gov/hi/nwis/gw.

Voss, C.I., 1999, USGS SUTRA code—history, practical use, and application in Hawaii, chap. 9 *of* Bear, J., Cheng, A.H.-D., Sorek, S., Ouazar, D., and Herrera, I., eds., Seawater intrusion in coastal aquifers—concepts, methods, and practices: Dordrecht, Kluwer Academic Publishers, p. 249–313.

Voss, C. I., and Provost, A.M., 2010, SUTRA, A model for saturated-unsaturated variable-density ground-water flow with solute or energy transport: U.S. Geological Survey Water-Resources Investigations Report 02–4231, version of September 22, 2010, 291 p., accessed November 15, 2018, https://doi.org/10.3133/wri024231.

Water Resource Associates, 1999, Waikolu Stream biological and hydrological monitoring study, Molokai, Hawaii: Hawaii Department of Agriculture, 42 p., plus figures and appendixes.

Weast, R.C., Lide, D.R., Astle, M.J., and Beyer, W.H., eds., 1989, CRC handbook of chemistry and physics (70th ed.): Boca Raton, Fla., CRC Press, variously paged.

Wentworth, C.K., 1939, The specific gravity of sea water and the Ghyben-Herzberg ratio at Honolulu: University of Hawaii Bulletin, v. 18, no. 8, 24 p.

Wentworth, C.K., and Macdonald, G.A., 1953, Structures and forms of basaltic rocks in Hawaii: U.S. Geological Survey Bulletin 994, 98 p., accessed November 15, 2018, at https://doi.org/10.3133/b994.

Appendixes 1–2

Appendix 1. Estimation of Recharge with a Water Budget

For this study, spatially distributed groundwater recharge on Molokaʻi was estimated using a water-budget computation. The water budget is designed to simulate, on a daily basis, the hydrological processes and physical conditions that affect groundwater recharge on Molokaʻi. Hydrological processes simulated by the water budget include rainfall, fog interception, irrigation, direct runoff, and evapotranspiration (ET). The water-budget method used in this study is similar to the methods used in previous U.S. Geological Survey (USGS) recharge studies of various parts of Hawaiʻi (Oki, 2002; Izuka and others, 2005; Engott and Vana, 2007; Engott, 2011; Johnson and others, 2018; Engott and others, 2017; Izuka and others, 2018). It is a "threshold-type" or "reservoir" method utilizing a variation of the Thornthwaite and Mather (1955) mass-balance procedure. The two generalized flow diagrams of the water budget—one for nonforest land covers and one for forest land covers—are shown in figure 1.1. See Engott and others (2017) for details on the water-budget equations used in this study. The water budget was used to estimate groundwater recharge under average climate conditions (1978–2007 rainfall), drought conditions (1998–2002 rainfall), and transient conditions during the seven decadal (or nearly decadal) time periods 1940–49, 1950–59, 1960–69, 1970–79, 1980–89, 1990–99, and 2000–12.

Water-Budget Subareas

The water-budget calculations for Molokaʻi subdivided the island into small areas with homogeneous properties, termed subareas. For each subarea, the water budget calculated recharge on a daily basis for the period of the scenario. The subarea map was generated using Esri ArcGIS software (www.esri.com) by intersecting (merging) spatial datasets that characterize the distribution of rainfall, fog, irrigation, reference ET, runoff, soil type, and land cover. Intersecting the spatial datasets resulted in 181,414 subareas—with an average area of about 0.9 acres—for the Molokaʻi water budget.

Input Data

Required input consists of data that quantify the spatial and temporal distributions of land cover, rainfall, fog interception, irrigation, ET, direct runoff, and soil properties.

Land Cover

Land-cover maps of Molokaʻi that are generally representative of conditions during the 1940s, 1950s, 1960s, 1970s, 1980s, 1990s, and 2000s were developed for this study. These maps identify 16 types of land cover (fig. 1.2) and were merged with other spatial datasets when creating the map of subareas for the water budget. The land-cover maps were created by modifying the LANDFIRE Existing Vegetation Type map for Molokaʻi (U.S. Geological Survey, 2010), herein referred to as the Landfire map. Modifications to the Landfire map included converting it from a raster to a vector dataset, combining similar land-cover classes, and superimposing the boundaries of agricultural fields appropriate for the time period. Information on crops and field boundaries during the time periods of interest was obtained from published maps and aerial images (Leopold and others, 1948; Harland Bartholomew and Associates, 1957; State of Hawaiʻi, 1966; Land Study Bureau, 1968; State of Hawaiʻi, 1969; U.S. Geological Survey, 1978; U.S. Department of Agriculture, 1983), supplemented with unpublished plantation maps and aerial images. Landfire groups "Hawaiian Dry Grassland," "Hawaiian Mesic Grassland," and "Introduced Perennial Grassland and Forbland" were combined to create the Grassland category for this study (fig. 1.2). Landfire groups "Hawaiian Dry Shrubland," "Hawaiian Mesic Shrubland," and "Introduced Upland Vegetation–Shrub" were combined to create the "Shrubland" category. Landfire groups "Hawaiian Dry Forest," "Hawaiian Mesic Forest," and "Hawaiian Rainforest" were combined to create the "Native-forest" category. The Landfire groups "Introduced Upland Vegetation–Treed," "Introduced Woody Wetland Vegetation," and "Managed Tree Plantation" were combined to create the "Alien-forest" category.

Monthly Rainfall

Gridded maps of monthly rainfall for each of the 876 months during 1940–2012 for the island of Molokaʻi (Giambelluca and others, 2013; Frazier and others, 2016) were used to define the spatial and temporal distributions of rainfall in the water-budget calculations. Rainfall maps are formatted 8.1-arcsecond grids, in which each grid cell covers an area of about 14 acres (770 by 820 ft) and has an estimated rainfall value for each month. Using Esri ArcGIS software, the monthly rainfall maps were converted from a raster grid to polygon format for use in the water budget. The rainfall polygons were intersected with the other spatial datasets when creating the map of subareas for the water budget.

Giambelluca and others (2013) developed mean monthly rainfall maps for the 1978–2007 period by interpolating mean monthly rainfall at rain-gaging stations rather than by computing the average rainfall in each grid cell from the monthly rainfall grids during 1978–2007. Cell-by-cell comparisons of mean monthly rainfall for the 1978–2007 period developed by interpolating mean monthly rainfall at rain-gaging stations and mean monthly rainfall computed for 1978–2007 from the monthly rainfall grids showed minor differences. For consistency, the monthly rainfall values were adjusted to produce the same mean monthly rainfall values for 1978–2007 as those developed by interpolating mean monthly rainfall at rain-gaging stations

Nonforest land covers

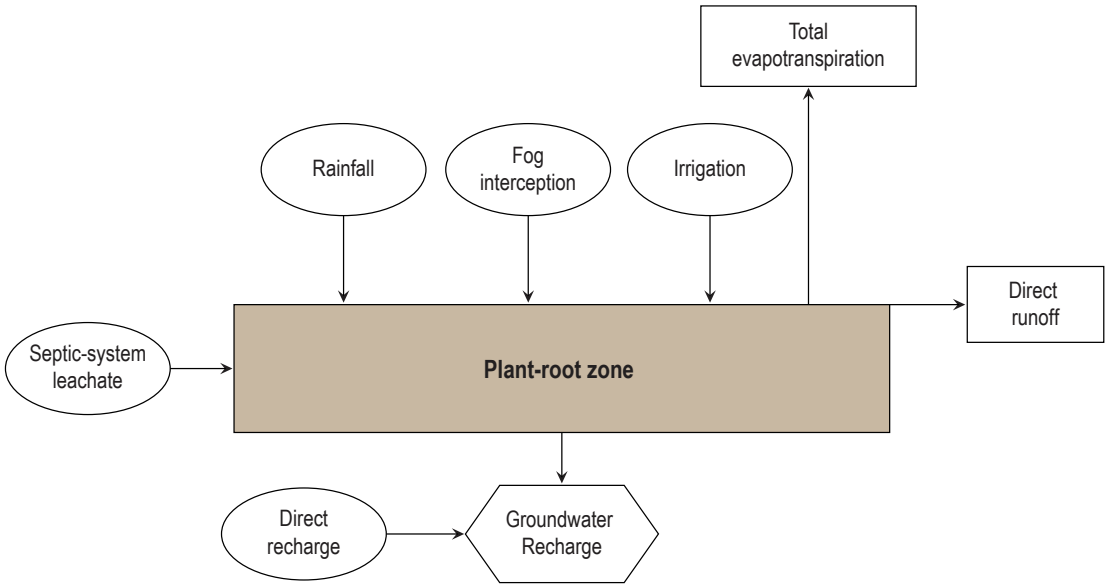

Forest land covers

(modified from McJannet and others, 2007)

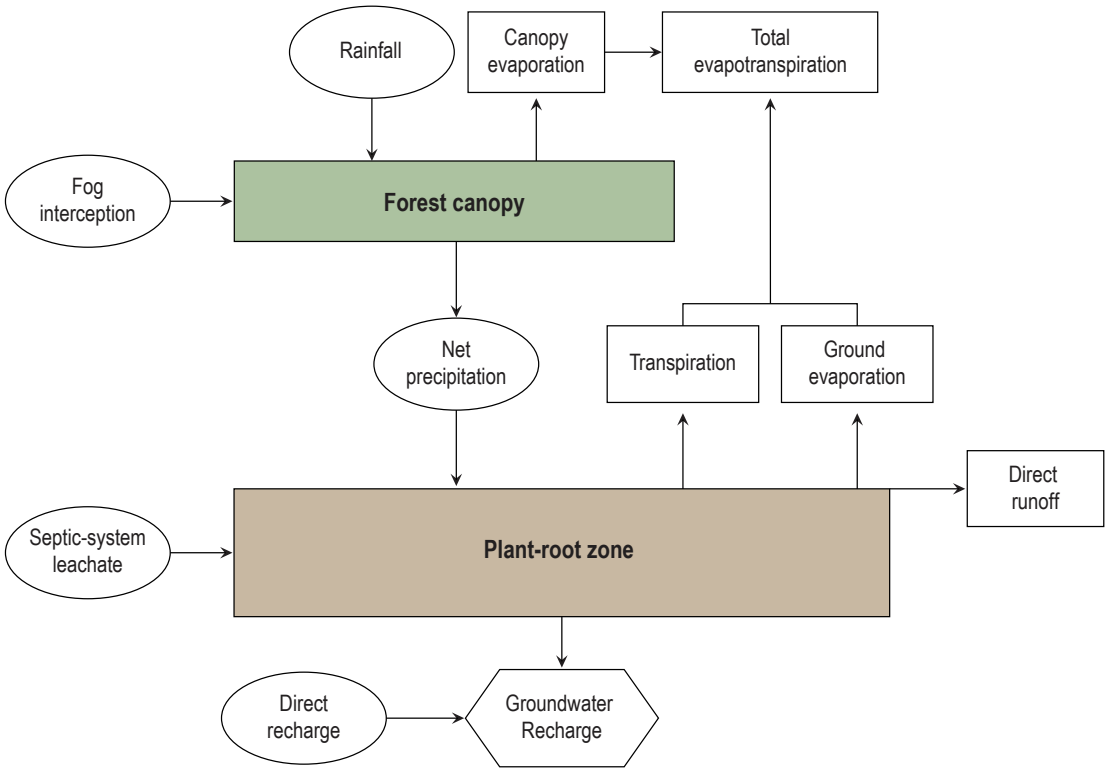

Figure 1.1. Generalized water-budget flow diagrams for nonforest and forest land covers.

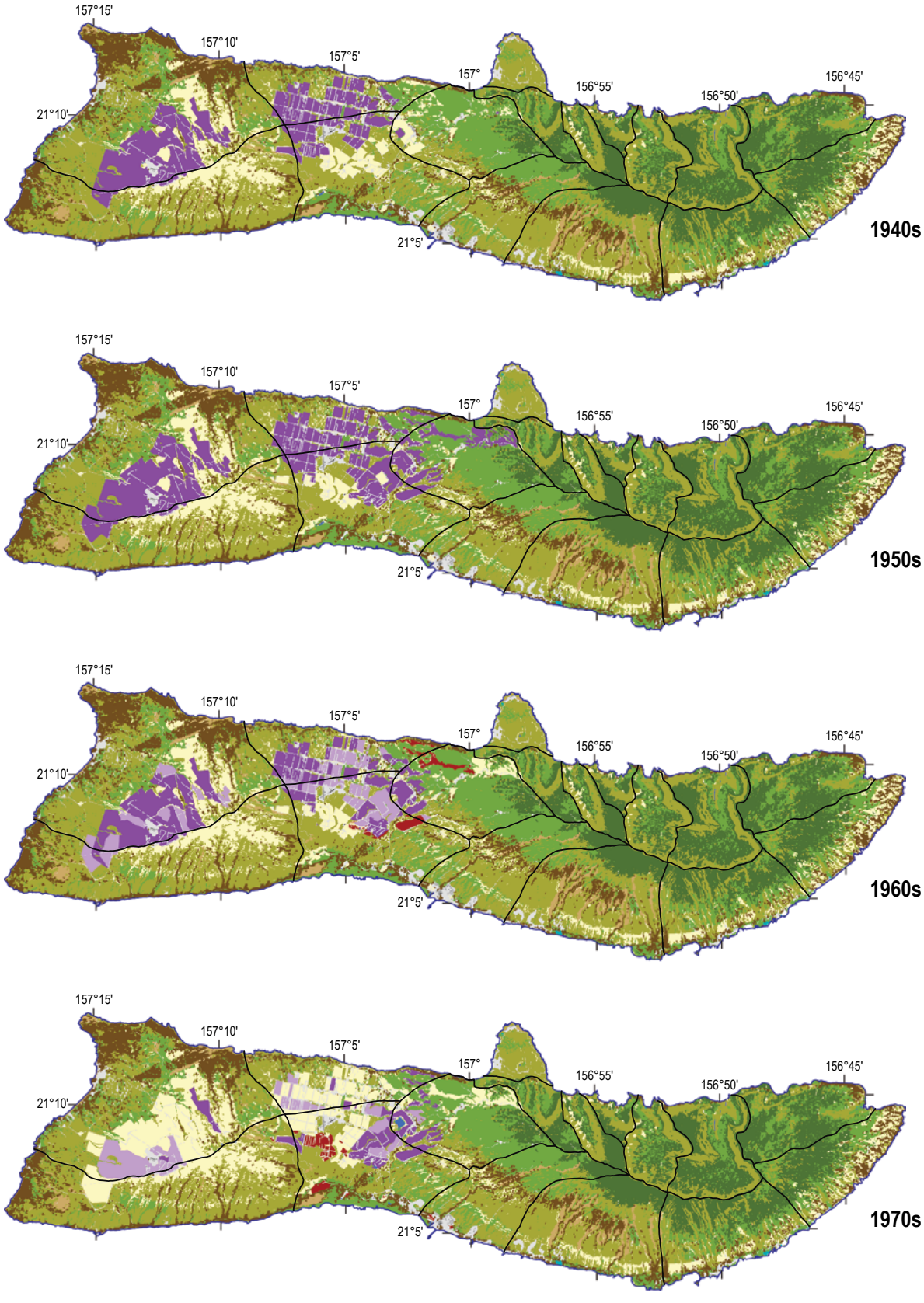

Figure 1.2. Maps of Molokaʻi, Hawaiʻi showing generalized land cover during selected decadal periods from 1940 to 2010.

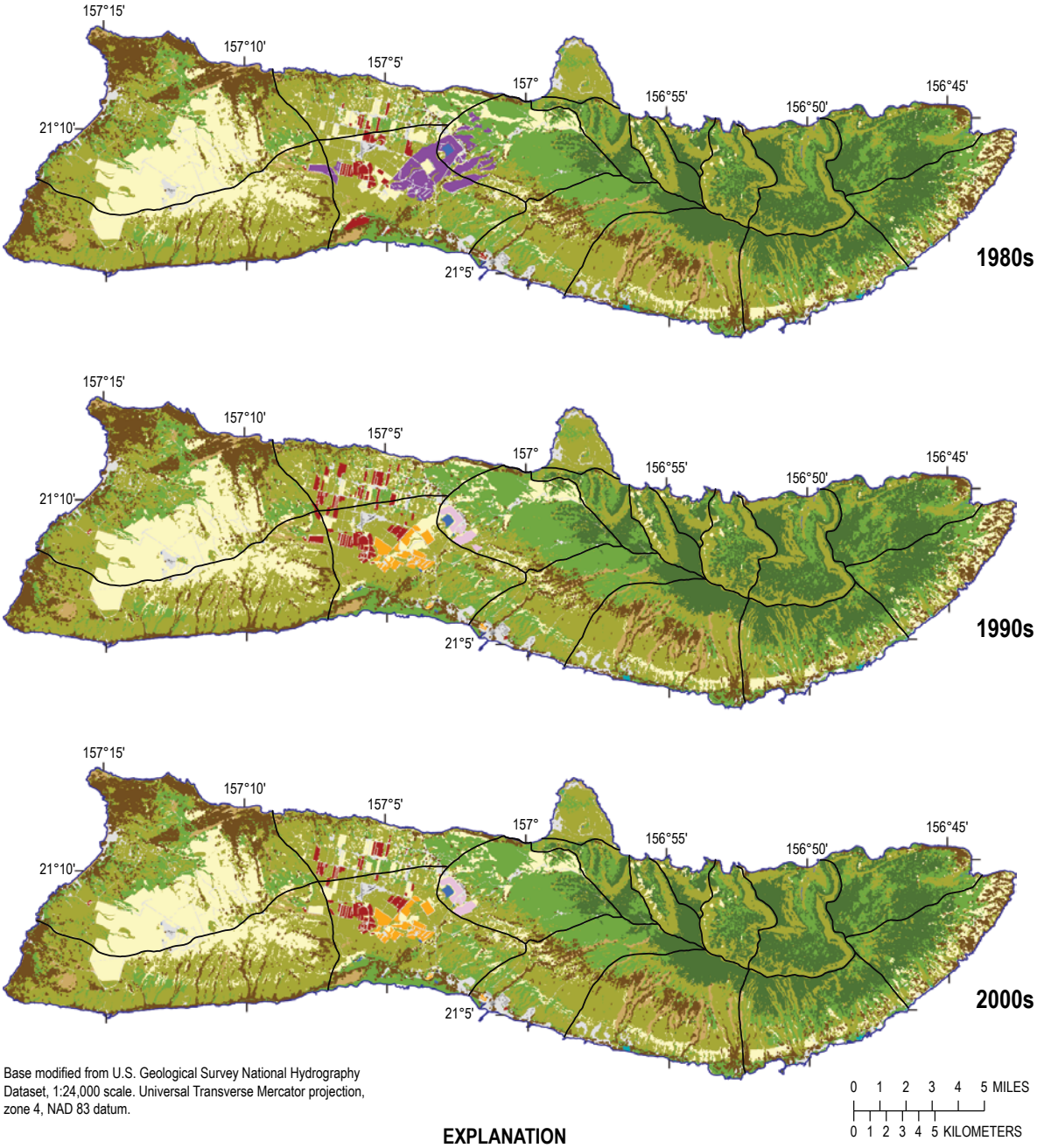

Figure 1.2.—Continued

(Giambelluca and others, 2013). A total of 12 monthly adjustment factors for each grid cell were determined as the ratio of the 1978–2007 mean monthly rainfall developed by interpolating mean monthly rainfall at rain-gaging stations (Giambelluca and others, 2013) to the 1978–2007 mean monthly rainfall calculated from the monthly values of each grid cell. In this study, the monthly rainfall for each grid cell was determined by multiplying the monthly rainfall by the appropriate monthly adjustment factor.

Daily Rainfall

Estimates of the actual daily rainfall distribution on Molokaʻi during 1940–2012 were not available and were not developed as part of this study. Although records of daily rainfall measurements at gages were available, reconstructing the actual daily rainfall pattern was not attempted because (1) records from many gages have considerable gaps, (2) the spatial interpolation of daily records for gages would have high uncertainty, and (3) the monthly rainfall maps (Giambelluca and others, 2013; Frazier and others, 2016) were considered to be the best dataset available for estimating historical rainfall patterns.

Daily rainfall was synthesized for input into the water budget by disaggregating the monthly values of the 1940–2012 rainfall distribution maps using the method of fragments (for example, Oki, 2002). The method of fragments creates a synthetic sequence of daily rainfall from monthly rainfall by imposing the rainfall pattern from a rain-gaging station with daily data. The synthesized daily rainfall data approximate the long-term average character of daily rainfall, such as frequency, duration, and intensity, but may not reproduce the historical daily rainfall record.

Daily rainfall measurements at 11 rain-gaging stations on Molokaʻi during 1949–2009 were used to disaggregate monthly rainfall into daily rainfall for the water budget. Rain-gaging stations were selected on the basis of location, and the length and completeness of daily records. Daily rainfall data from the period of record of each rain-gaging station were obtained from the National Climatic Data Center (www.ncdc.noaa.gov) and the USGS (http://waterdata.usgs.gov/hi/nwis/nwis). Thiessen polygons were drawn around each of the rain-gaging-station locations, and the daily rainfall pattern within each Thiessen polygon was assumed to be the same as the pattern at the rain-gaging station within the Thiessen polygon (fig. 1.3). Because of a lack of available daily rainfall data in northeastern Molokaʻi, where annual rainfall exceeds about 80 in., data from three rain-gaging stations on the northern part of the island of Hawaiʻi (stations 8548, 1864, and 0134 of fig. 3 from Engott, 2011) with similar annual rainfall and similar topography and orientation to the trade winds as northeastern Molokaʻi were used to define the daily rainfall pattern for that part of Molokaʻi.

Daily rainfall fragments of each rain-gaging station were calculated by dividing each daily rainfall measurement for a particular month by the total rainfall measured at the gage for that month. This resulted in a set of fragments for that particular month in which the total number of fragments was equal to the number of days in the month, and the sum of the fragments was equal to one. Fragment sets were compiled for every gage and every month in which complete daily rainfall measurements were available. Fragment sets were grouped by month of the year (12 months) and by rain-gaging station.

In the water-budget calculation, the fragment set used for a given gage and month was selected randomly from among all available sets for that gage and that month of the year. Daily rainfall for a given month was synthesized by multiplying total rainfall of that month (from the monthly rainfall maps) by each fragment in the set, thereby providing daily rainfall.

Fog Interception

Fog is persistent on the midaltitude mountain slopes of most Hawaiian Islands, occurring during periods of onshore, upsloping winds favorable for orographic cloud formation. Fog may be persistent at altitudes as low as about 2,000 to 3,000 ft (Juvik and Ekern, 1978). Orographic cloud formation is often limited or capped by the base of the trade-wind inversion, which commonly occurs between 5,000 and 10,000 ft (Giambelluca and Schroeder, 1998). This limitation on cloud formation hinders the growth of large raindrops and produces high ratios of fog to rain near or at the inversion-base altitude (Juvik and Ekern, 1978). Above the base of the inversion, fog tends to dissipate quickly in the drier air regime.

Where fog is persistent, the interception of this moisture by vegetation has been shown to be a substantial component of the water budget (Ekern, 1964; Juvik and Ekern, 1978; Juvik and others, 1993; 2011; Juvik and Nullet, 1995; Scholl and others, 2007). Fog interception occurs through the processes of turbulent diffusion and gravitational sedimentation of droplets onto vegetative surfaces, mainly leaves or needles (Bruijnzeel and others, 2005). Rates of fog interception are highly site dependent and influenced by both meteorological and biotic variables including (1) the duration and frequency of fog periods, (2) wind speed and direction, (3) liquid water content of fog, and (4) structural characteristics of the forest, such as height, size, spatial pattern, and the physical characteristics of leaves and epiphytes (Walmsley and others, 1996; Bruijnzeel and others, 2005; Villegas and others, 2007). The quantification of fog interception is a complex endeavor and is the subject of continuing research, both in Hawaiʻi and worldwide.

Site and species-specific information on fog-interception rates on Molokaʻi was not available for this study, and thus a simplified approach was used to estimate fog interception. For this study, the fog zone is assumed to occur in areas on Molokaʻi above 2,000 ft (fig. 1.3). For forested areas in the fog zone, the ratio of fog interception-to-rainfall was estimated as 0.16, which generally is consistent with fog-interception amounts for windward and leeward aspects of mountain ranges in Hawaiʻi (DeLay and Gaimbelluca, 2010).

Fog interception is primarily a phenomenon associated with trees and other tall vegetation because the magnitude of fog interception is directly related to the height of the

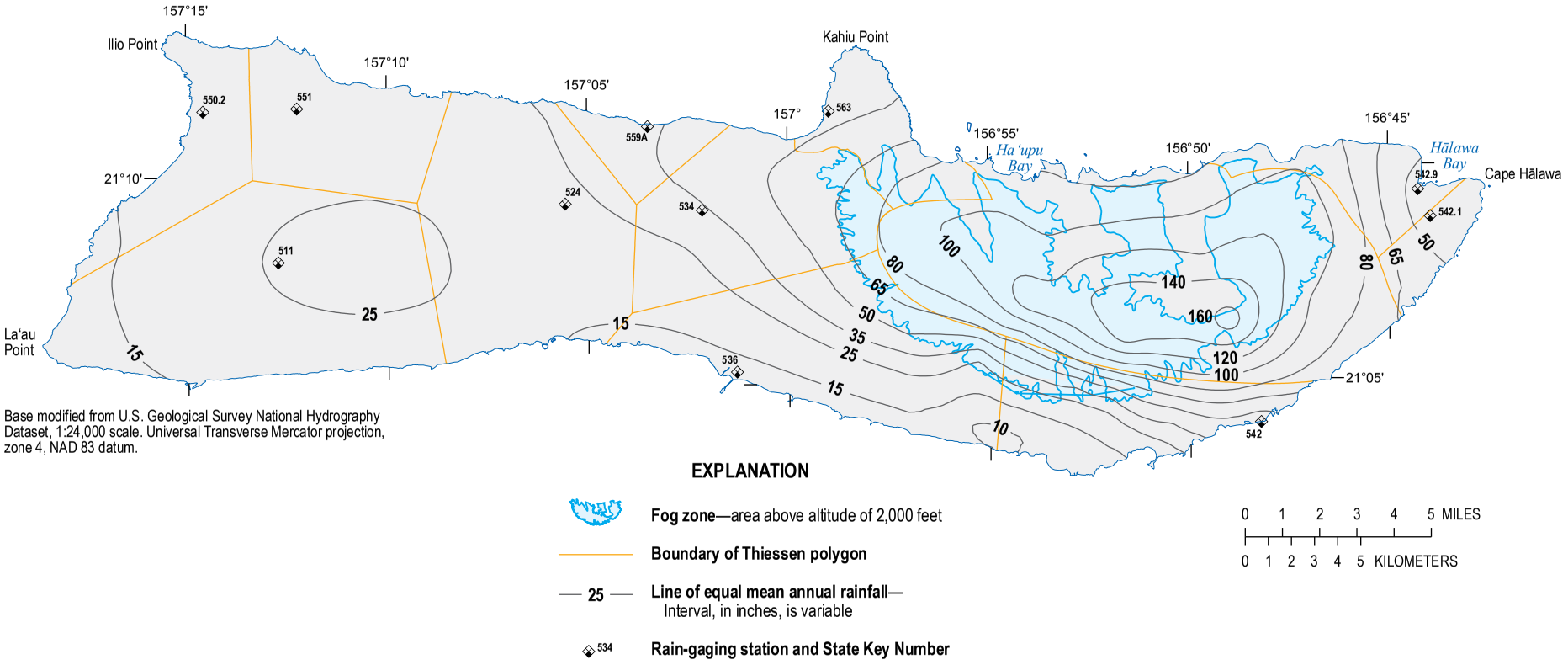

Figure 1.3. Map showing mean annual rainfall of 1978–2007 (modified from Giambelluca and others, 2013), locations of rain-gaging stations used in the water-budget calculations, and location of the fog zone (above 2,000 feet altitude) on Moloka'i, Hawai'i.

vegetated surface (Walmsley and others, 1996; Bruijnzeel and others, 2005). Accordingly, fog interception for nonforest land covers is assumed to be negligible, except for shrubland, which is assumed to intercept fog at one-half the rate of forest land-cover classes.

Irrigation

Irrigation was applied to four agricultural land-cover classes: corn, coffee, pineapple, and diversified agriculture (fig. 1.2). Irrigation was also applied to medium- and high-intensity developed subareas, which are of limited extent, to simulate the watering of urban landscapes. Irrigation rates were estimated using a demand-based approach. Irrigation demand for a given subarea was estimated on the basis of monthly rainfall, runoff, potential evapotranspiration, and irrigation-method efficiency.

$$I_m = [(PE)_m + U_m - R_m] / g$$

for $(PE)_m + U_m > R_m$ and

$$I_m = 0$$

for $(PE)_m + U_m \leq R_m$ (1-1)

where

$(PE)_m$ is potential evapotranspiration for month m [L] (varies by location),
U_m is amount of runoff for month m [L],
R_m is amount of rainfall for month m [L],
I_m is amount of irrigation for month m [L], and
g is irrigation-method efficiency [dimensionless].

Irrigation-method efficiency is the fraction of applied irrigation water that becomes available for plant consumption. Corn and diversified agriculture were assumed to use drip irrigation, which has an irrigation-method efficiency of 0.85 (University of Hawaiʻi, 2008). Coffee was assumed to use micro-spray irrigation, which has an irrigation efficiency of 0.80 (University of Hawaiʻi, 2008). Medium- and high-intensity developed land-cover classes were assumed to use sprinkler irrigation, which has an irrigation efficiency of 0.70 (University of Hawaiʻi, 2008). Pineapple, which on Molokaʻi was primarily grown prior to the 1990s, was assumed to have an irrigation efficiency of 0.85.

For all irrigated land-cover classes other than pineapple, monthly irrigation calculated using equation 1-1 was allocated in equal amounts for each day of a given month. Similar to the approach taken in Engott and Vana (2007) for pineapple irrigation, the monthly irrigation volume calculated for pineapple using equation 1-1 was uniformly distributed on days 1, 2, 3, 8, 9, 10, 15, 16, 17, 22, 23, 24, and 28 of each month. The pineapple cultivation cycle was not represented in this study. Corn irrigation for this study is based on a cultivation cycle of two crops per year. Only 25 percent of the corn land-cover class is cultivated at any one time, leaving the remaining 75 percent fallow/grassland. This approach was developed on the basis of cultivation practices on Molokaʻi (Ray Foster, Monsanto Company, acquired by Bayer in 2018, written commun., 2012).

An irrigation-estimation multiplier was used to adjust the irrigation estimate (equation 1-1) of the diversified agriculture land-cover class because of the relatively large uncertainty involved in selecting crop parameters, given the wide variety of crops represented by this category. An irrigation-estimation multiplier of 0.4 was used because of irrigation-supply information from fields served by the Molokaʻi Irrigation System in Central Molokaʻi (Santo, 2001). An irrigation-estimation multiplier of 0.37 also was used for the developed, medium- and high-intensity land-cover classes to calibrate the irrigation estimates from equation 1-1 to the rates used in Giambelluca (1983) and Giambelluca and others (2014) for urban irrigation in southern Oʻahu, Hawaiʻi. When pineapple was grown in western Molokaʻi near Mauna Loa during the 1940s through the 1970s, irrigation was very limited because of poor water supply (Baker, 1960; State of Hawaiʻi, 1966). For this study, no irrigation was applied to the western Molokaʻi pineapple fields; specifically, no irrigation was applied to the fields in the Kaluakoʻi and Punakou aquifer systems. An irrigation-estimation multiplier of 0.25 was used for the central Molokaʻi pineapple fields of the Hoʻolehua, Kualapuʻu, and Manawainui aquifer systems, where water supply for irrigation also was limited. This estimation is based on water-use information from Nance (1982).

Direct Runoff

Direct runoff is the fraction of rainfall that does not contribute to net moisture gain within the plant-root zone. Direct runoff of rainfall consists of overland flow and subsurface storm flow that rapidly returns infiltrated water to the stream (Oki, 2003). In the water-budget calculation, direct runoff was estimated as a fraction of rainfall using runoff-to-rainfall ratios. This approach was also used in previous water-budget studies of Hawaiʻi and other Pacific islands (for example, Izuka and others, 2005; Engott and Vana, 2007; Engott, 2011; Johnson, 2012; Johnson and others, 2018; Engott and others, 2017, Izuka and others, 2018) and provides reasonable estimates of regional average direct runoff using a minimal level of complexity.

The spatial variability of runoff-to-rainfall ratios depends on numerous factors including geology, climate, soil type, topography, and land use. Runoff-to-rainfall ratios are expected to be highest where the rainfall amount and intensity are high, permeability of the soils and substrate is low, slopes are steep, and soil moisture is high (Oki, 2003). The temporal variability in runoff-to-rainfall ratios reflects factors including antecedent soil moisture and rainfall intensity. In Hawaiʻi, runoff-to-rainfall ratios generally follow a seasonal pattern. Runoff-to-rainfall

ratios are highest during the wet-season months and lowest during the dry-season months.

In the water budget, daily direct runoff was calculated by multiplying daily rainfall by seasonal (wet and dry season) runoff-to-rainfall ratios assigned to catchment zones. The months of November through April and May through October were considered the wet and dry seasons, respectively for this study. Catchment zones of a stream network were delineated by Rea and Skinner (2012) using a 10-meter digital elevation model with a flow-accumulation threshold of 20,000 cells. For this study, each catchment zone was assigned two attributes: (1) gaged or ungaged, and (2) windward or leeward (fig. 1.4). The boundaries of the drainage basins of selected streamgaging stations were delineated by Rosa and Oki (2010), and the boundary between windward and leeward regions is based on topographic divides.

Mean seasonal runoff-to-rainfall ratios of ungaged basins were estimated using regression equations developed from streamflow data in Hawai‘i (Izuka and others, 2018). To estimate direct runoff in the water budget for average climate conditions and drought conditions, the mean seasonal runoff-to-rainfall ratios derived from the regional-regression equations were used. To estimate direct runoff in the water budget for transient climate conditions, the mean seasonal runoff-to-rainfall ratios derived from the regional-regression equations were modified to account for interannual variability (see table 4 and fig. 7 in Mair and others, 2019). For gaged basins, an average of the observed runoff-to-rainfall ratio and regional-regression-equation runoff-to-rainfall ratio was used because of uncertainty in rainfall and runoff estimates for the gaged basins of northeastern Moloka‘i. This approach was thought to provide the most reliable runoff estimate because an analysis of the water-budget results of this study indicated that recharge estimates using the observed seasonal runoff-to-rainfall ratios for northeastern Moloka‘i may be insufficient to account for base flow in several streams. Overly high observed runoff-to-rainfall ratios (possibly related to overestimated runoff or underestimated rainfall) were the likely cause. Thus, combining the observed and regression-equation runoff-to-rainfall estimates was considered an appropriate approach.

The estimated seasonal runoff-to-rainfall ratios for gaged drainage basins consisting of a single catchment zone were assigned to the catchment zone. For gaged drainage basins consisting of multiple catchment zones, the estimated seasonal runoff-to-rainfall ratios were spatially disaggregated to each catchment zone within the gaged basin (see for example Izuka and others, 2018).

Observed Seasonal Runoff-to-Rainfall Ratios

Runoff and rainfall data from drainage basins of 11 streamgaging stations on Moloka‘i (fig. 1.4) were used to derive seasonal runoff-to-rainfall ratios. Streamgaging stations selected for the runoff analysis had (1) at least eight complete years of daily mean discharge records between 1920 and 2007, and (2) a drainage-basin area greater than 0.2 mi^2. For drainage basins with more than one streamgaging station, only the station at the lowest altitude was used in the runoff analysis because it had the largest drainage basin to characterize runoff. Additionally, concurrent streamflow data from two stations within a drainage basin were generally absent or insufficient for improving direct runoff estimates. The drainage basins of the selected streamgaging stations were delineated using the USGS StreamStats application for Hawai‘i (Rosa and Oki, 2010). Rainfall within each drainage basin was calculated using gridded maps of monthly rainfall (Giambelluca and others, 2013; Frazier and others, 2016).

Because streamflow measured at most gaging stations consists of direct runoff and base flow, the base-flow component was estimated and subtracted from the total streamflow. Streamflow at stations 16411400 and 16414000 was ephemeral and was assumed to have no base flow. Base flow at the other gaged basins was estimated using a computerized base-flow separation method (Wahl and Wahl, 1995). This method has been used in numerous studies in Hawai‘i (for example, Izuka and others, 2005; Engott and Vana, 2007; Engott, 2011) and provides a reasonable estimate of base flow for perennial streams in Hawai‘i. The method defines local streamflow minimums within consecutive, nonoverlapping n-day periods and requires two parameters (1) f, the turning-point test factor, and (2) n, the number of days in a test window. In this study, the f value used for all stations was 0.9. The n values were determined to be 3 days for each station using the method described by Wahl and Wahl (1995) (table 1.1). Daily base flow was subtracted from daily streamflow to determine daily direct runoff. Streamflow measured at stations 16415000 and 16419500 is intermittent and likely reflects the effects of diversions, and therefore base flow may be underestimated at these stations.

Observed seasonal runoff-to-rainfall ratios (for a particular season and year) were calculated for 11 gaged drainage basins on Moloka‘i. Each observed seasonal runoff-to-rainfall ratio for the gaged drainage basins was calculated as the quotient of cumulative direct runoff and cumulative rainfall during the season. For example, the observed runoff-to-rainfall ratio of a gaged basin during the dry season of 2001 was calculated as the quotient of cumulative direct runoff and cumulative rainfall during May–October 2001.

Mean Seasonal Runoff-to-Rainfall Ratios

Mean seasonal runoff-to-rainfall ratios of each of the 11 selected gaged drainage basins were calculated for a period with rainfall and runoff conditions generally representative of those during 1978–2007 (table 1.1). The mean seasonal runoff-to-rainfall ratio of each gaged drainage basin was calculated as the quotient of cumulative direct runoff and cumulative rainfall during the appropriate season of the selected period. For example, the mean dry season runoff-to-rainfall ratio of streamgaging station 16400000 was calculated as the quotient of cumulative direct runoff and cumulative rainfall during May–October between 1978 and 2007.

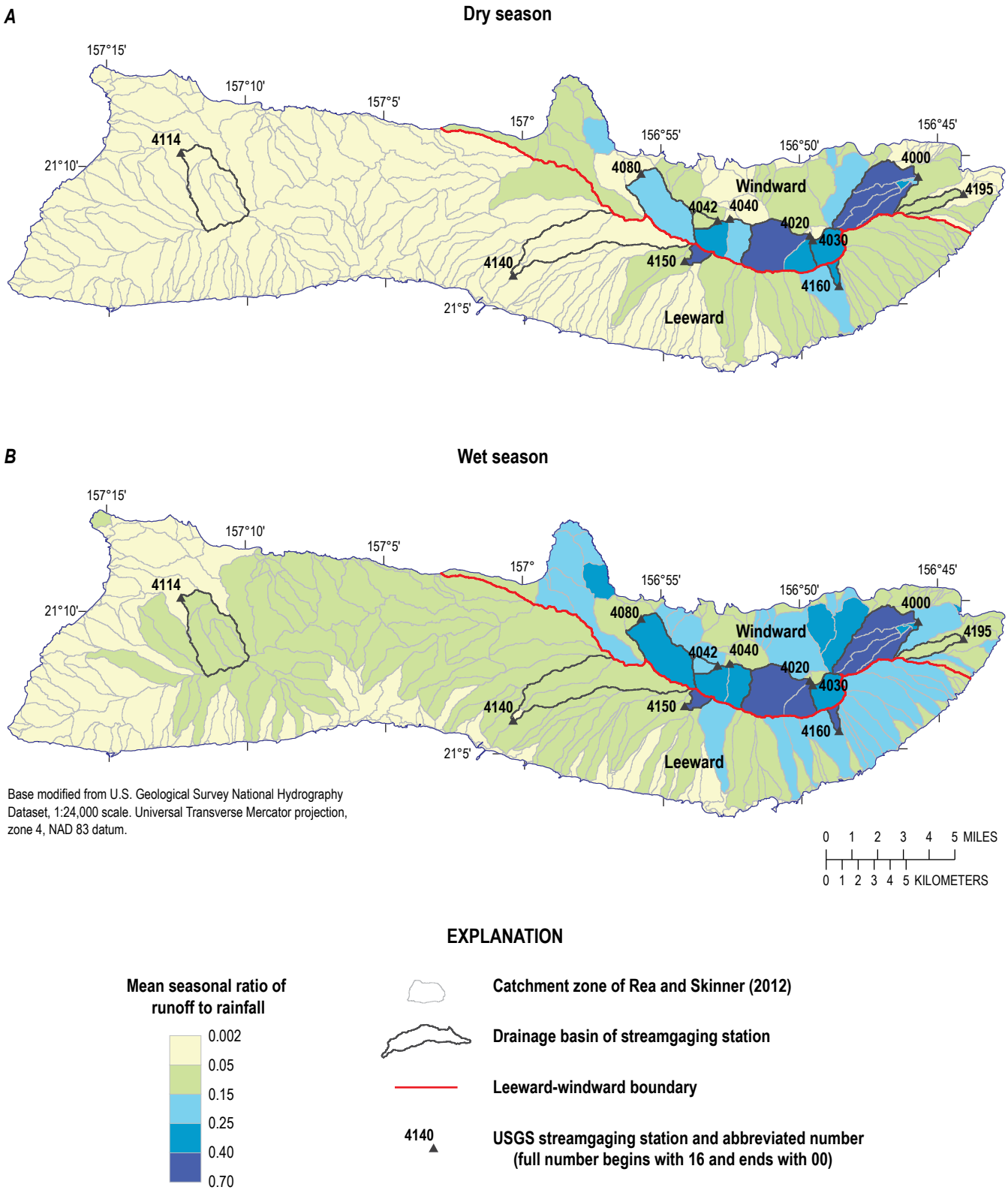

Figure 1.4. Maps of Molokaʻi, Hawaiʻi showing the mean runoff-to-rainfall ratios for the (*A*) dry-season months (May through October), and (*B*) wet-season months (November through April) from drainage basins of selected streamgaging stations and catchment zones (modified from Rea and Skinner, 2012).

Table 1.1. Mean seasonal runoff-to-rainfall ratios for drainage basins of streamgaging stations, Molokaʻi, Hawaiʻi.

[See fig. 1.4 for locations of drainage basins; *n*, number of days used for determining minimum flows in the base flow-separation program (Wahl and Wahl, 1995); E, ephemeral stream with no base flow]

Gaging-station number	Stream/gulch	Aspect	Area of drainage basin, in square miles	*n*	Period of record selected to compute mean runoff-to-rainfall ratios			Mean runoff-to-rainfall ratio calculated using streamgage data (method A)		Mean runoff-to-rainfall ratio calculated using regression equations (method B)	
					Start	End	Number of years	Wet season: November through April	Dry season: May through October	Wet season: November through April	Dry season: May through October
16400000	Hālawa Stream	Windward	4.681	3	1978	2007	30	0.61	0.59	0.25	0.17
16402000	Pūlena Stream	Windward	4.392	3	1938	1952	15	0.55	0.39	0.11	0.05
16403000	Waiakeakua Stream	Windward	1.405	3	1938	1956	19	0.38	0.32	0.15	0.08
16404000	Pelekunu Stream	Windward	2.637	3	1938	1947	10	0.37	0.26	0.12	0.06
16404200	Pilipililau Stream	Windward	0.465	3	1969	1996	28	0.17	0.06	0.14	0.07
16408000	Waikolu Stream	Windward	3.781	3	1949	1958	10	0.32	0.22	0.20	0.12
16411400	Kakaʻako Gulch	Leeward	5.041	E	1964	1971	8	0.06	0.04	0.06	0.02
16414000	Kaunakakai Gulch	Leeward	6.618	E	1951	1964	14	0.06	0.01	0.16	0.06
16415000	East fork Kawela Gulch	Leeward	0.440	3	1947	1970	23	0.55	0.53	0.15	0.08
16416000	Punaʻula Gulch	Leeward	0.276	3	1948	1971	24	0.41	0.29	0.19	0.17
16419500	Pāpio Gulch	Windward	0.993	3	1978	2005	28	0.12	0.07	0.12	0.06

Criteria for selecting periods of record were determined by examining temporal variations in seasonal runoff-to-rainfall ratios of streamgaging stations that were operational during 1978–2007. For these stations, the 1978–2007 mean seasonal runoff-to-rainfall ratios were compared with those calculated for smaller, subset periods during 1920–2007. The results of these comparisons show that the difference between 1978–2007 mean seasonal runoff-to-rainfall ratios and those calculated for subset periods decreases with increasing record length of the subset period and with decreasing differences between mean annual rainfall during 1978–2007 and the subset period. Accordingly, the period of record selected to calculate mean seasonal runoff-to-rainfall ratios consisted of (1) the entire period during 1978–2007 for streamgaging stations with at least 28 complete years of record during 1978–2007, (2) the longest contiguous period during 1920–2007 that had less than 5-percent difference in mean annual rainfall, relative to rainfall for 1978–2007, for all remaining streamgaging stations on perennial streams with base flow, and (3) the entire period of record for the four streamgaging stations on ephemeral or intermittent streams.

Runoff-to-Rainfall Ratios Assigned to Ungaged Catchment Zones

Ungaged catchment zones are outside of the drainage basins of the 11 selected streamgaging stations on Molokaʻi (fig. 1.4). Direct runoff for ungaged catchment zones was calculated using mean seasonal runoff-to-rainfall ratios derived from four regional-regression equations (table 1.2). These equations are the same as those used for Kauaʻi, Oʻahu, and Maui by Izuka and others (2018), Engott and others (2017), and Johnson and others (2018), in which the development method is described. Separate windward and leeward regression equations were derived for the wet and dry seasons. The regional-regression equations relate mean seasonal runoff-to-rainfall ratios and basin characteristics and were developed with methods consistent with discussion given in Helsel and Hirsch (1992). The performance statistics of the regression equations (table 1.2) are used to examine the sensitivity of recharge to runoff-to-rainfall ratios (see the Sensitivity Analysis section). Regression-equation errors for Molokaʻi may be related to uncertainties in estimated runoff

Table 1.2. Regional-regression equations used to calculate mean seasonal runoff-to-rainfall ratios for catchment zones, Molokaʻi, Hawaiʻi.

[See fig. 1.4 for locations of leeward and windward regions on Molokaʻi; RMSE, prediction root mean square error; RMSE and percentage bias for the gaged basins on the islands of Kauaʻi, Oʻahu and Maui were used to develop the regional-regression equations; Wet season is November through April; Dry season is May through October; mean wet-season rainfall and mean dry-season rainfall are from Giambelluca and others (2013) and are in inches; mean annual ETo and mean dry-season ETo, reference evapotranspiration, are from Giambelluca and others (2014) and are in inches; % HSG C is the percentage of area in a catchment zone that contains hydrologic soil group C; % HSG D is the percentage of area in a catchment zone that contains hydrologic soil group D; Areas of hydrologic soil groups were derived from U.S. Department of Agriculture (2006a, 2006b, 2006c, 2006d)]

Region	Season	Regression used to compute runoff-to-rainfall ratio	RMSE		Percentage bias	
			Overall	Molokaʻi	Overall	Molokaʻi
Leeward	Wet	0.00320 [mean wet-season rainfall]	0.06	0.18	0.6	−35
Leeward	Dry	0.00293 [mean dry-season rainfall]	0.07	0.20	3.8	−48
Windward	Wet	$[\%\ \text{HSG C}]^{0.185}\ [\%\ \text{HSG D}]^{0.247}\ [\text{mean annual ETo}]^{(-0.590)}$	0.12	0.25	−4.8	−56
Windward	Dry	$[\%\ \text{HSG C}]^{0.186}\ [\%\ \text{HSG D}]^{0.346}\ [\text{mean dry-season ETo}]^{(-0.947)}$	0.11	0.24	−5.8	−68

and rainfall or hydrologic differences with Kauaʻi, Oʻahu, and Maui.

Mean seasonal runoff-to-rainfall ratios derived from the regional-regression equations were used to estimate direct runoff in the water budget for average climate conditions and drought conditions. To estimate direct runoff of the seven time periods in the water budget (1940–49, 1950–59, 1960–69, 1970–79, 1980–89, 1990–99, and 2000–12), the mean seasonal runoff-to-rainfall ratios were modified to reflect interannual variability in rainfall using the method described by Mair and others (2019, table 4 and fig. 7).

Runoff-to-Rainfall Ratios Assigned to Gaged Basins with a Single Catchment Zone

Six of the selected streamgaging stations on Molokaʻi have drainage basins with a single catchment zone (16403000, 16404200, 16408000, 16415000, 16416000, and 16419500) (fig. 1.4). To estimate direct runoff for each single-catchment-zone basin in the water budget for average climate and drought conditions, an average of the observed mean seasonal runoff-to-rainfall ratio and regional-regression-equation runoff-to-rainfall ratio was used. To estimate direct runoff for single-catchment-zone basins during the seven transient time periods (1940–49, 1950–59, 1960–69, 1970–79, 1980–89, 1990–99, and 2000–12) in the water budget, seasonal runoff-to-rainfall ratios were determined as follows. For periods with observed seasonal runoff-to-rainfall ratios, the average of the observed seasonal runoff-to-rainfall ratio and the adjusted (Mair and others, 2019, table 4 and fig. 7) seasonal runoff-to-rainfall ratio derived from the appropriate regression equation was used. For periods without observed seasonal runoff-to-rainfall ratios, the average of the mean seasonal runoff-to-rainfall ratio and the seasonal runoff-to-rainfall ratio derived from the appropriate regression equation was computed, adjusted for interannual variability, and then used.

Runoff-to-Rainfall Ratios Assigned to Gaged Basins with Multiple Catchment Zones

Five of the selected streamgaging stations on Molokaʻi (16400000, 16402000, 16404000, 16411400, and 16414000) have drainage basins containing multiple catchment zones (fig. 1.4). Direct runoff for each of the catchment zones within these gaged basins was calculated using adjusted seasonal runoff-to-rainfall ratios determined from equation 1-2.

$$\widetilde{rr_{a,t}} = \widetilde{RR_a} \times \frac{rr_{b,t} \times rf_{b,t}}{\sum_{i=1}^{j} \widetilde{RR_i} \times rf_{i,t}} \qquad (1\text{-}2)$$

where

$\widetilde{rr_{a,t}}$ is adjusted runoff-to-rainfall ratio for catchment zone a during season t [dimensionless],

$\widetilde{RR_a}$ is mean runoff-to-rainfall ratio for catchment zone a estimated using the appropriate regional-regression equation (table 1.2) [dimensionless],

j is number of catchment zones in the gaged basin b [dimensionless],

$\widetilde{RR_i}$ is mean runoff-to-rainfall ratio for catchment zone i estimated using the appropriate regional-regression equation [dimensionless],

$rf_{i,t}$ is rainfall for catchment zone i during season t [L^3],

$rr_{b,t}$ is runoff-to-rainfall ratio for gaged basin b during season t [L^3] (see discussion below), and

$rf_{b,t}$ is rainfall for gaged basin b during season t [L^3].

Equation 1-2 uses the regional-regression models and seasonal rainfall to spatially disaggregate (Engott and others, 2017; Johnson and others, 2018; Izuka and others, 2018) observed

seasonal and mean seasonal runoff-to-rainfall ratios of a gaged basin for each catchment zone within a gaged basin. Hence, seasonal runoff-to-rainfall ratios were allowed to be spatially variable across the catchment zones within gaged drainage basins containing multiple catchment zones.

To estimate direct runoff for multiple-catchment-zone basins, an average of the seasonal runoff-to-rainfall ratio derived from basin data and the seasonal runoff-to-rainfall ratio derived from the regression equations was used in the water-budget analysis. To estimate direct runoff for each multiple-catchment-zone basin in the water budget for average climate and drought conditions, an average of the observed mean seasonal runoff-to-rainfall ratio and regional-regression-equation runoff-to-rainfall ratio was used.

To estimate direct runoff for multiple-catchment-zone basins during the seven transient time periods (1940–49, 1950–59, 1960–69, 1970–79, 1980–89, 1990–99, and 2000–12) in the water budget, seasonal runoff-to-rainfall ratios were determined as follows. For periods with observed seasonal runoff-to-rainfall ratios, the average of the observed seasonal runoff-to-rainfall ratio and the adjusted seasonal runoff-to-rainfall ratio (Mair and others, 2019, table 4 and fig. 7) derived from the appropriate regression equation was used. For periods without observed seasonal runoff-to-rainfall ratios, the average of the mean seasonal runoff-to-rainfall ratio and the seasonal runoff-to-rainfall ratio derived from the appropriate regression equation was computed, adjusted for interannual variability, and then used.

Adjustments to Runoff-to-Rainfall Ratios in Kawela and ʻUalapuʻe Aquifer Systems

At the higher altitudes of the Kawela and ʻUalapuʻe aquifer systems, an area consisting largely of native cloud forest (fig. 1.2), the runoff-to-rainfall ratios derived for ungaged basins using the regional-regression equations are lower than the ratios calculated for the drainage basins of streamgaging stations 16415000 and 16416000 in that area (fig. 1.4). Assuming that the local streamgaging station data are more reliable indicators of runoff conditions for that area than the regional-regression equations, native-forest land cover above the cloud zone was assigned the runoff-to-rainfall ratios from (1) streamgaging station 16415000 in the Kawela aquifer system and (2) streamgaging station 16416000 in the ʻUalapuʻe aquifer system.

Evapotranspiration

Evapotranspiration (ET) is the sum of all water that is evaporated or transpired from a vegetated surface and plant-root zone. Evapotranspiration can be divided into three main evaporative processes (1) canopy evaporation, which is evaporation of intercepted rain and fog from the surface of vegetation; (2) ground evaporation, which is evaporation of water from the soil surface and overlying litter and mulch layers; and (3) transpiration, the process by which soil moisture taken up by vegetation is eventually evaporated through plant pores (Viessman and Lewis, 2003).

Canopy evaporation in forested areas can substantially reduce the rainfall that reaches the ground beneath a forest canopy (Gaskill, 2004; DeLay, 2005; McJannet and others, 2007; Giambelluca and others, 2011; Safeeq and Fares, 2014). Because of the height of trees and their canopy structure, turbulent diffusion is much more efficient at removing intercepted water from forest canopies than from shorter vegetation. Moreover, canopy evaporation in forests tends to operate on much shorter time scales (hours) than transpiration (weeks or longer) (Savenije, 2004). Thus, accurate estimates of ET from forests generally require transpiration and canopy evaporation to be evaluated separately (Shuttleworth, 1993).

For this study, total ET from subareas of the forest land-cover classes is calculated by separately estimating forest-canopy evaporation and combined ground evaporation and transpiration derived from water in the plant-root zone (fig. 1.1). Evaporation from the forest canopy and evapotranspiration from the plant-root zone are added together to yield total ET. For subareas of nonforest land-cover classes, ET is calculated using a more traditional approach in which canopy evaporation, ground evaporation, and transpiration are not separately estimated (fig. 1.1). The concept of potential ET, combined with empirical models when soil moisture is limited, is used to estimate ground evaporation and transpiration for forest-land covers and total ET for all other land covers.

Forest-Canopy Evaporation and Net Precipitation

As rain falls on a vegetated surface, a fraction of the droplets will accumulate on the leaves, trunks, or stems of the vegetation. Additional moisture from fog interception may supplement the amount of water that accumulates on vegetation. Canopy evaporation is the part of precipitation that accumulates on and then evaporates from the vegetation (Gerrits and Savenije, 2011). Net precipitation is the part of precipitation that reaches the forest floor (fig. 1.1).

In this study, the Gash model (Gash and others, 1995) was used to calculate forest-canopy evaporation for the following reasons. First, the Gash model accounts for gaps in the forest canopy, and this allows for a sparse canopy to be differentiated from a dense canopy. Second, canopy evaporation during a period of precipitation is dependent on the amount of precipitation during that period. Third, the Gash model has the capacity to account for spatial differences in climate, including climate differences between windward and leeward forests. One disadvantage of the Gash model, however, is that it is theoretical. Therefore, one of the parameters of the Gash model used to calculate canopy evaporation in the water budget was calibrated to the wet-canopy evaporation maps of Giambelluca and others (2014) as described below. Use of the Gash model, instead of the mean wet-canopy evaporation maps, in the water budget allows forest-canopy evaporation to be calculated on a daily basis in response to daily variations in precipitation.

Forest-canopy evaporation is calculated in the water budget according to equations 4 and 5 in Engott and others (2017), which require values for rainfall and the following five parameters (1) canopy cover, (2) canopy capacity, (3) trunk-storage capacity, (4) proportion of precipitation diverted to stemflow (precipitation that flows to the ground along tree trunks or plant stems), and (5) the ratio of the mean evaporation rate to mean precipitation rate during saturated conditions, *V*. The values assigned to the first four parameters in the water-budget calculations were derived from published data for areas in Hawai‘i. The values assigned to *V* were derived using a method developed in a previous study (Johnson and others, 2018) that uses maps of mean wet-canopy evaporation for the islands of Kaua‘i, O‘ahu, and Maui (Giambelluca and others, 2014).

Canopy cover of forest land-cover classes varies spatially across Moloka‘i. The canopy cover of each forest land-cover class subarea in the water budget was estimated from a map of mean annual vegetation cover fraction (Giambelluca and others, 2014) and was assumed to be the same for each time period simulated. This map quantifies the vegetation cover fraction at a spatial resolution of about 14 acres. A canopy cover of 0 implies an absence of canopy cover, whereas a value of 1 implies a dense canopy with no gaps. The estimated canopy-cover values for subareas of forest land-cover classes used in the water budget range from 0.03 to 1.

Canopy capacity, trunk-storage capacity, and the proportion of precipitation diverted to stemflow were assumed to be the same for all forests for all time periods simulated (table 1.3). Canopy capacity was set at 0.05 inches, the mean of the average values reported for six forested sites in Hawai‘i (DeLay, 2005, p. 42; Takahashi and others, 2011, Safeeq and Fares, 2014). Trunk-storage capacity was set at 0.01 inches, the mean of the values reported for four forest sites in Hawai‘i (DeLay, 2005, p. 42; Safeeq and Fares, 2014). The proportion of precipitation diverted to stemflow was assumed to be 0.04, the mean of the values reported for eight forest sites in Hawai‘i (Gaskill, 2004; DeLay, 2005, p. 42; Takahashi and others, 2011; Safeeq and Fares, 2014). Forest sites of Takahashi and others (2011) and Safeeq and Fares (2014) with an abundance of *Psidium cattleianum* Sabine 1821 (strawberry guava) had relatively high stemflow estimates ranging from 29 to 34 percent of rainfall. In order to have conservative stemflow estimates in the water budget, the high stemflow values from these sites were excluded from the calculated stemflow mean of 0.04 used in the water budget.

The spatial distribution of *V* was estimated using the method described in Johnson and others (2018) and also used in Engott and others (2017) and Izuka and others (2018). The method is as follows:

$$V = 0.01$$

for $w < 0.009$,

$$V = 2.677 \times (w) - 0.014$$

for $0.009 \le w \le 0.192$, and

$$V = 0.050$$

for $w > 0.192$ (1-3)

where

w is the mean annual wind speed divided by mean annual rainfall (m/s/in).

The variable *w* is the quotient of (1) mean annual wind speed, in meters per second, which was derived from a map of mean annual wind speed at a height of about 100 ft above the land surface (AWS Truewind, 2004), and (2) 1978–2007 mean annual rainfall, in inches (Giambelluca and others, 2013). In general, estimates of *V* for wet areas are less than those for dry areas. An analysis of the sensitivity of the water-budget results to selected Gash-model parameters is included in the Sensitivity Analysis section of this appendix.

Potential Evapotranspiration

Potential evapotranspiration (ET) is the maximum rate that water can be removed from the plant-root zone by ET if soil moisture is nonlimiting (Giambelluca, 1983). The actual-ET rate is a function of potential ET, soil-moisture content, and threshold-moisture content (Engott and others, 2017, equation 13). The actual-ET rate becomes less than the potential rate with the onset of soil-moisture stress. As the soil dries, capillary and adsorptive forces bind the remaining water to the soil matrix, reducing water available to roots. Soil-moisture stress occurs when the reduced availability of water to the root system induces a response in the plant to slow down transpiration and prevent desiccation. The threshold-moisture content at which a plant begins to react to soil drying varies with the type of plant.

Potential ET is controlled by atmospheric conditions, topography, and land-cover characteristics (Giambelluca, 1983). Maps of mean monthly reference ET produced by Giambelluca and others (2014) were used in the water budget to represent the influence of atmospheric conditions (radiation, air temperature, air humidity, and wind speed) on potential ET. Crop coefficients were used to represent the integrated effects of land-cover and vegetation characteristics on potential ET. Potential ET of each subarea was calculated in the water budget as the product of mean monthly reference ET and the crop coefficient assigned to the land-cover class, and it was assumed to be constant within a given month.

Reference Evapotranspiration

Reference ET, as defined in this study, is the potential ET of a hypothetical grass surface with optimum soil-water conditions for given climatic conditions and is equivalent to Food and Agriculture Organization of the United Nations' (FAO) Penman-Monteith ET (Allen and others, 1998). Reference ET is similar to pan evaporation, which has been used in previous water-budget analyses for Maui and other Hawaiian Islands. Both pan

Table 1.3. Land-cover parameters used in the water-budget calculations, Moloka‘i, Hawai‘i.

[Crop coefficients for forests are used to compute the sum of transpiration and ground evaporation; canopy evaporation is computed separately. Crop coefficients for nonforest land covers are used to compute the sum of all evaporative components; N/A, not applicable]

Land-cover description	Root depth, in inches	Depletion fraction	Crop coefficient	Canopy capacity, in inches	Trunk-storage capacity, in inches
Forest land covers					
Alien forest	60	0.50	0.33[1], 0.44[2]	0.05	0.01
Native forest	30	0.50	0.30	0.05	0.01
Kiawe/Phreatophytes	71	1.00	0.84	0.05	0.01
Nonforest land covers					
Agriculture—					
Coffee	48	0.40	0.91	N/A	N/A
Corn	18	0.60	0.29–1.20[3]	N/A	N/A
Diversified	10	0.35	1.00	N/A	N/A
Pineapple	18	0.50	0.30	N/A	N/A
Pineapple–abandoned	29	0.55	0.63	N/A	N/A
Developed—					
Low-intensity	12	0.50	1.18	N/A	N/A
Medium-intensity	12	0.50	1.18	N/A	N/A
High-intensity	12	0.50	1.18	N/A	N/A
Grassland	39	0.60	0.95	N/A	N/A
Shrubland	12	0.50	1.00	N/A	N/A
Sparsely vegetated	5	0.50	1.18	N/A	N/A
Wetland	39	0.50	1.18	N/A	N/A
Water bodies	1	1.00	1.05	N/A	N/A

[1]Value used inside the cloud zone, which is above 2,000 feet altitude.

[2]Value used outside the cloud zone.

[3]Varies by month (see Crop Coefficients section for explanation).

evaporation and reference ET provide an index of the energy that is available for ET for a given area.

Maps of mean monthly reference ET (Giambelluca and others, 2014) for Moloka‘i were used in the water budget. These maps use the same grid as the monthly rainfall maps. Mean annual reference ET ranges from about 31 to 113 inches on Moloka‘i (fig. 1.5). In general, mean annual reference ET is highest in dry lowland areas, and is lowest in wet upland areas within the fog zone. In the water-budget calculation, monthly reference ET was not varied from year to year, and it was assumed to equal mean monthly reference ET. Reference ET was assumed to be the same each day of a given month.

Crop Coefficients

A crop coefficient is an empirically derived ratio of the potential ET of a certain type of land cover and reference ET. Crop coefficients provide an index of the integrated effect of vegetation characteristics (reflectance, roughness, and plant physiology) on potential ET. Crop coefficients were assigned to each land-cover class (table 1.3). Crop coefficients were assumed to be temporally constant for all classes other than corn. For nonforest land-cover classes, crop coefficients integrated the effects of transpiration, ground evaporation, and canopy evaporation. For forested land-cover classes (table 1.3), crop coefficients integrated the effects of transpiration and ground evaporation; canopy evaporation was accounted for separately (fig. 1.1).

Crop coefficients for nonforest land-cover classes were obtained from published values or were derived from pan coefficients used for the same or similar land-cover classes in previous water budgets for Hawai‘i. A Hawai‘i pan coefficient for a given land-cover class is the ratio of potential ET to pan evaporation, making it analogous to crop coefficients. Pan coefficients for land-cover classes other than sugarcane were converted to crop coefficients by dividing the pan coefficients by 0.85—a factor that Engott (2011) used to convert crop coefficients to pan coefficients. Crop coefficients for grassland, pineapple, wetland, and water-body land-cover classes were obtained from Allen and others (1998). The midpoint of the range of crop coefficients for grazing pasture (rotated grazing) was used for grassland. The mean of the crop coefficients for wetlands with no frost was used for wetland. The crop coefficient for open water in the tropics was used for the water body class. Crop coefficients for coffee were obtained from Fares (2008). Crop

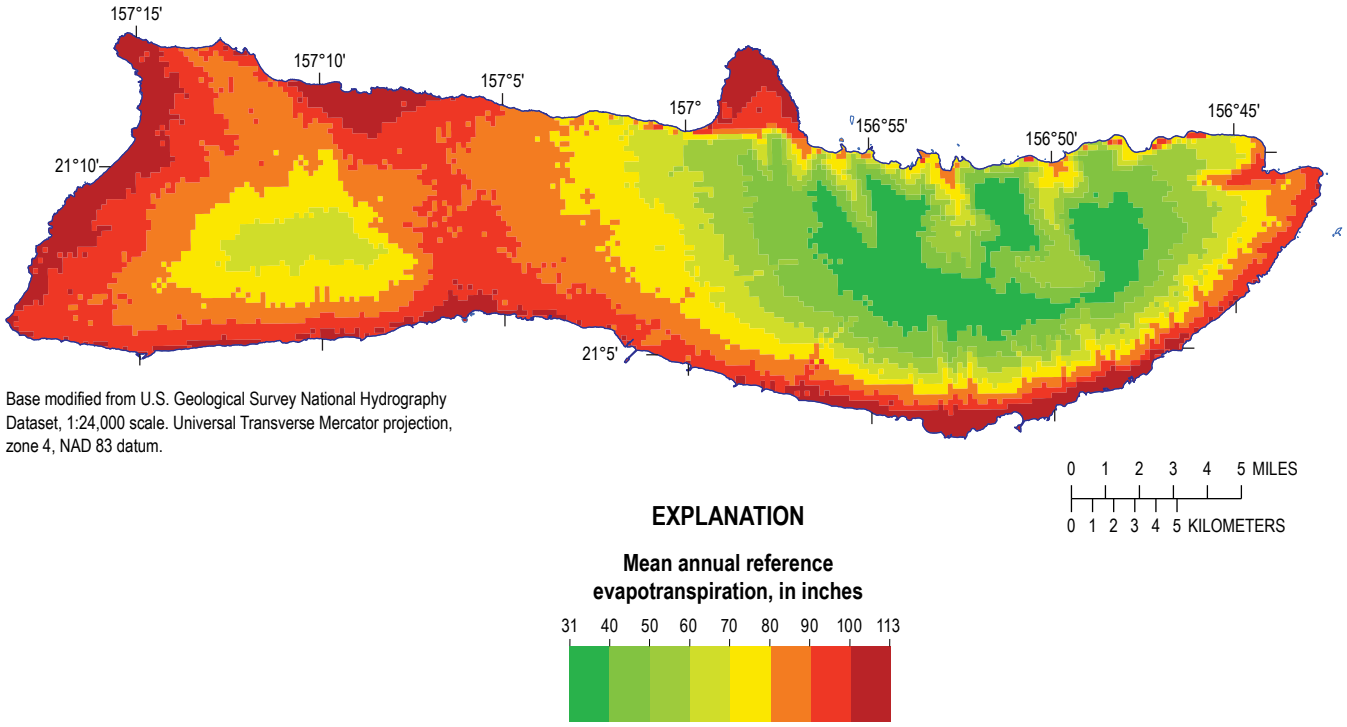

Figure 1.5. Map of Moloka‘i, Hawai‘i showing the mean annual reference evapotranspiration (modified from grass reference evapotranspiration in Giambelluca and others, 2014).

coefficients for developed land covers were derived from the pan coefficient used by Engott (2011) for developed land covers. Crop coefficients for diversified agriculture, shrubland, and sparsely vegetated land were also derived from pan coefficients used by Engott (2011). The crop coefficients for corn vary monthly and are based on information in the Hawai‘i Agricultural Water Use and Development Plan (University of Hawai‘i, 2008). The crop coefficients used for corn were 0.85, 0.50, 0.29, 0.40, 0.80, 1.20, 0.85, 0.50, 0.29, 0.40, 0.80, and 1.20 for the months of January through December (in chronological order). The crop coefficient for the pineapple–abandoned class is the average of the crop coefficients assigned to the pineapple and grassland land-cover classes. The crop coefficients for forested land-cover classes are the same as those used in Johnson and others (2018), Engott and others (2017), and Izuka and others (2018).

Moisture-Storage Capacity of the Plant-Root Zone

The moisture-storage capacity of the plant-root zone (fig. 1.6) was calculated as the product of available water capacity and root depth. A soil map and corresponding tables of available water capacities (U.S. Department of Agriculture, 2006d) were used to quantify the available water capacity of the soils on Moloka‘i. The tables list the minimum and maximum available water capacities of each soil unit for various ranges of depth. A depth-weighted mean available water capacity of each soil type was calculated for the water budget. However, all depths of the soil units “rock outcrop” and “gullied land” have zero available water capacity according to tables of U.S. Department of Agriculture (2006d). For this study, zero available water capacity for the “rock outcrop” and “gullied land” soil units was considered too low because many areas with this soil unit on Moloka‘i were mapped as grassland or shrubland. Therefore, for the water-budget calculations, available water-capacity values of the “rough broken land” soil unit were substituted for all subareas with the “rock outcrop” soil unit. The soil unit “rough broken land” was selected because it generally was mapped near “rock outcrop” soils and because its available water capacity exceeds zero in the top 8 inches of soil. Additionally, “gullied land” was given an available water capacity of 0.01 inches per inch.

Root depths for each land-cover class were assigned values on the basis of published values and root depths used in previous water budgets in the Hawaiian Islands (table 1.3). The root depth used for pineapple is the middle of the range of pineapple root depths reported in Fares (2008) and Allen and others (1998). The root depth used for “pineapple–abandoned” is the average of the root depths used for pineapple and grassland. The root depth used for diversified agriculture is near the middle of the range reported in Fares (2008) for typical diversified agriculture crops in the Hawaiian Islands. The root depth used for wetland is the same as that used for grassland. For all other land-cover classes, the root depths used are the same as those used by Engott and others (2017) in the water budget for the island of O‘ahu.

Direct Recharge

For this study, direct recharge is defined as water that passes directly to the groundwater system, completely bypassing the plant-root zone. Therefore, direct recharge is not subject to direct runoff or ET processes. Direct recharge was estimated for water bodies and subareas with distribution piping associated with the Moloka‘i Irrigation System (MIS). The water body land-cover category was broken into 3 different types for the purpose of estimating direct recharge—natural water bodies, estuarine/near-coastal water bodies, and the Kualapu‘u reservoir, which is part of the MIS. The direct-recharge rate from natural water bodies was set at 12 in/yr, which is consistent with previous Hawai‘i water budgets (Izuka and others, 2005; Engott and Vana, 2007; Engott, 2011). For estuarine/near-coastal water bodies, the recharge rate was set to zero, because these water bodies were assumed to produce no net recharge. The direct-recharge rate from leakage of the Kualapu‘u reservoir and distribution piping associated with the MIS was estimated to be 75 in/yr using inflow, outflow, and evaporation data (Santo, 2001).

Other Input

In addition to the aforementioned water-budget inputs, several other input parameter values were required. The initial moisture storage for the pervious fraction of subareas was set at 50 percent of the soil moisture-storage capacity. The rainfall-retention capacity for impervious surfaces was assumed to be 0.25 in. The initial moisture storage for the impervious fraction of subareas was set at 0.125 in, which is calculated as 50 percent of the rainfall-retention capacity of 0.25 in. These values were also used for other recent Hawai‘i water budgets (Johnson and others, 2018; Engott and others, 2017; Izuka and others, 2018). The impervious fractions of low-, medium-, and high-intensity developed land-cover classes were estimated to be 20, 50, and 85 percent, respectively, by using the analysis of an impervious-surface map for O‘ahu (National Oceanic and Atmospheric Association, 2008) and the 2010 O‘ahu land-cover map in Engott and others (2017). High-intensity developed areas on Moloka‘i have very limited spatial extent but are included in the analysis. All other land-cover categories were assumed to have an impervious fraction of zero.

Exclusions and Limitations

Several exclusions were made to simplify the water budget. Reinfiltration of direct runoff, water that runs off one subarea and then infiltrates the plant-root zone of a different subarea, was not explicitly considered in the water budget. Reinfiltration of direct runoff within gaged basins was assumed to be included in streamflow records used to derive runoff-to-rainfall ratios. Spatial variations in the reinfiltration of direct runoff within a drainage basin, however, were not accounted for in the model. For example, if reinfiltration of direct runoff was considerable within streambeds, then recharge may have been underestimated in intrachannel (streambed) areas and overestimated in inter-channel (nonstreambed) areas. Additionally, direct runoff from upland areas that seeps into the streambed of lower reaches near the coast was not quantified.

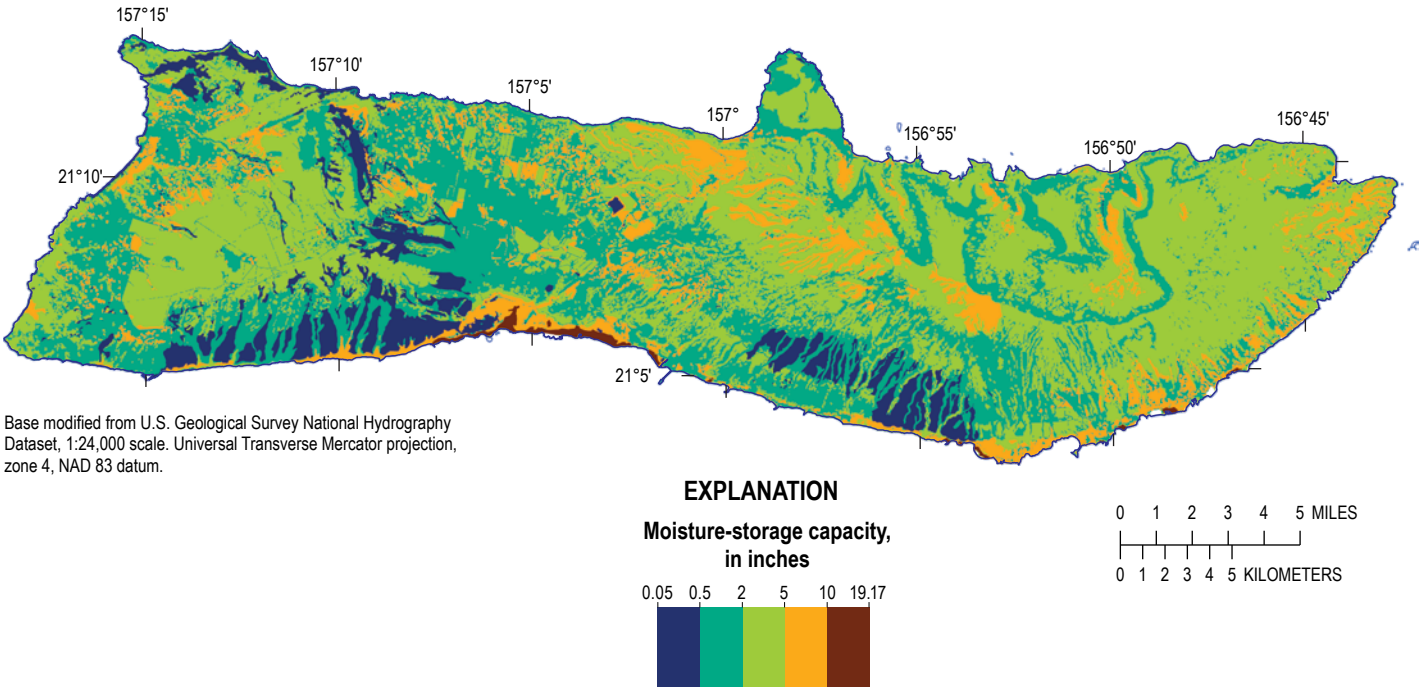

Figure 1.6. Map of Moloka‘i Hawai‘i showing calculated moisture-storage capacity of the plant-root zone for land-cover conditions during the 2000s.

Because of the lack of complete daily information and the use of synthesized daily rainfall, the water budget did not reconstruct the actual distributions of the water-budget components (rainfall, fog interception, irrigation, septic-system leachate, runoff, evapotranspiration, and recharge) on Molokaʻi for each simulated day. The reconstruction of actual daily runoff was also precluded by the use of seasonal runoff-to-rainfall ratios. Additionally, runoff may have been overestimated by the model on days with light rain and underestimated on days with intense rain. The water budget, however, reproduced the spatial distribution of (1) monthly rainfall on Molokaʻi during 1940–2012 that was estimated by Frazier and others (2016), and (2) mean monthly and mean annual rainfall on Molokaʻi during 1978–2007 that was estimated by Giambelluca and others (2014).

Some parameters and conditions not included in the calculations of the water budget were inherent in other parameters used in the model. For example, the permeability and vertical hydraulic conductivity of the plant-root zone and underlying substrate were not included in the water-budget calculations. Their effect on direct runoff, however, would be inherent in streamflow records used to derive runoff-to-rainfall ratios that were used to calculate direct runoff in the model. For subareas with forest land covers, a reduction in the potential ET of the plant-root zone in response to evaporation from the forest canopy was not included in the model calculations. However, the effects of forest-canopy evaporation on the potential-ET rate likely were accounted for in the forest crop coefficients, which were calibrated to the estimates of mean transpiration and ground evaporation produced by Giambelluca and others (2014).

Some processes and conditions were excluded from the water-budget calculations. Potential ET was assumed to be uniform each day of the month and consequently may have been overestimated on cloudy days and underestimated on clear days. For subareas with impervious surfaces, potential ET was not reduced to account for evaporation from impervious surfaces. Adjustments to reference ET at scales less than the spatial resolution of the reference ET maps, such as those related to shading in rugged terrain, were not accounted for in the model. Other conditions not considered in the model include the variability of soil moisture with regard to depth within the soil root zone, the effect of soil texture on irrigation demand, and removal of water from saturated groundwater zones by transpiration. Additionally, daily irrigation estimates were based on monthly variations in rainfall, runoff, and potential ET instead of daily variations. The daily irrigation estimates of the water budget may also differ from actual irrigation rates because, in addition to the model not reproducing actual daily rainfall, the model does not account for other factors—field observations, nonirrigation water needs, and water availability—that may be considered by irrigation managers each day. Direct recharge from cesspools and County watermain leakage was excluded from the analysis.

Water-Budget and Groundwater-Recharge Estimates

The water budget was used to calculate average recharge for average climate conditions, drought conditions, and seven historical periods. Monthly rainfall during 1978–2007 and 1998–2002 were used to represent average climate conditions and drought conditions, respectively. For the average climate conditions and drought conditions, 2000s land-cover conditions were used. For the seven historical periods, 1940–49, 1950–59, 1960–69, 1970–79, 1980–89, 1990–99, and 2000–12, monthly rainfall and land-cover conditions corresponding to the time period being represented were used. For all conditions and periods, mean monthly reference evapotranspiration was used.

Average Climate Conditions

Mean annual recharge of the island of Molokaʻi is about 227 Mgal/d for average climate conditions (table 1.4). Recharge is about 37 percent of rainfall and is about 35 percent of total inflow (sum of rainfall, fog interception, irrigation, and direct recharge). Expressed as a depth of water uniformly distributed across the island, mean annual recharge is about 18 inches.

The spatial pattern of mean annual recharge on Molokaʻi for average climate conditions resembles that of mean annual rainfall, but the pattern also reflects (1) spatial variations in vegetation and soils, (2) irrigation in agricultural and developed areas, (3) seepage from Kualapuʻu reservoir, and (4) persistent cloud layers where fog interception supplements rainfall (fig. 1.7). Recharge is highest along the eastern Molokaʻi mountain crest, where it is as much as about 130 in/yr near the boundary between the ʻUalapuʻe and Wailau aquifer systems. Recharge is much lower outside of the mountainous areas of the island. In undeveloped and nonagricultural areas at low altitude, recharge is commonly less than 5 in/yr. Detectable at these lower altitudes are the footprints of irrigated agricultural fields in central Molokaʻi, which contribute higher rates of recharge than adjacent, unirrigated areas. The additional recharge from seepage from the Kualapuʻu reservoir also is evident. A discontinuity in the recharge distribution exists along the border of the Hālawa Stream drainage basin, 16400000, and adjacent areas in northeastern Molokaʻi. Estimated recharge is considerably lower in the Hālawa Stream drainage basin than in the adjacent areas. The primary reason is the higher estimated mean runoff-to-rainfall ratios in the Hālawa Stream drainage basin compared to adjacent areas (fig. 1.7).

For most of Molokaʻi, the fraction of total water inflow that becomes groundwater recharge is less than 40 percent (fig. 1.8). The areas with the highest fraction, over 60 percent, are mainly in east Molokaʻi where mean annual rainfall exceeds 80 in. This roughly corresponds to the areas with highest recharge, where consistently wet conditions keep the soil moisture high. Other notable areas with a fraction over 60 percent include (1) the midaltitude areas of Kamiloloa and

Table 1.4. Mean annual water-budget estimates for average and drought conditions for each aquifer system, Molokaʻi, Hawaiʻi.

[See fig. 2 for locations of aquifer systems; Mgal/d, million gallons per day; Canopy evap, forest canopy evaporation; Total ET, total evapotranspiration, which includes forest-canopy evaporation. Average climate conditions for this study are 1978–2007 rainfall and land-cover condition during the 2000s. Drought conditions for this study are 1998–2002 rainfall and land-cover conditions during the 2000s. Components may not balance because of rounding and direct recharge from cesspools and reservoirs. The source of water for direct recharge may be from external sources, including groundwater and imported streamflow. Some recharge may discharge to streams as base flow]

Aquifer system	Aquifer code	Hypothetical condition	Water-budget component (Mgal/d)							
			Rain	Fog	Irrigation	Direct recharge	Runoff	Canopy evap.	Total ET	Recharge
Kaluakoʻi	40101	Average	45.52	0.00	0.05	0.02	1.86	5.69	36.34	7.42
		Drought	29.69	0.00	0.05	0.02	1.13	4.03	26.47	2.69
Punakou	40102	Average	34.26	0.00	0.02	0.01	1.38	2.68	25.37	7.60
		Drought	21.77	0.00	0.03	0.01	0.80	1.87	18.49	2.82
Hoʻolehua	40201	Average	17.87	0.00	1.12	0.02	1.06	2.48	15.24	2.71
		Drought	10.92	0.00	1.25	0.02	0.60	1.67	11.13	0.61
Manawainui	40202	Average	24.50	0.00	2.87	0.17	1.23	2.05	21.53	4.96
		Drought	13.71	0.00	3.23	0.17	0.65	1.30	15.64	1.30
Kualapuʻu	40203	Average	42.83	1.54	0.89	0.42	4.11	10.10	29.32	12.51
		Drought	27.80	1.10	1.06	0.42	2.58	7.30	23.02	5.23
Kamiloloa	40301	Average	37.25	3.04	0.18	0.03	3.26	6.69	19.20	18.05
		Drought	27.05	2.48	0.19	0.03	2.33	5.39	16.15	11.31
Kawela	40302	Average	46.47	4.17	0.00	0.00	10.71	6.38	23.22	16.70
		Drought	36.38	3.42	0.00	0.00	8.58	5.44	20.75	10.54
ʻUalapuʻe	40303	Average	68.70	4.13	0.01	0.00	13.72	10.63	31.72	27.38
		Drought	55.66	3.43	0.01	0.00	10.92	9.31	28.76	19.46
Waialua	40304	Average	53.13	1.51	0.00	0.00	7.40	9.40	29.38	17.83
		Drought	38.66	1.15	0.00	0.00	5.29	7.76	25.00	9.56
Kalaupapa	40401	Average	9.57	0.00	0.02	0.01	1.71	0.41	6.40	1.50
		Drought	6.85	0.00	0.02	0.01	1.20	0.31	5.18	0.54
Kahanui	40402	Average	20.49	1.59	0.00	0.00	2.70	3.42	9.52	9.86
		Drought	16.33	1.31	0.00	0.00	2.11	2.98	8.79	6.70
Waikolu	40403	Average	21.41	1.56	0.00	0.00	5.19	2.13	7.76	10.01
		Drought	18.41	1.34	0.00	0.00	4.47	1.97	7.60	7.64
Haʻupu	40404	Average	11.25	0.73	0.00	0.00	1.82	1.30	4.76	5.39
		Drought	9.35	0.61	0.00	0.00	1.51	1.18	4.57	3.86
Pelekunu	40405	Average	38.88	1.64	0.00	0.00	5.53	2.99	13.22	21.75
		Drought	31.82	1.35	0.00	0.00	4.43	2.78	12.87	15.83
Wailau	40406	Average	75.43	4.09	0.00	0.05	16.80	7.09	22.90	39.83
		Drought	61.22	3.33	0.00	0.05	13.47	6.48	21.95	29.09
Hālawa	40407	Average	59.97	4.43	0.00	0.00	16.18	10.95	24.90	23.30
		Drought	43.32	3.31	0.00	0.00	11.66	9.13	21.99	12.92
Island of Molokaʻi		Average	607.51	28.44	5.16	0.73	94.65	84.40	320.78	226.81
		Drought	448.95	22.83	5.83	0.73	71.72	68.90	268.36	140.10

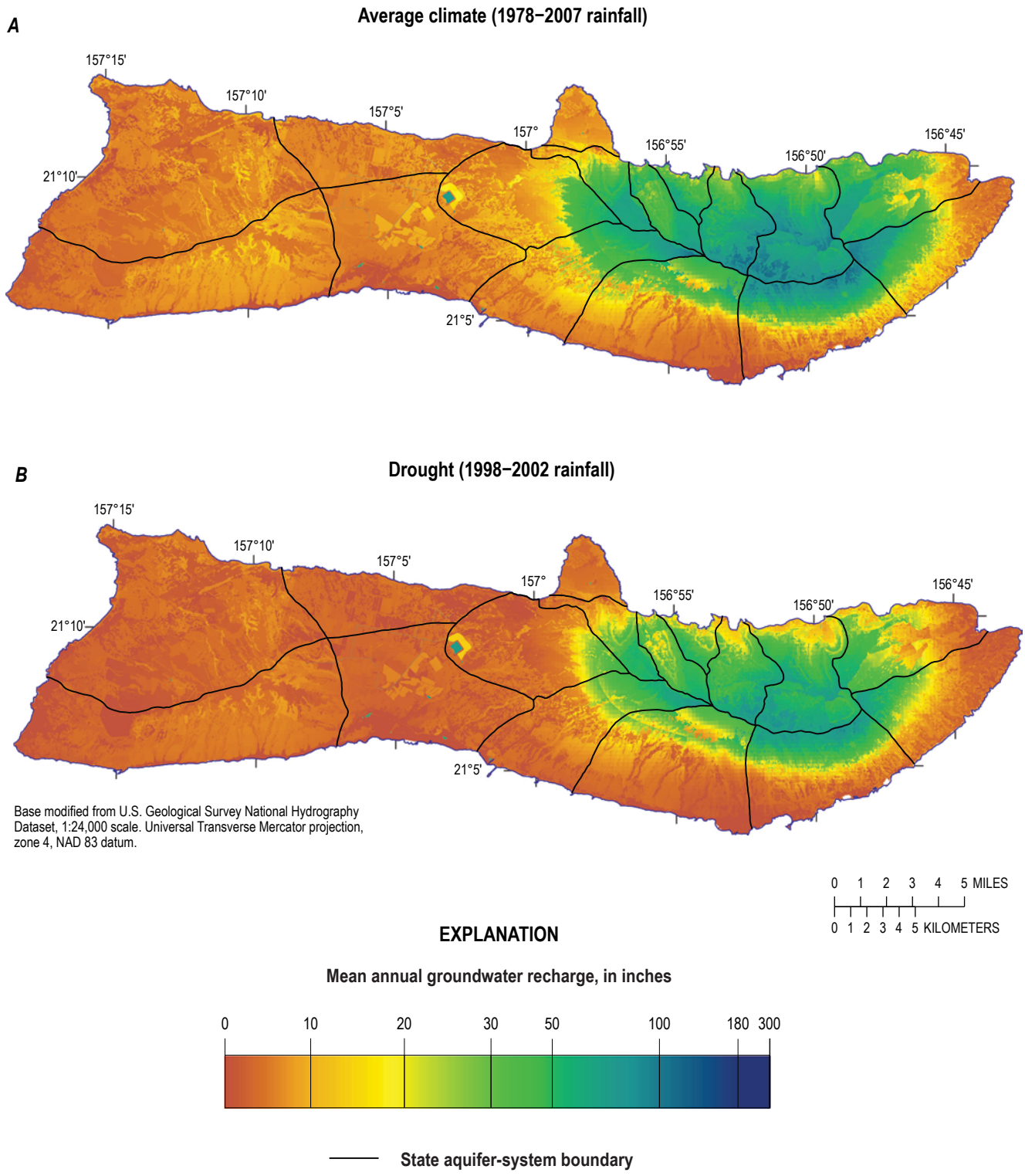

Figure 1.7. Maps of Moloka‘i, Hawai‘i showing the distribution of mean annual groundwater recharge, calculated with a water budget, for land-cover conditions during the 2000s and (*A*) average climate conditions (1978–2007 rainfall) and (*B*) drought conditions (1998–2002 rainfall).

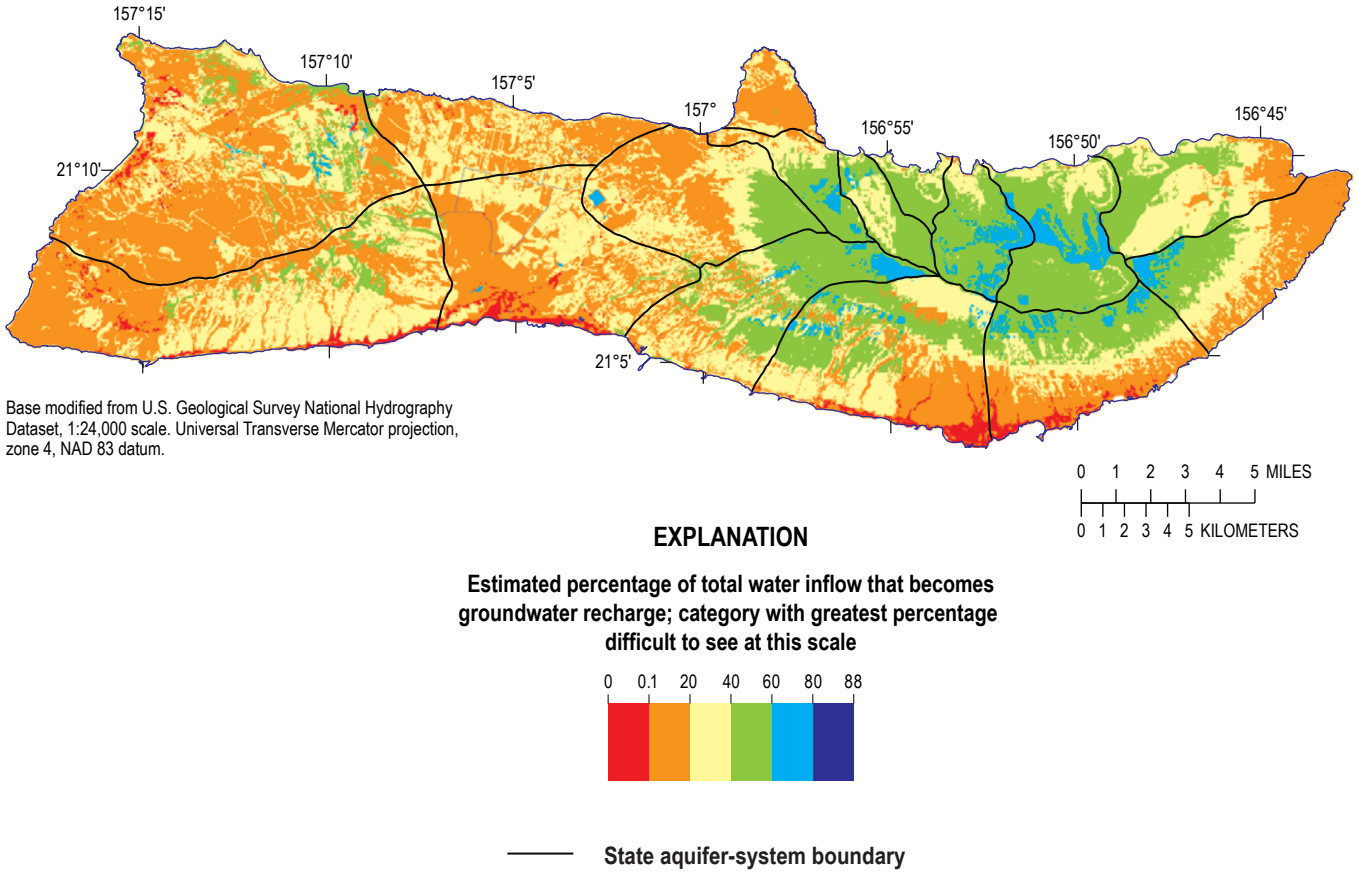

Figure 1.8. Map of Molokaʻi, Hawaiʻi showing estimated percentage of total water inflow (rainfall, fog interception, irrigation, and direct recharge) that becomes groundwater recharge in the water budget for average climate (1978–2007 rainfall) and using land-cover conditions during the 2000s.

Kawela aquifer systems, (2) patches of west Molokaʻi, where very low soil-moisture storage capacity is primarily responsible (fig. 1.6); and (3) the Kualapuʻu reservoir.

Comparison with the 1990 Water Resources Protection Plan

The 1990 Water Resources Protection Plan (State of Hawaiʻi, 1990; referred to as the 1990 WRPP) used water-budget methods to generate recharge estimates for each aquifer system on Molokaʻi. Island wide, the recharge estimate in this study for average climate conditions is 58 percent higher than in the 1990 WRPP (table 1.5). Recharge estimates from this study are higher than estimates in the 1990 WRPP for 11 of the 16 aquifer systems.

The reasons for differences in the recharge estimates between the 1990 WRPP and this study are related to (1) the different computational intervals used, (2) the different methods and datasets used to estimate individual water-budget components, and (3) the inclusion or exclusion of other components (table 1.6). The 1990 WRRP used an annual computational interval, whereas this study uses a daily interval. In general, uncertainty in recharge estimates is less for water budgets calculated using the shortest computational interval that is consistent with the physical processes being represented (Oki, 2008). The 1990 WRPP states that ET was estimated as (1) 40 in/yr for areas where mean rainfall was at least 55 in/yr, and (2) 73 percent of rainfall for areas where mean rainfall was less than 55 in/yr. In this study, ET is calculated daily on the basis of spatially distributed mean monthly potential ET, soil moisture, vegetative cover, and soil type. The runoff-rainfall relations used to estimate runoff in the 1990 WRPP were developed from streamflow measurements without subtracting base flow. In contrast, base flow was subtracted from streamflow measurements when developing the runoff-rainfall relations for this study. Fog interception is included in this study, but not in the 1990 WRPP. Rainfall estimates of the WRPP are based on 1916–83 mean isohyets (Giambelluca and others, 1986), whereas estimates of this study are based on 1978–2007 monthly rainfall maps (Frazier and others, 2016). Different spatial extrapolation techniques were used to prepare these two rainfall datasets; therefore, the difference in the rainfall values for any given area may not be attributable only to the different periods of record. Additionally, the 1990 WRPP did not account for irrigation, seepage from reservoirs, and leaks from the MIS distribution system.

Table 1.5. Comparison of water-budget estimates from this study with two previous studies, Molokaʻi, Hawaiʻi.

[Total ET, total evapotranspiration, which includes forest-canopy evaporation; 1990 WRPP, Water Resources Protection Plan (State of Hawaiʻi, 1990); values in million gallons per day; values for this study are for average-climate conditions calculated using 1978–2007 rainfall and land-cover conditions during the 2000s, rounded to the nearest whole number]

Aquifer system	Aquifer code	Water inflow			Runoff			Total ET			Recharge		
		This study	1990 WRPP	Shade (1997)	This study	1990 WRPP	Shade (1997)	This study	1990 WRPP	Shade (1997)[a]	This study	1990 WRPP	Shade (1997)[b]
Kaluakoʻi	40101	46	43	43	2	2	5	36	34	31	7	7	7
Punakou	40102	34	28	25	1	2	3	25	20	18	8	6	5
Hoʻolehua	40201	19	19	18	1	1	2	15	14	13	3	4	4
Manawainui	40202	28	21	22	1	1	2	22	15	16	5	5	4
Kualapuʻu	40203	46	34	39	4	2	4	29	25	23	13	9	11
Kamiloloa	40301	40	29	27	3	2	3	19	21	15	18	7	9
Kawela	40302	51	54	37	11	3	4	23	39	20	17	11	13
ʻUalapuʻe	40303	73	58	69	14	6	10	32	34	35	27	18	24
Waialua	40304	55	53	43	7	6	6	29	28	24	18	19	13
Kalaupapa	40401	10	10	8	2	1	1	6	7	4	2	3	3
Kahanui	40402	22	16	24	3	1	3	10	10	9	10	4	12
Waikolu	40403	23	18	25	5	4	6	8	9	8	10	6	11
Haʻupu	40404	12	10	15	2	2	3	5	5	5	5	3	8
Pelekunu	40405	41	35	39	6	10	6	13	14	14	22	12	19
Wailau	40406	80	62	75	17	16	13	23	25	24	40	20	38
Hālawa	40407	64	44	43	16	7	17	25	26	16	23	10	10
Island of Molokaʻi		642	534	552	95	66	88	321	326	275	227	144	191

[a]Values shown are from the "average AE" column in table 6 of Shade (1997).

[b]Values shown are from the "average recharge" column in table 6 of Shade (1997).

Comparison with Shade (1997)

Shade (1997) also used water-budget methods (method 1 and method 2) to generate recharge estimates for each aquifer system on Molokaʻi. Shade (1997) calculated recharge using two different accounting sequences. In method 1, recharge was calculated prior to subtracting ET from soil moisture in the plant-root zone. In method 2, recharge was calculated after subtracting ET. In table 6 of Shade (1997), estimates for recharge using method 1, method 2, and the average of the recharge calculated using the two methods are presented for each aquifer system. For this study, comparisons are made to "average recharge" presented in table 6 of Shade (1997) because these were used by the State Commission on Water Resource Management to update the 1990 WRPP (State of Hawaiʻi, 2008). Island wide, the recharge estimate in this study for average climate conditions is 19 percent higher than Shade (1997) (table 1.5). Recharge estimates from this study are higher than estimates in Shade (1997) for 10 of the 16 aquifer systems.

As with the 1990 WRPP, differences in the recharge estimates between Shade (1997) and this study are related to (1) the different computational intervals used, (2) the different methods and datasets used to estimate individual water-budget components, and (3) the inclusion or exclusion of other components (table 1.6). Shade (1997) used a monthly computational interval, whereas this study uses a daily interval, which is generally more accurate. Fog interception is included in this study, but not in Shade (1997). Rainfall estimates in Shade (1997) are based on 1916–83 mean monthly isohyets (Giambelluca and others, 1986), whereas estimates of this study are based on 1978–2007 monthly rainfall maps (Frazier and others, 2016). Outside of the drainage basins for streamgaging stations 16400000, 16404200, and 16408000, which encompass a very small percentage of the area of Molokaʻi, runoff-to-rainfall ratios in Shade (1997) were taken from results of a water budget for southern Oʻahu (Giambelluca, 1983) and applied to areas on Molokaʻi with similar rainfall and soils characteristics. Shade (1997) uses pan-evaporation estimates as estimates of potential ET without adjusting for land-cover

Table 1.6. Important differences between the recharge-estimation methods used in this study and the recharge-estimation methods used in the Water Resources Protection Plan (State of Hawai‘i, 1990) and Shade (1997).

[1990 WRPP, Water Resources Protection Plan (State of Hawai‘i, 1990); comparing to “average recharge” in table 6 of Shade (1997)]

Factor	This study	1990 WRPP and Shade (1997)	Effect on amount of recharge estimated in this study relative to the 1990 WRPP and Shade (1997) recharge estimates[1]
Fog interception	Included	Not included	More
Direct recharge[2]	Included	Not included	More
Rainfall	1978–2007 monthly rainfall (Frazier, 2012)	1916–1983 mean annual rainfall (Giambelluca and others, 1986)	Indeterminate (depends on area being considered)

Factor	This study	1990 WRPP	Effect on amount of recharge estimated in this study relative to the 1990 WRPP recharge estimates[1]
Computational interval	Daily	Annual	More
Irrigation	Included	Not included	More
Direct runoff	Estimated as the difference between streamflow and base flow	Estimated as being equal to streamflow (without subtracting base flow)	More
Total evapotranspiration (ET)	Estimated using potential ET derived from crop coefficients, decreasing ET with soil-moisture depletion; canopy evaporation is separately estimated and included for forests	Estimated on the basis of mean annual rainfall; canopy evaporation is not separately estimated	Indeterminate (depends on area being considered)

Factor	This study	Shade (1997)	Effect on amount of recharge estimated in this study relative to the Shade (1997) recharge estimates[1]
Computational interval	Daily	Monthly	More
Direct runoff outside gaged basins	Estimated using regional regression equations derived from basin characteristics	Estimated from results of a water budget for southern O‘ahu (Giambelluca, 1983) and applied to areas on Moloka‘i with similar rainfall and soils characteristics	Indeterminate (depends on area being considered)
Total evapotranspiration (ET)	Estimated using potential ET derived from crop coefficients, decreasing ET with soil-moisture depletion; canopy evaporation is separately estimated and included for forests	Estimated using pan evaporation with no land-cover/crop adjustment, no decreasing ET rate with soil-moisture depletion; canopy evaporation is not separately estimated	Indeterminate (depends on area being considered)
Water-budget accounting sequence	ET is subtracted from soil moisture prior to calculating recharge	ET is taken as the average of 2 methods: (1) ET is subtracted from soil moisture after calculating recharge and (2) ET is subtracted from soil moisture prior to calculating recharge	Less

[1]All other factors being equal.

[2]Includes leakage from the Kualapu‘u reservoir, leakage from the distribution piping associated with the Moloka‘i Irrigation System, and seepage from other water bodies.

conditions, whereas crop coefficients are used in this study to account for variation in potential ET related to land-cover class. In Shade (1997), the rate of actual ET is assumed to occur at the potential (maximum) ET rate even as soil moisture decreases to the wilting point, ignoring the effects of soil-moisture stress, which tend to reduce the rate of actual ET as soil-moisture is depleted (Allen and others, 1998). Recharge estimates in wet areas are sensitive to factors that include forest-canopy evaporation (Johnson and others 2018); a factor separately accounted for in this study but not by Shade (1997).

Drought Conditions

Rainfall during 1998–2002 was selected to represent drought conditions on Moloka‘i. This period had the lowest 5-year moving average of total rainfall on the island during 1920–2012 (fig. 1.9) (Giambelluca and others, 2013; Frazier and others, 2016). Other than rainfall, all inputs to the water budget were the same as those used for average climate conditions. Although other factors during 1998–2002, including potential ET, may have differed from the average climate condition, data were not available to characterize their distributions on Moloka‘i during this drought period. Furthermore, rainfall is the largest component of the water budget and therefore using rainfall during 1998–2002 is generally representative of drought conditions.

Groundwater recharge of the island of Moloka‘i for drought conditions is about 140 Mgal/d, which is 38 percent lower than recharge for average climate conditions (table 1.4). Rainfall in individual aquifer systems for drought conditions ranges from 14 to 44 percent lower than corresponding rainfall for average climate conditions (table 1.4). Recharge in individual aquifer systems for drought conditions ranges from about 24 to 77 percent lower than corresponding recharge for average climate conditions. The reduction in recharge for drought conditions, as a percentage (fig. 1.10), tends to be more pronounced in areas with lower mean annual rainfall. The reduction in recharge for drought conditions is directly related to the reduction in rainfall relative to average climate conditions, except in areas with inflows from irrigation and direct recharge.

1940–2012 Conditions

Groundwater recharge was estimated for seven time periods; 1940–49, 1950–59, 1960–69, 1970–79, 1980–89, 1990–99, and 2000–12; using the corresponding land-cover conditions (fig. 1.2) and rainfall of each time period. Island-wide recharge was highest during 1960–69 and lowest during 1970–79 (table 1.7), corresponding to the time periods with highest and lowest island-wide rainfall, respectively. In nonagricultural areas, the relative spatial distribution of recharge of each time period (fig. 1.11) strongly resembles the distribution discussed for average climate conditions. In agricultural areas, recharge generally is enhanced by irrigation. In the pineapple fields, recharge is additionally enhanced by the very low water use of the crop. Differences in the relative spatial distributions of recharge among the time periods are due primarily to changing agricultural land use.

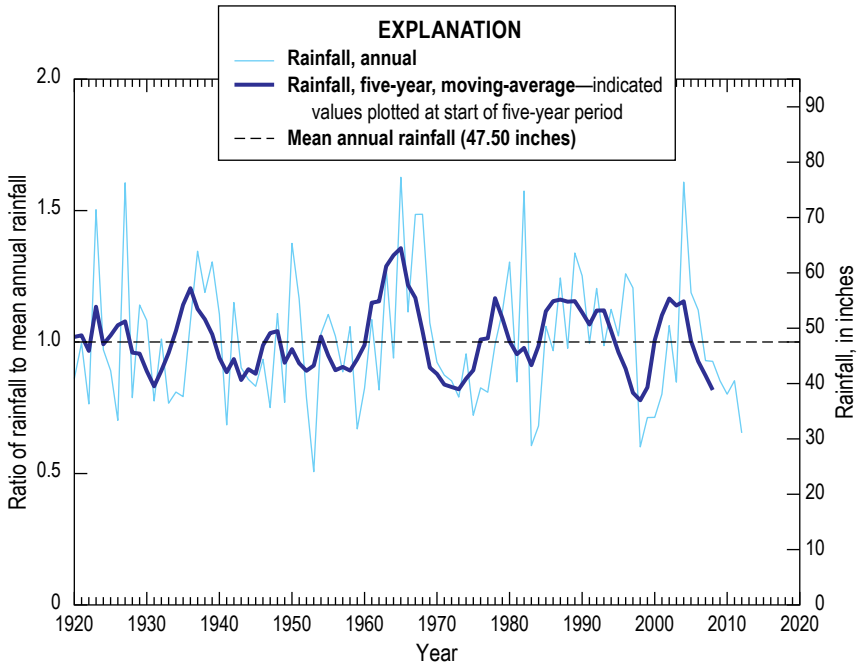

Figure 1.9. Graph showing annual and five-year, moving-average rainfall during 1920 to 2012 on Moloka‘i, Hawai‘i (data from Giambelluca and others, 2013).

Table 1.7. Estimated mean annual groundwater recharge in million gallons per day for seven time periods during 1940–2012 for each aquifer system, Moloka‘i, Hawai‘i.

Aquifer system	Aquifer code	1940–49	1950–59	1960–69	1970–79	1980–89	1990–99	2000–12
Kaluako‘i	40101	10.15	11.29	15.83	6.37	8.01	5.56	6.83
Punakou	40102	6.98	7.82	12.43	6.78	7.62	6.01	7.49
Ho‘olehua	40201	4.06	4.27	5.49	2.43	3.04	2.13	2.21
Manawainui	40202	4.47	6.39	7.53	3.72	5.32	3.51	4.24
Kualapu‘u	40203	10.68	13.34	15.47	9.97	15.83	10.47	8.39
Kamiloloa	40301	16.24	16.64	19.42	14.17	18.44	16.71	15.23
Kawela	40302	15.79	17.36	20.42	15.75	18.37	18.18	17.07
‘Ualapu‘e	40303	22.56	24.90	32.68	22.35	26.22	29.23	27.05
Waialua	40304	15.85	16.71	21.26	13.79	18.99	17.41	15.81
Kalaupapa	40401	1.51	1.52	2.11	1.31	1.71	1.18	1.15
Kahanui	40402	10.36	9.70	11.47	7.99	11.15	9.58	7.36
Waikolu	40403	10.84	9.82	12.14	8.87	11.13	10.79	9.17
Ha‘upu	40404	5.35	5.10	6.33	4.60	5.72	5.35	4.64
Pelekunu	40405	19.08	19.11	24.39	18.55	21.65	21.78	20.00
Wailau	40406	34.60	36.66	45.06	33.98	40.69	41.55	38.18
Hālawa	40407	19.70	21.17	25.78	18.65	26.40	23.06	19.96
Island of Moloka‘i		208.23	221.81	277.82	189.28	240.29	222.51	204.79

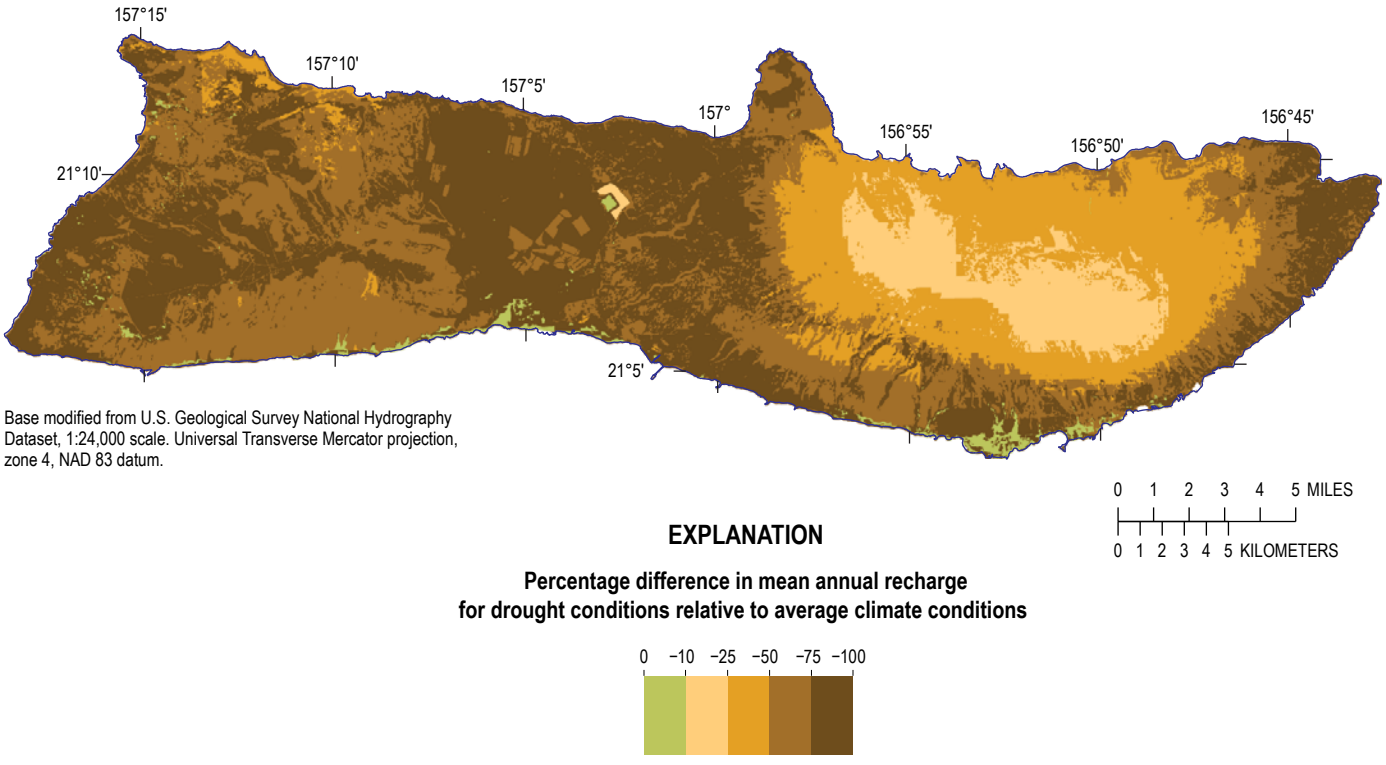

Figure 1.10. Map of Moloka‘i, Hawai‘i showing percentage difference in mean annual groundwater recharge for drought conditions (1998–2002 rainfall) relative to average climate conditions (1978–2007 rainfall).

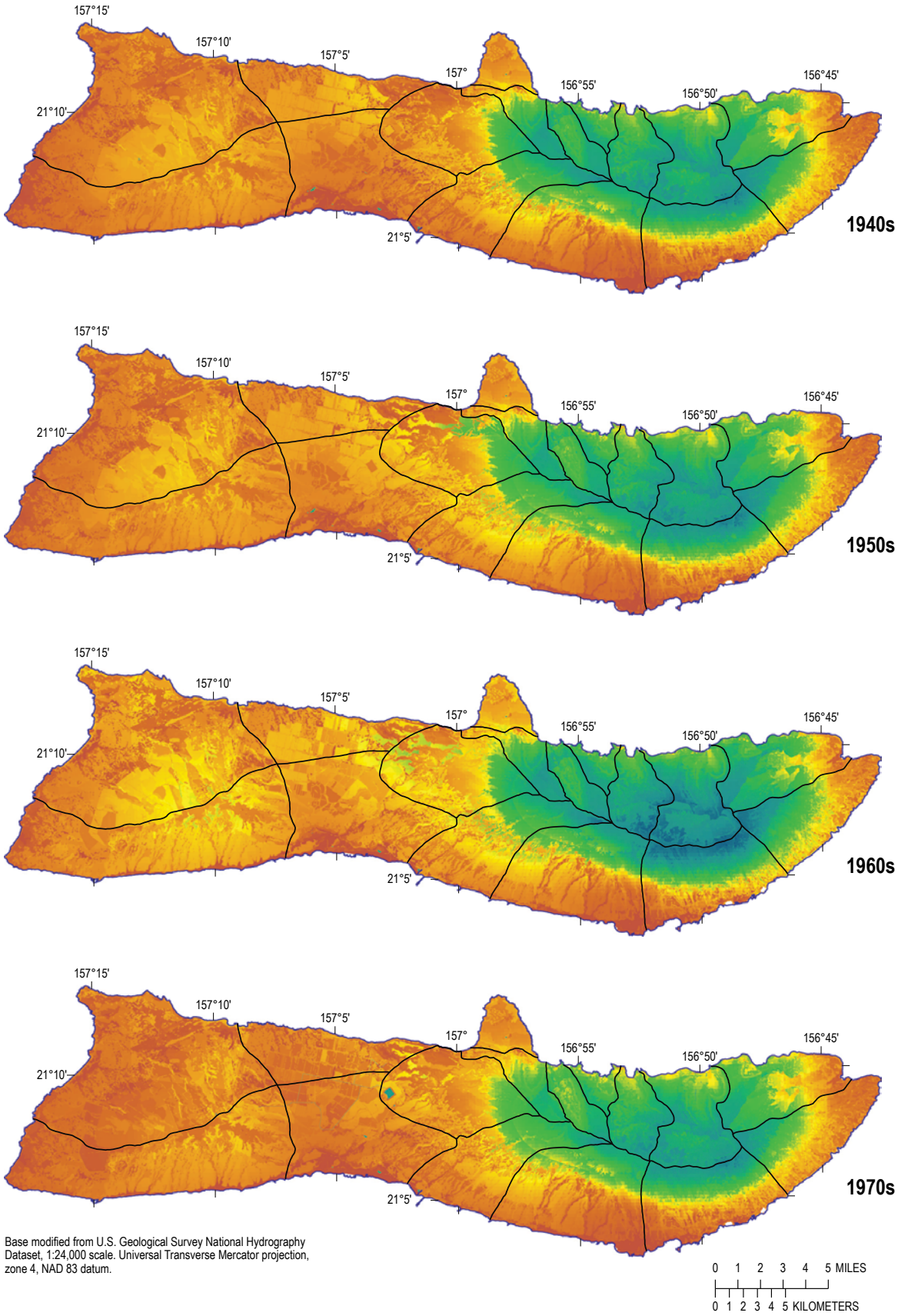

Figure 1.11. Maps of Molokaʻi, Hawaiʻi showing distribution of mean annual groundwater recharge for seven time periods during 1940–2012, calculated with a water budget.

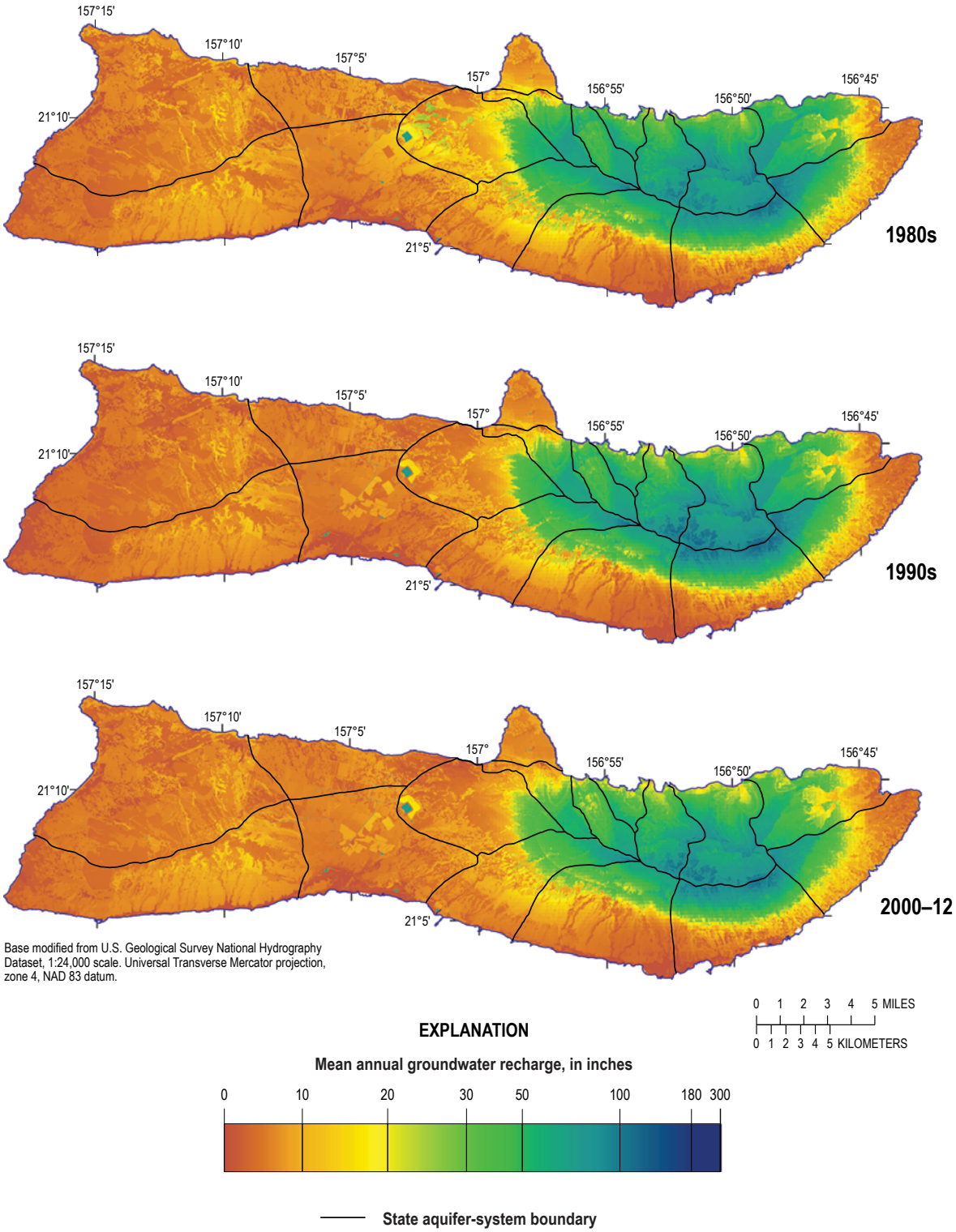

Figure 1.11.—Continued

Sensitivity Analysis

Uncertainty exists in many of the water-budget inputs used in this study. To analyze the effect that uncertainty in water-budget inputs has on estimated recharge, the water budget was rerun, changing one input value at a time within a reasonable range. The parameters tested were (1) available water capacity, (2) fog interception-to-rainfall ratio, (3) root depth, (4) runoff-to-rainfall ratio, (5) crop coefficient, and (6) canopy capacity. For available water capacity, the high and low published values (U.S. Department of Agriculture, 2006d) were tested. For fog interception-to-rainfall ratio and root depth, the values used in the water-budget calculations were increased and decreased by 50 percent relative to the original values. Runoff-to-rainfall ratios were adjusted on the basis of bias and root-mean-square-error statistics of the runoff regression models (table 1.2). For crop coefficients, values were increased and decreased by 20 percent relative to the original values. Canopy capacity values of 0.08 and 0.02, corresponding to an increase and decrease of 0.03 from the baseline value, were tested.

The recharge estimates for the sensitivity analysis are compared with recharge estimates for average climate conditions for the entire island of Molokaʻi, as well as the Hoʻolehua, Kawela, and Waikolu aquifer systems (table 1.8). These three aquifer systems cover a range of climates and land-cover conditions on Molokaʻi. The Hoʻolehua aquifer system is representative of the windy central plain of Molokaʻi, where reference ET is high, rainfall is moderate, and agriculture is a primary land use. The Kawela aquifer system is representative of leeward east Molokaʻi. It encompasses a wide variety of land-cover and climate conditions from fog forest at the higher altitudes to dry, shrub- and grassland near the coast. The Waikolu aquifer system is important for the MIS and is representative of the highly eroded valleys of windward east Molokaʻi, where rainfall is high.

For the entire island of Molokaʻi and the three individual aquifer systems tested, recharge estimates are very sensitive to changes in runoff-to rainfall ratios (table 1.8). Available water capacity, root depth, and crop coefficients also have substantial effects on recharge in the Hoʻolehua aquifer system. All three parameters are related to ET estimation, showing the importance of this component of the water budget in an area where annual reference ET is substantially higher than rainfall. For the Kawela aquifer system, recharge estimates were also very sensitive to changes in the fog interception-to-rainfall ratio because recharge in this aquifer system is highest in the fog forest. Recharge in the Waikolu aquifer system is also sensitive to the fog interception-to-rainfall ratio for the same reason. For both the Kawela and Waikolu aquifer systems, crop coefficients have a smaller but substantial effect on recharge compared to the fog interception-to-rainfall ratio.

Table 1.8. Results of sensitivity testing for selected water-budget parameters performed for selected aquifer systems and the island of Molokaʻi, Hawaiʻi.

[See fig. 2 for locations of aquifer systems; baseline parameters are those used for average climate conditions; %, percent; RMSE, prediction root-mean-square error of regional runoff-to-rainfall ratio regression]

Parameter	Adjusted parameter value	Percentage difference in recharge relative to scenario for average climate conditions for aquifer systems and the island of Molokaʻi			
		Hoʻolehua	Kawela	Waikolu	Island of Molokaʻi
Available water capacity	High reported value[1]	−13.8	−1.5	−0.4	−2.0
	Low reported value[1]	26.3	1.7	0.5	2.7
Fog interception−to−rainfall ratio	50% of baseline	0.0	−10.1	−7.0	−5.5
	150% of baseline	0.0	10.2	7.0	5.5
Root depth	150% of baseline	−23.0	−4.0	−1.4	−3.6
	50% of baseline	41.8	7.4	3.2	7.1
Runoff−to−rainfall ratio	Regression bias adjustment[2]	−6.2	−4.5	−1.7	−7.7
	Increase by regression RMSE[3]	−41.8	−23.9	−8.8	−26.9
	Decrease by regression RMSE[3]	18.1	12.6	2.9	16.4
Crop coefficient	120% of baseline	−9.7	−7.4	−7.6	−7.2
	80% of baseline	13.7	8.9	8.9	8.6
Canopy capacity	Increase by 0.03 units	−0.7	−4.3	−4.7	−4.8
	Decrease by 0.03 units	0.9	5.2	5.5	5.8

[1]Low and high values reported in U.S. Department of Agriculture (2006d).

[2]For leeward areas, runoff-to-rainfall ratios were increased by 35 and 48 percent for the wet and dry seasons, respectively. For windward areas, runoff-to-rainfall ratios were increased by 56 and 68 percent for the wet and dry seasons, respectively.

[3]For leeward areas, runoff-to-rainfall ratios were adjusted by 0.18 and 0.20 units for the wet and dry seasons, respectively. For windward areas, runoff-to-rainfall ratios were adjusted by 0.25 and 0.24 units for the wet and dry seasons, respectively.

Suggestions for Future Study and Additional Data Collection

Lack of data or sparse, uneven distribution of data in space and time, and poor understanding of some hydrologically relevant processes limit the accuracy of study results. This section discusses information that could advance future efforts to more accurately assess the distribution of groundwater recharge on Molokaʻi.

Rainfall is an essential dataset for estimating recharge. The placement of gages and their periods of operation generally have been dictated by the water-supply needs of humans—particularly agriculture (Giambelluca and others, 1986). Rain gages are scarce in areas that are less populated or unfavorable for agriculture, such as in the high-altitude interiors of islands or areas having rugged terrain. Although these tend to be the wettest areas of the islands and the areas where most recharge occurs, estimates of rainfall for these areas have greater uncertainty (Giambelluca and others, 2013). Recharge estimates can be improved with rainfall data from these sparsely gaged areas.

Fog-interception data are particularly scant. Fog interception provides a substantial part of the water available for groundwater recharge over large areas of the Hawaiian Islands but has been quantified by only a few studies in a few places. As a result, fog-interception distribution was applied in a very generalized fashion in the recharge calculation. Recharge estimates can be improved with a better quantification of the spatial and temporal variability of fog-interception rates, and the ability of different types of vegetation to intercept fog.

An acknowledged limitation of the water budget is that monthly reference ET is uniformly distributed among each day of the month, regardless of the daily rainfall distribution over the month. In reality, reference ET should be lower during cloudy, rainy days than during sunny days. Recharge estimates could be improved with more measurements of the daily variations of reference ET across the study area.

Another ET-related limitation of this study is the current lack of data needed to more accurately differentiate ET parameters among native and alien species of plants. Replacement of native forest by invasive alien plants like *P. cattleianum* (strawberry guava) has occurred in many forested areas in Hawaiʻi. More data could be used to develop better crop coefficients for native and alien plants. These improvements would help to better estimate the difference in recharge that could be expected in native relative to alien-dominated forests.

The accuracy of the modified Gash canopy-interception model used in this study is limited by the quantity, quality, and spatial distribution of data used to develop model parameters. Field measurements of one parameter, the ratio of the mean evaporation rate to the mean precipitation rate during saturated canopy conditions (V), are especially lacking. Additional measurements of canopy-evaporation and related parameters could be used to better confirm and calibrate the canopy-evaporation estimates of the modified Gash model.

Runoff is perhaps the most uncertain parameter in the recharge analysis. The runoff-to-rainfall ratio method in the water budget of this study was improved, relative to methods used in studies prior to 2014 for Hawaiʻi water-budget analyses, by developing regression equations relating the ratio to drainage-basin characteristics. These regression equations were used to estimate runoff-to-rainfall ratios in ungaged basins. Additional streamflow data from basins throughout Hawaiʻi, including Molokaʻi, could lead to development of improved regression equations. For Molokaʻi, the number of ungaged basins was far greater than the number of gaged basins, and ratios had to be extrapolated to some ungaged basins having characteristic values that were beyond the range of values used to develop the regression equations. Streamflow data from more basins with a wider range of characteristic values are needed to improve the regression approach to regionalizing runoff-to-rainfall ratios or to develop watershed models for estimating runoff.

Concurrent daily direct runoff and high-resolution rainfall data could improve understanding of the processes controlling temporal variability in runoff estimates. Results of the regional-regression analysis indicate that runoff in windward and leeward basins differ statistically. Better understanding of the physical basis of this statistical difference would improve conceptualization of runoff processes.

The water budget used in this study applies the runoff-to-rainfall ratios at the catchment-zone level. Ratios do not vary spatially within a catchment zone, even though the catchment zone may encompass a variety of land-cover conditions, soil types, slopes, and a range of climates. The catchment-zone-level application of runoff-to-rainfall ratios limits the ability of the model to assess differences in runoff and groundwater recharge that may exist between different areas within the catchment zone, such as between forested and deforested areas. Part of the limitation stems from the scarcity of studies assessing the variation in runoff rates for different vegetation, soil, and slope characteristics in Hawaiʻi. In a study comparing adjacent deforested rangeland and reforested areas on the southern slope of Haleakalā, Maui, Perkins and others (2012; 2014) found that the reforested areas had soil hydraulic properties that favored rapid and deep infiltration of water. This finding suggests that runoff may be lower from the forested area than from the deforested area of their study, but runoff was not measured. Better understanding of the processes and distribution of hydrogeological characteristics at the catchment-zone scale are important for answering questions that are often posed about watershed management, such as the effect of forest restoration on water resources.

References Cited

Allen, R.G., Pereira, L.S., Raes, D., and Smith, M., 1998, Crop evapotranspiration; guidelines for computing crop water requirements: Food and Agriculture Organization of the United Nations, FAO Irrigation and Drainage Paper 56, 300 p.

AWS Truewind, LLC, 2004, Wind Energy Resource Maps of Hawaiʻi: Prepared for Hawaiʻi Department of Business, Economic Development, and Tourism Strategic Industries Division, Honolulu, Hawaiʻi, 17 p, accessed January 25, 2012, at http://planning.Hawaii.gov/gis/download-gis-data/.

Baker, H.L., 1960, Molokai—present and potential land use: University of Hawaiʻi, Land Study Bureau Bulletin no. 1, 99 p.

Bruijnzeel, L.A.S., Eugster, W., and Burkard, R., 2005, Fog as a hydrologic input, chap. 38 *of* Anderson, M.G., ed., Encyclopedia of Hydrological Sciences: Hoboken, New Jersey, John Wiley and Sons, Ltd., p. 559–582.

DeLay, J.K., 2005, Canopy water balance on an elfin cloud forest at Alakahi, Hawaiʻi: Honolulu, University of Hawaiʻi, M.S. thesis, 78 p., accessed November 15, 2018, at http://hdl.handle.net/10125/11633.

DeLay, J.K., and Giambelluca, T.W., 2010, History of fog and cloud water interception research in Hawaiʻi, in Bruijnzeel, L.A., Scatena, F.N., and Hamilton, L.S., eds., Tropical montane cloud forests—Science for conservation and management: New York, Cambridge University Press, p. 332–341.

Ekern, P.C., 1964, Direct interception of cloud water on Lanaihale, Hawaii: Soil Science Society of America Proceedings, v. 28, no. 3, p. 419–421.

Engott, J.A., Johnson, A.G., Bassiouni, M., Izuka, S.K., and Rotzoll, K., 2017, Spatially distributed groundwater recharge for 2010 land cover estimated using a water-budget model for the Island of Oʻahu, Hawaiʻi (ver. 2.0, December 2017): U.S. Geological Survey Scientific Investigations Report 2015–5010, 49 p., accessed October 1, 2018, at https://doi.org/10.3133/sir20155010.

Engott, J.A., 2011, A water-budget model and assessment of groundwater recharge for the Island of Hawaiʻi: U.S. Geological Survey Scientific Investigations Report 2011–5078, 53 p., accessed October 1, 2018, at https://doi.org/10.3133/sir20115078.

Engott, J.A., and Vana, T.T., 2007, Effects of agricultural land-use changes and rainfall on ground-water recharge in central and west Maui, Hawaiʻi, 1926–2004: U.S. Geological Survey Scientific Investigations Report 2007–5103, 56 p., accessed October 1, 2018, at https://doi.org/10.3133/sir20075103.

Fares, A., 2008, Water management software to estimate crop irrigation requirements for consumptive use permitting in Hawaii: State of Hawaiʻi, Commission on Water Resource Management, accessed March 13, 2009, at, http://dlnr.hawaii.gov/cwrm/info/publications/.

Frazier, A.G., Giambelluca, T.W., Diaz, H.F., and Needham, H.L., 2016, Comparison of geostatistical approaches to spatially interpolate month-year rainfall for the Hawaiian Islands: International Journal of Climatology, v. 36, no. 3, p. 1459–1470, at http://dx.doi.org/10.1002/joc.4437.

Gash, J.H.C., Lloyd, C.R., and Lachaud, G., 1995, Estimating sparse forest rainfall interception with an analytical model: Journal of Hydrology, v. 170, p. 79–86.

Gaskill, T.G.R., 2004, Hydrology of forest ecosystems in the Honouliuli Preserve; implications for groundwater recharge and watershed restoration: Honolulu, University of Hawaiʻi, Ph.D. dissertation, 177 p., accessed November 15, 2018, at http://hdl.handle.net/10125/12116.

Gerrits, A.M.G, and Savenije, H.H.G., 2011, Interception, chapter 2.04 *of* Wilderer, Peter, ed., Treatise on Water Science, Volume 2: The Science of Hydrology, 2102 p.

Giambelluca, T.W., 1983, Water balance of the Pearl Harbor-Honolulu basin, Hawaiʻi, 1946–1975: University of Hawaiʻi Water Resources Research Center Technical Report no. 151, 151 p., accessed November 15, 2018, at http://hdl.handle.net/10125/1992.

Giambelluca, T.W., Chen, Q., Frazier, A.G., Price, J.P., Chen, Y.-L., Chu, P.-S., Eischeid, J.K., and Delparte, D.M., 2013, Online rainfall atlas of Hawaiʻi: Bulletin of the American Meteorological Society, v. 94, no. 3, p. 313–316, at https://rainfall.geography.Hawaii.edu/.

Giambelluca, T.W., DeLay, J.K., Nullet, M.A., Scholl, M.A., and Gingerich, S.B., 2011, Canopy water balance of windward and leeward Hawaiian cloud forests on Haleakalā, Maui, Hawaiʻi: Hydrological Processes, v. 25, p. 438–447, at https://doi.org/10.1002/hyp.7738.

Giambelluca, T.W., Nullet, M.A., and Schroeder, T.A., 1986, Rainfall atlas of Hawaiʻi: State of Hawaiʻi, Department of Land and Natural Resources, Report R76, 267 p.

Giambelluca, T.W., and Schroeder, T.A., 1998, Climate, *in* Juvik, S.P., and Juvik, J.O., eds., Atlas of Hawaiʻi, (3d ed.): Honolulu, University of Hawaiʻi Press, p. 49–59.

Giambelluca, T.W., Shuai, X., Barnes, M.L., Alliss, R.J., Longman, R.J., Miura, T., Chen, Q., Frazier, A.G., Mudd, R.G., Cuo, L., and Businger, A.D., 2014, Evapotranspiration of Hawaiʻi, final report: submitted to U.S. Army Corps of Engineers–Honolulu District and Commission on Water Resource Management, State of Hawaiʻi, 168 p., accessed November 15, 2018, at https://evapotranspiration.geography.hawaii.edu/downloads.html.

Harland Bartholomew and Associates, 1957, An inventory of available information on land use in Hawaii, vol. 1, evaluation and recommendations: Economic Planning and Coordination Authority, Territory of Hawai‘i, 100 p.

Helsel, D.R., and Hirsch, R.M., 1992, Statistical methods in water resources; studies in environmental science, volume 49: Amsterdam, Elsevier, 522 p.

Izuka, S.K., Engott, J.A., Rotzoll, K., Bassiouni, M., Johnson, A.G., Miller, L.D., and Mair, A., 2018, Volcanic aquifers of Hawai‘i —hydrogeology, water budgets, and conceptual models (ver. 2.0, March 21018): U.S. Geological Survey Scientific Investigations Report 2015–5164, 158 p., accessed November, 15, 2018, at https://doi.org/10.3133/sir20155164.

Izuka, S.K., Oki, D.S., and Chen, C., 2005, Effects of irrigation and rainfall reduction on ground-water recharge in the Lihue Basin, Kauai, Hawaii: U.S. Geological Survey Scientific Investigations Report 2005–5146, 48 p., accessed November 15, 2018, at https://doi.org/10.3133/sir20055146.

Johnson, A.G., 2012, A water-budget model and estimates of groundwater recharge for Guam: U.S. Geological Survey Scientific Investigations Report 2012–5028, 53 p., accessed November 15, 2018, at https://doi.org/10.3133/sir20125028.

Johnson, A.G., Engott, J.A., Bassiouni, M., and Rotzoll, K., 2018, Spatially distributed groundwater recharge estimated using a water-budget model for the Island of Maui, Hawai‘i, 1978–2007 (ver. 2.0, February 2018): U.S. Geological Survey Scientific Investigations Report 2014–5168, 53 p., accessed November 15, 2018, at https://doi.org/10.3133/sir20145168.

Juvik, J.O., DeLay, J.K., Kinney, K.M., and Hansen, E.W., 2011, A 50th anniversary reassessment of the seminal Lana‘i fog drip study in Hawai‘i: Hydrological Processes, v. 25, p. 402–410, accessed August 29, 2019, at https://onlinelibrary.wiley.com/doi/full/10.1002/hyp.7803.

Juvik, J.O., and Ekern, P.C., 1978, A climatology of mountain fog on Mauna Loa, Hawai‘i Island: University of Hawai‘i Water Resources Research Center Technical Report no. 118, 63 p., accessed November 15, 2018, at https://hdl.handle.net/10125/2006.

Juvik, J.O., and Nullet, D., 1995, Relationships between rainfall, cloud-water interception, and canopy throughfall in a Hawaiian montane forest, chap. 11 *of* Hamilton, L.S., Juvik, J.O., and Scatena, F.N., eds., Tropical montane cloud forests: New York, Springer-Verlag, p. 165–182.

Juvik, J.O., Nullet, D., Banko, P., and Hughes, K., 1993, Forest climatology near the tree line in Hawai‘i: Agricultural and Forest Meteorology, v. 66, nos. 3–4, p. 159–172.

Land Study Bureau, 1968, Detailed land classification, island of Molokai: University of Hawai‘i L.S.B. Bulletin no. 10, 90 p.

Leopold, L.B., Burn, S., and Stidd, C.K., 1948, A key to rain gages in Hawaii: The Hawaiian Planters’ Record, v. 52, nos. 3 and 4, p. 201–246.

McJannet, D., Wallace, J., Fitch, P., Disher, M., and Reddell, P., 2007, Water balance of tropical rainforest canopies in north Queensland, Australia: Hydrological Processes, v. 21, p. 3473–3484.

Mair, A., Johnson A.G., Rotzoll, K., and Oki, D.S., 2019, Estimated groundwater recharge from a water-budget model incorporating selected climate projections, Island of Maui, Hawai‘i: U.S. Geological Survey Scientific Investigations Report 2019–5064, 46 p., accessed August 15, 2019, at https://doi.org/10.3133/sir20195064.

Nance, T., 1982, Molokai water systems plan: Belt, Collins and Associates, prepared for the Maui County Department of Water Supply, 106 p.

National Oceanic and Atmospheric Administration, 2008, Coastal Change Analysis Program (C-CAP) Land Cover Atlas, O‘ahu, Hawai‘i 2005: Coastal Services Center, at https://coast.noaa.gov/ccapftp/#/.

Oki, D.S., 2002, Reassessment of ground-water recharge and simulated ground-water availability for the Hawi area of North Kohala, Hawaii: U.S. Geological Survey Water-Resources Investigations Report 02–4006, 62 p., accessed November 15, 2018, at https://doi.org/10.3133/wri20024006.

Oki, D.S., 2003, Surface water in Hawaii: U.S. Geological Survey Fact Sheet 045–03, accessed November 15, 2018, at https://doi.org/10.3133/fs04503.

Oki, D.S., 2008, The significance of accounting order for evapotranspiration and recharge in monthly and daily threshold-type water budgets: U.S. Geological Survey Scientific Investigations Report 2008–5163, 11 p., accessed November 15, 2018, at https://doi.org/10.3133/sir20085163.

Perkins, K.S., Nimmo, J.R., and Medeiros, A.C., 2012, Effects of native forest restoration on soil hydraulic properties, Auwahi, Maui, Hawaiian Islands: Geophysical Research Letters, v. 39, no. 5, 4 p., at https://doi.org/10.1029/2012GL051120.

Perkins, K.S., Nimmo, J.R., Medeiros, A.C., Szutu, D.J., and von Allmen, E., 2014, Assessing effects of native forest restoration on soil moisture dynamics and potential aquifer recharge, Auwahi, Maui: Ecohydrology, v. 7, no. 5, p. 1437–1451, https://doi.org/10.1002/eco.1469.

Rea, A., and Skinner, K.D., 2012, Geospatial datasets for watershed delineation and characterization used in the Hawaii StreamStats web application: U.S. Geological Survey Data Series 680, 12 p., at http://pubs.usgs.gov/ds/680/.

Rosa, S.N., and Oki, D.S., 2010, Hawaii StreamStats—A web application for defining drainage-basin characteristics and estimating peak-streamflow statistics: U.S. Geological Survey Fact Sheet 2010–3052, 4 p., at https://water.usgs.gov/osw/streamstats/hawaii.html.

Safeeq, M., and Fares, A., 2014, Interception losses in three non-native Hawaiian forest stands: Hydrological Processes, v. 28, no. 2, p. 237–254, at https://doi.org/10.1002/hyp.9557.

Santo, L.T., 2001, Assessment and improvement recommendations for the Molokai Irrigation System: Hawaiʻi Agriculture Research Center, 52 p.

Savenije, H.H.G., 2004, The importance of interception and why we should delete the term evapotranspiration from our vocabulary: Hydrological Processes, v. 18, p. 1507–1511.

Scholl, M.A., Giambelluca, T.W., Gingerich, S.B., Nullet, M.A., and Loope, L.L., 2007, Cloud water in windward and leeward mountain forests; the stable isotope signature of orographic cloud water: Water Resources Research, v. 43, W12411, 13 p.

Shade, P.J., 1997, Water budget for the island of Molokai, Hawaii: U.S. Geological Survey Water-Resources Investigations Report 97–4155, 20 p., accessed November 15, 2018, at https://doi.org/10.3133/wri974155.

Shuttleworth, W.J., 1993, Evaporation, chap. 4 *of* Maidment, D.R., ed., Handbook of hydrology: New York, McGraw-Hill, p. 4.1–4.53.

State of Hawaiʻi, 1966, Water resources development—Molokai: Department of Land and Natural Resources, Bulletin B16, 69 p.

State of Hawaiʻi, 1969, Island of Molokai, Waikolu and Pelekunu Valleys water resources feasibility study: Department of Land and Natural Resources, Division of Water and Land Development, prepared by Parsons Brinckerhoff-Hirota Associates, variously paged.

State of Hawaiʻi, 1990, Water resources protection plan, volumes I and II, June 1990: State of Hawaiʻi, Commission on Water Resource Management, variously paginated.

State of Hawaiʻi, 2008, Water resource protection plan, June 2008: State of Hawaiʻi, Commission on Water Resource Management, variously paginated, accessed November 15, 2018, at https://dlnr.hawaii.gov/cwrm/planning/hiwaterplan/wrpp/wrpp2008/.

Takahashi, M., Giambelluca, T.W., Mudd, R.G, DeLay, J.K., Nullet, M.A., and Asner, G.P., 2011, Rainfall partitioning and cloud water interception in native forest and invaded forest in Hawaiʻi Volcanoes National Park: Hydrological Processes, v. 25, no. 3, p. 448–464, https://doi.org/10.1002/hyp.7797.

Thornthwaite, C.W., and Mather, J.R., 1955, The water balance: Publications in Climatology, v. 8, no. 1, p. 1–104.

U.S. Department of Agriculture, 1983, Agricultural land use in the State of Hawaii, island of Molokai, November 1982: Fort Worth, Texas, map.

U.S. Department of Agriculture, 2006a, Soil survey geographic (SSURGO) database for the island of Oʻahu: U.S. Department of Agriculture, Natural Resources Conservation Service, accessed June 8, 2011, at http://SoilDataMart.nrcs.usda.gov/.

U.S. Department of Agriculture, 2006b, Soil survey geographic (SSURGO) database for the island of Maui: U.S. Department of Agriculture, Natural Resources Conservation Service, accessed October 3, 2011, at http://SoilDataMart.nrcs.usda.gov/.

U.S. Department of Agriculture, 2006c, Soil survey geographic (SSURGO) database for the island of Kauaʻi: U.S. Department of Agriculture, Natural Resources Conservation Service, accessed September 4, 2012, at http://SoilDataMart.nrcs.usda.gov/.

U.S. Department of Agriculture, 2006d, Soil survey geographic (SSURGO) database for the island of Molokaʻi: U.S. Department of Agriculture, Natural Resources Conservation Service, accessed December 20, 2011, at http://SoilDataMart.nrcs.usda.gov/.

U.S. Geological Survey, 1978, 7.5-minute series orthophoto quads, Ilio Point, Molokai Airport, and Kaunakakai, Hawaii: 1:24,000 scale maps.

U.S. Geological Survey, 2010, LANDFIRE Existing Vegetation Type (Refresh08): Earth Resources Observation and Science Center, U.S. Geological Survey, at http://landfire.cr.usgs.gov/viewer.

University of Hawaiʻi, 2008, Hawaii agricultural water use and development plan: report submitted to Hawaiʻi Department of Agriculture by College of Tropical Agriculture and Human Resources, Department of Natural Resources and Environmental Management, University of Hawaiʻi at Mānoa, Honolulu, Hawaiʻi, 556 p.

Viessman, W., Jr., and Lewis, G.L., 2003, Introduction to hydrology (5th ed.): Upper Saddle River, N.J., Prentice Hall, 612 p.

Villegas, J.C., Tobon, C., and Breshears, D.D., 2007, Fog interception by non-vascular epiphytes in tropical montane cloud forests; dependencies on gauge type and meteorological conditions: Hydrological Processes, v. 22, no. 14, p. 2484–2492.

Wahl, K.L., and Wahl, T.L., 1995, Determining the flow of Comal Springs at New Braunfels, Texas: Proceedings of Texas Water ’95, a component conference of the American Society of Civil Engineers International Conference on Water Resources Engineering, 1st, San Antonio, Texas, p. 77–86.

Walmsley, J.L., Schemenauer, R.S., and Bridgman, H.A., 1996, A method for estimating the hydrologic input from fog in mountainous terrain: Journal of Applied Meteorology, v. 35, no. 12, p. 2237–2249.

Appendix 2. Sensitivity Analysis for Three-Dimensional Numerical Groundwater Model

The sensitivity of the three-dimensional numerical groundwater-flow and salinity model of Molokaʻi to selected hydraulic parameters was evaluated by varying one parameter in the model at a time. Selected parameters tested consisted of: (1) the vertical distribution of withdrawal from selected wells; (2) transverse dispersivity; (3) longitudinal dispersivity; (4) effective porosity; (5) horizontal hydraulic conductivity of the dike barrier east of existing wells in the Kualapuʻu area; (6) vertical anisotropy of hydraulic conductivity near well 0901–01; and (7) and vertical anisotropy of hydraulic conductivity near wells 0801–01 to –03. In general, simulated water levels were not sensitive (less than a foot change) to selected parameters, with the possible exception of effective porosity (within the range of effective-porosity values tested, water-levels differed by about 2 ft in places). Thus, for the sensitivity analysis, model results are presented in terms of the simulated chloride concentration of water withdrawn from selected production wells.

Vertical Distribution of Withdrawal

The model developed for this study assumed that withdrawals were uniformly distributed with depth, with the exception of two wells in the Kualapuʻu area. For the two exceptions (wells 0801–01 and 0801–02), withdrawals were assumed to be distributed nonuniformly because information from well 0801–01 indicated improved production when the well was deepened from an altitude of about −51 ft to −91 ft. In the model, 90 percent of the withdrawals from wells 0801–01 and 0801–02 were distributed to the bottom node of the vertical column of nodes representing each well and the remaining 10 percent of the withdrawals were assigned to the other nodes representing each well. Model sensitivity to the vertical distribution of withdrawal from wells 0801–01 and 0801–02 was evaluated by assuming withdrawal was uniformly distributed with depth, which is consistent with all other wells (fig. 2.1). Model results indicate that the simulated chloride concentration of water withdrawn from wells 0801–01 and 0801–02 is reduced if the withdrawal is uniformly distributed with depth because less water is withdrawn from near the bottom of the well.

Transverse Dispersivity

The model developed for this study assumed a transverse-dispersivity value of 0.16 ft (in all directions) throughout. Model sensitivity to transverse dispersivity was evaluated by testing values of 0.08 ft and 0.33 ft in the model (fig. 2.2). Model results indicate that the simulated chloride concentration of water withdrawn from wells generally increases as the transverse dispersivity in the model increases. Increased values of transverse dispersivity enhance dispersion in the model.

Longitudinal Dispersivity

The model developed for this study assumed longitudinal-dispersivity values of 250 ft in the maximum and middle hydraulic-conductivity directions (horizontal longitudinal and transverse directions) and 5 ft in the minimum hydraulic-conductivity direction (vertical direction) throughout. Model sensitivity to longitudinal dispersivity was evaluated by halving and doubling these values in the model (fig. 2.3). Model results indicate that the simulated chloride concentration of water withdrawn from wells generally increases as the longitudinal dispersivity in the model increases. Increased values of longitudinal dispersivity enhance dispersion in the model.

Effective Porosity

The model developed for this study assumed an effective porosity value of 0.05 throughout. Model sensitivity to effective porosity was evaluated by halving (0.025) and doubling (0.1) the original value in the model (fig. 2.4). Model results indicate that the simulated chloride concentration of water withdrawn from wells in the Kualapuʻu area is sensitive to the effective porosity value (within the range tested) and generally increases as the effective porosity in the model decreases. Decreased effective porosity values in the model result in greater groundwater velocities and more rapid changes in water levels and salinity.

Hydraulic Conductivity of Eastern Dike Barrier

The model developed for this study assumed a horizontal hydraulic-conductivity value of 3 ft/d for the eastern dike barrier (between inflow zones 4 and 5 in fig. 16), east of existing production wells in the Kualapuʻu area. The ratio of horizontal-to-vertical hydraulic-conductivity ratio was assumed to be 10, and this value was held constant for the sensitivity analysis. Model sensitivity to the hydraulic conductivity of the eastern dike barrier was evaluated by decreasing (0.3 ft/d) and increasing (30 ft/d) the original value by a factor of 10 in the model (fig. 2.5). Model results indicate that the simulated chloride concentration of water withdrawn from wells in the Kualapuʻu area decreases as the hydraulic conductivity of the eastern dike barrier increases by a factor of 10, but chloride concentration does not change much if the hydraulic conductivity of the eastern dike barrier decreases by a factor of 10. An increased hydraulic-conductivity value for the eastern dike barrier in the model appears to cause greater inflow of fresh groundwater from the east toward the Kualapuʻu production wells.

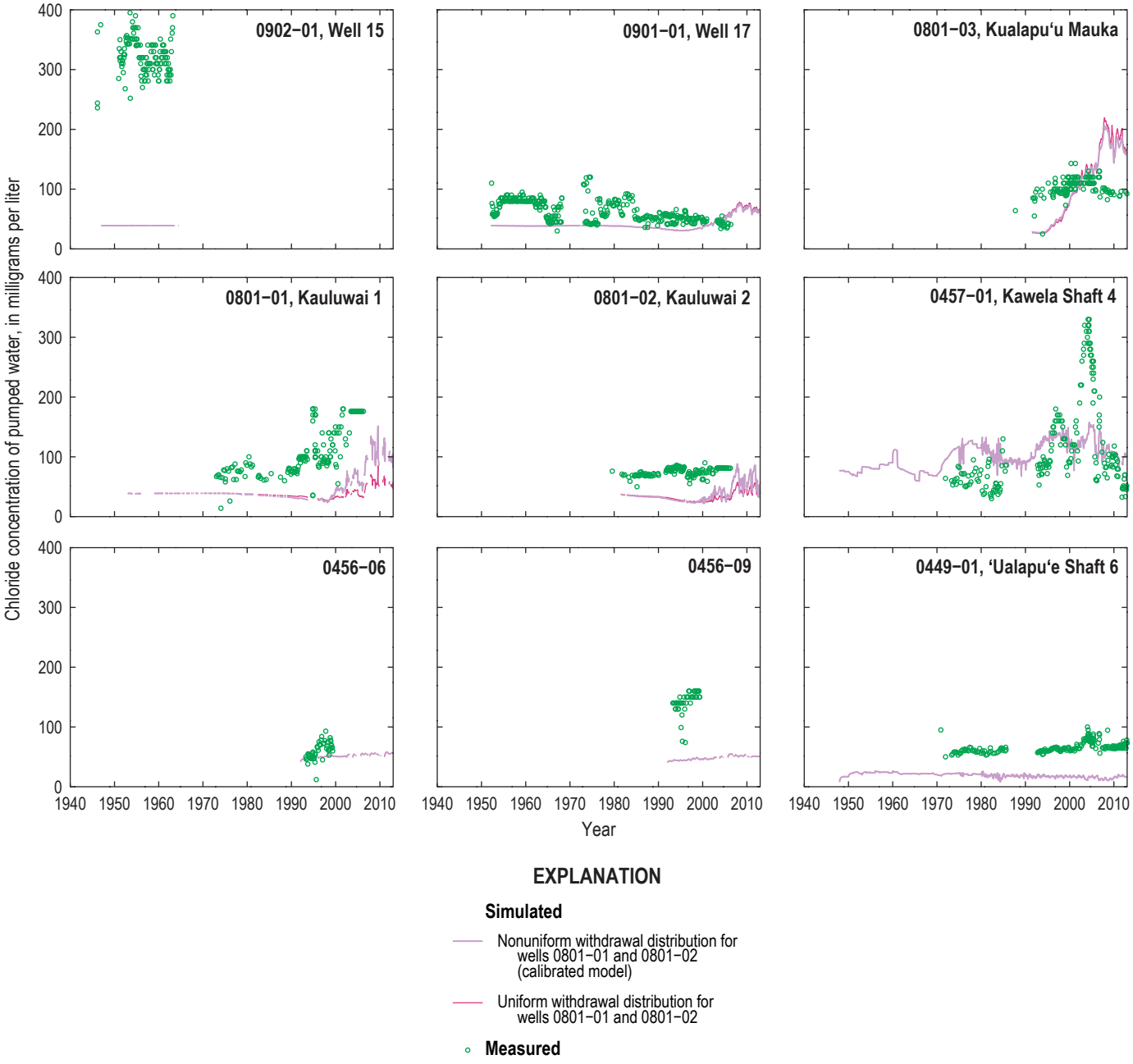

Figure 2.1. Multiple time-series graphs showing model sensitivity to vertical withdrawal distribution from selected pumped wells (0801−01 and 0801−02) in terms of simulated chloride concentration of water withdrawn from selected wells during 1940−2012, Moloka‘i, Hawai‘i.

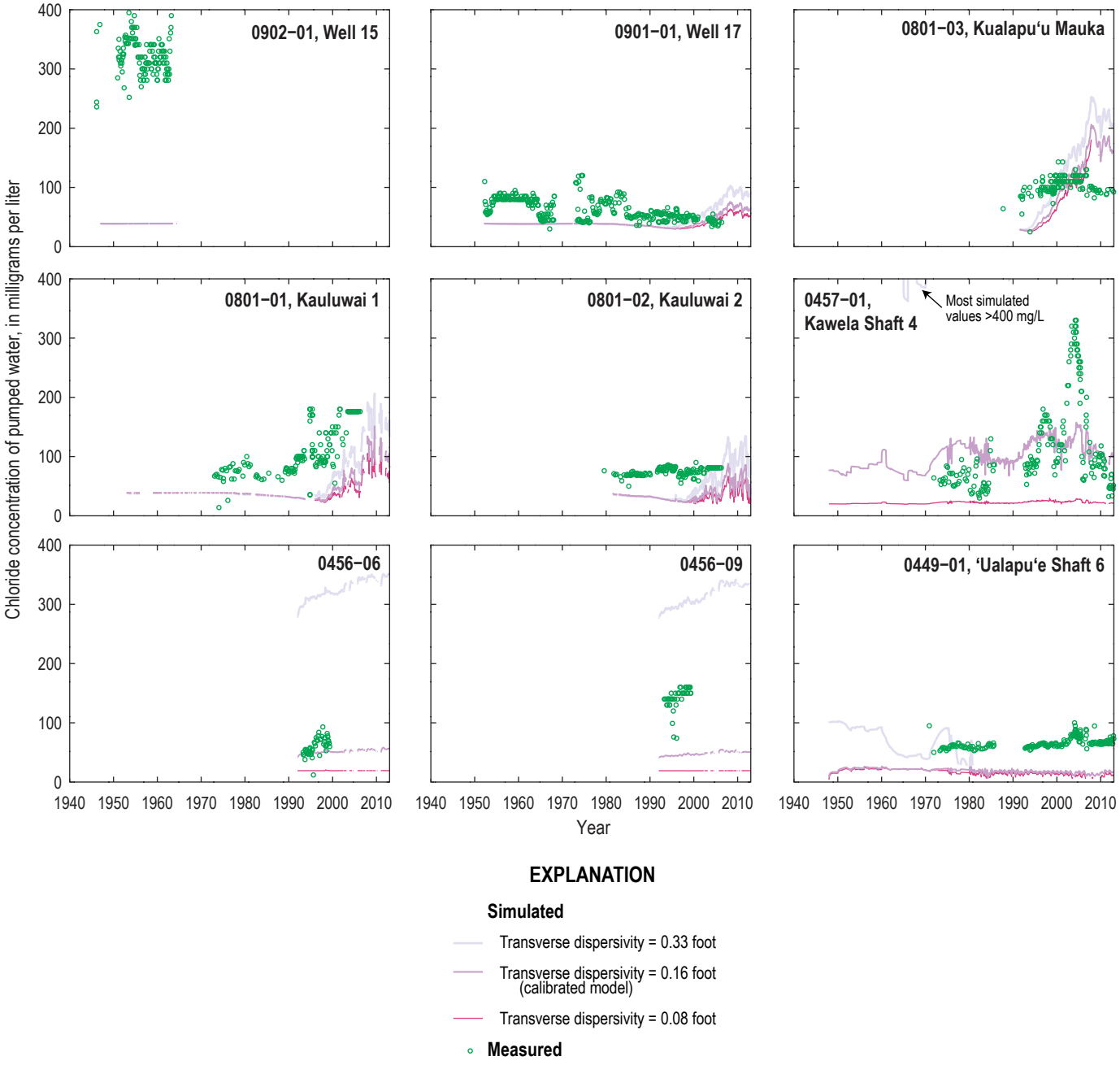

Figure 2.2. Multiple time-series graphs showing model sensitivity to transverse dispersivity in terms of simulated chloride concentration of water withdrawn from selected wells during 1940–2012, Moloka‘i, Hawai‘i. For well 0449–01 (transverse-dispersivity values of 0.33 and 0.08 foot) and well 0801–03 (transverse dispersivity of 0.08 foot), simulated chloride concentrations are not plotted during some periods because of numerical errors (negative values).

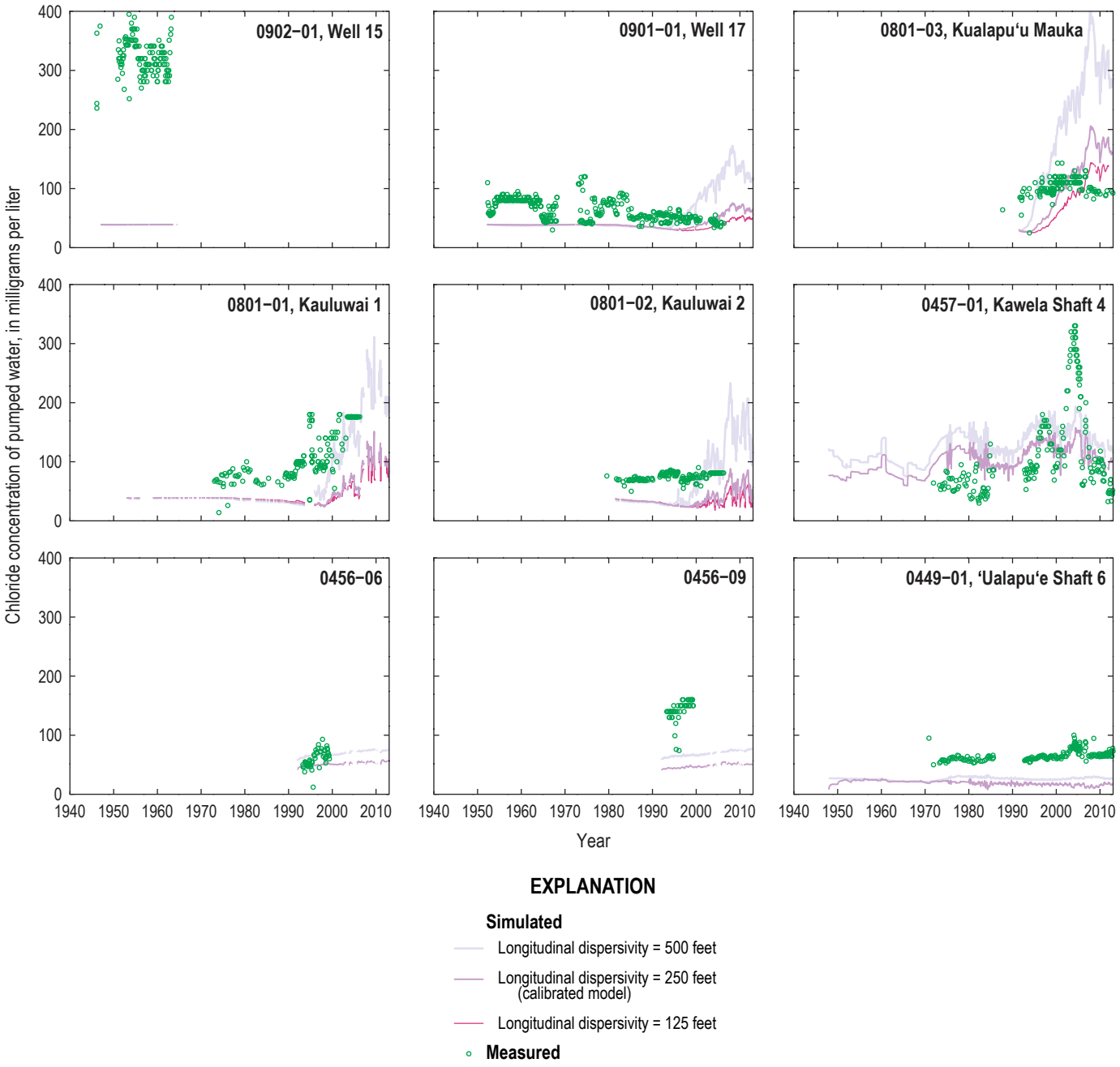

Figure 2.3. Multiple time-series graphs showing model sensitivity to longitudinal dispersivity in terms of simulated chloride concentration of water withdrawn from selected wells during 1940−2012, Moloka‘i, Hawai‘i. For wells 0801−03, 0457−01, 0456−06, 0456−09, and 0449−01 simulated chloride concentrations for a longitudinal dispersivity of 125 feet are not plotted during some periods because of numerical errors (negative values).

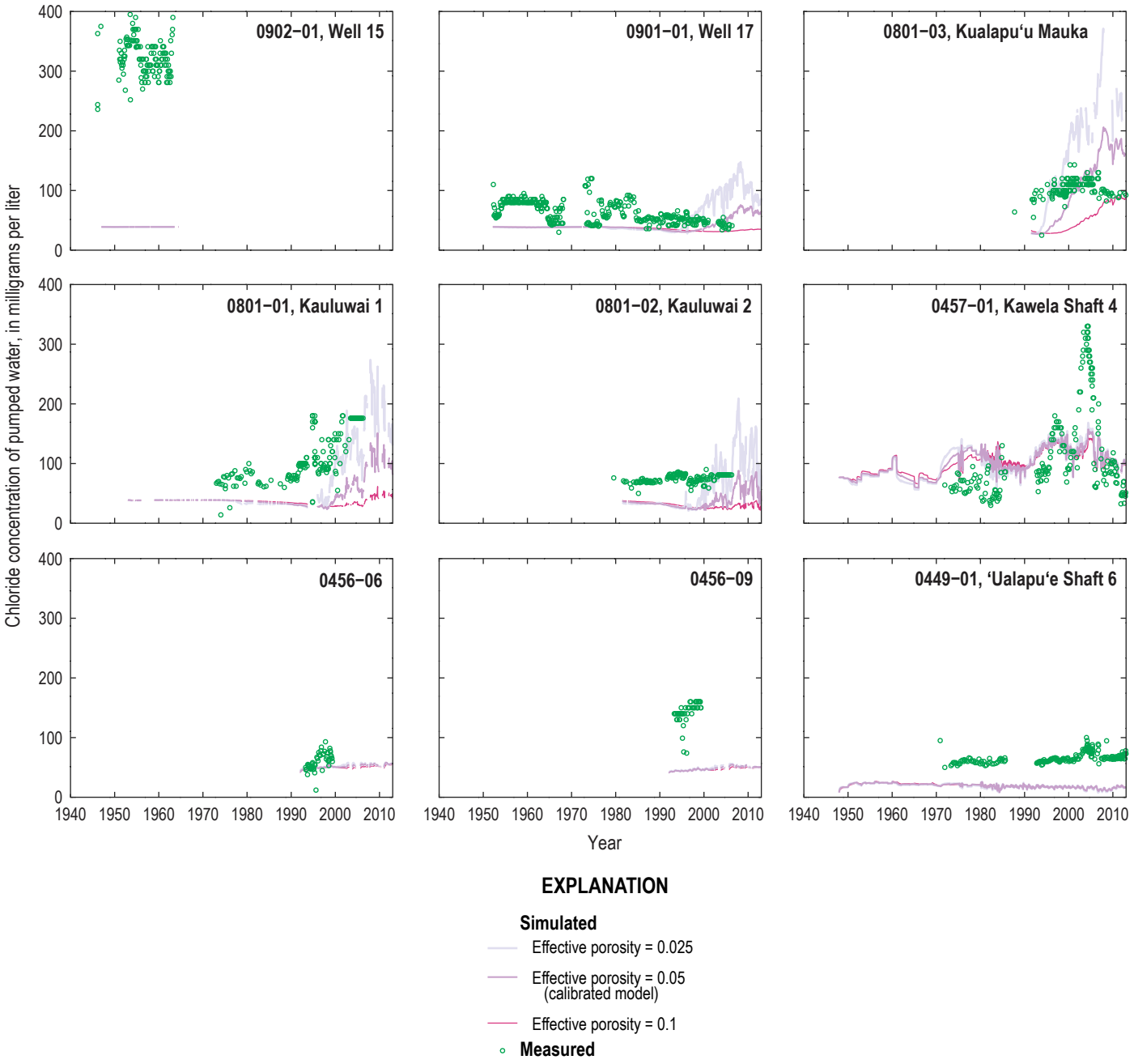

Figure 2.4. Multiple time-series graphs showing model sensitivity to effective porosity in terms of simulated chloride concentration of water withdrawn from selected wells during 1940–2012, Moloka‘i, Hawai‘i. For well 0801–03, simulated chloride concentrations for an effective porosity of 0.025 are not plotted during some periods because of numerical errors (negative values).

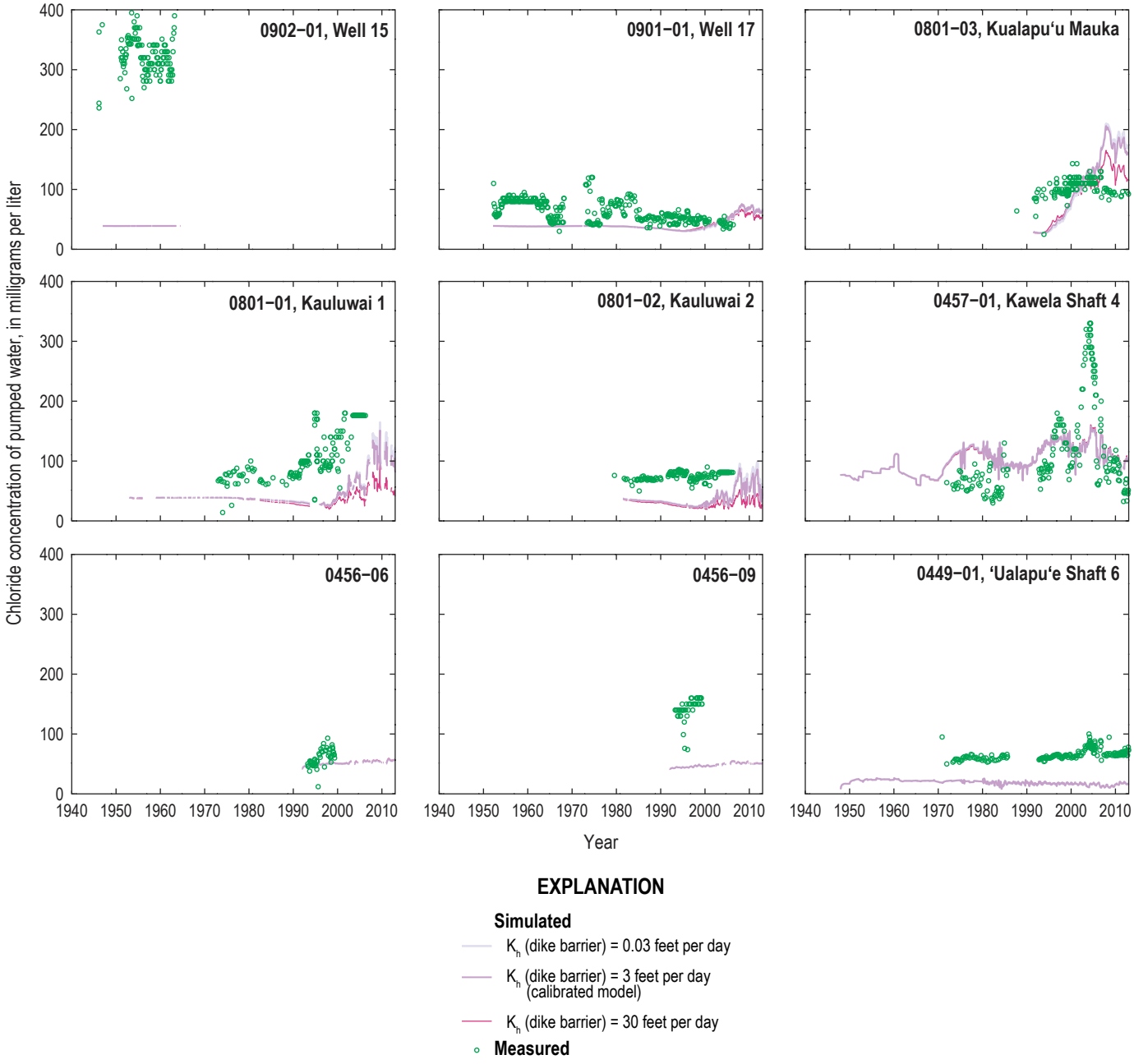

Figure 2.5. Multiple time-series graphs showing model sensitivity to horizontal hydraulic conductivity (K_h) of dike barrier east of wells 0801−01 and 0801−02 in terms of simulated chloride concentration of water withdrawn from selected wells during 1940−2012, Molokaʻi, Hawaiʻi.

Vertical Anisotropy Near Well 0901–01

The model developed for this study assumed a horizontal-to-vertical hydraulic-conductivity ratio of 350 near well 0901–01 in the Kualapu‘u area (downgradient of inflow zone 3 in fig. 16). The horizontal hydraulic-conductivity value was assumed to be 1,000 ft/d, and this value was held constant for the sensitivity analysis. Model sensitivity to the horizontal-to-vertical hydraulic-conductivity ratio near well 0901–01 was evaluated by decreasing (150) and increasing (550) the original value in the model (fig. 2.6). Model results indicate that the simulated chloride concentration of water withdrawn from well 0901–01 increases as the horizontal-to-vertical hydraulic-conductivity ratio decreases. By maintaining a constant horizontal hydraulic-conductivity value for the sensitivity analysis, the vertical hydraulic-conductivity value increases as the horizontal-to-vertical hydraulic-conductivity ratio decreases. In the model, higher vertical hydraulic-conductivity values (lower horizontal-to-vertical hydraulic-conductivity ratios) tend to enhance upward movement of brackish water near pumped wells.

Vertical Anisotropy Near Wells 0801–01, 0801–02, and 0801–03

The model developed for this study assumed a horizontal-to-vertical hydraulic-conductivity ratio of 150 near wells 0801–01, 0801–02, and 0801–03 in the Kualapu‘u area (downgradient of inflow zone 4 in fig. 16). The horizontal hydraulic-conductivity value was assumed to be 1,000 ft/d, and this value was held constant for the sensitivity analysis. Model sensitivity to the horizontal-to-vertical hydraulic-conductivity ratio near wells 0801–01, 0801–02, and 0801–03 was evaluated by decreasing (100) and increasing (350) the original value in the model (fig. 2.7). Model results indicate that the simulated chloride concentrations of water withdrawn from wells 0801–01, 0801–02, and 0801–03 increases as the horizontal-to-vertical hydraulic-conductivity ratio decreases. In the model, higher vertical hydraulic-conductivity values (lower horizontal-to-vertical hydraulic-conductivity ratios) tend to enhance upward movement of brackish water near pumped wells.

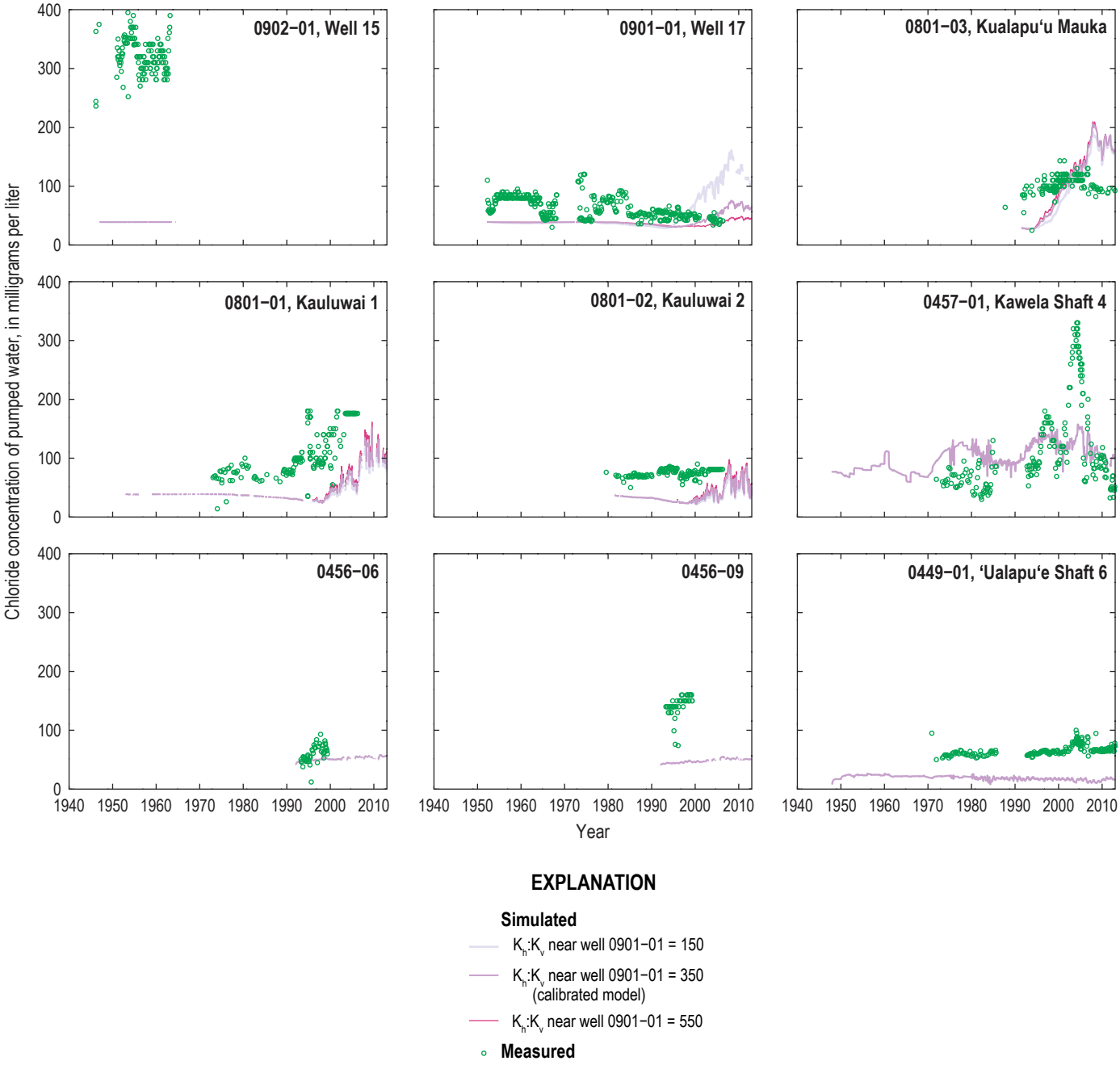

Figure 2.6. Multiple time-series graphs showing model sensitivity to vertical anisotropy (ratio of horizontal hydraulic conductivity to vertical hydraulic conductivity, K_h:K_v) of the volcanic rocks near well 0901−01 in terms of simulated chloride concentration of water withdrawn from selected wells during 1940−2012, Moloka‘i, Hawai‘i. For testing model sensitivity to vertical anisotropy, the horizontal hydraulic conductivity of the volcanic rocks near well 0901−01 was set at 1,000 feet per day. For well 0901−01, simulated chloride concentrations for K_h:K_v = 150 are not plotted during some periods because of numerical errors (negative values).

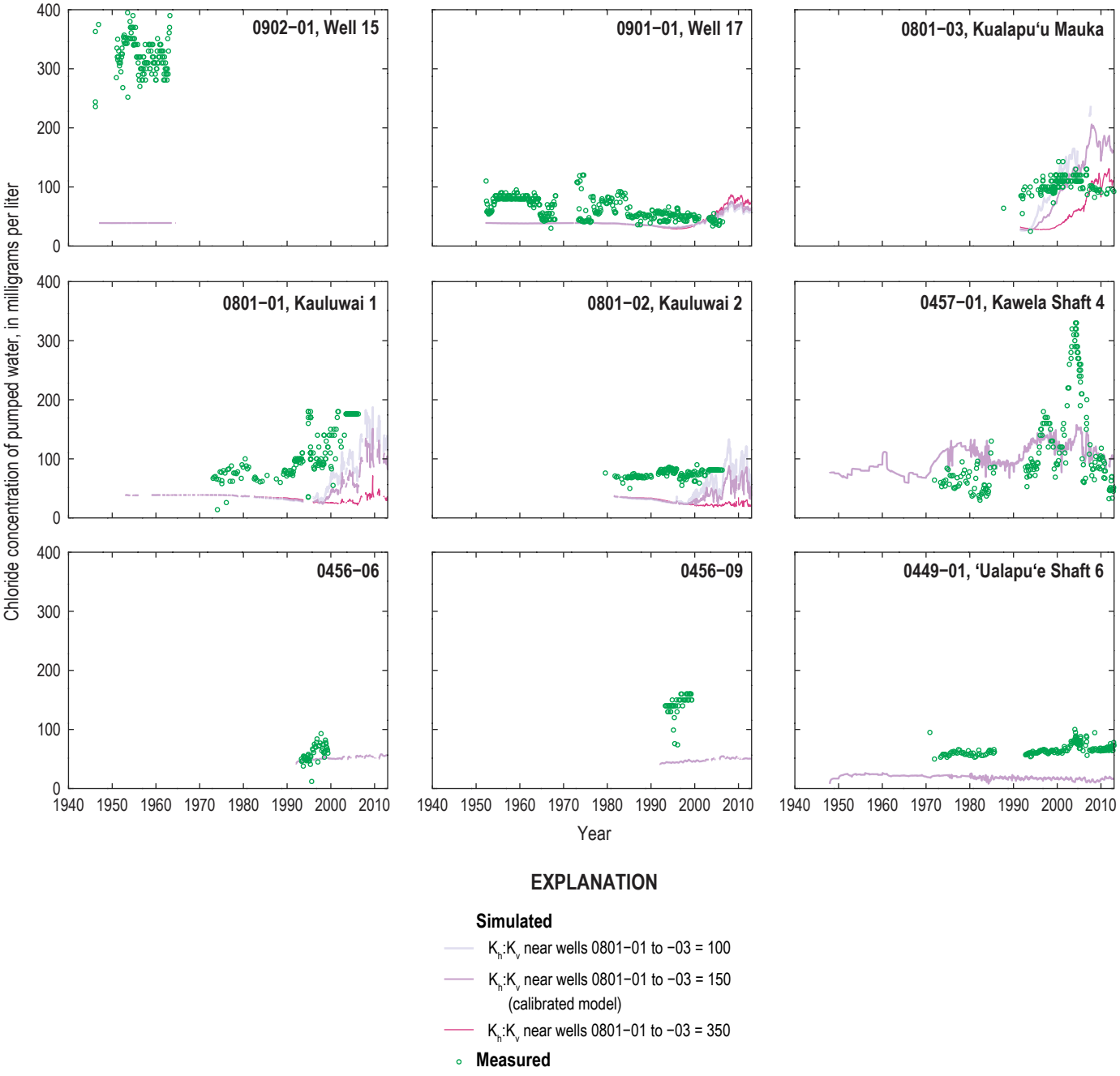

Figure 2.7. Multiple time-series graphs showing model sensitivity to vertical anisotropy (ratio of horizontal hydraulic conductivity to vertical hydraulic conductivity, K_h:K_v) of the volcanic rocks near wells 0801−01, 0801−02, and 0801−03 in terms of simulated chloride concentration of water withdrawn from selected wells during 1940−2012, Moloka‘i, Hawai‘i. For testing model sensitivity to vertical anisotropy, the horizontal hydraulic conductivity of the volcanic rocks was set at 1,000 feet per day. For well 0801−03, simulated chloride concentrations for K_h:K_v = 100 are not plotted during some periods because of numerical errors (negative values).

Menlo Park Publishing Service Center, California
Manuscript approved for publication December 26, 2019
Edited by Phil A. Frederick
Layout and design by Cory Hurd

ISSN 2328-0328 (online)
https://doi.org/10.3133/sir20195150